Kerstin Schmoltner

Environmentally Stable Organic Field-Effect Transistor based Sensor Devices

DOCTORAL THESIS

For obtaining the academic degree of

Doktorin der technischen Wissenschaften

Doctoral Programme of Technical Sciences
Technical Physics

Graz University of Technology

Supervisor:
Ao. Univ.-Prof. Dipl.-Ing. Dr.techn. Emil J. W. List-Kratochvil
Institute of Solid State Physics
in cooperation with:
NanoTecCenter Weiz Forschungsgesellschaft mbH

Graz, July 2014

EIDESSTATTLICHE ERKLÄRUNG

AFFIDAVIT

Ich erkläre an Eides statt, dass ich die vorliegende Arbeit selbstständig verfasst, andere als die angegebenen Quellen/Hilfsmittel nicht benutzt, und die den benutzten Quellen wörtlich und inhaltlich entnommenen Stellen als solche kenntlich gemacht habe. Das in TUGRAZonline hochgeladene Textdokument ist mit der vorliegenden Dissertation identisch.

I declare that I have authored this thesis independently, that I have not used other than the declared sources/resources, and that I have explicitly indicated all material which has been quoted either literally or by content from the sources used. The text document uploaded to TUGRAZonline is identical to the present doctoral dissertation.

Datum / Date	Unterschrift / Signature

To Roland

Acknowledgements

I would like to express my sincere gratitude to a number of people for their help and support during my PhD research. First of all I would like to thank my supervisor Prof. Emil J. W. List-Kratochvil for giving me the opportunity to work in his team on this interesting field of research and for his guiding ideas.

I wish to express my greatest thanks to Johannes Kofler for intense collaboration, many fruitful discussions and for your inspiring enthusiasm and ideas as well as friendship. Special thanks goes also to Sebastian Nau for your support, valuable discussions and being a good friend and Florian Kolb for your eagerness to help, your valuable feedback and friendship. Thank you for creating such a joyful atmosphere and all good laughs. It was such a great pleasure working with you.

Among the collaborators and co-authors, in particular I would like to thank Florian Schlütter within the group of Prof. Klaus Müllen for providing the novel semiconducting polymer, Stefanie Winkler within the group of Prof. Norbert Koch for the UPS investigation and the group of Prof. Roland Resel for the XRD measurements. Moreover I would like to thank the whole team of the NanoTecCenter Weiz Forschungsgesellschaft mbH for the great collaboration and their assistance, in particular, Andreas Klug, who allocated the funding with the research project BioOFET2, which gave me the opportunity to work on this interesting field of research. Furthermore like to express my sincere gratitude to Markus Postl and Stefan Sax for their support, especially for the design and realization of the 3D printed measurement setup and Alexander Blümel for being the AFM expert. Special thanks goes also to Josef Harrer, Cornelia Ranz and Angelika Nigg for always being available for technical problems or chemical stuff. Among others I also wish to thank Katrin Koren, Manuel Auer, Christoph Wolf and Patrick Hierzer for their help in the lab and creating an enjoyable research environment.

For funding I want to acknowledge the research project BioOFET2 and MIEC-DEVs (EFRE).

Moreover I want to thank my family and friends, for all the good times and your support. In particular I deeply want to thank my parents, Monika und Wolfgang and my sister, Martina, for your love and continuous encouragement and for helping me to also focus on what really matters in life. Last, but most important I like to thank Roland for believing in me, your tremendous support, your understanding, and your endless love.

Abstract

Organic field-effect transistors (OFETs) have already been proven to be excellent candidates as transducers for various chemical and biological sensing applications. Such sensor systems combine the unique properties of organic materials such as cost-efficient production, integration on flexible substrates and biocompatibility with those of field-effect transistors. The latter offer distinct advantages, like intrinsic signal amplification, leading to higher sensitivity, low power consumption and the possibility of miniaturization and integration into complex circuits for further signal processing. Aside from sensor key features such as sensitivity, selectivity, reversibility and response time, the device stability is another important factor. Within this context a novel air-stable p-type heterotriangulene polymer (PTA) for large-area OFET applications was investigated concerning morphological, optical, electrical and interface related properties. PTA FETs exhibit excellent air stability over several months and a superior performance compared to the widely used poly(3-hexylthiophene) (P3HT) based OFETs. Furthermore, the investigations of the influence of photolithographic processing on the device performance of P3HT BG/BC OFETs highlight the importance to focus not only on the constituting materials but also on the manufacturing process.

In addition, for the emerging fields of biomedical diagnostics and environmental monitoring, sensing of ions (e.g. Na^+, K^+, Cl^-, Ca^{2+}) in appropriate aqueous media is of particular interest. Therefore a water-stable operation of OFET-based sensor elements is crucial. Within this thesis electrolyte-gated OFETs (EGOFETs) are discussed as the transducer of choice. Due to an electric double layer of high electrical capacitance at the electrolyte - organic semiconductor interface, low voltage operation and thus a water-stable operation is obtained. A combined study of P3HT-based EGOFETs on various substrates is presented, including the investigations of the influence of different electrolytes and various gate electrode materials. Furthermore, the limits of a stable operating voltage window are evaluated and the effects when abandoning the latter are discussed. Based on these findings, the first electrolyte-gated OFET for selective and reversible ion detection is demonstrated. A sensitive and selective response to sodium ions was obtained by introducing a state of the art ion-selective membrane (ISM). Based on this novel modular sensor concept, a sensitive linear response in the range of 10^{-6} to 10^{-1} M Na^+ with a slope of ~62 mV/dec was achieved. Furthermore, this potentiometric sensor showed a reversible response and its selectivity was successfully tested against K^+ ions. These results constitute an important step towards a low-cost integrated sensor array for multiple ion detection, facilitated by the integration of different state of the art ISMs.

Kurzfassung

Organische Feldeffekttransistoren (OFETs) haben sich bereits als Messwandler in der chemischen und biologischen Sensorik bei vielen Anwendungsbeispielen bewährt. Ihr Einsatz ermöglicht die Verknüpfung der Vorteile zweier Technologien: Organische Materialien bieten den Vorteil einer einfachen und kostengünstigen Herstellung selbst auf flexiblen Substraten sowie eine gute Umweltverträglichkeit (Biokompatibilität). Feldeffekttransistoren als aktive Sensoreinheit zeichnen sich durch die Vereinigung von Sensor und Verstärker in einem Bauteil aus. Neben der höheren Empfindlichkeit aufgrund der intrinsischen Verstärkung des Messsignals wird durch die Möglichkeit der Integration in komplexen Schaltkreisen die weitere Signalverarbeitung erleichtert. Als weiteren Vorteil ist der geringe Energieverbrauch von Transistor-basierten Sensorsystemen zu nennen. Neben den wichtigsten technischen Merkmalen von Sensoren wie Sensitivität, Selektivität, Reversibilität und Ansprechzeit stellt die Stabilität eine wesentliche Voraussetzung für deren praktische Anwendung dar. In diesem Zusammenhang wurde ein neuartiges p-Typ Heterotriangulen-basiertes Polymer (PTA) in OFETs eingesetzt und untersucht. Dieses amorphe halbleitende Polymer wurde bezüglich Stabilität und morphologischer, optischer, elektrischer und Grenzflächen-Eigenschaften im Detail studiert. Die in dieser Arbeit präsentierten PTA-basierten OFETs zeigen eine hervorragende Stabilität über mehrere Monate selbst bei Betrieb an Luft. Im Vergleich zu den üblicherweise verwendeten Poly(3-hexylthiophen) (P3HT) basierten OFETs, weisen die PTA-FETs eine deutlich verbesserte Performance auf. Zudem wurde die Bedeutung des Herstellungsprozesses von OFETs, im speziellen mit der Untersuchung der Einflüsse photolithographischer Prozesse auf die Bauteil Performance von P3HT BG/BC OFETs, hervorgehoben.

In Hinblick auf biomedizinische Diagnostik wie auch Überwachung und Kontrolle von Umweltsystemen ist die Detektion von Ionen wie Na^+, K^+, Cl^-, Ca^{2+} etc. von großer Bedeutung. Allerdings muss, um Ionen detektieren zu können, als Grundvoraussetzung ein stabiles Betreiben der OFET-Sensoren in wasserbasierten Medien gewährleistet sein. Hinsichtlich dieser Anforderung stellten sich „electrolyte-gated“ organische Feldeffekttransistoren (EGOFETs) als die Messwandler der Wahl heraus. Im Vergleich zur konventionellen Elektronik nutzen EGOFETs den direkten Kontakt mit Wasser bzw. dem wässrigen Analyten aus. Die Formierung einer elektrischen Doppelschicht zwischen organischen Halbleiter und Elektrolyt (Analyt) führt zu einer sehr hohen elektrischen Kapazität, die ein stabiles Betreiben des Transistors bei sehr niedrigen Spannungen im jeweiligen wässrigen Medium ermöglicht. In diesem Zusammenhang wurde der Einfluss unterschiedlicher Elektrolyte und Gateelektroden-Materialien auf die Charakteristika P3HT-basierter EGOFETs untersucht. Die wesentlichen Parameter für einen stabilen Betrieb wurden

festgelegt und die Auswirkungen bei Verlassen dieses Betriebsfensters studiert. Basierend auf diesen Erkenntnissen wird im Zuge dieser Arbeit gezeigt, dass mit „electrolyte-gated“ OFETs Ionen reversibel und selektiv detektieren werden können. Durch Einsatz spezieller ionenselektiver Membranen (ISM) gelang der Nachweis von Na^+ Ionen in einem sehr großen Konzentrationsbereich von 10^{-6} mol/L bis 10^{-1} mol/L Na^+ mit einer Sensitivität von ~62 mV/dec. Die Selektivität des Na^+ sensitiven EGOFETs wurde des Weiteren erfolgreich gegen das interferierende Kalium-Ion getestet. Außerdem zeigte der potentiometrische Ionensensor auch ein ausgezeichnetes reversibles Verhalten. Durch die einfache Integration von unterschiedlichen ISMs, schafft diese Arbeit die Grundlage für ein voll integrierbares kostengünstiges Sensor-Arrays zur zeitlich-parallelisierten Detektion von unterschiedlichen Ionenarten.

List of included Publications

This thesis is mainly based on work that has been published within the journals mentioned below. The author of this thesis is also the first author of the listed publications and wrote the manuscripts, unless otherwise noted. The permission to reproduce the content was obtained from each journal and indicated within the corresponding chapters. Parts of the reproduced content have been modified and the original work can be found in the appendix.

[1] Photolithographic processing and its influence on the performance of organic field-effect transistors

K. Schmoltner, A. Klug, J. Kofler and E. J.W. List

Proceedings of SPIE 8479, Organic Semiconductors in Sensors & Bioelectronics V, 84790J, (**2012**)

Contribution: All experimental work. SEM images were recorded together with J. Kofler. Wrote the manuscript and did the final editing with the co-authors.

[2] A heterotriangulene polymer for air-stable organic field-effect transistors

K. Schmoltner, F. Schlütter, M. Kivala, M. Baumgarten, S. Winkler, R. Trattnig, N. Koch, A. Klug, E. J. W. List and K. Müllen

Polymer Chemistry 4, 5337-5344 (**2013**)

Contribution: All experimental work concerning film preparation and organic field-effect transistors. All electrical characterizations and contributed equally in the optical measurements together with Roman Trattnig. Wrote the manuscript expect for the polymer synthesis and did the final editing with the co-authors.

[3] Electrolyte-gated field-effect transistors for sensing applications in aqueous media

K. Schmoltner, J. Kofler, A. Klug and E. J. W. List-Kratochvil

Proceedings of SPIE 8831, Organic Field-Effect Transistors XII; Organic Semiconductors in Sensors & Bioelectronics VI, 88311N (**2013**)

Contribution: All experimental work. Wrote the manuscript and did the final editing with the co-authors.

[4] Electrolyte-gated field-effect transistor for selective and reversible ion detection

K. Schmoltner*, J. Kofler*, A. Klug and E. J. W. List-Kratochvil,

Advanced Materials 25 (47), 6895–6899 (**2013**)

*both authors contributed equally.

Contribution: All experimental work concerning EGOFETs. The author contributed equally with J. Kofler to experiments related to the ion-selective EGOFETs and sensor characterization. Wrote the manuscript, finalized the manuscript together with J. Kofler and did the final editing with the co-authors.

List of not included Publications

Variable tunneling barriers in FEBID based PtC metal-matrix nanocomposites as a transducing element for humidity sensing
F. Kolb, K. Schmoltner, M. Huth, A. Hohenau, J. Krenn, A. Klug, E. J. W. List, H. Plank
Nanotechnology 24, 305501 (**2013**)

Hydrogen ion-selective electrolyte-gated field-effect transistor for pH-sensing
J. Kofler[*], K. Schmoltner[*], A. Klug, E. J. W. List-Kratochvil
Applied Physics Letter 104, 193305 (**2014**)
[*]both authors contributed equally.

Highly robust electron beam lithography lift-off process using chemically amplified positive tone resist and PEDOT:PSS as a protective coating
J. Kofler, K. Schmoltner, A. Klug, E. J. W. List-Kratochvil
Accepted for publication in Journal of Micromechanics and Microengineering (**2014**)

Table of Contents

Acknowledgements i

Abstract ii

Kurzfassung iii

List of included Publications v

List of not included Publications vi

1 Introduction and Scope of the Thesis 1

2 Theoretical Background 5

2.1 Organic Semiconductors 5

2.1.1 Organic Semiconducting Materials 7

2.1.2 Charge Carriers and Charge Carrier Transport 9

2.2 Organic Field-Effect Transistors 13

2.2.1 Basic Operation and Transistor Equations 13

2.2.2 Transistor Characteristics and Parameters 17

2.2.3 OFET Architectures and Design Rules 20

2.3 OFETs as Sensing Elements in Aqueous Media 22

2.4 EGOFETs for Sensing Applications in Aqueous Media 25

2.4.1 Operation of EGOFETs – EDL Formation 26

2.4.2 Requirements of EGOFET based Sensors 28

3 Experimental Methods – Manufacturing and Characterization of OFETs and EGOFETs 31

3.1 Device Fabrication 31

3.1.1 Structuring of Source/Drain Electrodes 32

3.1.2 Surface Modifications 34

3.1.3 Film Deposition 34

3.1.4 Electrolytes and PDMS Replica Molding 35

3.2 Materials and Film Characterization Methods 36

3.3 Electrical Characterization 37

4 Photolithographic Processing and its Influence on the Performance of Organic Field-Effect Transistors 39

4.1 Introduction 39

4.2 Influence of Photoresist Residuals on the OFET Performance 40
4.3 Influence of the Lift-Off Chemicals on the OFET Performance 43
4.4 Conclusion 47

5 A Heterotriangulene Polymer for Air-Stable Organic Field-Effect Transistors 49
5.1 Introduction 49
5.2 Synthesis and Materials Characterization 51
5.3 Thin Film Morphology 53
5.4 Energy Levels and Optical Properties 53
5.4.1 UV/Vis Absorption and Photoluminescence Spectra 53
5.4.2 Ultraviolet Photoelectron Spectroscopy - Energy levels of PTA 58
5.5 Characterization of Organic Field-Effect Transistors based on a Novel Heterotriangulene Polymer 61
5.5.1 Influence of N-protonation on the OFET Performance 65
5.6 Ambient Stability Investigations 66
5.7 Conclusion 69

6 Electrolyte-Gated Field-Effect Transistors for Sensing in Aqueous Media 71
6.1 Introduction 71
6.2 P3HT-based EGOFETs 72
6.3 Influence of the Ion Concentration within the Electrolyte 75
6.4 Influence of Various used Gate Electrodes 77
6.5 Stability Investigations of EGOFETs 78
6.6 Conclusion 85

7 Ion-Selective Electrolyte-Gated Field Effect Transistor 87
7.1 Introduction 87
7.2 Novel Ion Sensing Concept 89
7.3 Fabrication of Ion-Selective EGOFETs 91
7.4 Characterization of the Na^+ selective ISM within an Ion-Selective Electrode . 93
7.5 Characterization of Ion-Selective EGOFETs 95
7.5.1 Reversibility and Selectivity 99
7.6 Conclusion 101

8 Summary and Conclusion 103

References 107

Appendix 113

1 Introduction and Scope of the Thesis

From electronics to organic bioelectronics

The basic idea of a transistor as a solid state device was proposed by E. J. Lilienfeld in the late 1930s, aiming to replace the bulky and power-consuming vacuum triode.[5] About 20 year later (1947) J. Bardeen and W. Brattain constructed the first transistor at the Bell Laboratories.[6,7] This transistor was a germanium point-contact device but based on a different principle than originally proposed. This invention ignited intense research on inorganic semiconductors and led to further discoveries such as the bipolar transistor by Shockley et al. in 1948. It took another 10 years of research until the first metal-oxide-semiconductor field-effect transistor (MOSFET) was demonstrated by Atalla and Kahng[8], also from the Bell Labs. These inventions had an immense impact on the computers design, ushering in the "computer age". Nowadays we are surrounded by billions of MOSFETs, which are the basic building block of modern electronics including personal computers, mobile phones and many other microelectronics devices. The transistor is regarded as one of the greatest technological innovations of the 20th century. Accordingly, W. Shockley, J. Bardeen and W. Brattain were awarded with the Nobel Prize in Physics in 1956 "for their researches on semiconductors and their discovery of the transistor effect".[9,10]

The discovery of conducting properties of plastics in 1977 created new unprecedented opportunities.[11] Before that, these materials were solely regarded as insulating materials. Due their outstanding properties and ease of fabrication, they have already found widespread applications in the early 1900s replacing other materials such as wood, glass, leather, metals and ceramics. Plastics are basically organic polymers, which are mainly composed of carbon based compounds.[12] The discovery of electrical conductivity of organic materials can be traced back to the beginning of the 20th century, starting with the report on the photoconductivity of anthracene crystals.[13] However, there was only little of interest until the big milestone was set with the discovery of the high electrical conductivity of iodine doped polyacetylene by Hideki Shirakawa, Alan G. Mac. Diarmid, Alan J. Heeger and co-workers in 1977. It induced a new area of research, the "organic electronics", and was awarded with the Nobel Prize in Chemistry in the year 2000 "for the discovery and development of conductive polymers".[14] The fast advancing progress in research on

small molecule and π-conjugated polymer based organic semiconductors has led to successful realizations of organic light emitting diodes (OLEDs),[15] organic field-effect transistors (OFETs),[16,17] organic solar cells,[18] light-emitting electrochemical cells[19] as well as sensors.[20]

Although, organic semiconductors cannot compete with high performing inorganic semiconductors such as crystalline silicon, they feature other properties which are beneficial for certain applications. Most of the organic semiconductors can be processed from solution at low-temperature, allowing for low-cost large-scale printing techniques on a variety of flexible substrates such as plastic foils or paper. Today charge carrier mobilities of organic semiconductors (> 1 cm^2 $V^{-1}s^{-1}$)[21,22] already exceed the benchmark values of amorphous hydrogenated silicon, which is of high interest e.g. for thin film transistor application in radio-frequency identification tags,[23] drivers of flexible large-area displays[24] or sensing devices.[25] Organic light emitting diodes, for example, have already been implemented in displays of mobile phones and cameras, and will be soon also available for lightweight flexible and large screens.

More distant aims like reaching marketability of wearable electronics equipped with various organic based sensors (E-textiles) e.g. to monitor the health conditions, still require intense research and development. Within this context, organic field-effect transistors (OFET) have been proven to be promising candidates as transducers for several types of physical and chemical sensors.[25] They combine the unique properties of organic materials with those of field-effect transistors, such as low power consumption and the possibility of miniaturization and integration into complex circuits for further signal processing. Organic compounds offer a distinct advantage compared to inorganics that is the possibility to modify or functionalize the chemical structure in order to obtain a certain sensitivity and selectivity to target analytes. Moreover, they benefit from their “soft” nature and good biocompatibility,[26-28] which is highly important for biomedical applications. Hence, new possibilities are available for the envisioned human interfacing e.g. in-situ measurements of vital parameters, neuronal recordings, drug delivery, or artificial skin applications. Accordingly, there is a clear future trend towards “organic bioelectronics”,[29] which might lead to devices at the edge of human-machine interface technology in the near future.

Scope of this thesis

One of the current challenges of organic electronics is to overcome stability problems of organic based devices. Besides the above mentioned advantages, organic semiconductors often suffer from poor environmental stability. Within this thesis, these reliability issues, which are a basic requirement for all OFET applications are addressed by the investigation of a novel air-stable heterotriangulene polymer as well as by studying instabilities originating from OFET processing.

Interestingly, it was exactly the sensitivity of organic compounds to many environmental influences, which has led to the first realizations of OFET based chemical sensors for the detection of O_2, humidity as well as other gasses. However, for other chemical sensing applications such as the detection of ions or biomolecules, sensing in appropriate aqueous media is required. Especially, within the emerging fields of medical diagnostics and environmental monitoring, sensor arrays for in-situ sensing of ions (e.g. Na^+, K^+, Ca^{2+}, pH) are of particular interest. Thus, in addition to the air stable performance, a water-stable operation of OFET sensor elements is crucial. Consequently the second aim of this thesis was to develop a novel OFET based sensing concept for selective and reversible ion detection.

Chapter 2 is intended to give a basic introduction on organic semiconductors and organic field-effect transistors. The first part discusses the chemical and physical properties of organic semiconductors whereas the second part presents the basic operation principles of OFETs, including theoretical models describing the current voltage characteristics as well as important device parameters. Thereafter, an additional section gives an overview of OFET based sensors and reviews OFETs operating in aqueous media and their sensing applications. In particular electrolyte-gated OFETs are described in more detail. Specifically, the electric double layer formation and basic requirements for further sensing applications are discussed.

Chapter 3 presents the general fabrication methods of bottom-gate/bottom contact (BG/BC) OFETs and electrolyte-gated FETs (EGOFETs), such as structuring of S/D electrodes, film deposition etc. Moreover an overview of the analytical methods to investigate organic materials and films and the electrical characterization of OFETs is given.

Chapter 4 deals with the influence of photolithographic processing of source/drain electrodes on the device performance of regioregular poly(3-hexylthiophene) P3HT-based BG/BC OFETs. In particular, the effects of photoresist residuals within the active channel region and the influence of various lift-off chemicals, modifying the dielectric-semiconductor and/or electrode-semiconductor interfaces were morphologically and electrically investigated. The content of this chapter is based on work that has been published in [1].

Chapter 5 presents a novel air-stable p-type heterotriangulene polymer (PTA) for organic field-effect transistor (OFET) applications. This newly synthesized amorphous organic semiconductor was characterized concerning morphological, optical, electrical and interface related properties. In the course of optimization, the influence of several interface modifications and the effect of hydrochloric acid in chloroform (used as solvent), leading to protonation of the nitrogen atom on the PTA, was investigated. Finally, the ambient stability of BG/BC PTA OFETs was studied in detail over months and compared with P3HT devices. The content of this chapter is mainly based on work that has been published in [2].

Chapter 6 focuses on a combined study of P3HT-based electrolyte-gated OFETs gated via different aqueous solutions, demonstrating that EGOFETs constitute the transducer of choice for sensing applications within water. In particular, the influences of different ion concentrations in the electrolyte and various gate electrode materials have been investigated. The device stability as a central issue for a reliable sensor response was addressed by the evaluation of the stable operational window of EGOFETs. Moreover the effects when abandoning the latter as well as long time stability are discussed. The content of this chapter is mainly based on work that has been published in [3].

Within chapter 7 the first electrolyte gated poly(3-hexylthiophene) thin film transistor for selective and reversible ion detection is presented. A detailed description of the novel concept based on an EGOFET in combination with a state of the art ion-selective membrane and of its function is given. Moreover the ion-selective EGOFETs were electrically characterized with respect to sensitivity and selectivity to sodium. This potentiometric sensor was tested with respect to reversibility and selectivity against interfering potassium ions, demonstrating an important step towards a low-cost integrated ion sensor array for selective multiple ion detection, facilitated by a simple integration of different state of the art ion-selective membranes. The content of this chapter is mainly based on work that has been published in [4].

The final chapter 8 summarizes the work.

2 Theoretical Background

2.1 Organic Semiconductors

Organic materials are compounds mainly based on carbon in combination with other atoms, like hydrogen, oxygen, nitrogen, sulfur, etc. Carbon, as the central element in organic chemistry, allows for a large variety of molecules to be created due to different reasons: As a 4^{th}-main group element covalent bonds can be formed with virtually all materials due to its moderate electronegativity. Its chemical versatility is further increased due to hybridization of carbon allowing for the formation of single, double or triple bonds. Moreover the steric hindrance in carbon-based molecules is reduced, due to its small size. As a result of their specific mechanical, optical and electrical properties, carbon-based materials can be found in numerous applications in our everyday´s life. Depending on the type of chemical bonds different electrical properties are obtained. For instance when all 4 valence electrons of the outer shell are involved in strong single covalent bonds (σ-bonds), the material is insulating due to a large energy gap between bonding (σ) and antibonding (σ^*) orbitals. These compounds are called saturated hydrocarbons and are well-known from daily routines such as polyethylene (PE) e.g. for packaging (plastic bags, plastic films, container, bottels etc.). The formation of 4 single bonds is based on sp^3 hybridization (formation of 4 sp^3 orbital), whereas the unique properties of organic semiconductors are based on sp^2 hybridization leading to so called unsaturated hydrocarbons.

As the electronic configuration of carbon in its ground state is $1s^2 2s^2 2p^2$, where two electrons of the 2p orbital are unpaired, only two covalent bonds should be allowed to be formed. However, the energy difference between the 2s and the 2p state is small enough so that an electron can be easily promoted from the 2s orbital to the unoccupied 2p state, leading to four unpaired valence electrons available for bonding. According to the number of p orbitals, being combined with the 2s orbital, either a sp, sp^2 or sp^3 hybrid orbital can be formed.[30]

As already stated, in case of organic semiconductors the sp^2 hybridization is of particular importance. Here the sp^2 orbitals form strong covalent σ-bonds, while the unaltered p_z orbital, which is oriented perpendicular to the σ orbitals, overlaps with neighboring p_z orbitals forming

π-bonds. This gives a double bond. An example for a double bonded pair of carbon atoms (ethylene) is shown in Figure 2.1 (a).

Organic semiconductors are based on an alternation of single and double bonds, which is also called conjugation. One of the simplest examples of conjugated polymers from a structural point of view but with a huge historic impact is polyacethylene (see Figure 2.1 (b)). The σ-bonds account for the geometric structure of the molecule, whereas π-bonds overlap and are responsible for the semiconducting properties. Electrons which are bonded through π-bonds have a higher degree of freedom. They are not associated with any specific atoms or bonds and thus are delocalized forming a π-system which extends over the whole conjugated chain.

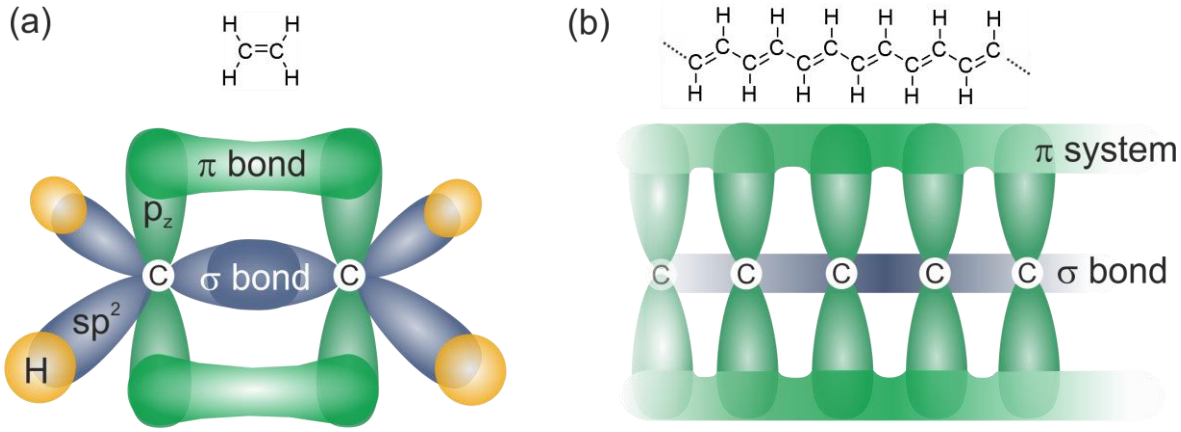

Figure 2.1: Schematic illustration of the sp^2 and p_z orbitals for a double bonded pair of carbon atoms (ethylene) forming a σ- and a π-bond (a) and for polyacethylene (b) with their corresponding chemical structure.

Since the π-bonds are weaker compared to the strong σ-bonds, the energy difference of the π-bonding and the π^*-antibonding orbital is less than between the σ- and σ^*-orbitals. According to the molecular orbital theory, the orbital occupied by electrons with the highest energy is called the highest occupied molecular orbital (HOMO) and the orbital with the lowest energy being unoccupied is called lowest unoccupied molecular orbital (LUMO). The number of the π and π* orbitals is proportional to the number of carbon atoms in a conjugated system. Therefore, as the number of carbon atoms increases, the individual energy levels (π and π*) become closer spaced and for infinitely long chains even lead to zero energy difference between the energy levels resulting in continuous energy bands rather than discrete levels.[30] This is shown in Figure 2.2 for alkene molecules (from ethylene to polyacethylene). The band gap of organic semiconductors, which is typically in the range of few eV, is determined by the structure of the material and decreases for increasing polymer chain length. [31,32] In analogy to inorganics semiconductors, the filled π-band (HOMO) is often also called valence band and the empty π^*-band (LUMO) is referred

to as conduction band. Moreover, in real systems the π-conjugation is generally limited to few repeating units due to twist, kinks and/or other defects on the molecular chain.

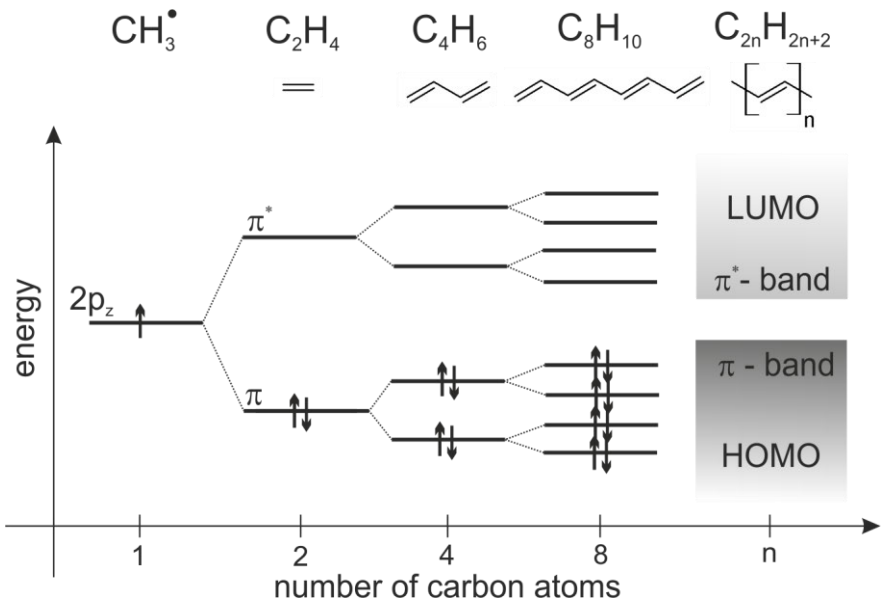

Figure 2.2: Energy levels (π and π) of alkenes with increasing number of carbon atoms, becoming closer spaced and finally leading to continuous energy bands.*

2.1.1 Organic Semiconducting Materials

Organic semiconductors can be regarded as van der Waals solids, as the intermolecular interactions are based on weak van der Waals forces compared to the strong covalent bonds of their backbone. They can be classified in conjugated small molecules and conjugated polymers, whereas latter are typically solution processable. Moreover, due to the excellent film forming properties of conjugated polymers thin films can be fabricated by various methods including spin coating, inkjet or gravur printing etc. In contrast, conjugated small molecules are usually not solution processable due to their poor solubility. They are mostly deposited by thermal evaporation or other vapor phase deposition methods, where the film formation can be influenced by the temperature of the substrate and the deposition rate.

In general the performance of conjugated materials i.e. charge carrier mobility (μ) is strongly dependent on their structural arrangement. A high degree of order of polymer chains or small molecules with respect to each other allow for a good π orbital overlap of adjacent molecules (π-π stacking), leading to a good interchain charge transport. Small molecules generally exhibit high charge carrier mobilities, caused by the formation of well-organized polycrystalline films with μ up to 5 $cm^2 V^{-1}s^{-1}$as well as single crystalline films with μ as high as 15 - 40 $cm^2 V^{-1}s^{-1}$.[33,34,42] An example for a high mobility small molecule is pentacene (μ ~ 5 $cm^2 V^{-1}s^{-1}$), shown in Figure 2.3.[35]

In contrast, the charge carrier mobilities of conjugate polymers are typically lower, especially for fully amorphous semiconductors such as polytriarylamines (PTAA), which possesses mobilities in the range of 10^{-3} – 10^{-2} cm^2 $V^{-1}s^{-1}$ (see Figure 2.3). However, in case of the widely investigated regioregular poly(3-hexylthiophene) (P3HT), mobilities of up to ~ 0.1 cm^2 $V^{-1}s^{-1}$ have been reported.[36] This can be ascribed to the self-organization into ordered lamellar structures, which results in microcrystalline films. Therefore the charge carrier transport is highly anisotropic, depending on how structures are oriented on the surface.[37] Unfortunately, P3HT is susceptible to oxidation and therefore exhibits a poor air-stability (see chapter 5).[2,38] In literature several approaches have been presented to improve the stability, resulting in a large variety of new materials.[39-41] An extensive review by Wang et al. summarizes these achievements (160 different kinds of π-conjugated systems), including many semiconductors with mobility values $\mu > 1$ cm^2 $V^{-1}s^{-1}$.[42]

Each of the so far presented semiconductors is hole transporting (p-type). In general for most of the conjugated materials the loss of an electron is energetically favored over its gain. To obtain electron transporting (n-type) properties the conjugated backbones need to be electron deficient so that the LUMO level is lower and gaining an electron becomes possible.[31] Figure 2.3 depicts examples of n-type semiconductors. However, compared to p-type materials lower charge carrier mobilities are often reported for electrons, which can be attributed to inefficient charge injection and charge carrier trapping in presence of water and oxygen. N-type organic semiconductors with low ionization energies are generally not air stable, due to reduction processes of hydrogen and oxygen to H_2O.[43] Nevertheless fluorinated compounds such as hexadecafluorocopper-phthalocyanine (F16CuPc, μ ~ 0.03 cm^2 $V^{-1}s^{-1}$)[44,45] are natively relatively stable as well as several newly developed n-type polymers, which have been designed to be air stable. One example is the naphthalenedicarboximide-based copolymer P(NDI2OD-T2) with an electron mobility as high as 0.85 cm^2 $V^{-1}s^{-1}$ under ambient conditions.[21] These novel semiconductors constitute promising materials for future applications especially for complementary circuitry as a corner stone of microelectronics.

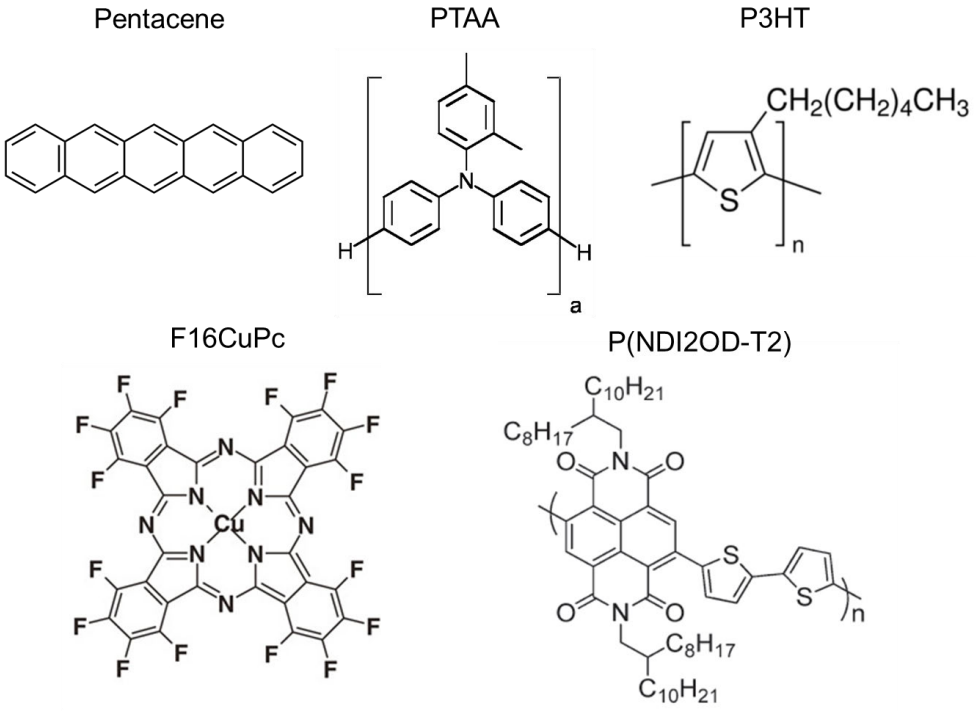

Figure 2.3: Chemical structure of well-known organic semiconductors.

2.1.2 Charge Carriers and Charge Carrier Transport

Charge carrier transport as well as excited states in organic semiconductors departs from those in inorganic semiconductors. This can be ascribed to the weak van der Waals forces in organic solids, which results in *localized* states. On the contrary, crystalline inorganic semiconductors (e.g. Si, Ge) form strong covalently bonded lattice structures, resulting in *delocalized* exited states (band transport).[46] Also, in organic perfect single crystals with high intermolecular π orbital overlap one would expect band-like transport in extended states (π-system), leading to high mobility values. Nevertheless the band model is unable to describe the charge transport within these molecular crystals, due to the neglected polarization phenomena. In principle when a charge resides on a molecular site it tends to polarize its environment. This polarization cloud is moving with the charge as an entity. In other words, these charges are accompanied with a local deformation of its surrounding bonds (structural relaxation). Such quasi-particles are called *polarons*, and are delocalized only over few repeating units. Within band diagrams they are often described through the creation of localized states in the gap between the HOMO and the LUMO, as shown in Figure 2.4 for polythiophene. Corresponding to their charge, either a positive or a negative polaron is formed. Moreover if two polarons are involved, for some system it is energetically more favorable to form bipolarons. By adding more electrons (holes) to the polymer chain (e.g. by doping) energy bands within the gap can be created.[31]

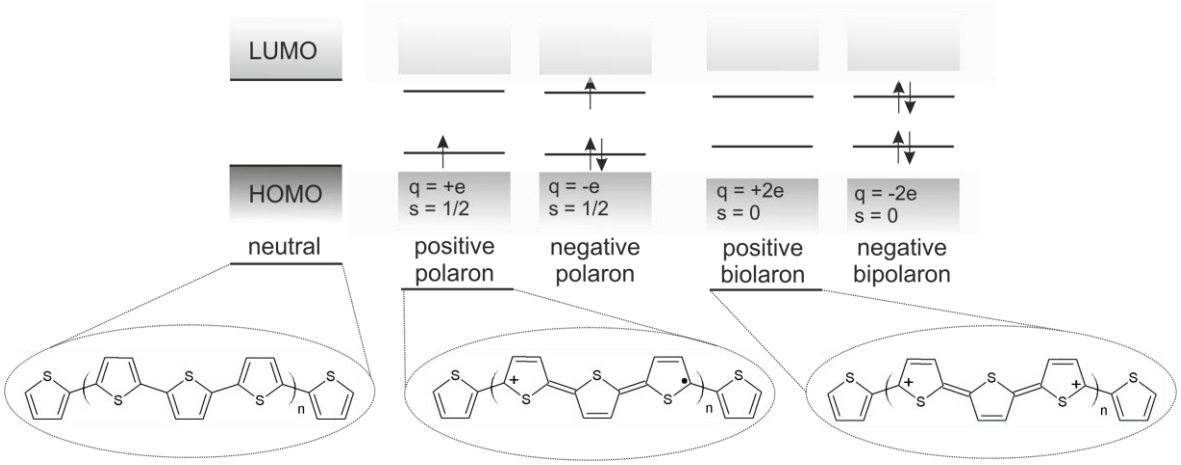

Figure 2.4: Band diagrams with polaronic states within the ππ-gap and corresponding examples of a neutral polythiophene (aromatic, left) and after formation of a positive polaron (middle) and bipolaron (right) on the polythiophene (quinoid) with certain charge q and spin s.*

Charge Carrier Transport

In contrast to the band transport of inorganic single crystal semiconductors, the charge carrier transport in organic semiconductors occurs via hopping of charges between localized states. Thus the delocalized transport is limited by phonon scattering (scattering of the carriers at thermal lattice vibrations), while the localized transport is phonon assisted. Accordingly, in contrast to conventional semiconductors the charge carrier mobilities of organic semiconductors usually increase with temperature.

The charge carrier mobility, as a central parameter, is a relation between the charge carrier speed in a material and the applied electric field. As described in section 2.1.1 the charge carrier mobilities strongly varies according to the microstructures as well as chemical structure and impurities of the organic semiconductors from 10^{-5} cm^2 $V^{-1}s^{-1}$ – 10^{-2} cm^2 $V^{-1}s^{-1}$ in the case of amorphous polymers to 1 – 40 cm^2 $V^{-1}s^{-1}$ in highly ordered single crystals.[42] Accordingly to account for different degrees of disorder several charge transport models have been developed.[47]

For well-ordered semiconductors such as polycrystalline films of small molecules the thermal activated mobility has been first described by the multiple trap and release model (MTR)[48,49]. It assumes that the charges can move in narrow delocalized bands but most of the carriers are trapped in localized states (in the HOMO-LUMO gap), originating from structural or chemical defects. The effective charge carrier mobility is then determined by trapping and thermally activated releasing of the charges. [50] However this model could not explain the often observed temperature independence of the mobility at low temperatures. Another model, called the grain boundary model[51], which accounts for that particular independence, assumes that the charge transport is limited by grain boundaries. It divides the semiconductor into a trap free region (crystal grain, high μ) and a region with a high trap density (grain boundaries, low μ). At low temperatures the charge

transport is governed by tunneling through the grain boundaries, explaining the temperature independent mobility. For intermediate temperatures this tunneling is thermally activated, while for high temperatures the charge transfer at grain boundaries occurs via thermionic emission.

In comparison, the charge transport in conjugated polymers (disordered semiconductors) is generally described as thermally activated hopping in a distribution of localized states. Accordingly, different models have been proposed, giving a qualitative description of the hopping transport.[52] For example Bässler et al.[53] developed a model which described the localized states (density of states) in a Gaussian distribution to account for the spatial and energetic disorder. The charge transport is set on the same level with a random walk described by a typical equation of the Miller–Abrahams form.[54] Another model for hopping rates is given by the Marcus theory.[47] Moreover, Vissenberg and Matters introduced the variable-range hopping (VRH) model,[55] describing the charge transport by hopping short distances with high activation energies or long distances with low activation energies. They used an exponential distribution of the localized states as the tail states of a Gaussian distribution. This model describes a thermally activated mobility and predicts an increase of mobility with increasing charge carrier density.

Doping

The conductivity of intrinsic organic semiconductors is generally low (10^{-10} – 10^{-5} S cm^{-1}).[56] Due to a relatively large band gap (2 - 4 eV) only few charge carriers are thermally activated. The conductivity is given by: $\sigma = n \cdot e \cdot \mu$ with n the charge carrier density, e the elementary charge and μ the charge carrier mobility. By basically increasing the charge carrier density n via doping the conductivity can be increased by several orders of magnitude. This can even lead to metallic conductivities (1 - 10^3 S cm^{-1}) for highly doped materials such as for poly(3,4-dioxythiophene):polystyrenesulphonate (PEDOT:PSS).[57,58] However, the processes are different from those used for inorganic semiconductors, where a dopant atom replaces a lattice atom. In contrast, the doping process is related to a charge transfer process, during which the doped materials gets oxidized (p-doped) or reduced (n-doped). Commonly used methods include the chemical and the electrochemical doping. Moreover the charge injection in case of diodes or field-effect transistors as well as photoexitaction in photovoltaic are also often referred to as interfacial and photochemical doping, respectively.[14]

In the case of chemical doping a redox reaction is involved between a dopant and the conjugated molecule. For p-doping, an electron is transferred from the HOMO of the conjugated molecule to the dopant (acceptor). On the other hand for n-doping an electron is transferred from the dopant

(doner) to the LUMO of the conjugated molecule. One of the most famous examples is the doping of polyacetylene with iodine as dopant.

Electrochemical doping can be explained with an electrochemical cell consisting of a working electrode in direct contact with the conjugated material an electrolyte and a counter electrode. By applying a specific potential the polymers can be either oxidized or reduced until an electrochemical equilibrium (doping level) is reached, depending on the applied potential. In detail, electrochemical p- (n-) doping happens when a hole (electron) is injected from the electrode onto the polymer chain and at the same time the hole (electron) is counterbalanced by a negative (positive) ion which diffuses into the polymer, to keep electroneutrality.

2.2 Organic Field-Effect Transistors

The basic idea of field-effect transistors (FET) dates back to the mid-1920s,[5] however it lasted almost 40 years until the concept was successfully demonstrated with the invention of the metal-oxid-semiconductor FET (MOSFET) by Kahng and Atalla from the Bell labs.[8] Nowadays FETs are one of the most important components in modern microelectronics, both as discrete devices and in integrated circuits. First field-effect measurements on organic semiconductors were reported in the 1970s.[59] A significant milestone was set by Tsumara and coworkers[60] in 1986 with the demonstration of the first organic field-effect transistor (OFET) based on an in-situ polymerized polythiophene with recognizable current gain. The excitement about printed organic electronics was ignited by Jen et al.[61] who developed a soluble form of polythiophene which was then applied to OFETs by Assadi et al.[62], allowing for various large-area solution processing techniques. The performance of OFETs has continuously improved, following the improvements and development of high-mobility organic semiconductors. Due to intense studies, OFETs can compete with amorphous hydrogenated silicon (a-Si:H) thin film transistors (TFTs),[42,63] which are preferred in applications where large-area is needed such as flat panel displays. TFTs are a special kind of FETs, differing from MOSFETs in that the conduction channel is formed by accumulation rather than by an inversion layer. In particular, TFTs have been proven their applicability for low conductivity materials (intrinsic semiconductors) such as a-Si:H. Accordingly, the TFT architecture is also applied for OFETs. Driven by the outstanding properties of organic compounds, which enable the realization of low-cost, lightweight, large-area, flexible electronic circuits[64,65] OFETs have developed rapidly. Successful realizations include flexible displays,[24,66,67] radio-frequency identification tags[23,68] as well as OFET-based sensors[25,27,29].

2.2.1 Basic Operation and Transistor Equations

Figure 2.5 shows an illustration of an OFET. It can be regarded as a three-terminal device, where two electrodes, the source and the drain are in direct contact with the organic semiconductor (OSC), the active part of the device. The third electrode, the gate is electrically isolated from the OSC by an insulating layer also referred as gate dielectric. The distance between the source and the drain is called the channel length L, while the transverse dimension of the electrodes is the channel width W. The gate and the drain voltages V_{GS} and V_{DS} are applied with respect to the grounded source electrode.

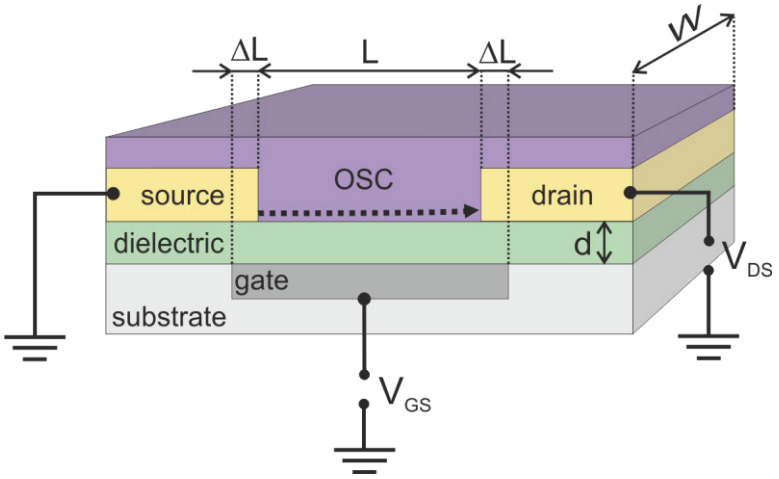

Figure 2.5: Three-dimensional illustration of an organic thin film transistor.

The stack of metal-insulator-semiconductor (MIS) formed by the gate, the dielectric and the OSC constitutes the core of the device. By applying a gate voltage charge carriers are induced and form an accumulation layer at the semiconductor/insulator interface, thus creating a conductive channel between source and drain. This *channel* can be either *n*- or *p*- conducting depending on induced charges/applied gate voltage (positive voltage for electron accumulation, negative voltage for hole accumulation). Materials which can conduct both are denoted as ambipolar. Upon applying a voltage between source and drain (V_{DS}) these charges are driven across the channel and a current flows. Hence by varying the electric field across the dielectric layer (varying V_{GS}) the conductivity of the channel is modified and the device can be switched between an "on" and "off" state, for which ideally no current is needed. In contrast to MOSFETs, OFETs are operating in accumulation regime, thus charge carriers which are responsible for the off-current conduction and the on-current are from the same type.

Nevertheless, in a first approximation the popular equations describing current-voltage characteristics of MOSFETs can be also used for OFETs.[16,31,69] However, this simplification relies on several assumptions that are not always fulfilled in real devices. This includes: (1) The transverse electric field induced by the gate is much larger than the longitudinal electric field induced by the applied drain voltage, also known as the so-called gradual channel approximation. It is fulfilled as long as the insulator thickness is much smaller than the channel length L ($d \ll L$). (2) The mobility is constant all over the channel and for different electric fields. This is generally not the case, since the mobility in real devices show a gate and drain voltage dependence as well as an influence of the contact resistance. Moreover the bulk current is assumed to be negligible and the diffusion of charges is also not considered. Nevertheless the following derived equations are often used to quantify the OFET performance. The channel current at a position *x*, which is solely based on the drift of charges is given by eq. 2.1 with W the channel width, μ the charge carrier mobility,

Q*(x)* the charge density at position *x* and *E(x)* the electric field in the direction of the channel at position *x*.

$$I_D(x) = W\mu Q(x)E_x(x) \tag{2.1}$$

The charge density *Q* at $V_{DS} = 0$, when the semiconductor is grounded depends on the capacitance per unit area C_i of the gate dielectric and the applied gate voltage. However, the conducting channel is only formed upon exceeding a certain gate voltage, which is called the threshold voltage V_{th}. For OFETs which are operating in accumulation this voltage should ideally be zero. However, this is practically not the case due to localized states (traps) at the semiconductor-insulator interface, residual charges within the bulk of the OSC or difference in work function of semiconductor and gate material.[31] By considering this nonzero V_{th} the charge density can be written as follows:

$$Q = C_i(V_{GS} - V_{th}) \tag{2.2}$$

When a source-drain voltage V_{DS} is applied the potential within the semiconductor is a function of the position *x* in the channel. The voltage gradually increases from zero at the source contact (*x* = 0) to V_{DS} at the drain contact (*x* = *L*). Thus, the charge density is a function of the position *x* as well:

$$Q = C_i\big(V_{GS} - V_{th} - V(x)\big) \tag{2.3}$$

Substituting this equation of the charge density and inserting *E(x)* = *dV(x)/dx* into eq. 2.1 gives eq. 2.4 and finally the integration over the channel from source to drain leads eq. 2.5, describing the current-voltage curves of OFETs:

$$I_D(x)dx = W\mu C_i\big(V_{GS} - V_{th} - V(x)\big)dV(x) \tag{2.4}$$

$$I_D = \frac{W\mu C_i}{L}\left[(V_{GS} - V_{th})\,V_{DS} - \frac{{V_{DS}}^2}{2}\right] \tag{2.5}$$

According to applied voltages the operation of OFETs can be divided into two regimes the *linear* and the *saturation regime*. Basically, if a gate voltage larger than the threshold voltage is applied $V_{GS} > V_{th}$ a uniform charge layer is induced (see Figure 2.6 (a)). Consequently, a current flows upon applying a drain voltage and charge density gradually decreases from the source to the drain contact. If this applied drain voltage is small ($V_{DS} \ll V_{GS} - V_{th}$) the resistance of the channel will remain unchanged along the channel. Within this so called linear regime, the drain current increases proportional to the applied drain voltage (see Figure 2.6 (a)) and can be derived from eq. 2.5 by neglecting the quadratic term:

$$I_{Dlin} = \frac{W\mu C_i}{L} (V_{GS} - V_{th}) V_{DS} \tag{2.6}$$

The field-effect mobility in the linear regime is therefore given by:

$$\mu_{lin} = \frac{L}{WC_iV_{DS}} \frac{\partial I_{Dlin}}{\partial V_{GS}} \tag{2.7}$$

As the drain voltage increases to V_{GS} - V_{DS} < V_{th} the current reduces its rate of increase. In particular, when V_{GS} - V_{th} = V_{DS} the charge concentration at the drain contact is zero and the channel is said to "pinch off" (see Figure 2.6 (b)). By further increasing the drain voltage V_{DS} > V_{GS} - V_{th} this pinch off point P (charge carrier concentration = 0) will move closer to the source contact (see Figure 2.6 (c)). A depletion layer is formed between P and the drain contact, where a space charge limited current flows. The number charge carriers arriving at P remains constant independent of the applied drain voltage, since the potential drop between P and the source remains also constant. In other words the current is said to saturate above the pinch off at V_{sat} = V_{GS} - V_{th}. Accordingly, this operation region is called the saturation regime and the equation of the drain current within this regime can be expressed by substituting V_{DS} = V_{GS} - V_{th} in eq. 2.5 as

$$I_{Dsat} = \frac{W\mu C_i}{2L} (V_{GS} - V_{th})^2 \tag{2.8}$$

The field-effect mobility in the saturation regime can be written as:

$$\mu_{sat} = \frac{2L}{WC_i} \left(\frac{\partial \sqrt{I_{Dsat}}}{\partial V_{GS}} \right)^2 \tag{2.9}$$

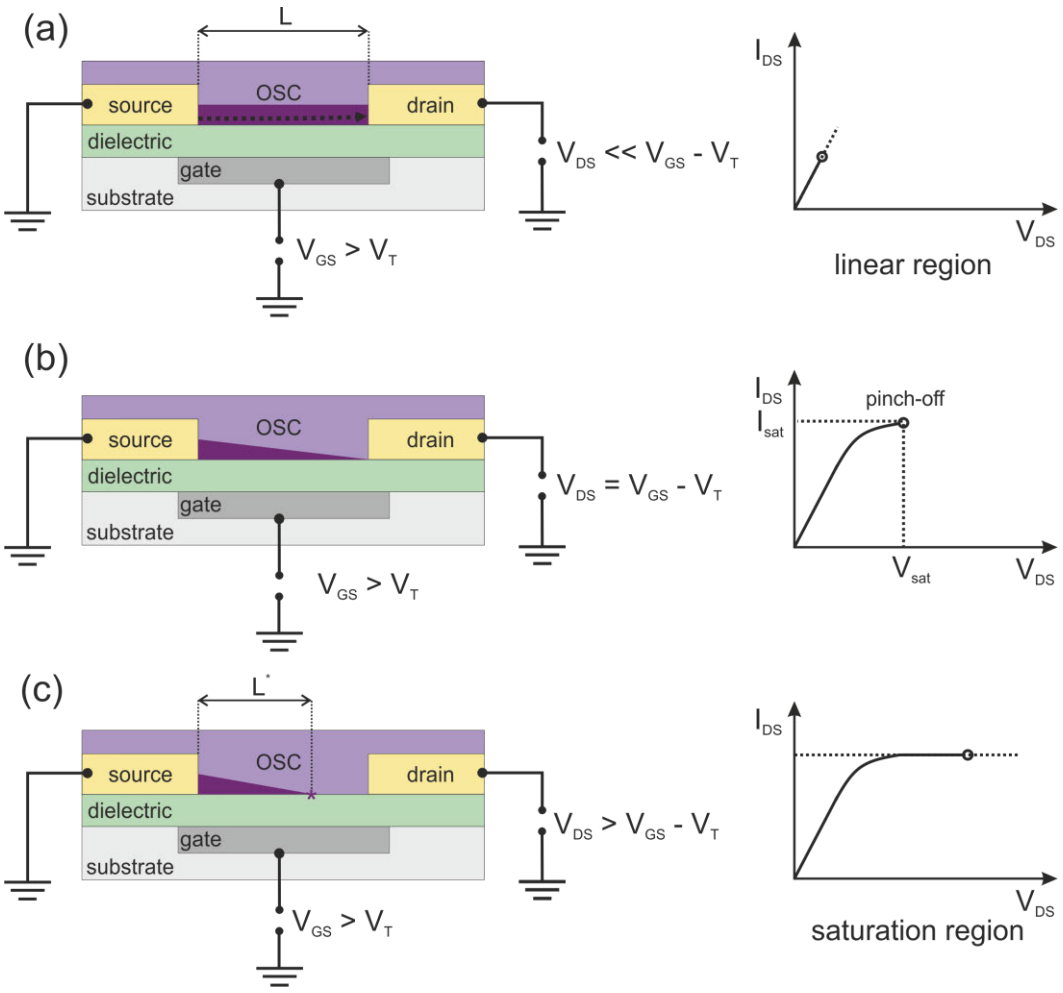

Figure 2.6: Illustration of the working principle of OFETs including charge carrier distribution and current-voltage characteristics in linear (a), pinch off (b) and saturation regime (c).

2.2.2 Transistor Characteristics and Parameters

The most common I-V characteristics for OFETs are the *output* and the *transfer characteristics*. The output characteristics, which are shown in Figure 2.7, are obtained by sweeping the drain voltage V_{DS} for constant gate voltages V_{GS}. The two regions, the linear and saturation region can be clearly distinguished. The onset of saturation is indicated with a fitted parabola (dashed line) of the pinch-off points ($V_{DS} = V_{GS} - V_{th}$). Figure 2.7 (b) shows the transfer characteristics, showing the drain current dependence when the V_{GS} is swept while V_{DS} is set constant, either in linear or saturation regime. In comparison to the output curves, the transfer curves are swept over broad accumulation range. Consequently the drain current varies over several orders of magnitude and is therefore often plotted semilogarithmically (see Figure 2.7 (b)). The transfer characteristics generally provide information of the switching property, stability and charge carrier mobility of the device. Moreover the recording of forward and reverse sweep gives information about charge

trapping at the OSC/insulator interface or ionic drifts within the insulator by the appearance of a hysteresis.

At low gate voltage the current is determined by the leakage current and bulk current of the device which is not modulated by the gate and is desired to be low. This region is called the off-state. In contrast the highest obtained drain current above the threshold is called the on-current. The *on/off current ratio* can be easily extracted from the transfer curve and is a fundamental parameter to assess the transistor performance. Naturally, a high on/off current ratio is desired for well performing OFETs in order to clearly distinct between on and off state.

The region between the off-state and the threshold voltage is the *subthreshold* region where current increases exponentially expected from purely diffusive transport.[31] Its slope depends on the capacitance of gate dielectric and interfacial trap density. The inverse slope of the curve within this region is denoted as the *subthreshold slope* S (see eq. 2.10) which can be extracted from a linear fit of $\log|I_{DS}|$ vs V_{GS} as shown in Figure 2.7 (b):

$$S = \frac{\partial V_{GS}}{\partial\,(log\, I_{DS})} \tag{2.10}$$

It determines the sharpness of the transition from the off to the on state and is defined as the gate voltage needed to increase the current for one decade. Small S values are favorable, implicating a fast switching. Moreover since S is strongly related to the quality of the semiconductor/insulator interface, altering values can indicate changes in the doping or trapping density.

The voltage, where the subthreshold region starts (current starts to increase exponentially), is also called *switch-on voltage* V_{so} (or onset voltage). It represents the gate voltage at which all traps are filled and the conducting channel starts to form. In contrast, the *threshold voltage* V_{th} is the voltage, where the conductive channel has been formed and the current is not limited by the charge concentration, showing an ohmic behavior. The threshold voltage can be estimated from the intersection of the gate voltage axis with the linear fit of the drain current in linear regime or the square root of the drain current in saturation regime (see Figure 2.7 (b)).[70] However, this extrapolation approach has several limits, e.g. when significant current flows below V_{th} due to slow subthreshold turn-on, or non-linear current increase due to the field depending mobility. There have been presented other techniques to determine the threshold voltage more accurately.[71]

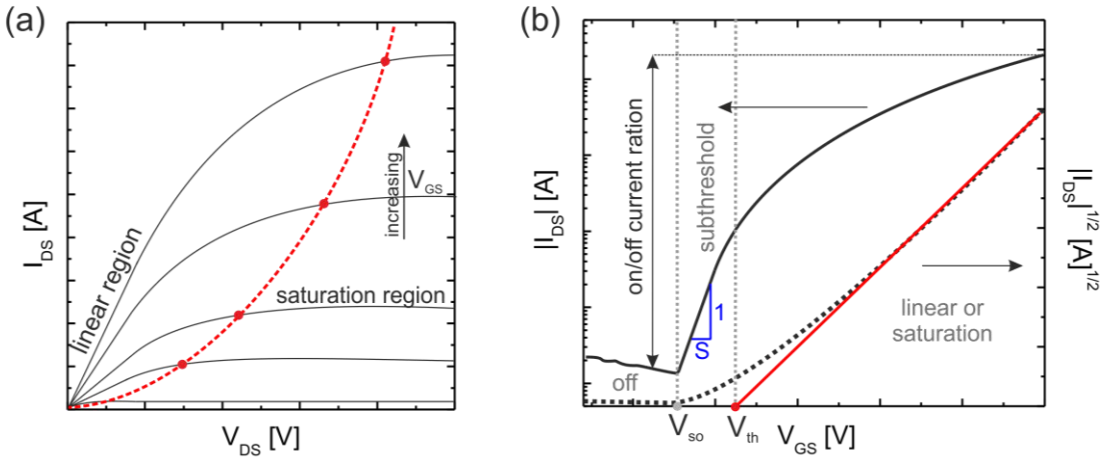

Figure 2.7: Typical I-V characteristics of OFETs: (a) output characteristics with a clear linear and saturation regime, (a) transfer characteristics semilogarithmically (solid line) and linear plotted (dashed line) with indication of different regime (off state, subthreshold and linear/saturation regime) and corresponding OFET parameter.

Another important parameter is the field-effect mobility. As mentioned above, upon exceeding the threshold voltage the drain current can be described by eq. 2.6 and 2.8. Accordingly, the linear and saturation field-effect mobilities can be calculated from the transfer characteristics with eq. 2.7 and eq. 2.9, respectively. However, it must be considered that the assumptions made by the presented model above, might not hold for real devices and more elaborated models must be applied for proper mobility extraction.[31,72]

Moreover the transconductance g_m, constitutes another fundamental and representative device parameter. It is determined as the conductance of the channel and describes how the drain current varies with the gate voltage for a constant drain voltage.

$$g_m = \frac{\partial I_{DS}}{\partial V_{DS}} \tag{2.11}$$

According to the model above (eq. 2.6 and eq. 2.8) the transconductance in linear and saturation regime are described as follows:

$$g_{mlin} = \frac{W\mu}{L\,C_i}\,V_{DS} \tag{2.12}$$

$$g_{msat} = \frac{2W\mu}{L\,C_i}\,(V_{GS} - V_{th}) \tag{2.13}$$

2.2.3 OFET Architectures and Design Rules

OFETs can basically be fabricated in four different architectures shown in Figure 2.8. These structures are named depending on the position of the gate, namely bottom-gate (Figure 2.8 (a) and (b)) or top-gate (Figure 2.8 (c) and (d)). Accordingly, the source-drain electrodes can also be either bottom-contact ((a) and (c)) or top-contact ((a) and (b)). For a proper OFET design several criteria have to be considered. The gate electrode should be directly aligned under the channel in order to avoid stray capacitance or edge effects. These parasitic gate-source/drain capacitances originating from the gate overlap with the source/drain electrodes can have a significant influence on the cut-off frequency, which is especially important for the dynamic transistor performance.[73] For such applications the channel length L should be small. In accordance, small L and large W are also desirable for low voltage operation, whereupon for too small L short channel effects can be observed.[74,75] From a fabricational point of view it is important to consider that the consecutive deposition of layers do not dissolve/alter the underlying layer or increase the roughness at the interface. In particular the OSC/insulator interface, where the charge carrier transport happens, should be of high quality. Each of the four architectures have advantages but also drawbacks.

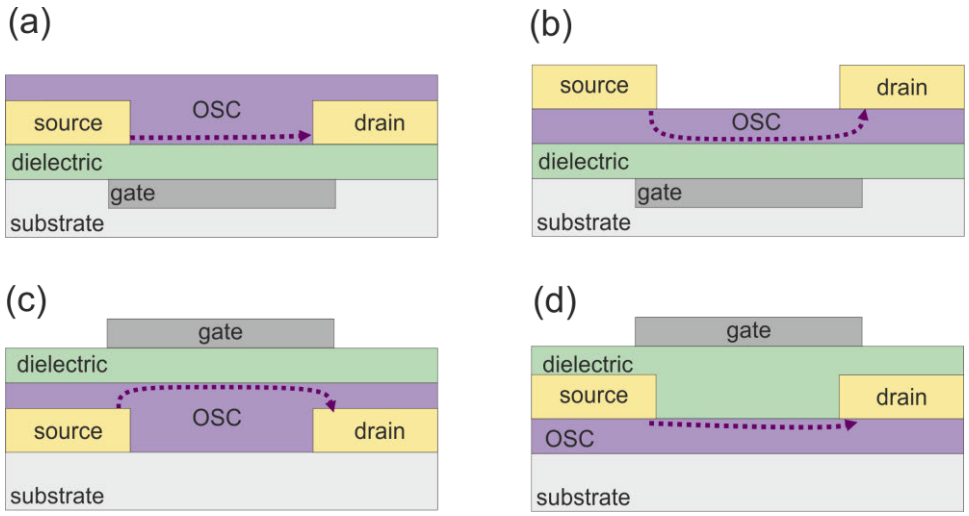

Figure 2.8: Basic TFT architectures: (a) bottom-gate bottom-contact BG/BC, (b) bottom-gate top-contact BG/TC, (c) top-gate bottom-contact TG/BC, (d) top-gate top-contact TG/TC.

For the bottom-gate/bottom-contact (BG/BC) architecture the source/drain electrodes can be directly structured on the dielectric layer for example with well-established photolithographic techniques, yielding highly defined channels. Subsequently solution processable organic compounds can be deposited by means of spin-casting, drop-casting or inkjet-printing.

Although same materials have been applied, different device performance for different OFET structures are obtained. Bottom-gate/top-contact (BG/TC) structure, where the source/drain electrodes are deposited on top of the semiconductor, exhibit very homogeneous films in

comparison to the BG/BC structure, where the film morphology near the electrodes can differ from that within the channel.[76] This leads to a better device performance for BG/TC OFETs. However, the injected charges have to cross the undoped region in order to reach the conductive channel and thus the thickness of the semiconducting layer becomes an important parameter for this type of architecture (see Figure 2.8 (b)).[77] This is also the case for the TG/BC structure. On the other hand they benefit from a larger injection area leading to lower contact resistance. The injection area is not explicitly defined by the gate overlap but is also influenced by the edges of the source (current crowding).[77,78] Moreover, top gate architectures also benefit from the encapsulation of the organic semiconductor by the dielectric layer leading to an increased environmental stability.

Furthermore, the metal of the source drain electrodes must be chosen according to the HOMO for p-type semiconductors and LUMO for n-type in order to fit the work function and allow for sufficient charge injection.[31,79] An energy mismatch (high injection barrier) results in an increased contact resistance, which can also be observed by an non-linear current increase in the output characteristics. Besides the correlation of the contact resistance to the work function difference and the barrier height and width, the contact resistance also depend on the morphology of the materials, trap concentrations, doping level near the interface, interfacial dipole layers, chemical and physical reactions near the interface region, temperature and sample geometry.[79] The contact resistance can be reduced by applying a self-assembled monolayer on the electrode surface which induces a counterbalancing dipole[79] or treated via UV/ozone to improve charge injection[80] (see section 5.5).

2.3 OFETs as Sensing Elements in Aqueous Media[i]

Aside from the main application of organic field-effect transistors (OFETs) in display and integrated circuit technology,[62,65] OFETs have been proven to be excellent candidates as transducers for many sensing applications.[25,29,81-83] Owing to the outstanding features of organic devices, which are processable at low temperatures, economic production, miniaturization and integration on flexible substrates are feasible, leading to smart (disposable) sensor assemblies for health-, food- and environmental monitoring.[20,84] Another property of organic compounds is the good biocompatibility,[27,28,85] which is of high importance when it comes to biomedical applications and the envisioned human interfacing, e.g. artifical skin, in-situ measurements of vital parameters, or monitoring the health conditions via E-textiles. Benefiting from the "soft" nature as well as the similarity of building blocks, organic materials outperform the inorganic counterparts significantly.[26] Moreover, the chemical and physical properties of organic compounds can be tailored to obtain a distinct sensitivity and selectivity with respect to target analytes or to meet a specific requirement.

Another advantage of transistors compared to other sensor concepts (e.g. based on resistors), is the inherent signal amplification, which results in higher sensitivity.[86,87] OFET-based sensors are transducers and amplifiers at the same time and there are well established methods to miniaturize and integrate them into complex circuits for further signal processing. They benefit also from fast response times and low power consumption. In view of these exceptional features, integrated low-cost (disposable) sensor tags for multi-analyte detection are not a future vision anymore. Accordingly, several examples of OFET-based chemical sensors have been demonstrated, ranging from detection of small molecules such as NH_3,[88] NO_2,[89,90] O_2,[91] vapors (e.g. 1-hexanol, ethanol)[92-94] and humidity[95] to ions[2,96], and complex biomolecules[27,97,98]. In addition to these chemical sensors including gas, chemical vapor and biosensors, physical sensors based on OFETs have been realized as well.[99] Such physical sensor examples are pressure and thermal sensors, targeting "electronic skin" applications.[100-102] However, since the focus of this section is, to give a basic overview of OFET architectures operating in aqueous media for chemical sensing applications, physical sensors are not further discussed.

For the emerging fields of biomedical diagnostics and environmental monitoring, sensing of ions (e.g. Na^+, K^+, Ca^{2+}, pH,…) and biological substances (e.g. DNA, enzymes, hormones, …) in

[i] Parts of the content within this chapter is based on work that has been published: K. Schmoltner, J. Kofler, A. Klug, E. List, „*Electrolyte-gated organic field-effect transistors for sensing in aqueous media*", Organic Field-Effect Transistors XII; and Organic Semiconductors in Sensors and Bioelectronics VI, Zhenan Bao; Iain McCulloch; Ruth Shinar; Ioannis Kymissis, Editors, Proc. of SPIE 8831, 88311N (2013).Copyright 2013 Society of Photo Optical Instrumentation Engineers.

appropriate aqueous media is of particular interest.[29] Therefore a water-stable performance of OFET-based sensors is crucial, demanding for a low-voltage operation. In general low voltage operation is obtained by applying gate insulators with a high capacitance (using thin high-k dielectrics or electrolytes).[103-105] Moreover, degradation and delamination of the semiconductor under aqueous conditions are highly unwanted. Accordingly, several approaches using different OFET architectures for a stable operation in aqueous environment have been presented (see Figure 2.9) and are summarized by several excellent reviews.[20,25,29,81,82,106,107]

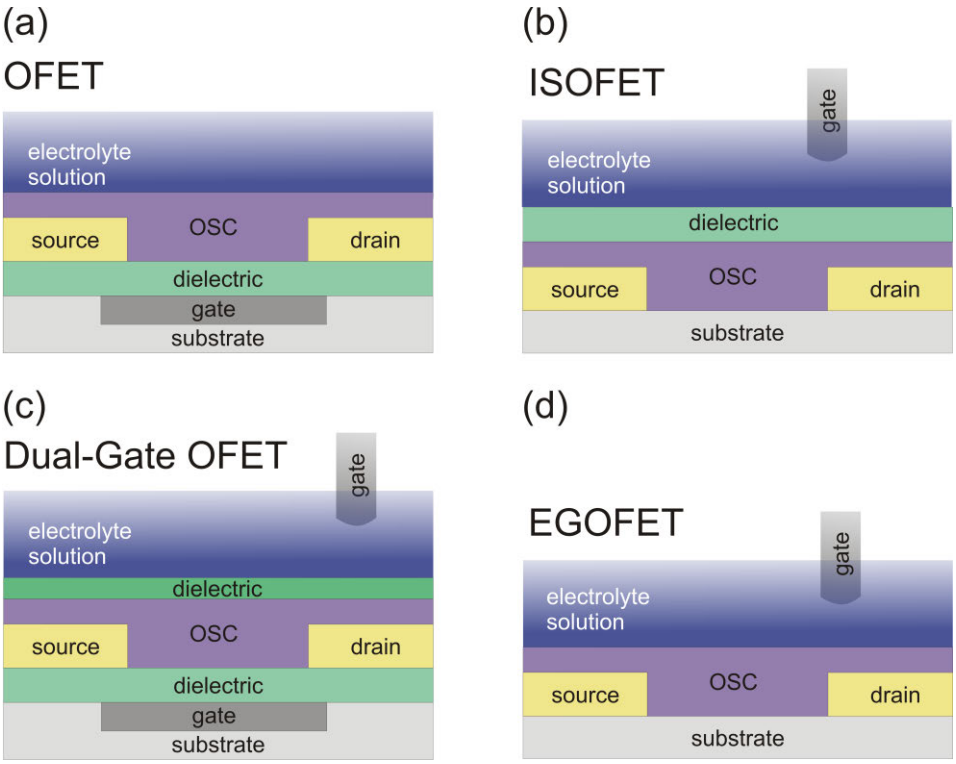

Figure 2.9. Scheme of a BG/BC OFET exposed to an aqueous environment (a), an ion-sensitive organic field-effect transistor (ISOFET) (b), a dual-gate OFET (c) and an electrolyte-gated organic field-effect transistor (EGOFET).

Classical OFET operating in aqueous media

Someya et al. were the first to address this challenge by using a standard BG OFET architecture (see Figure 2.9 (a)), where the semiconductor is in direct contact with water (or aqueous solutions). The source drain electrodes, where considerably high electric fields occur, were encapsulated by a fluorinated polymer, in order to limit the water exposure to the channel region and allow for a microfluidic flow.[27,29] Pentacene and α-sexithiophene were used as semiconductor and as sensing layer to detect glucose and lactic acid in aqueous solution. Generally, the key issues for devices operating in liquid solutions are a low voltage operation to avoid unwanted electrochemical reactions and environmental stable organic materials.

Based on this first step, others have shown that the operation voltage can be reduced by using a thin, crosslinked dielectric layer and that the stability can be improved by applying a stable organic semiconductor (5,5-bis-(7-dodecyl-9H-fluoren-2-yl)-2,2-bithiophene (DDFTTF)). With this device changes in pH and low concentrations of chemicals, such as trinitrobenzene, cysteine, methylphosphonic acid, and glucose in water were detected.[108] Although such examples[109] exhibit high sensitivity, they suffer from a lack of true selectivity, since it relies on the semiconductors inherent sensitivity to many chemical compounds. In general in order to obtain a selective response, the semiconductors can be chemically altered[110] e.g. functionalized with specific recognition groups (e.g enzymes, antibodies etc.)[130] or an additional sensing layer[111], can be introduced. Based on this standard BG OFET architecture, selective detection of mercury(II) in water was achieved by utilizing functionalized gold nanoparticles applied onto the surface of an organic transistor.[112]

Ion-sensitive OFET

In analogy to the inorganic semiconductor technology, organic ion-sensitive FETs (ISOFETs) are one of the most widley investigated FETs operating in aqueous media.[96,113,114,] Here the electrolyte is in direct contact with the gate dielectric and a reference electrode is used as the gate electrode (see Figure 2.9 (b)). The electric field across the insulating gate dielectric is influenced by the ions at the electrolyte-dielectric interface, thus modulating the channel current. With this potentiometric concept successful detection of pH changes has been realized using silicon nitride as proton-sensitive layer.[96] Furthermore sensing of biomolecules (e.g. glucose) has been demonstrated by immobilization of an enzymatic layer (glucose oxidase) on a tantalum oxide dielectric.[98] This proved that the selectivity towards a certain analyte can be induced by modifying the gate dielectric with a proper functionalization. Moreover, attempts for the detection of specific ions have been reported by Ritjareonwattu et al. [115] or Ji et al.[116], but no reversible and selective ion sensor based on the conventional ISOFET concept has been presented so far.

Dual-gate OFET

Similar to the classical ISFET design dual-gate OFETs (see Figure 2.1 (c)), where the semiconductor layer is prodected by a hydrophopbic dielectric layer and the source-drain electrodes are buried, have been presented as another potentiometric pH sensing concept.[117] Nonetheless, the reference electrode is essential to fix the potential of the electrolyte. Similar to ISOFETs, the detection relies on changes of the surface potential which lead to threshold voltage shifts. It was shown that by changing the capacitance ratio of the top and bottom gates, the sensitivity of the sensor can be increased. A different dual-gate approach uses a floating gate as the second gate

which is coupled to a gate in contact with the semiconductor by a common dielectric layer. This floating gate was further functionalized in order to detect pH changes as well as DNA.[118,119]

Electrolyte-gated OFET

In contrast to conventional ISOFETs, where the aqueous analyte is in contact with a solid gate dielectric, electrolyte-gated OFETs (EGOFETs) benefit from a direct contact between the organic semiconductor and the analyte. Due to the formation of an electric double layer at the electrolyte-organic semiconductor interface, they exhibit a very high capacitance allowing for low voltage operation (< 1V), which is crucial for a water-stable performance. In this context, EGOFETs seem to be ideal candidates as transducers for potentiometric sensors. Accordingly, several different sensing concepts based on EGOFETs have been demonstrated so far.[120] This includes also our recently presented novel, modular and versatile EGOFET-sensor platform for reversible and selective ion detection. A sensitive and selective response to sodium ions was obtained by introducing a state of the art ion-selective membrane (see chapter 7).[4] The next section will give more information about EGOFETs in general, including the basic operation, EDL formation, and basic electrochemical consideration concerning a stable EGOFET performance.

2.4 EGOFETs for Sensing Applications in Aqueous Media

Owing to the exceptional property of high capacitance, EGOFETs were also subject of intense research in the field of low-voltage/low-power applications. They are good alternatives to conventional OFETs based on solid dielectrics such as oxide gate insulators, high-k dielectrics or ultrathin organic layers.[121] A large variety of different electrolytic systems, including polyelectrolytes,[122] polymer electrolytes,[104] ionic liquids,[123] ion gels[124],[125] and electrolyte solutions[126,127] have been employed. An important milestone for sensing of biomolecules was then set by Kergoat et al., who reported on the stable operation of water-gated OFETs, making in-situ sensing of ions and biological substances in an appropriate aqueous medium possible.[127] Recent advances in this field include the successful detection of biomolecules such as DNA, dopamine, enzymes, proteins[128-131] as well as studies of the influence of pH and ionic strength on the performance of electrolyte-gated FETs[3,132]. These achievements are excellently reviewed by Kergoat et al.[127] and Cramer et al.[120], demonstrating that the utilization of EGOFET-based sensors ushered in a new era of biological and ion sensing.

2.4.1 Operation of EGOFETs – EDL Formation

As already mentioned the excellent low voltage operation (below 1V) of EGOFET relies on the electric double layer (EDL) formation at the electrolyte-organic semiconductor interface exhibiting a very high capacitance (on the order of ~1-10 µF/cm^2)[127,132,133]. Figure 2.10 illustrates a p-type EGOFET in case of a negative applied gate potential, leading to the formation of an EDL at the gate-electrolyte and the semiconductor-electrolyte interface via migration of cations and anions to the respective interfaces. In detail, the EDL at the gate side consists of electrons within the metal and cations in the electrolyte, while at the semiconductor side holes and anions form the EDL.

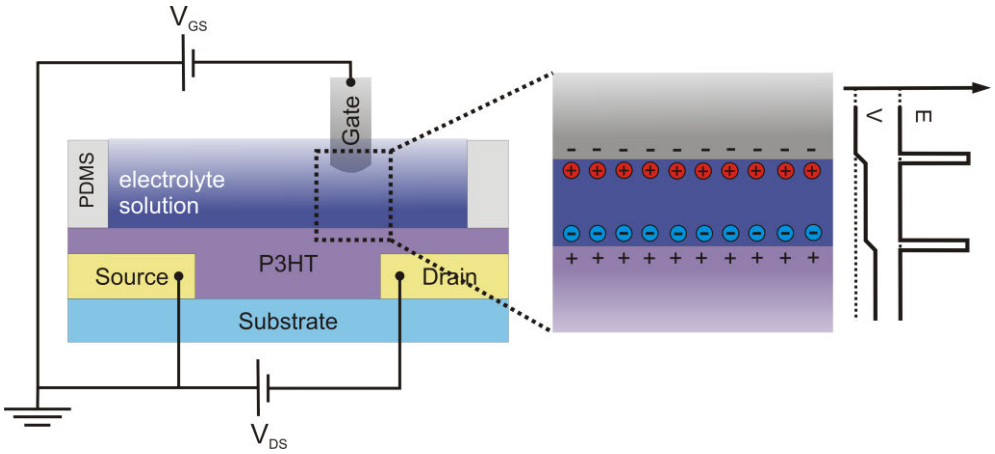

Figure 2.10: Scheme of an electrolyte-gated p-type organic field-effect transistor and corresponding illustration of the voltage and electric field distribution at the interfaces.

According to Gouy-Chapmann-Sterns (CGS) model, which describes the charge distribution of an EDL, the electrolyte is composed of 2 layers, the Helmholtz layer and the diffusion layer (see Figure 2.11). The first basically consist of solvent molecules and can contain also specifically adsorbed species (ions or molecules) and is often referred to as inner Helmholtz plane (IHP). The outer Helmholtz plane (OHP), comprises solvated ions whose interaction with the charged interface involves only long range electrostatic forces and does not depend on the specific properties of these ions (nonspecific adsorbed ions). This Helmholtz layer forms a parallel plate capacitor with the charged interface with a very small distance in between, leading to a steep linear potential drop (see Figure 2.11). The diffusion layer, on the other hand, describes the layer of the nonspecific adsorbed ions, which migrate under electrostatic interaction and thermal motion. The excess of these ions decreases with increasing distance from the gate- or semiconductor-electrolyte interface, exhibiting an exponential potential drop.[134] Since the total potential drops only at the interface of the double layer, which typically exhibits very small thickness on the order of few nm, very high capacitance

values (few tens of μF/cm^2) are obtained.[ii] The total capacitance of the electrolyte layer of an EGOFET is given by the series capacitance of the EDLs at the semiconductor and the gate side. Thus, it is determined by the smaller of the two EDL capacitors. This is usually the EDL at the semiconductor-electrolyte interface with capacitance values of ~1-10 μF/cm^2. Consequently, by applying low gate voltages (< 1 V) high charge carrier densities are induced, allowing for transistor operation within a water-stable window.

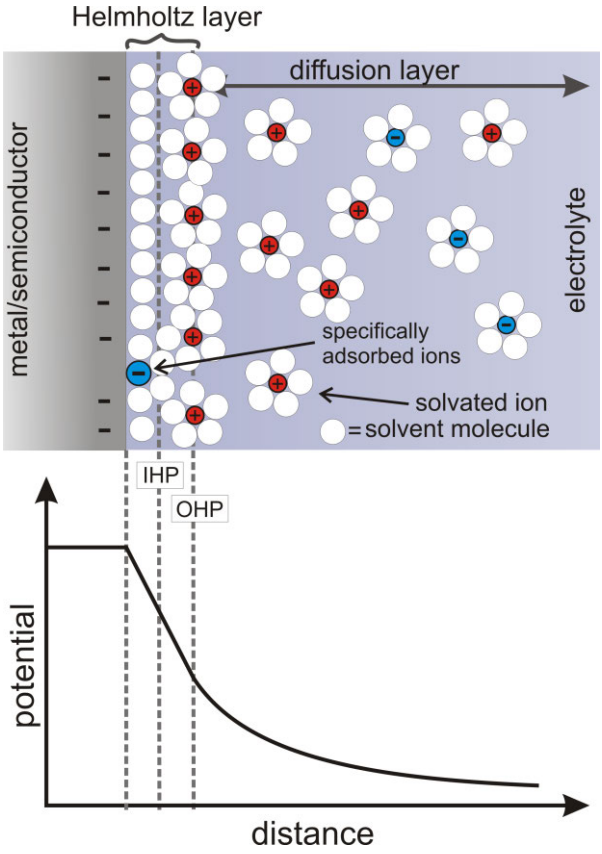

Figure 2.11: Schematic illustration of the electric double layer consisting of the Helmholtz layer and the diffusion layer with the corresponding potential profile.

While electrochemical doping of the semiconductor is highly unwanted in case of EGOFETs, the working principle of OECTs[135] relies exactly on this process. In comparison to EGOFETs, where the conducting channel is formed via charge accumulation due to the application of a sufficiently high gate field, OECTs are turned on or off via electrochemical doping or dedoping mechanisms, altering the conductivity of the electrically conducting polymer (see Figure 2.12). Basically the architecture of OECTs is the same as for EGOFETs (see Figure 2.9). However, a charge-transfer process (faradaic current) across the electrolyte-polymer interface is required. In general the concept of electrolyte-gating is not a new one. First OECT-based chemical sensors were reported

[ii] These capacitances are often a function of the applied voltage, in contrast to the real capacitors whose capacitances are independent of the voltage across them (see ref.134 p.12).

by Wrighton et al. in 1985, where transistors based on polyaniline operated in an aqueous electrolyte solution, showing a response to small changes in pH as well as to redox reagents.[136] However, the drawback of OECTs is the slow switching speed and therefore slow response times.

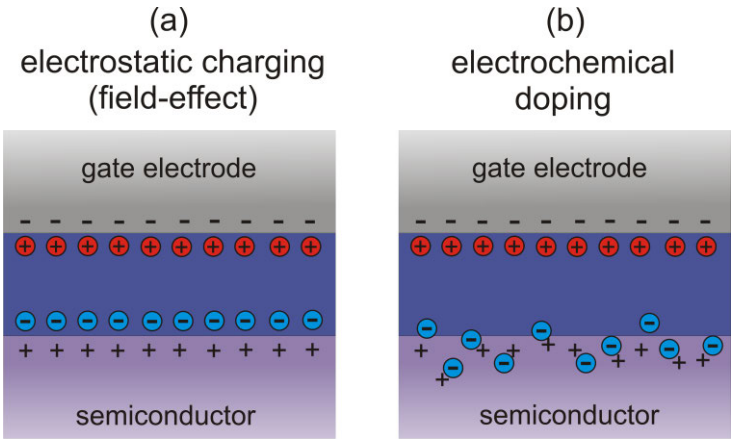

Figure 2.12: Comparison of field-effect vs. electrochemical operation mode.

2.4.2 Requirements of EGOFET based Sensors

In order to use EGOFETs as transducers for potentiometric sensors, certain requirements have to be fulfilled. Accordingly, within the following sections the demands on the semiconductor-electrolyte and the gate-electrolyte interface are discussed.

Semiconductor-Electrolyte Interface

Ideally no faradaic current should pass at the semiconductor-electrolyte interface, so that the applied potential drops at this interface and a proper OFET performance with negligible leakage current is obtained. Such an interface would correspond to an ideal polarizable electrode (IPE), where no charge-transfer process occurs regardless of the applied potentials.[134] Consequently, the charges arrange at the electrolyte-semiconductor interface forming charged layer, known as the EDL. However, no real electrode can behave as an IPE over the whole voltage region available in a solution. Though some certain electrode-solution systems can approach this behavior over a limit potential range (see horizontal current-potential curve in Figure 2.13(a)).[iii] Nevertheless, there is always a very small current flowing due to charge transfer of trace impurities (oxygen, organic species, metal ions). The same holds also for real EGOFET systems: within limited potential window the semiconductor-electrolyte interface is polarizable and therefore only limited faradaic (leakage) current flows and the transistors performance is solely based on field-enhanced conduction. This window can be altered by adding electroactive substances with a small

[iii] Mercury is an example of an ideal polarizable electrode.

electrochemical window (depolarizer), meaning that they are easily oxidized or reduced when exceeding the small voltage window.[134] Thus current is flowing and the interface is not polarizable anymore. This should be taken into account when choosing the electrolyte for an appropriate EGOFET performance.

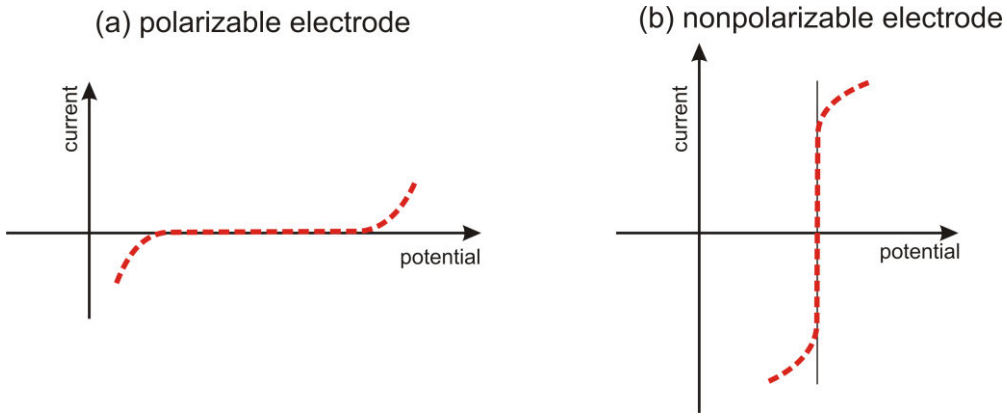

Figure 2.13: Current-potential curves for a polarizable (a) and nonpolarizable (b) electrode approaching ideal behavior for a limited potential or current range.[134]

Gate-Electrolyte Interface

In contrast, the gate-electrolyte interface should ideally be nonpolarizable so that a faradaic current can freely pass, and the potential does not change upon passage of a current (see vertical current-potential curve in Figure 2.13 (b)). This constant electrode potential is required in order to attribute any obtained potential changes to a modified semiconductor-electrolyte interface, where ideally the whole potential drops. Examples of nonpolarizable electrodes are standard reference electrodes with a fixed potential such as standard hydrogen electrode (SHE), saturated calomel electrode (SCE, Hg/Hg_2Cl_2) or the silver/silver chloride (Ag/AgCl) electrode.[134] To obtain a stable electrode potential a redox-system is employed, where each component is present with sufficient concentration. In the case of the Ag/AgCl electrode, a silver wire is coated with a thin layer of silver chloride which is immersed in a saturated potassium chloride inner filling solution. The electrode is in contact with the environment via a liquid junction (provided by a porous plug). For example by using a 3 M KCl inner filling solution a standard electrode potential E^0 of 0.210 V vs the SHE is obtained. Accordingly, the electrode potential of a standard reference electrode with a constant inner filling solution is constant and independent of the sample concentration. This is important in order to ascribe any changes occurring, to the sensing interface.

3 Experimental Methods – Manufacturing and Characterization of OFETs and EGOFETs

In the following chapter the general fabrication methods of bottom-gate/bottom-contact (BG/BC) OFETs and electrolyte-gated OFETs (EGOFETs) based on different materials are described. Additionally, the analytical methods to characterize the materials, to investigate the semiconductor films as well as the electrical characterizations of OFETs are presented.

3.1 Device Fabrication

Within this thesis two different OFET architectures were applied: BG/BC OFETs (see Figure 3.1, left) were used to characterize the electrical properties of a novel heterotriangulene semiconducting polymer and to study the influence of interface modifications on the OFET performance. In order to investigate the air-stability of this new material BG/BC architecture is preferred over others, since the semiconductor is directly exposed to ambient conditions. Secondly, EGOFETs (see Figure 3.1, right) were applied as transducer for sensing application within aqueous media, due to their excellent water-stability. This device architecture is based on a BC OFET structure, where the semiconductor is in direct contact with the electrolyte and gated via a standard reference electrode. As shown in Figure 3.1, both architectures rely on BC OFETs and therefore the corresponding fabrication processes are the same. In the next sections, manufacturing steps for structuring source/drain electrodes, the deposition of the semiconductor including surface modifications and the replica molding for electrolyte reservoirs are presented.

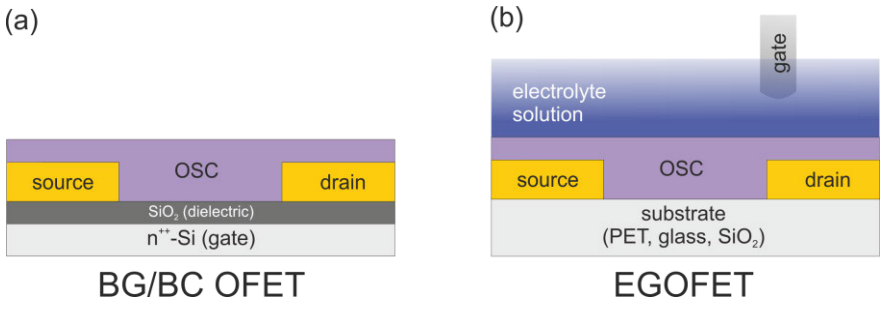

Figure 3.1: Scheme of a BG/BC OFET (a) and a typical EGOFET (b) with TG/BC architecture.

3.1.1 Structuring of Source/Drain Electrodes[iv]

For structuring the source/drain electrodes of OFETs conventional photolithographic patterning via lift-off was applied. It is one of the well-developed and widely used processes[137] asides from several other processing techniques such as inkjet printing,[138] other printing techniques (screen-, offset-, gravure-printing), soft lithography[139] and imprint lithography. It provides a straightforward method to process large-area substrates, enabling parallel patterning as well as down-scaling with feature sizes as low as ~40 nm[140]. Moreover it is a well-established method in today's integrated circuit technology based on inorganic semiconductors and therefore the available knowledge can be exploited for its application in organic electronics. However, there are significant drawbacks including high process and equipment costs and limitations when pattering the organic semiconductor (e.g. delamination, degradation effects).

The basic photolithographic pattering via lift-off process includes following steps (illustrated in Figure 3.2): the preparation of the substrate surface, coating of a photoresist, softbake, alignment and exposure through a photomask, post-exposure bake, development, metallization and removal.

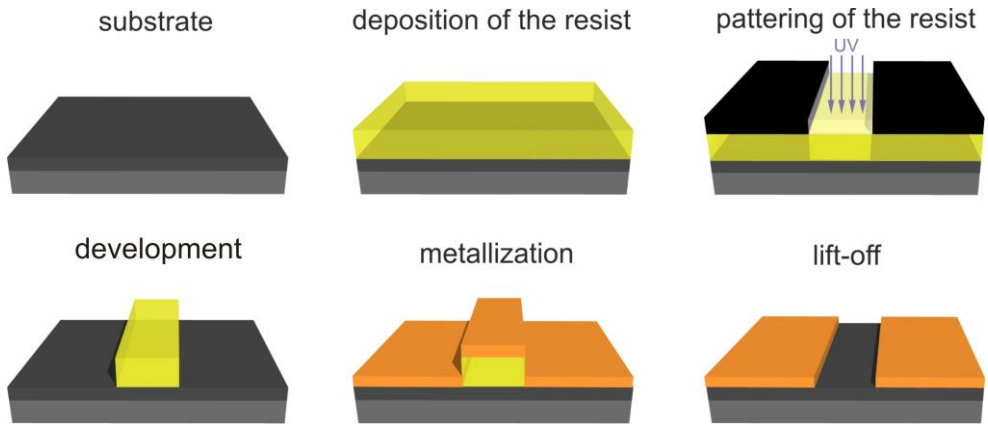

Figure 3.2. Schematic illustration of photolithographic pattering via lift-off (negative resist) of metal source/drain electrodes.

In our case, the source/drain electrodes of BG/BC OFETs were structured on highly n-doped silicon (n^{++}-Si) substrates (dimensions: 1″ x 1″) with thermally grown 200 nm thick silicon dioxide (SiO_2). n^{++}-Si was used as common bottom gate and SiO_2 as gate dielectric ($C_i \sim 17.3$ nF cm^{-2}). Additionally, glass (microscope slides) and polyethylenterephthalat (PET) (Melinex®, DuPont Teijin Films) substrates were used for EGOFETs, where the highly doped n^{++}-Si is not needed.

[iv] Parts of the content within this chapter is based on work that has been published: K. Schmoltner, A. Klug, J. Kofler, E. List, *„Photolithographic processing and its influence on the performance of organic field-effect transistors"*, Proc. of SPIE 8479, Organic Semiconductors in Sensors and Bioelectronics V, Zhenan Bao; Iain McCulloch; Ruth Shinar; Ioannis Kymissis, Editors, Proc. of SPIE 8479, 84790J, (2012).Copyright 2012 Society of Photo Optical Instrumentation Engineers.

First, the substrate surfaces were prepared by cleaning with acetone, isopropanol (ultrasonic bath) and deionized water, followed by a dehydration bake at 200 °C for ~5 min. For the PET substrates the acetone and the dehydration was skipped to avoid etching and shrinking effects, respectively. After cooling the glass and SiO_2 substrates to room temperature the negative photoresist AZ® nLof 2035 (MicroChemicals)[141] was spin-cast (obtaining a resist high of ~3 µm) and softbaked at 100 °C for 180 s. After that the resist was exposed to UV-light through a chromium-patterned quartz mask in proximity mode using an EVG 620 mask aligner (exposure dose: 65 - 75 mJ cm^{-2}). Subsequently a post-exposure bake (~105 °C, 40 s – 120 s, time was adjusted according to the different substrates) was performed to promote crosslinking initiated by UV-light exposure. The development of the resist, using an AZ® 826 MIF developer[141] (40 s – 60 s), was followed by the metallization with a 2 nm thick chromium adhesion layer and a 50 nm thick gold layer via thermal evaporation ($p < 1 \times 10^{-6}$ mbar). Finally, the lift-off process was completed by immersing the sample into NMP (1-methyl-2-pyrrolidone) remover at 65°C in an ultrasonic bath for 5 min. The substrates were then rinsed with deionized water and spin-dried. It was necessary to introduce a second removing step with TechniStrip™ NI555 (for 5 min at 65°C)[142] for glass and SiO_2 substrates with subsequent rinsing using deionized water and spin-drying, in order to remove resist residuals. A detailed investigation of the effects of these resist residuals on the device performance as well as the optimization process to prevent its appearance is given in chapter 4.[1]

Figure 3.3 shows typical substrates for BG/BC OFETs (top) and EGOFETs (bottom) with 12 (L ~ 2.5 µm, ~ 10 µm, ~ 25 µm, ~ 50 µm) and 3 (L ~ 5 - 7 µm) structured source/drain electrodes with channel width of 2.85 mm and 3 mm, respectively. Corresponding micrographs, of source/drain electrodes on different substrates are also included.

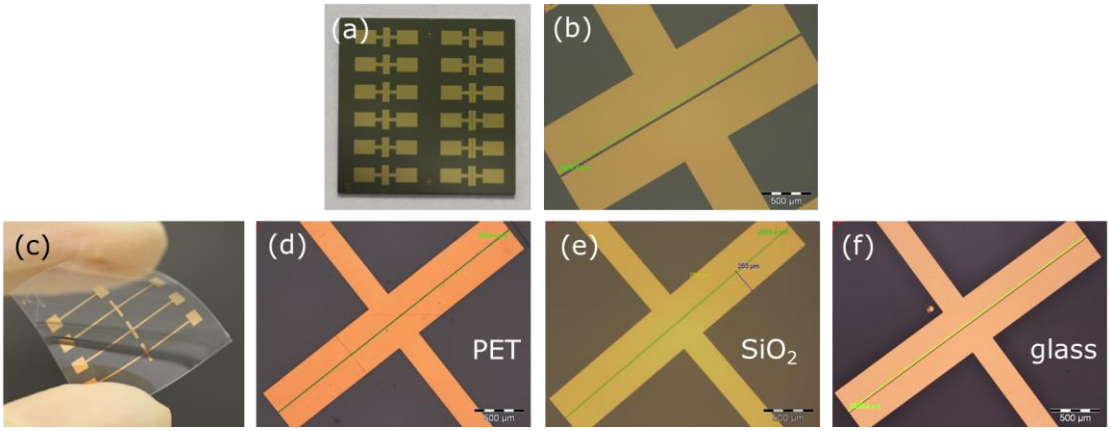

Figure 3.3: BG/BC OFET substrate (a) with 12 structured gold source/drain electrodes and corresponding micrograph (b). EGOFET substrate (c) with 3 structured gold source/drain electrodes on PET and corresponding micrographs of source/drain electrodes on PET (d), SiO_2 (e) and glass (f).

3.1.2 Surface Modifications

In order to optimize the device performance and to investigate the influence of several surface treatments onto the device performance, the surface of some samples (SiO_2 and glass) was modified before depositing the semiconductor.

Hexamethyldisilazane (97% purity degree) was applied via vapor phase deposition for various exposure times (SSE Optihot VB20 hotplate). The application of hexamethyldisilazane (HMDS) reduces the surface energy by replacing hydroxyl groups (OH-) on the surface (SiO_2 or glass) by polar methyl groups.[143,144] Figure 3.4 shows the results of the static advancing contact angle measurements (Krüss DSA 100) using deionized water (DI H_2O). The contact angle is increasing (more hydrophobic) for longer exposure times (see Figure 3.4 (b-e)). In contrast O_2-plasma treatment leads to very hydrophilic surfaces by inducing a high density of OH-groups (see Figure 3.4 (f)). The O_2-plasma treatment was done using a Femto plasma etch plant (diener electronic) with exposure times of 5 min and a power of 100 W.

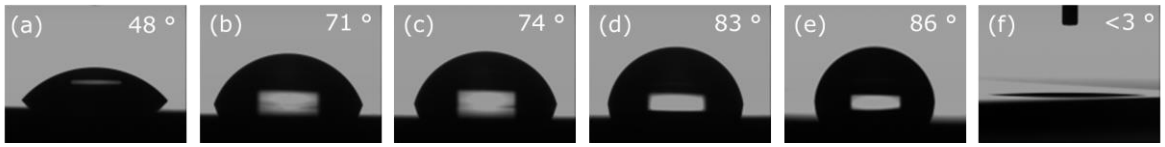

Figure 3.4: Contact angle of water with cleaned SiO_2 substrate without (a) and with 1 x 5 s HMDS (b), 1 x 60 s HMDS (c) 1 x 5 min HMDS (d) 3 x 5 min HMDS (e) and O_2-Plasma treatment (f). The contact angle of a liquid droplet is defined as the angle between the liquid/vapour interface and the solid surface and is determined by Young's equation.[145]

As a third surface modification UV/ozone treatment to hydrophilize the surface and form a thin AuO_x layer on the gold electrodes[80] was applied in order improve the charge carrier injection.[146] A UV-lamp 6035 Hg (Ar) was used for 10 min UV-light exposure of the SiO_2 surface and the gold electrodes in close proximity of ~ 5 mm in ambient conditions.

3.1.3 Film Deposition

Aside from the novel heterotriangulene polymer (PTA), regioregular poly(3-hexylthiophene) (P3HT, Plexcore® OS) was used as semiconducting layer for EGOFETs. In general, these conjugated polymers were dissolved in toluene or chloroform (HPLC) with concentrations of 2 - 4 g/L. In case of P3HT, solutions were stirred for ~5 min at temperatures of ~60 °C.

Generally, all devices were assembled under inert atmosphere in argon-filled glove boxes, except those used for ambient stability investigations. Before the deposition of the semiconductor, adsorbed water on the surface was removed by a dehydration bake at 120 °C in high vacuum ($p \sim 4 \times 10^{-5}$ mbar) for 1 h. The semiconductor was then applied by spin-coating (1000 – 1500 rpm,

40 – 60 s), achieving a film thickness between 20 – 40 nm. Afterwards, the thin films were first dried at 60 °C in argon for approximately 10 min and subsequently at 120 °C in high vacuum ($p \sim 4x10^{-5}$ mbar) for 1h. The gate of BG/BC OFETs was then contacted with conductive silver to a cooper plate for the followed electrical characterization (see Figure 3.5 (a) and (b)). Whereas in case of EGOFETs, the electrolyte must be confined on top of the semiconducting layer in a next step (see Figure 3.5 (c)).

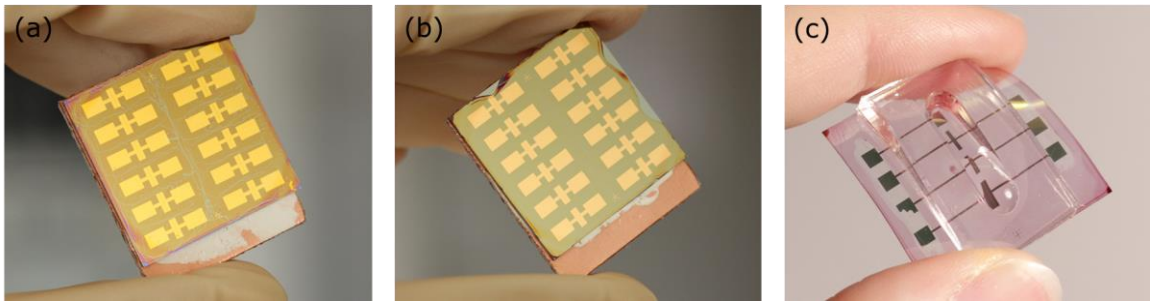

Figure 3.5: Sample of 12 BG/BC OFETs based on the PTA polymer (a) and P3HT (b) and a typical sample of 3 EGOFETs in contact with DI water without the Ag/AgCl electrode.

3.1.4 Electrolytes and PDMS Replica Molding

For EGOFETs deionized (DI) water and various saline solutions, which were prepared in concentrations varying from 10^{-4} M to 10^{-2} M NaCl (99.5%, p.a., ACS, ISO) in DI water, were used as electrolytes. In order to confine these electrolytes on top of the semiconductor, a reservoir (electrolyte well) made of polydimethylsiloxane (PDMS, Sylgard 184) was fabricated by replica molding. First, the master was fabricated by simply using optical slides with structured (cut) glass on top of it (see Figure 3.6 (a)). Then the PDMS prepolymer was cast on the master, followed by a curing step of ~1 h at 100 °C.[147] The prepolymer, which consists of a liquid base and a curing agent (10:1 base : curing agent ratio) undergoes a crosslinking reaction, resulting in an elastomeric solid. It can be peeled from the master and shaped into final form by cutting with a scalpel.

These glass masters were further replaced by more elaborated masters fabricated by 3D printing (Objet30 Pro). However, these masters, made of verogray ink (Fullcure®850) have to be subjected to a certain cleaning treatment before PDMS casting. Otherwise, it was observed that the crosslinking of the prepolymer was impeded in contact with the master. This can be ascribed to NaOH residuals, originating from the removal of the support materials where the objects are immersed into a NaOH solution. Therefore to minimize the appearance of these residuals the 3D printed masters were immersed into DI water, rinsed with DI water and isopropanol and then annealed at ~80 °C in the vacuum oven for 1h. Figure 3.6 (b) and (c) show examples of a successfully fabricated PDMS reservoir and the flow cell cast from 3D printed masters. The access

for the gate electrode and the tubing can be added by appropriate placements (c) or punched out of the cured replica.

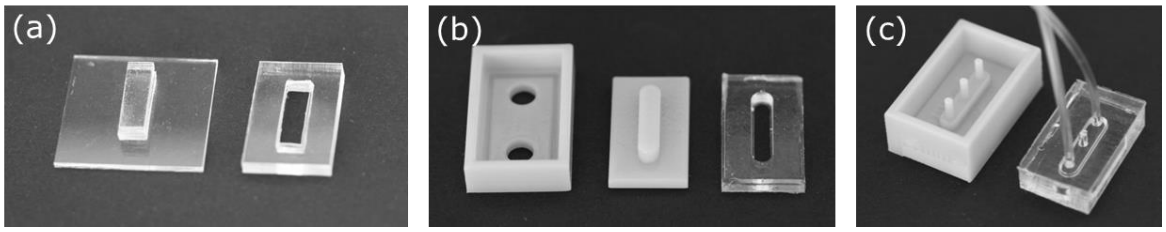

Figure 3.6: Typical master made of glass (a) and by 3D printing (b,c) with corresponding PDMS reservoirs (a,b) and flow cell (c).

3.2 Materials and Film Characterization Methods

Optical absorption, photoluminescence and photoelectron spectroscopy as well as atomic force microscopy was used to investigate the novel heterotriangulene polymer, in terms of morphological, optical, and interface related properties in comparison to P3HT.

Diluted solutions of 5 x 10^{-3} g/L and 1 g/L of the PTA polymer in $CHCl_3$ and toluene as well as thin films (spin-coated from 2 g/L toluene and $CHCl_3$) on quartz glass were prepared for the optical spectroscopy. Optical absorption spectra were measured by a Perkin Elmer Lambda 900 UV/VIS – spectrometer. A spectrofluorophotometer Shimadzu RF-5301PC was used to record photoluminescence and all spectra were corrected according to the detector characteristics.

Furthermore, to investigate the surface morphology of the thin semiconducting films of OFETs, atomic force microscopy (AFM) (Veeco Dimension V AFM equipped with a Nanoscope V controller) was used in tapping mode.

For ultraviolet photoelectron spectroscopy (UPS) studies the polymer solutions (1 g/L) were spin-coated from toluene solution on $Si/SiO_2/Au$ substrates, with the gold layer being thermally evaporated and subsequently exposed to lift-off chemicals in order to obtain the same conditions as with the OFETs. The UPS measurements[v] were performed using a multitechnique ultra high vacuum (UHV-) apparatus (base pressure: 1 x 10^{-10} mbar) and a Helium-gas-discharge lamp (21.218 eV) with a very low photon flux (ca. 100 times attenuated compared to standard commercial sources) in order to reduce any irradiation damage. All spectra were recorded at room temperature and normal emission using a hemispherical Specs Phoibos 100 energy analyzer with

[v] The UPS investigations were performed by Stefanie Winkler within the group of Prof. Norbert Koch from Helmholtz Zentrum Berlin für Materialien und Energie GmbH Elektronenspeicherring BESSY II and Physics Intstitute at Humboldt University Berlin.

120 meV energy resolution for UPS. To determine the work function, secondary electron cutoffs were recorded with the sample biased to -10 V to clear the analyzer work function.

3.3 Electrical Characterization

The electrical measurements were performed in an argon-filled glove box and/or in air at ambient conditions. The electrodes of a BG/BC OFETs were contacted with micromanipulators on a probe station (PM5 Krüss), whereas the EGOFETs were electrically characterized within a 3D printed measurement setup (Figure 3.7 (a)). Figure 3.7 shows an EGOFET device before (b) and after (c) implementation of the reservoir and the flow cell. The big advantage of this setup is that the flow cell alignment and sealing can be done independently of the electrical conduction by an appropriate fixture. In order to seal the flow cell it is important to apply a constant pressure all-over the device, which was perfectly achieved by the new designed set up.

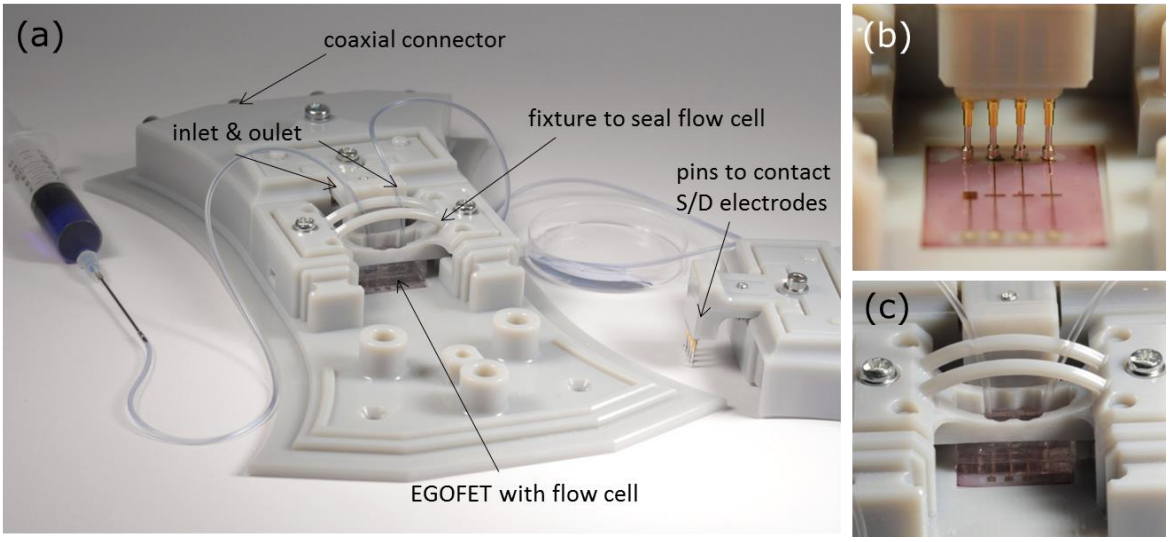

Figure 3.7: (a) 3D printed measurements setup for electrical characterization of EGOFET based sensors. (b) EGOFET without the electrolyte reservoir but electrically contacted with pogo pings and (c) after the implementation of the reservoir and the flow cell with an appropriate fixture to seal the flow cell, but without the implemented gate electrode.

The current-voltage characteristics such as transfer and output characteristics were measured using an Agilent B1500A Parameter Analyzer which is equipped with four source-measure-units (SMUs). The SMUs can supply a voltage or current while simultaneously measure voltage and/or current. Each terminal of the OFET was connected to one SMU. The transfer characteristics were performed by measuring the source-drain current while sweeping the gate voltage and keeping the drain voltage constant. The gate voltage was swept within a potential window chosen to extend the off- and on-state of the device. This sweep was recorded in forward and reverse direction and repeated for several drain voltages including the linear regime and the saturation regime. After

measuring the transfer characteristics, the output characteristics were recorded in a similar manner. Here the source-drain current was measured as the drain voltage was swept while the gate voltage is kept constant. This was repeated for a several equally spaced gate voltages. Additionally to the basic OFET characterization other measurement protocols were used such as time dependend recording of the channel current at a constant working point. OFET parameters like field-effect mobility, threshold voltage or substhreshold slope were extracted as described in section 2.2.2 applying the gradual channel approximation.[72]

Furthermore, other electrical characterization methods e.g. potentiometric measurements of ion-selective electrode are presented in the respective chapter.

4 Photolithographic Processing and its Influence on the Performance of Organic Field-Effect Transistors

Photolithography is a well-established method in today's integrated circuit technology based on inorganic semiconductors, whereupon its adoption in organic electronics implicates some limitations. In the following chapter, we report on the influence of photolithographic processing of source/drain electrodes on the device performance of regioregular poly(3-hexylthiophene)-based bottom-gate bottom-contact (BG/BC) organic field-effect transistors (OFETs). In particular, the effects of photoresist residuals within the active channel region and the influence of the application of various lift-off chemicals were thoroughly investigated by contact angle measurements, scanning electron microscopy, atomic force microscopy and electrical characterization of OFET-based devices. By modifying the dielectric-semiconductor and/or electrode-semiconductor interfaces, applied chemicals are shown to affect the device performance in terms of switch-on voltage, subthreshold swing and on/off-current ratio. Thus, we highlight the importance to focus not only on the constituting OFET materials but also on the manufacturing process for obtaining reproducible well-performing OFET devices.[1]

The content of this chapter is based on work that has been published and was partly modified: K. Schmoltner, A. Klug, J. Kofler, E. List, *„Photolithographic processing and its influence on the performance of organic field-effect transistors“*, Organic Semiconductors in Sensors and Bioelectronics V, Zhenan Bao; Iain McCulloch; Ruth Shinar; Ioannis Kymissis, Editors, Proc. of SPIE 8479, 84790J, (2012). Copyright 2012 Society of Photo Optical Instrumentation Engineers.

4.1 Introduction

Recent advances within the field of OFETs were not only possible due to extensive research and development of high-mobility[148] and solution-processable organic semiconductors[149] but also

because of the technological progress concerning the manufacturing processes. Accordingly, besides the optimization of organic semiconductors, whose charge-carrier mobility values (of 0.1 - 1 $cm^2 V^{-1}s^{-1}$)[21,22] already exceed the benchmark values of amorphous silicon, big focus is also set on improving the OFET performance from the device physics and manufacturing point of view (e.g. downscaling for low-voltage applications and higher operational frequencies[150]). It is generally known that the processing conditions of the organic semiconductor as well as a specific treatment of the substrate surface with SAMs or chemicals such as hexamethyldisilazane (HMDS) or n-octadecyltrichlorosilane (OTS) significantly influence the OFET performance.[151]

Within this chapter it is demonstrated that it is already the photolithographic processing to structure the electrodes prior to the deposition of the organic semiconductor, influencing the interface (dielectric-semiconductor and/or electrode-semiconductor) properties. Accordingly also the electrical performance of BG/BC OFETs is affected. In particular, the effects of photoresist residuals within the active channel region and the influence of the application of various lift-off chemicals were thoroughly investigated in OFETs based on P3HT (see Figure 4.1). The present study emphasizes the necessity for the optimization of the manufacturing process in order to obtain reproducible high-performing OFETs and OFET-based sensors.

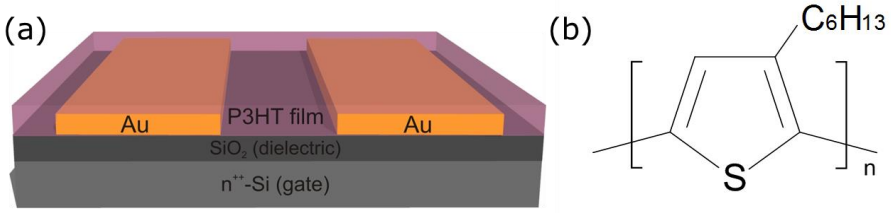

Figure 4.1: (a) Bottom-gate/bottom-contact (BG/BC) OFET architecture; (b) chemical structure of regioregular P3HT.

4.2 Influence of Photoresist Residuals on the OFET Performance

P3HT-based BG/BC OFETs were fabricated as presented in chapter 3.1, except for the lift-off process, where different lift-off chemicals were used and the number of removing process steps was varied. After photolithographic structuring of the source/drain electrodes the samples were investigated with scanning electron microscopy (SEM, Raith e-line) and atomic force microscopy (AFM, Veeco Instruments) in tapping-mode. Figure 4.2 (a) and (b) show SEM and AFM images of the channel between the gold source/drain electrodes after lift-off with n-methyl-2-pyrrolidon (NMP). The SEM image reveals areas with dark spots on the SiO_2 surface, which are also observable in the AFM image in terms of height variations up to ~8 nm. Since SiO_2 usually has a

very smooth surface and the SEM image shows significant material contrast, these features most likely can be ascribed to photoresist residuals. Their origin might be a high degree of crosslinking of the negative resist, being increased for higher temperatures. The temperature input in combination with the corresponding radiation during thermal evaporation of the metal might lead to enhanced crosslinking and therefore reducing removability.[152] In order to remove these resist residuals, alternative removers (TechniStripTM NI555 and P1316) were used, which rather dissolve the crosslinked resist than peeling it off the substrate. SEM and AFM images confirmed the successful removal of the photoresist with these strippers (Figure 4.2 (d,e,f)). The corresponding line section of the AFM image shows a very smooth SiO_2 surface within the channel without any residual chemicals.

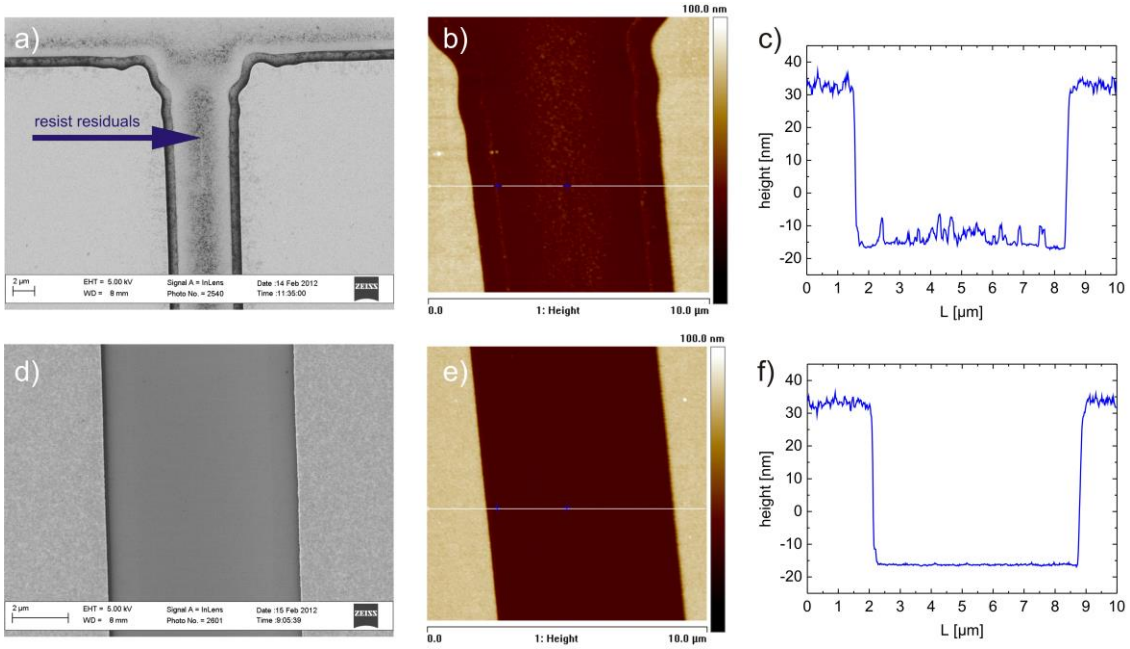

Figure 4.2: SEM (a,d) and AFM (b,e) images and line sections (c,f) of the structured channel on SiO_2 after lift-off with NMP showing photoresist residuals (top) and without residuals after using the remover TechniStrip™ P1316 (bottom).

To study the influence of photoresist residuals on the electrical performance of the organic semiconductor, BG/BC OFETs based on P3HT ($CHCl_3$ solution) were characterized. Figure 4.3 compares the output characteristics of a device exhibiting resist residuals on the SiO_2 surface with those of a BG/BC OFET without photoresist within the source/drain channel region. The former showed a decreased OFET performance in terms of lower on-currents (40 % lower), decreased field-effect mobility values and a larger subthreshold slope (see Table 4.1). This significant performance reduction can be ascribed to the rough semiconductor/dielectric interface and/or dissolution of the resist residuals by the solvent of the P3HT solution, followed by a possible intermixing with the semiconducting polymer. These chemical and structural impurities can act as additional traps decreasing the charge carrier mobility.[153-156] In general, the surface roughness of the

dielectric significantly affects the electrical performance of OFETs,[157-159] since the charge transport takes place in the first few monolayers close to the interface with the dielectric.

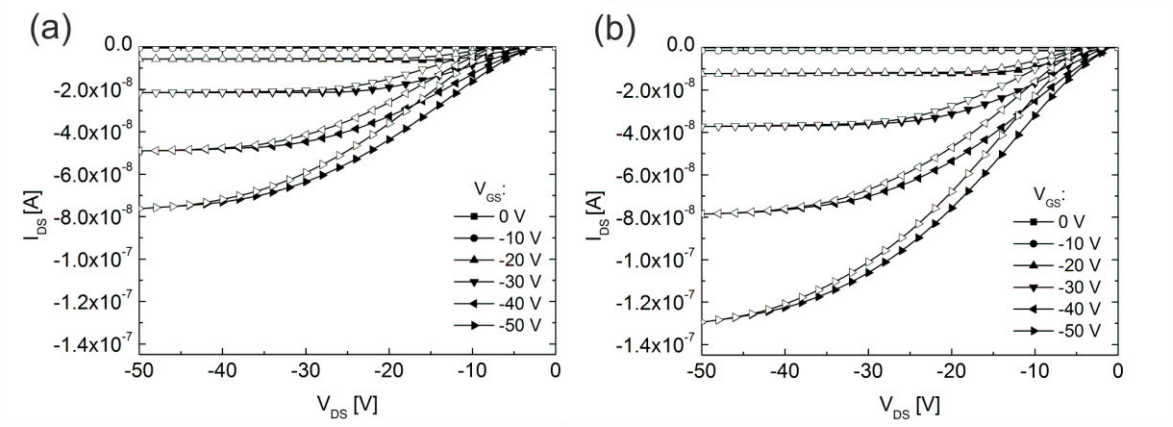

Figure 4.3: Output characteristics of a P3HT-based OFET with photoresist residuals (a) and after removing the residuals with NI555 (b); filled symbols: sweeps from positive to negative voltages; open symbols: reverse sweep.

Moreover, the smaller value of the I_{on} *(O-T)* in Table 4.1, which indicates a larger difference between the source-drain channel current values in the output and transfer characteristics at a particular drain voltage and gate voltage, is also a sign for higher trap densities in the device with resist residuals. Gate-bias stress is responsible for the fact that the channel current at a particular V_{DS} and (high) V_{GS} is often lower in the output characteristics than in the transfer characteristics, because a high gate voltage (leading to charge trapping) is longer applied in the former. In addition, a thin layer of residual resist can change the polarity of the surface, which for nanocrystalline films formed by P3HT might influence the morphology as well. For both devices the absence of a distinct linear channel current behavior at low drain voltages indicates a significant contact resistance, resulting from a non-negligible injection barrier[79] between gold and P3HT.

Table 4.1: Relevant OFET parameters of typical P3HT-based BG/BC devices (L ~ 25 µm, W ~ 2.85 mm) fabricated on SiO_2 with and without resist residuals.

Substrate	Remover	Mobility μ_{sat} [a] ($cm^2\ V^{-1}\ s^{-1}$)	*I* (on/off) [b]	V_{so} (V)	*S* (V/dec)	I_{on} *(O-T)* [c] (%)
SiO_2 + resist residuals	NMP	9.1×10^{-5}	1.3×10^{3}	-6	7.2	64
SiO_2	NMP – NI555	1.2×10^{-4}	3.5×10^{3}	-5	3.0	73

[a] saturation field-effect mobility μ_{sat} at V_{DS} = -50 V, V_{GS} = -35 V calculated according to gradual channel approximation
[b] on/off-current ratio I(on/off) (I_{on}: V_{GS} = -50 V, I_{off}: V_{GS} = 0 V at V_{DS} = -50 V)
[c] percentage of I_{DS} at $V_{DS} = V_{GS}$ = -50 V in output characteristics with respect to value in transfer characteristics I_{on}(O-T)

Due to the fact that the application of additional removers (TechniStrip™ NI555 or P1316) was an essential step for minimizing the sample-to-sample variation of BG/BC OFETs before the

deposition of the organic semiconductor, the next section deals with a thorough investigation of the influence of various lift-off chemicals on the device performance.

4.3 Influence of the Lift-Off Chemicals on the OFET Performance

Figure 4.4 depicts AFM height images of P3HT films of OFETs fabricated on n^{++}-Si/SiO_2 substrates, where either remover NI555 or P1316 was additionally used in the lift-off process. The films exhibit a very smooth surface with a root-mean-square roughness of ~ 0.4 nm and ~ 0.3 nm, respectively. On P1316 treated substrates the P3HT grain size seems to be larger. Furthermore, the corresponding AFM image seems to be more blurry, which is typical for a more hydrophilic modified surface resulting from adsorbed water molecules.[160]

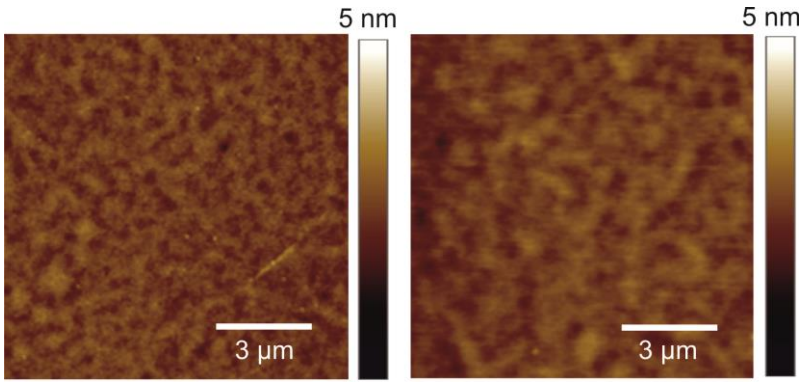

Figure 4.4: AFM height images of P3HT on SiO_2 when different removers were used for the lift-off process: (left) NMP-NI555 and (right) NMP-P1316.

Besides the morphological investigations, the contact angles of deionized water (DI H_2O) and diiodomethane on the SiO_2 surface were determined in order to investigate the influence of the applied lift-off chemicals on the surface polarity. Table 4.2 summarizes the results, also including relevant device parameters of corresponding P3HT-based BG/BC OFETs. The application of P1316 significantly changed the SiO_2 surface energy from more hydrophobic (contact angle of DI H_2O ~70 °), when NMP and NI555 was used, to hydrophilic (contact angle of DI H_2O ~12 °). Not only the surface energy of SiO_2 was affected, but also the gold surface showed modified contact angles of DI H_2O and diiodomethane, being an issue for morphology changes at the electrode/semiconductor interface and therefore being relevant for injection properties. Moreover, an additional cleaning step with acetone, isopropanol and rinsing with deionized water slightly changed the contact angles as well, in particular rendering the surface more hydrophobic (contact angle of DI H_2O from 12 ° to 32 °) when applied after removing with P1316.

Table 4.2: Contact angles on SiO_2 and gold (thermally evaporated) after using different lift-off chemicals and relevant OFET parameters of corresponding P3HT-based BG/BC devices (L ~ 25 µm, W ~ 2.85 mm)

Substrate	Treatment	Contact angle (°)		Mobility μ_{sat} [a]	I	V_{so}	I_{on} (O-T) [c]
		H_2O	Diiodmethan	($cm^2 V^{-1} s^{-1}$)	(on/off) [b]	(V)	(%)
SiO_2	NMP – NI555	70.6	59.9	1.8×10^{-4}	5.6×10^3	-4	82
Gold	NMP – NI555	59.5	22.6				
SiO_2	NMP-NI555 – acetone–ISO	71.5	60.2	1.9×10^{-4}	6.8×10^3	-4	82
Gold	NMP-NI555 – aceton–ISO	63	24.5				
SiO_2	NMP – P1316	11.7	47.3	2.1×10^{-4}	1.5×10^4	-12	73
Gold	NMP – P1316	32.1	4.4				
SiO_2	NMP-P1316 – acetone-ISO	32.1	53.3	1.6×10^{-4}	1.6×10^4	-9	72
Gold	NMP-P1316 – acetone-ISO	40.2	14.7				

[a] saturation field-effect mobility μ_{sat} at V_{DS} = -50 V, V_{GS} = -35 V calculated according to gradual channel approximation
[b] on/off-current ratio I(on/off) (Ion: V_{GS} = -50 V, I_{off}: V_{GS} = 0 V at V_{DS} = -50 V)
[c] percentage of I_{DS} at $V_{DS} = V_{GS}$ = -50 V in output characteristics with respect to value in transfer characteristics I_{on}(O-T)

Figure 4.6 depicts the output characteristics, the semilogarithmic transfer curves as well as the square-root of the channel current vs. gate voltage of typical P3HT-based BG/BC OFETs when different lift-off chemicals were applied. Accordingly, Figure 4.5 shows a combined comparison of semilogarithmic transfer curves of the differently treated OFETs. As indicated above and shown by other research groups,[161,162] chemicals modifying the surface properties of the dielectric significantly influence the performance of organic field-effect transistors. OFETs treated with remover P1316 showed a more negative switch-on voltage and a larger hysteresis (see Figure 4.6 (e)), indicating a higher trap density due to a larger number of OH-groups on the more hydrophilic surface.[155,163] This is in agreement with the results of the contact angle measurements. Moreover, by comparing the maximum currents in Figure 4.6, the OFETs treated with P1316 (more hydrophilic surface) yielded ~16 % lower drain current (at V_{GS} = -50 V, V_{DS} = -50 V) as well as a lower I_{on} *(O-T)* ratio (see Table 4.2), which again is a sign for a larger trap density. Although OFETs with NI555-treated SiO_2 exhibited lower channel currents in the reverse sweep as well, the effect ascribed to charge-carrier trapping is not as pronounced as for OFETs with the hydrophilic SiO_2 surface (P1316 treated). In accordance with the results of the contact angle measurements, an additional cleaning step of the sample with isopropanol and acetone after the lift-off process did not significantly change the performance of P3HT-based OFETs when NI555 was used, while showing a slight influence in terms of a switch-on voltage shift for P1316-treated surfaces. The performance variations might, however, also result from a change in the morphology of the semiconductor due to a modified SiO_2 surface. In addition, the application of different lift-off chemicals also changed the surface properties of the gold electrodes, resulting in altered contact angles (see Table 4.2).

Thus a modification of the electrode-semiconductor interface (injection barrier) is highly likely. This is in good agreement with results presented by other groups, which showed that already the structuring process of the source/drain electrodes (e.g. cleaning, hydrocarbon contaminations) can significantly influence the contact resistance and injection properties.[79,164]

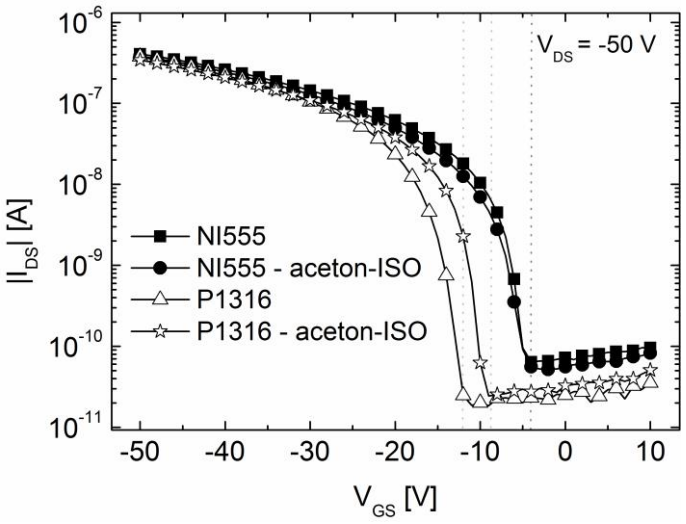

Figure 4.5. Comparison of semilogarithmic transfer curves at V_{DS} = -50 V (right) of several P3HT-based OFETs when different lift-off chemicals were applied: NMP-NI555 (squares), NMP-NI555 with additional cleaning step (circles), NMP-P1316, (triangles,) NMP-P1316 with additional cleaning step (stars).

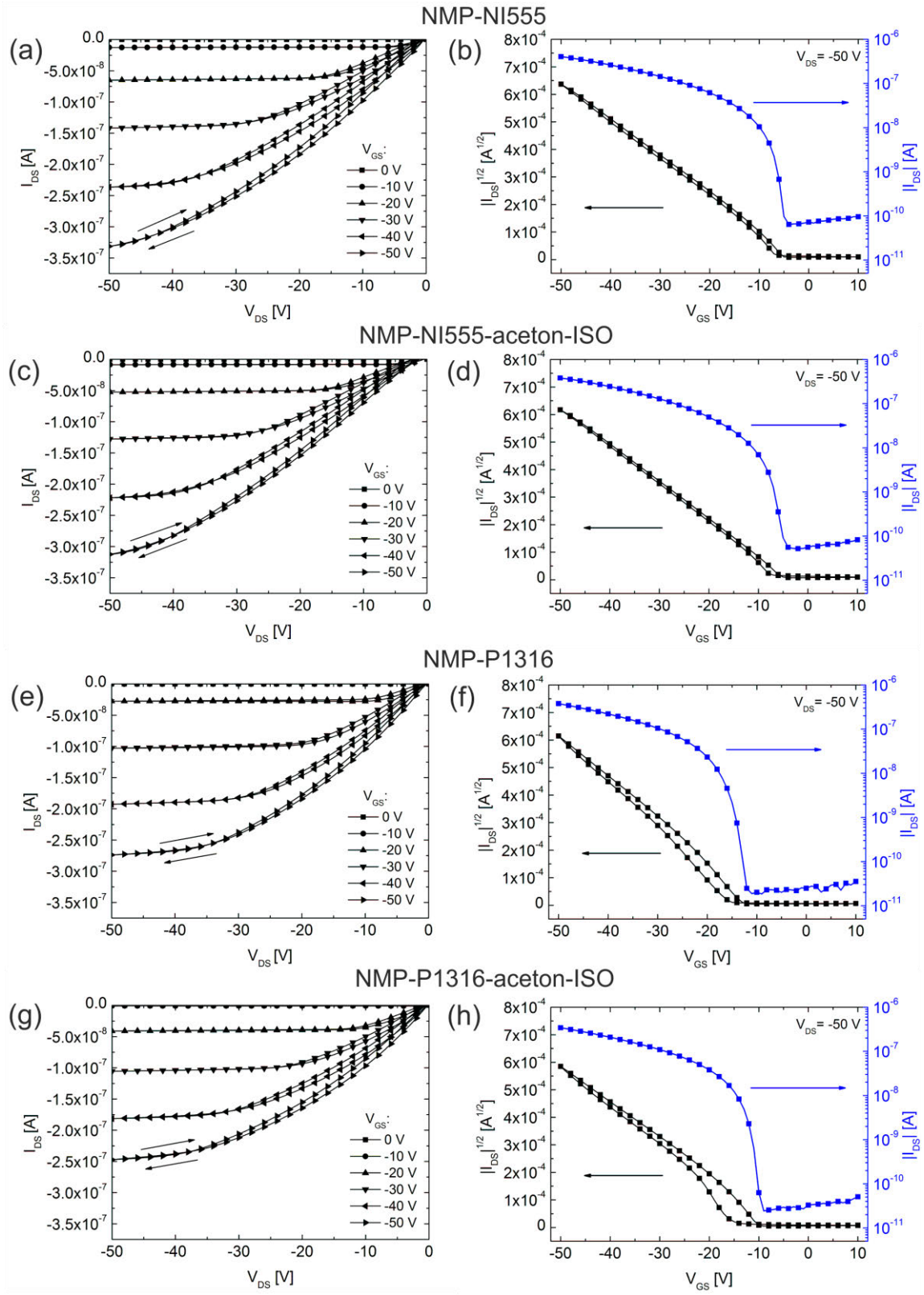

Figure 4.6. Output characteristics (left), square root of the channel current vs. gate voltage and semilogarithmic transfer curves at V_{DS} = -50 V (right) of several P3HT-based OFETs when different lift-off chemicals were applied: (a,b) NMP-NI555, (c,d) NMP-NI555 with additional cleaning step, (e,f) NMP-P1316, (g,h) NMP-P1316 with additional cleaning step; the hysteresis between forward and reverse sweep showed a lower current for the latter.

4.4 Conclusion

In summary, we demonstrated that photolithographic processing to structure the source/drain electrodes of organic field-effect transistors can significantly influence the dielectric-semiconductor and/or electrode-semiconductor interfaces, leading to a modification of the electrical performance of bottom-gate bottom-contact OFETs based on P3HT. In particular, photoresist residuals within the channel of OFETs lead to decreased field-effect mobilities, lower on/off-current ratios and higher subthreshold slopes, originating from a substantial increase of the surface roughness and the associated charge carrier trap density. The application of additional remover chemicals successfully dissolved the observed photoresist residuals affecting the OFET performance. If, however, a remover chemical was used which renders the substrate surface more hydrophilic, the corresponding devices showed significantly larger negative threshold voltages indicating higher trap densities at the semiconductor/dielectric interface originating from a larger number of OH-groups on the surface. To conclude, the presented results clearly demonstrate that process chemicals have a distinct influence on the device performance of organic field-effect transistors, making it inevitably necessary to focus not only on the constituting OFET materials but also on the manufacturing process for obtaining reliable well-performing OFETs and OFET-based sensors.

5 A Heterotriangulene Polymer for Air-Stable Organic Field-Effect Transistors

Within this chapter a novel air-stable p-type heterotriangulene polymer (PTA) for large-area organic field-effect transistor (OFET) applications is presented. This newly synthesized amorphous organic semiconductor[vi] was characterized concerning morphological, optical, electrical and interface related properties. In order to optimize the performance of PTA-based BG/BC OFETs, the influence of several interface modifications was investigated. Moreover, in the course of optimization the influence of different solvents on the device performance revealed that hydrochloric acid in chloroform leads to protonation of the nitrogen atom on the PTA polymer. Finally, the ambient stability of BG/BC PTA OFETs was studied in detail over months and compared with P3HT devices.[2]

The content of this chapter is based on work that has been published and was partly modified: K. Schmoltner, F. Schlütter, M. Kivala, M. Baumgarten, S. Winkler, R. Trattnig, N. Koch, A. Klug, E.J.W. List, and K. Müllen, "*A heterotriangulene polymer for air-stable organic field-effect transistors*", Polym. Chem. 4 (20), 5337-5344 (2013). Reproduced by permission of The Royal Society of Chemistry, http://dx.doi.org/10.1039/c3py00089c.

5.1 Introduction

During the past two decades the fast progress in research on novel small molecule and π-conjugated polymer based organic semiconductors[17,42,165] has led to successful realizations of simple electronic circuits for low-cost radio-frequency identification tags,[23,68] flexible large-area displays, [24,65] as well as for sensing devices[25,29]. In particular, to enable cost-effective, simple large-scale roll-to-roll production, solution-processable organic semiconductors with good electric properties in OFETs, *i.e.* high charge carrier mobilities, high on/off current ratios and low threshold

[vi] The novel heterotriangulene polymer was synthesized by Florian Schlütter within the group of Martin Baumgarten and Klaus Müllen from Max-Planck-Institute for Polymer Research at Mainz.

voltages, are imperative. π-Conjugated oligomers and polymers have proved to be good candidates with excellent performance, reaching the benchmark of amorphous silicon with charge carrier mobilities of 0.1 – 6.2 $cm^2 V^{-1}s^{-1}$.[22,166-169] Regioregular poly(3-hexylthiophene) (P3HT), for example, is by far one of the most widely investigated p-type polymers exhibiting charge carrier mobility values up to 0.1 - 0.4 $cm^2 V^{-1}s^{-1}$.[36,170] However, P3HT forms microcrystalline films and its mobility is strongly influenced by morphological changes depending on processing conditions.[37,171] In comparison, amorphous polymers such as poly(triarylamines) (PTAAs) cannot compete with the mobilities of crystalline ones (~10^{-3} to 10^{-2} $cm^2 V^{-1}s^{-1}$), although their ease of processing with high reproducibility as well as robust electrical performance are beneficial.[161,172,173] Since most of large-scale roll-to-roll printing techniques are applied under ambient conditions, air stability of organic semiconductors is required. In this context, P3HT shows poor performance, due to a relatively low ionization potential leading to degradation effects in the presence of light.[38,75,174,175] In general, a significant improvement in air stability can be obtained by increasing the ionization potential above 5 eV.[39,176]

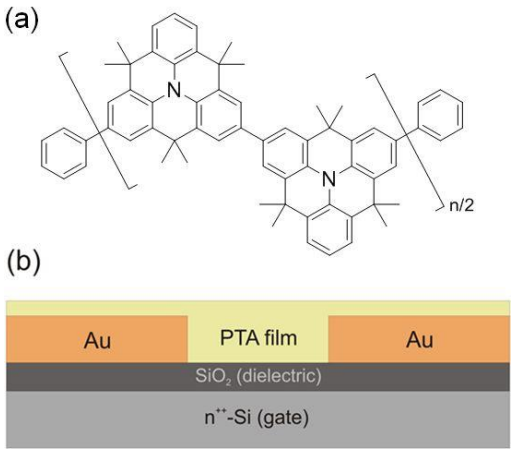

Figure 5.1: (a) Chemical structure of PTA polymer. (b) Schematic representation of bottom-gate/bottom-contact (BG/BC) OFETs (not to scale).

Here we report on a heterotriangulene polymer (**PTA**) as an alternative organic semiconductor for air stable organic field-effect transistors synthesized in a straightforward procedure (see Figure 5.1 and section 5.2). Due to the bridging dimethylmethylene-groups good solubility of **PTA** in organic solvents is ensured without the attachment of additional solubilizing groups (e.g. long alkyl chains), leading to thermally stable amorphous films with enhanced device stability.[177] Furthermore, the electron delocalization between the central nitrogen and the benzene moieties is enhanced by the planarization, which results in an improved conjugation along the polymer chains. The crucial air stability is, however, provided by the low lying HOMO level (E_{HOMO} = 5.1 eV) and wide bandgap (E_g = 2.9 eV) of **PTA**. The high potential of heterotriangulenes as p-type semiconductor was recently shown by dendrimeric derivatives of **PTA**, exhibiting an enhanced hole transporting

ability in organic light emitting diodes (OLEDs) together with an improved thermal and morphological stability.[178,179]

Within the next sections the characterization of this novel amorphous organic semiconductor concerning morphological, optical and interface related properties by means of AFM, UV-vis absorption, photoluminescence and ultraviolet photoelectron spectroscopy, is shown. Aside from the intrinsic properties of the organic semiconductor, the device architecture, its interfaces and thus the applied surface treatments are determining the OFET stability under ambient conditions.[151] We focus on bottom-gate/bottom-contact (BG/BC) OFETs based on **PTA** (see Figure 5.1 (b)) and investigate the influence of several surface treatments onto the device performance (see section 5.5). We show that the utilization of chloroform as solvent leads to a protonation of the nitrogen atom on the **PTA** polymer, which has a significant influence on the electrical characteristics of OFETs. The protonation reaction and its effects are discussed in detail within the optical properties section 5.4. In section 5.6, the ambient stability of **PTA** OFETs over months is benchmarked against P3HT OFETs.

5.2 Synthesis and Materials Characterization

The synthesis of **PTA** as well as the basic materials characterization including ^{1}H NMR spectroscopy, size-exclusion chromatography, thermogravimetric analysis and cyclic voltammetry was done by Florian Schlütter within the group of Martin Baumgarten and Klaus Müllen. For that reason, only a short summary of the synthesis and the materials characteristics is given here. The full work including the experimental details is presented in [2].

The straightforward synthetic route towards polymer **PTA** is shown in Figure 5.2. The dimethylmethylene-bridged triarylamine **DTPA** (4,4,8,8,12,12-hexamethyl-8,12-dihydro-4H-benzo[1,9]quinolizino[3,4,5,6,7-defg]acridine) was prepared according to literature in three steps.[180,181] Monomer **DTPABr$_2$ (**2,6-dibromo-4,4,8,8,12,12-hexamethyl-8,12-dihydro-4H-benzo[1,9]quinolizino[3,4,5,6,7-defg]acridine**)** was obtained after twofold bromination using *N*-bromosuccinimide (NBS) in stoichiometric amounts. Following standard Yamamoto conditions and endcapping using bromobenzene, **PTA** was obtained.[182,183] After removal of the low molar mass fraction by repeated Soxhlet extraction and precipitation, the weight-average molecular weight of **PTA** was determined by size-exclusion chromatography (SEC) using a poly(styrene) standard in THF and was found to be 17,800 g/mol (PDI = 1.7), which corresponds to a molecular structure of approximately 49 **DTPA** repeating units. **PTA** showed good solubility in organic solvents, *e.g.*, THF, toluene, dichloromethane and 1,2-dichlorobenzene.

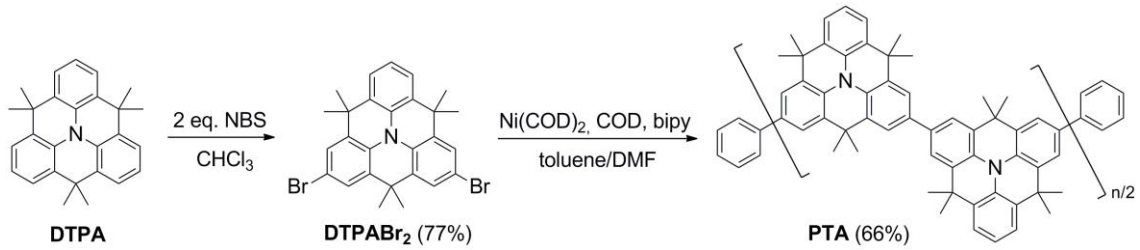

Figure 5.2: Schematic representation of the synthesis of PTA. COD = 1,5-cyclooctadiene, bipy =2,2'-bipyridine, NBS = N-bromosuccinimide, DMF = N,N-dimethylformamide.

Thermogravimetric analysis (TGA) showed good thermal stability up to 400 °C (see Figure 5.3 (a)) (decomposition temperature at 5% weight loss is 456 °C). Cyclic voltammetry of PTA was measured at room temperature (see Figure 5.3 (b)) and the HOMO level of the polymer in solution was estimated using the onset oxidation potential relative to the ferrocene standard according to equation 5.1.[184] This resulted in a HOMO energy level of 5.01 eV (see below and Table 5.1).

$$E^{HOMO} = [\ (\ E_{onset}^{\ ox} - E_{onset}^{\ reference}\ ) + 4.8\ ]\ \text{eV} \qquad (5.1)$$

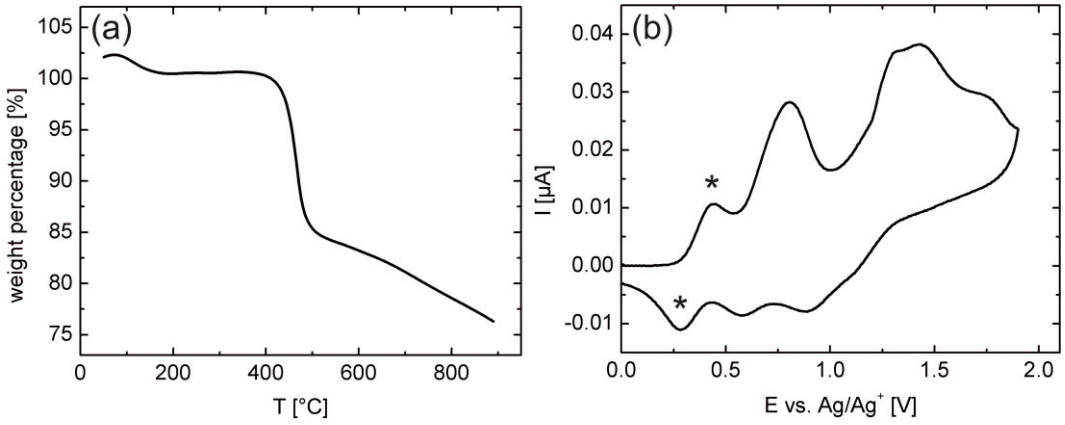

Figure 5.3: (a) TGA of PTA at a heating rate of 10 K/min under nitrogen atmosphere. (b) Cyclic voltammogram of PTA reported vs. ferrocene (anodic scans are shown, 10^{-3} M in 0.1 M Bu_4PF_6 – CH_2Cl_2 at a scan rate of 50 mV·s^{-1}). The asterisks denote the Fc^+/Fc oxidation/reduction process.

5.3 Thin Film Morphology

Figure 5.4 shows the topographic image of a typical PTA and P3HT film on SiO_2 after annealing at 120°C for 1h in high vacuum (p ~ 4 x 10^{-5} mbar). Both films exhibit a very smooth surface with a root-mean-squared roughness of ~0.4 nm. The amorphous, disordered morphology of the PTA film was confirmed by X-ray diffraction analysis, where no scattering patterns were observed (Siemens D501, Cu-tube in Bragg-Brentano configuration).[vii]

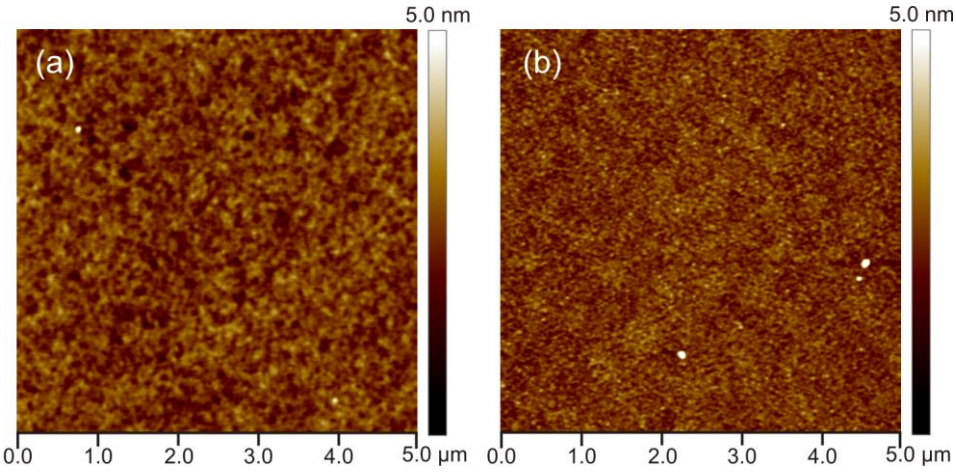

Figure 5.4: AFM topographic image of a typical PTA (a) in comparison to a P3HT (b) film on SiO_2 (scan size 5 µm x 5 µm).

5.4 Energy Levels and Optical Properties

5.4.1 UV/Vis Absorption and Photoluminescence Spectra

To investigate the photophysical properties of the PTA polymer, UV/Vis absorption spectra and photoluminescence (PL) spectra were recorded in diluted solutions of toluene and $CHCl_3$ (5 x 10^{-3} g/L) (Figure 5.5 and Table 5.1). The UV/Vis absorption maximum of PTA in toluene and $CHCl_3$ is at 383 nm and a second maximum is found at ~323 nm. The PL spectra of PTA in toluene (black line) and $CHCl_3$ (red line) differ significantly. The fluorescence spectrum of the toluene solution exhibits a maximum at 425 nm. In contrast, for the $CHCl_3$ solution the initial blue emission (at 425 nm) is significantly decreased and a second emission peak appears at 547 nm. Accordingly, a coloration of the $CHCl_3$ solution (from colorless to brown) was observed within a few seconds when the solutions were prepared under ambient light or exposed to UV-light (see Figure 5.5 (b)), while equivalent toluene solutions remained colorless.

[vii] The XRD investigations were performed by Alfred Neuhold within the group of Prof. Roland Resel, Institute of Solid State Physics, TU Graz.

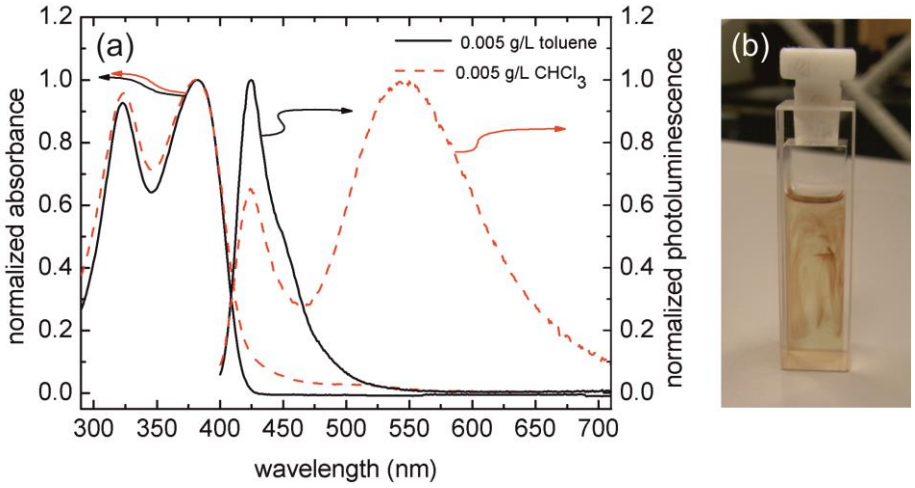

Figure 5.5: (a) UV/Vis absorbance and photoluminescence emission spectra of PTA in toluene (solid black line) and in chloroform (dashed red line); (b) corresponding PTA chloroform solution after UV/Vis absorption specotroscopy.

Table 5.1 UV/Vis maximum absorption wavelength and maximum emission wavelength (λ_{max}), bandgap energy (E_g), ionization potential (E_{HOMO}) and energy of LUMO level (E_{LUMO}) of PTA polymer.

Solution	Absorption (λ_{max}, nm)	Emission (λ_{max}, nm)	E_g^{opt} (eV)[a]	E_{HOMO} (eV)	E_{LUMO} (eV)[d]
toluene	323, 382	425	2.9	5.1[b]	2.2
$CHCl_3$	324, 382	424, 547		5.0[c]	

[a] Estimated from the onset of absorption in solid state. [b] Obtained from ultraviolet photoelectron spectroscopy.
[c] HOMO levels were calculated from the measured first oxidation potential versus Fc/Fc+ according to eq 5.1.
[d] Calculated using optical bandgap energy.

Influence of UV-light on PTA Solutions in Chloroform and Toluene

The influence of UV-light on PTA solutions was further investigated by preparing 1 g/L PTA toluene and chloroform solution under different light conditions. Figure 5.6 compares the fluorescence spectra of solutions prepared under ambient condition (black line), under yellow light (and kept in dark until the measurements) (blue dashed line) and exposed to UV-light (~10 s, λ = 254 nm and 366 nm) (red dashed/dotted line). In contrast to the toluene (a), the chloroform (b) solution spectra exhibit a significant influence of the ambient/UV-light exposure. A second peak appears around ~565 nm. The ~15 nm blue-shift of these emission peaks in comparison to the spectra of 0.005 g/L solution shown in Figure 5.4 can be ascribed to the high concentration (1 g/L) resulting in self-absorption effects of these solutions.

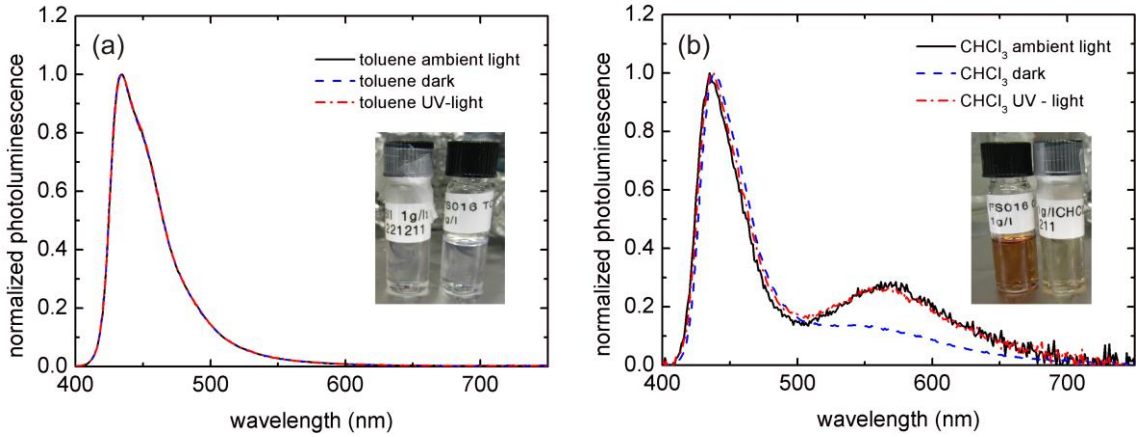

Figure 5.6: Photoluminescence emission spectra of 1g/L PTA solution in toluene (a) and chloroform (b) after preparation under ambient conditions (black solid line), in dark (blue dashed line) and after exposure to UV-light (red dashed/dotted line). Inset: corresponding solutions when prepared under ambient light (left) and in dark (right).

The inset depicts the accompanied color change of the $CHCl_3$ solution from colorless to brown solution when exposed to UV-light. This suggests that the coloration is caused by a halochromic effect, resulting from the well-known dissociation of $CHCl_3$ under UV-light (MUV, 200 – 300 nm) at which hydrochloric acid (HCl) is formed leading to protonation of the central nitrogen (N-protonation).[185-188] Reactions 1-3 describe the expected photolysis of $CHCl_3$ forming HCl: *hv* is the energy of the incident light with *h* the Planck constant and *v* the frequency, k_a and k_b are the corresponding reaction rates. In particular, when $CHCl_3$ is irradiated at $\lambda < 260$ nm $CHCl_3$ dissociates in chlorine atoms and dichlormethyl radicals (1), which further react with chloroform molecules: (2) dissociated chlorine atoms abstract hydrogen from $CHCl_3$ to form HCl with a rate of k_a; (3) the reaction of dichlormethyl radicals with $CHCl_3$ lead to dichlormethan CH_2Cl_2 and CCl_3 radicals with a rate of k_b.

$$CHCl_3 \xrightarrow{hv} Cl + CHCl_2 \quad (1)$$

$$Cl + CHCl_3 \xrightarrow{k_a} HCl + CCl_3 \quad (2)$$

$$CHCl_2 + CHCl_3 \xrightarrow{k_b} CH_2Cl_2 + CCl_3 \quad (3)$$

The formed hydrochloric acid within the PTA chloroform solution can then further protonate the basic nitrogen atom (nitrogen with a lone pair of electrons), leading to alterations of the photophysical properties (see Figure 5.7). It was reported, that in case of other nitrogen containing conjugated polymers, especially pyridine based materials, the effect of protonation have attracted considerable interest. For example it can be exploited as pH responsive materials for sensor applications or utilized to fine tune the optical properties.[187-190]

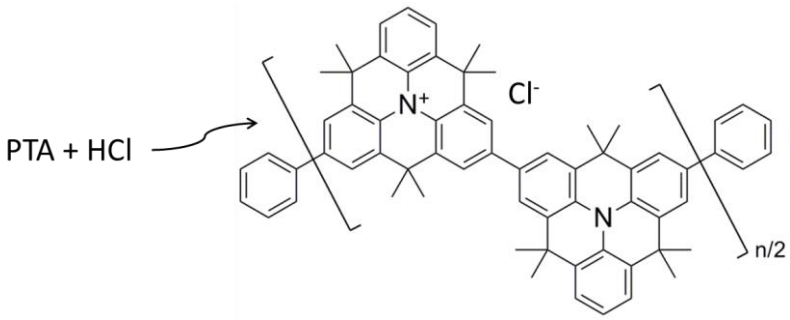

Figure 5.7: Illustration of a possible protonation reaction of hydrochloric acid with the central nitrogen atom on the PTA polymer.

In general, upon protonation an absorption band at higher energies is decreased while a red-shifted absorption peak appears. Similar behavior is observed for photoluminescence spectra, where an initial blue emission peak decreases and a red-shifted emission band increases for the protonated species.[187] For PTA, a significant influence was observed for the luminescence spectra, while for the absorption spectra only a slight non-vanishing tail for higher wavelength was recorded (see Figure 5.5 (a)). This might be a hint for low concentration of protonated species within the solution already at this stage. Since the solutions are exposed to UV light during the absorption measurements[viii] and the PL investigations were done afterwards the protonated amount is significantly higher for the latter, indicated by accompanied coloration (see Figure 5.5 (b)).

Moreover, Figure 5.6 shows that even if the $CHCl_3$ solution was prepared under yellow light and kept in dark, a non-negligible emission from 500 nm to 650 nm appears but is not as pronounced as for solutions prepared under ambient light or exposed to UV-light before the measurements. Besides considering the UV light exposure during the absorption measurements the light exposure during mounting the sample in the spectrofluorophotometer has to be taken into account. Moreover, it cannot be excluded that the used $CHCl_3$ has already contained a small amount of HCl. However for the 1 g/L solutions which were prepared under different conditions the absorption measurement cannot be conducted because of a too high solid content and therefore strong absorption.

Furthermore, to investigate the pH-dependent origin of the altered photophysical properties when chloroform is used, trifuoroacetic acid (TFA) and triethylamine (TEA) (base) was added to a PTA toluene solution in order to protonate and deprotonate the nitrogen atom, respectively. In this regard when using organic solvents, it is important to consider the solvent dependent pK_a values as well as the solvent basicity scale in order to avoid e.g. reactions of the acid with the solvent molecule instead of the polymer.[187,191]

[viii] Note that the absorption spectra is recorded from low to high energies.

Figure 5.8 (b) shows the toluene solution after adding 60 µl TFA (CF_3CO_2H), exhibiting a brown color, similar to chloroform solutions after exposure to ambient light (UV light) (Figure 5.9 (b)). The reversibility was shown by adding 80 µl TEA (Et_3N). For both protonated solutions (toluene + TFA, $CHCl_3$ + UV light) the addition of the base leads to deprotonation (colorless solution) (see Figure 5.8 (d) and Figure 5.9 (c)). Moreover, Figure 5.9 (a) depicts a $CHCl_3$ solution which was stored after exposure to UV-light in dark (several days), showing that the formation of HCl (and corresponding protonation) is also reversible.[186,187]

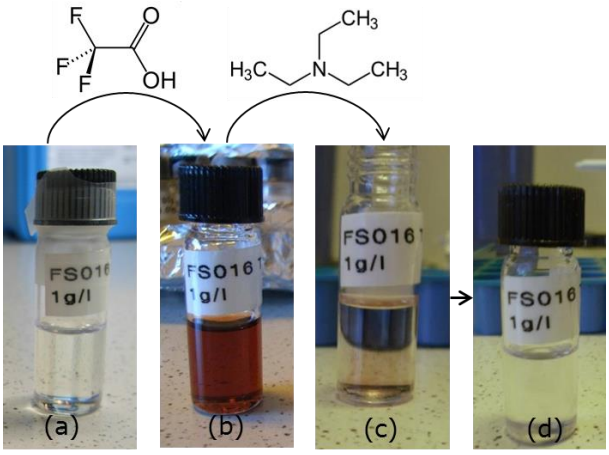

Figure 5.8: PTA toluene solutions under ambient light (a) after adding TFA to protonate (b) and TEA (c,d) to deprotonate the nitrogen.

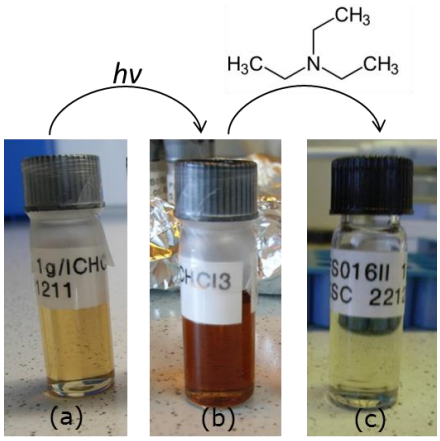

Figure 5.9: PTA chloroform solutions under ambient light after storing in dark (a) after exposure to UV light to protonate (b), after adding a base (TEA) (c) to deprotonate the nitrogen.

UV/vis Absorption and Photoluminescence Spectra of PTA in Solid State

Furthermore, UV/Vis absorption and photoluminescence measurements were also performed in solid state. Figure 5.10 displays corresponding spectra of PTA films spin-coated from 2 g/L toluene and chloroform solutions. The UV/Vis absorption maxima of PTA films were at 383 nm and

325 nm. An optical bandgap of 2.9 eV can be estimated from the onset of absorption with $E = hc/\lambda$ (h: Planck constant, c: speed of light).

The fluorescence spectrum of films prepared from toluene and $CHCl_3$ solution exhibits a maximum at 434 nm and 436 nm, respectively (see Figure 5.10). Compared to the results obtained for PTA solutions, the spectra of films showed no significant influence of the used solvent, which can be explained by the fact that the solutions for film deposition were prepared and spin-coated under inert atmosphere in absence of UV-light (no discoloration, no protonation effects were observed). Subsequently the films were dried under high vacuum ($p \sim 4 \times 10^{-5}$ mbar) at 120 °C to remove residual solvent.

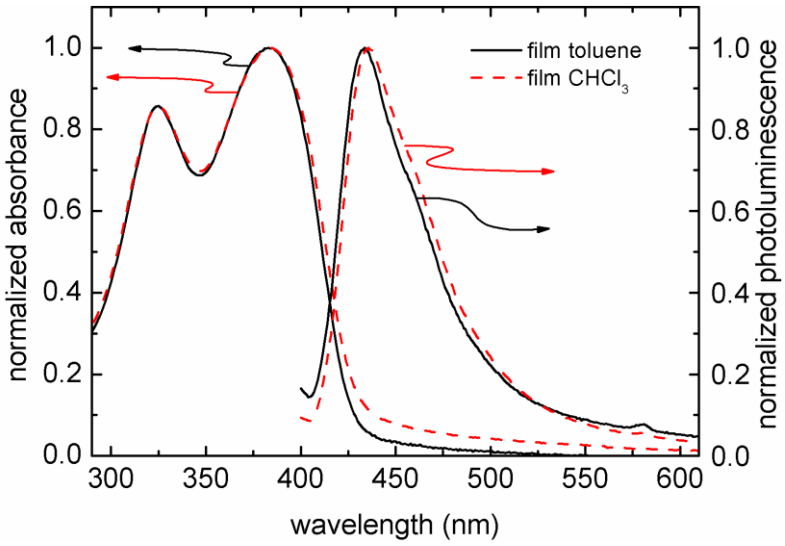

Figure 5.10: UV/Vis absorbance and photoluminescence emission spectra of PTA films prepared from toluene (solid black line) and chloroform (dashed red line) solutions.

5.4.2 Ultraviolet Photoelectron Spectroscopy - Energy levels of PTA

The energy levels of the PTA polymer and their alignment with respect to the Au Fermi-level was determined by ultraviolet photoelectron spectroscopy (UPS) (see chapter 3.2 for experimental details).[ix] PTA´s low binding energy onset is 0.7 eV below the Fermi-level (E_F) (Figure 5.11 (a)). Together with the work function (Φ = 4.4 eV, Figure 5.11 (a)) determined from the secondary electron cutoff, the ionization energy (IE) is 5.1 eV (Table 5.1). This is in good agreement with the result from cyclic voltammetry (E_{HOMO} = 5.0 eV, see section 5.2). The lowest unoccupied molecular orbital level was estimated by taking into account the optical energy gap of 2.9 eV (Table 5.1), resulting in the energy level scheme in Figure 5.11 (b). The deep HOMO level and the

[ix] The UPS investigations were performed by Stefanie Winkler within the group of Prof. Norbert Koch from Helmholtz Zentrum Berlin für Materialien und Energie GmbH Elektronenspeicherring BESSY II and Physics Intstitute at Humboldt University Berlin.

wide bandgap are responsible for the good stability of the PTA polymer under ambient conditions. In contrast, P3HT has its ionization energy at 4.5 eV (see below).

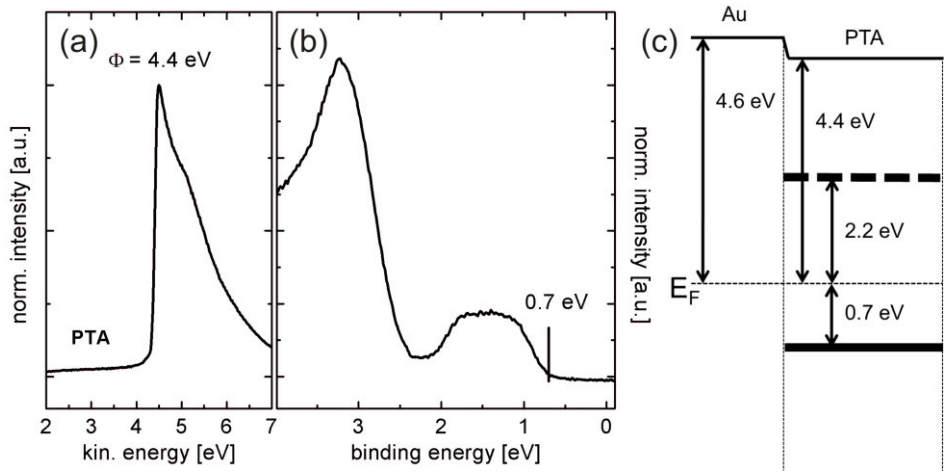

Figure 5.11: (a) Secondary electron cut-off and (b) valence region UPS spectra of PTA on Au/SiO_2 substrates. (c) Schematic energy levels of PTA with respect to gold.

Additionally, focus was set on the polymer-gold interface in order to correlate injection properties with the electrical characteristics. The hole injection barrier between gold and PTA is 0.7 eV and the interface dipole $\Delta\Phi$ is -0.2 eV. The determined work function of gold with 4.6 eV is rather low, but can be explained by hydrocarbon contaminations on the gold due to handling in air and exposure to chemicals used in the lift-off process, reducing the surface dipole (as shown by Rentenberger and coworkers[80]). In accordance, it is demonstrated that depending on the conditions prior to the measurements, different Au work function values were measured varying between 4.4 eV and 4.7 eV.

Work Function of differently treated Au

To determine the influence of different treatments and storing conditions on the work function of gold, various gold substrates were investigated. To resemble the conditions in the device after evaporation of gold, the sample was exposed to the lift-off chemicals used during the source/drain structuring process and stored in argon. The work function of these gold films was determined to be 4.58 eV (**Au**, Table 5.2). When the samples were stored in air (for ~2-3 days), the work function was lowered by about 0.15 eV ($\mathbf{Au_{air}}$, Table 5.2). Films exposed to the lift-off chemicals, which were additionally treated with 15 min HMDS, showed a work function of 4.53 eV ($\mathbf{Au^{HMDS}}$). The highest work function of 4.65 eV (still low due to storing in air) was obtained for gold films without any additional treatment ($\mathbf{Au_{air}^{pristine}}$, Table 5.2). The obtained values are in good agreement with results from literature.[80,192]

Table 5.2: Work functions Φ of differently treated gold films.

Sample	Au	Au_{air}	Au^{HMDS}	$Au_{air}^{pristine}$
Φ (eV)	4.58	4.43	4.53	4.65

Au: exposed to lift-off chemicals and stored in Ar,
Au^{air}: exposed to lift-off chemicals and stored in air,
Au^{HMDS}: exposed to lift-off chemicals and HMDS, then stored in Ar,
$Au_{air}^{pristine}$: without treatment but stored in air.

Energy Levels of P3HT

Figure 5.12 shows the results of ultraviolet photoelectron spectroscopy (UPS) of the P3HT polymer to determine the absolute location of the energy levels of P3HT and the relative alignment at the interface to gold. The secondary electron cut-off was found at 4.2 eV with respect to the Fermi level (E_F) and, in conjunction with the binding energy of the emission onset of 0.3 eV below the Fermi level, the corresponding ionization energy could be determined to 4.5 eV (see Figure 5.12 (a)). The LUMO can be estimated (E_{LUMO} = 2.6 eV) by using the optical gap energy of 1.9 eV, determined from UV/Vis absorption measurements in solid state (film of 2 g/L toluene, not shown). The corresponding energy level scheme is shown in Figure 5.12 (b).

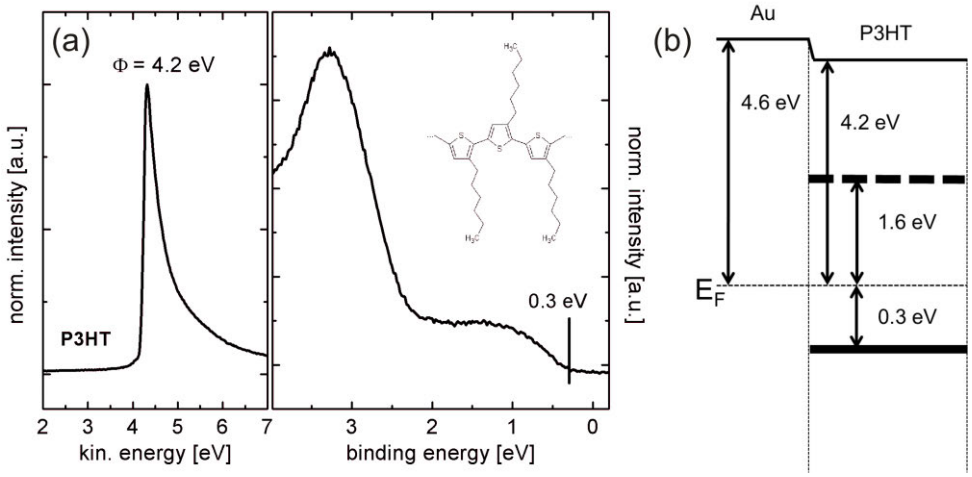

Figure 5.12: (a) Secondary electron cut-off and (b) valence region UPS spectra of P3HT on Au/SiO_2 substrates. (c) Schematic energy levels of P3HT with respect to gold.

5.5 Characterization of Organic Field-Effect Transistors based on a Novel Heterotriangulene Polymer

Investigations of PTA-based BG/BC OFETs revealed a clear p-type transport of the novel material with a rather strong influence of the applied surface treatments. Figure 5.13 (a) shows the transfer characteristics of PTA OFETs with different surface treatments (Table 5.3). The highest saturation mobility of 4.2 x 10^{-3} cm^2 $V^{-1}s^{-1}$ and on/off current ratio of ~10^5 were obtained for OFETs with HMDS treatment. These results are similar to literature values of other fully amorphous semiconductors such as PTAAs.[172] Figure 5.13 (b) depicts the output characteristics of a typical device, showing a negligible hysteresis.

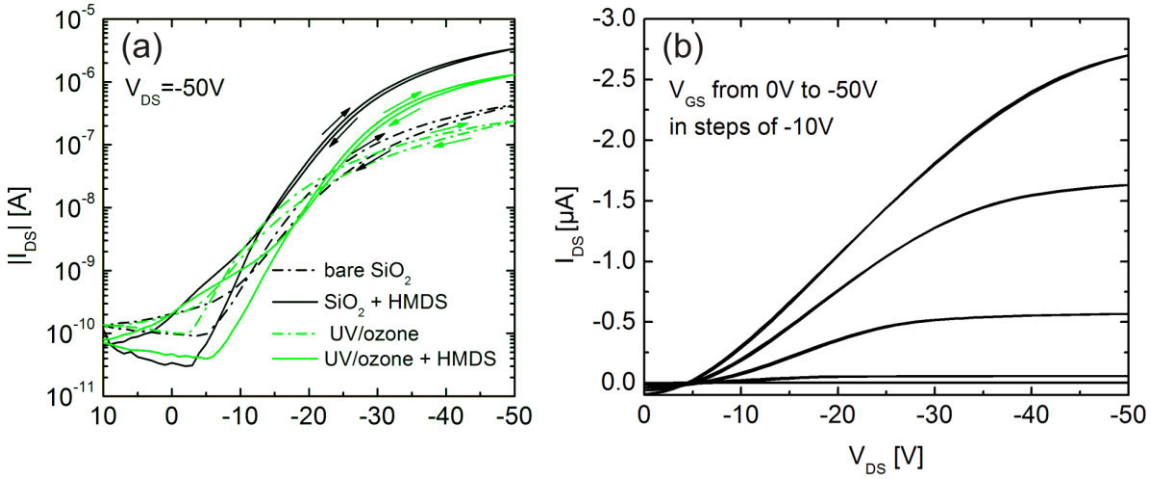

Figure 5.13: (a) Transfer characteristics of PTA OFETs with different surface treatments: bare SiO_2 (dashed black line), 15 min HMDS treatment (solid black line), UV/ozone treatment with (dashed green line) and without (solid green line) HMDS. (b) Output characteristics of a typical PTA OFET with HMDS treatment.

However, the absence of a clear linear characteristics at low drain voltage indicates a significant contact resistance, which can be ascribed to a high hole injection barrier, resulting from the energy mismatch of the PTA HOMO level and the low gold work function due to storing (of the S/D structures) in air. This emphasizes that the fabrication process is strongly correlated with charge injection/contact resistance of the electrodes. [79,192] To improve the injection of charge carriers, the gold contacts were UV/ozone and O_2 plasma treated inducing a thin AuO_x layer which increases the work function.[80,146,193] The treatment improved the linear region of the output characteristics (shown below in Figure 5.15), but at the same time one order of magnitude lower source-drain currents and mobility values (~2 x 10^{-4} cm^2 $V^{-1}s^{-1}$) were obtained (see Figure 5.13 (a) and Table 5.3). This can be also seen in Figure 5.14, where a comparison of O_2 plasma treated samples with samples without or solely HMDS treatment is shown. The observed lower on-currents, lower mobilities and higher subthreshold slopes *S* can be ascribed to a higher density of hydroxyl (OH-)

groups induced by UV/ozone or O_2 plasma treatment, which act as traps on the SiO_2 dielectric.[155,156] Additionally, O_2 plasma treated devices showed a positive switch-on voltage (V_{so}), and low on/off current ratios (high off-currents, high subthreshold slope) (see Table 5.3), which is most likely due to doping of the semiconductor and higher leakage currents.[194] By deactivating the OH-groups and decreasing the polar component on SiO_2 with HMDS treatment, the mobility could be increased again (~2.1 x 10^{-3} cm^2 $V^{-1}s^{-1}$, Figure 5.13 (a)). [162,195] In general, the modified performance of the PTA FETs due to different interface treatments can be attributed to a change of the hole injection barrier, the surface polarity, consequently an in-/decreased charge carrier trap density and doping, rather than changes in morphology.[161]

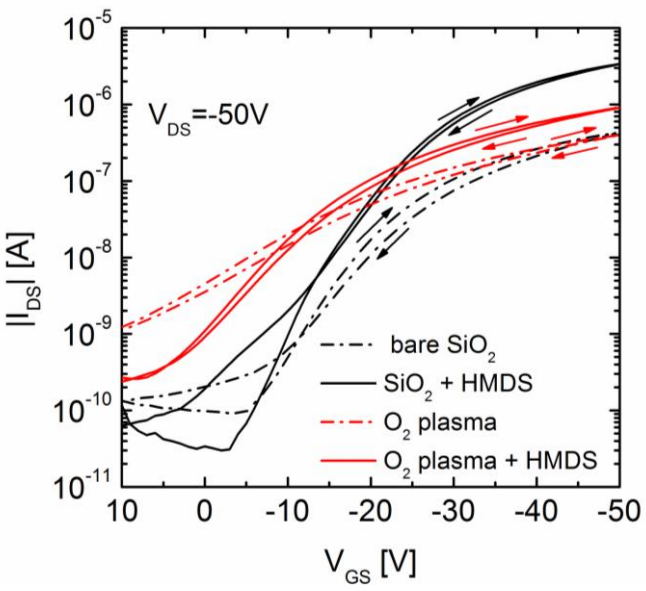

Figure 5.14: Comparison of transfer characteristics of PTA OFETs with different surface treatments: bare SiO_2 (dashed black line), 15 min HMDS treatment (solid black line), O_2 plasma treatment with (dashed green line) and without (solid green line) HMDS.

Table 5.3: Device parameters of BG/BC OFETs based on PTA with different surface treatments.

Surface modification	**HMDS treatment**[a]	**Mobility μ_{sat}**[b] **(cm^2 V^{-1} s^{-1})**	**I (on/off)**[c]	**V_{so} (V)**	**S (V/dec)**
O_2 plasma	-	$1.8 \cdot 10^{-4}$	$8.8 \cdot 10^{1}$	>10	15.7
UV/ozone	-	$1.5 \cdot 10^{-4}$	$2.3 \cdot 10^{3}$	-3	5.5
bare SiO_2	-	$4.1 \cdot 10^{-4}$	$4.4 \cdot 10^{3}$	-5	5.9
O_2 plasma	HMDS 15 min	$4.9 \cdot 10^{-4}$	$8.3 \cdot 10^{2}$	7	8.3
UV/ozone	HMDS 5s	$2.1 \cdot 10^{-3}$	$2.8 \cdot 10^{4}$	-6	5.3
bare SiO_2	HMDS 15 min	$4.2 \cdot 10^{-3}$	$1.0 \cdot 10^{5}$	-3	4.3

[a] different exposure times had to be used due to wetting problems,
[b] μ_{sat} was calculated according to the gradual channel approximation,
[c] on-current extracted at V_{GS} = -50 , V_{DS} = -50 V and off-current at V_{GS} = 0 V, V_{DS} = -50 V.

Output Characteristics of PTA-based OFETs with different Interface Treatments

Figure 5.15 depicts output characteristics of PTA-based OFETs with UV/ozone (b) and O_2 plasma (c) treatment of the dielectric surface and the electrodes compared to a reference device without surface modification (a). All samples were prepared without HMDS treatment. Figure 5.15 (b) shows that the UV/ozone treatment of the source/drain electrodes slightly improves charge carrier injection, indicated by an improved linear characteristics at low drain voltages. Moreover, the channel current is lower which can be explained by a higher density of OH-groups on SiO_2 (caused by the UV/ozone exposure), leading to charge carrier trapping. The output characteristics of OFETs with O_2 plasma exposure of the electrode-/dielectric surface show good saturation without injection problems (see Figure 5.15 (c)), being ascribed to (contact-) doping.

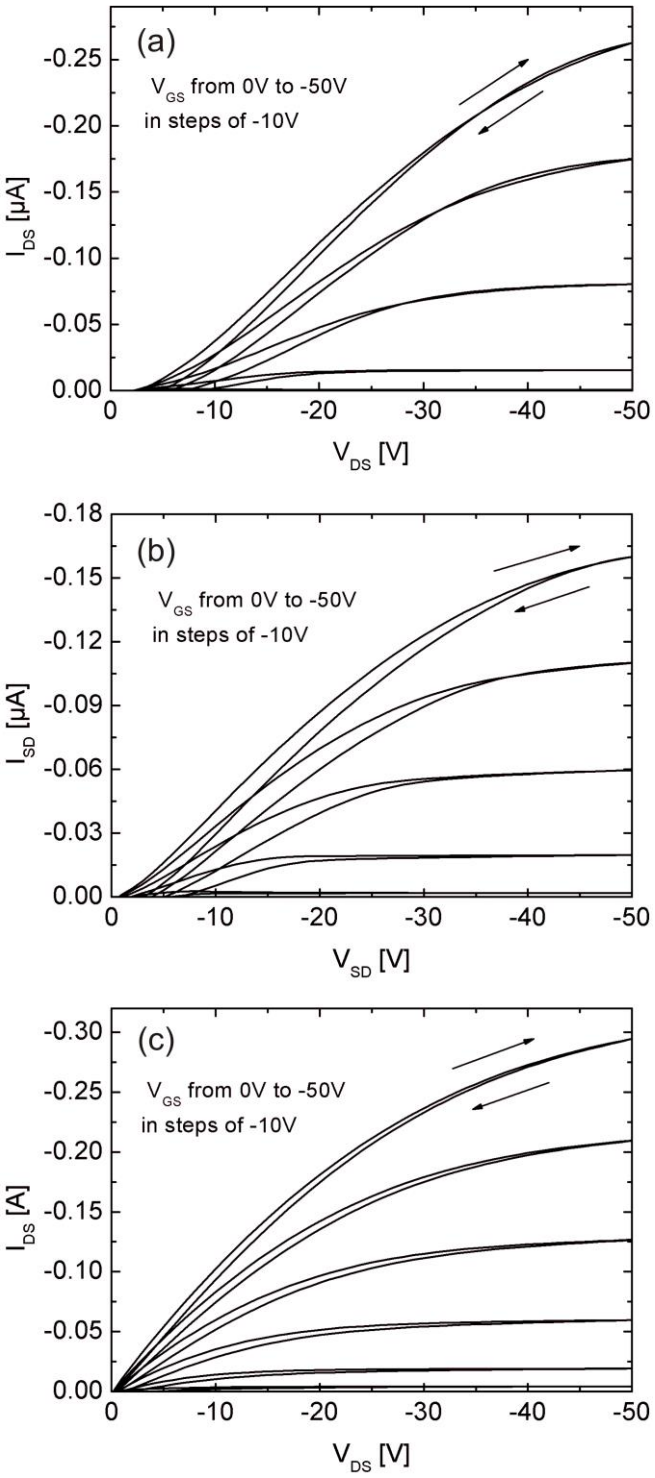

Figure 5.15: Output characteristics of PTA OFETs with different interface treatments: (a) bare SiO_2, (b) UV/ozone and (c) O_2 plasma treatment, (L = 25 µm, W = 2.85 mm, without HMDS exposure).

5.5.1 Influence of N-protonation on the OFET Performance

BG/BC OFETs were also fabricated to investigate the influence of $CHCl_3$ as solvent and the corresponding protonation reaction on the electrical properties of the PTA polymer. Figure 5.16 (a) displays the output characteristics of a PTA OFET (protonated) when the $CHCl_3$ solution was exposed to UV-light (~10 s, wavelength of 254 nm and 366 nm) prior to spin-coating. Solutions of reference OFETs (non-protonated) also shown were not exposed to UV-light and ambient light was kept at a minimum. For these devices, similar to the results for toluene, the output characteristics show a significant contact resistance. This is not the case with protonated (UV-light exposed) $CHCl_3$ solution, indicated also by good saturation behavior. Accordingly, the transfer curves show a higher off-current and a shift of the switch-on voltage to more positive values (see Figure 5.16 (b)). Both effects are most probable assigned to (contact-) doping of the PTA polymer.

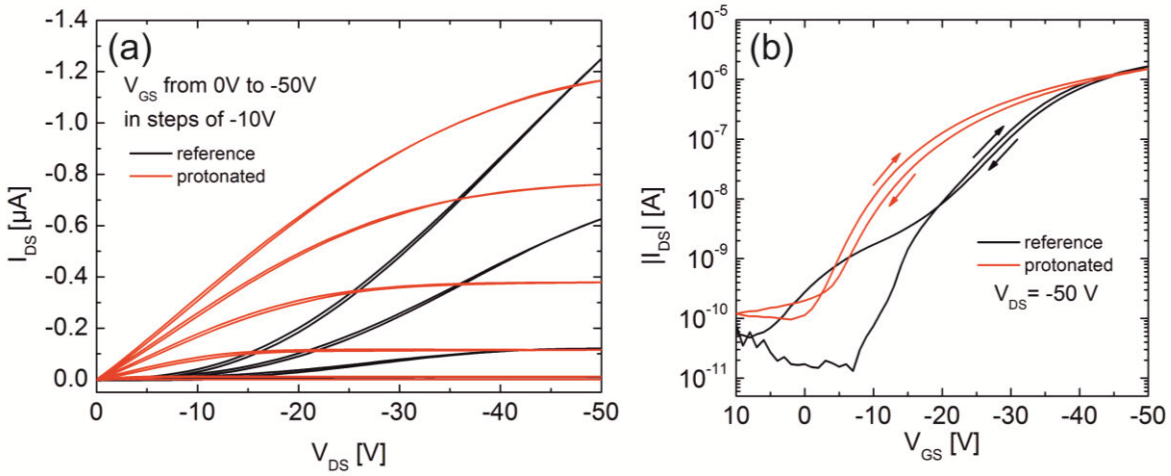

Figure 5.16: Output (a) and transfer (b) characteristics of PTA OFETs with (red lines) and without (black lines) UV-light exposure of the $CHCl_3$ solution prior to spin-coating in argon atmosphere.

The corresponding UV/Vis absorption and photoluminescence spectra of protonated PTA films ($CHCl_3$ solution was exposed to UV-light prior to spin-coating) showed in comparison to reference films (solution was not exposed to UV-light) no significant influence of the UV exposure. The maxima at 384 nm and 325 nm for the UV/vis absorption and 434 nm for the fluorescence spectrum are in good agreement with results obtained for PTA toluene films.

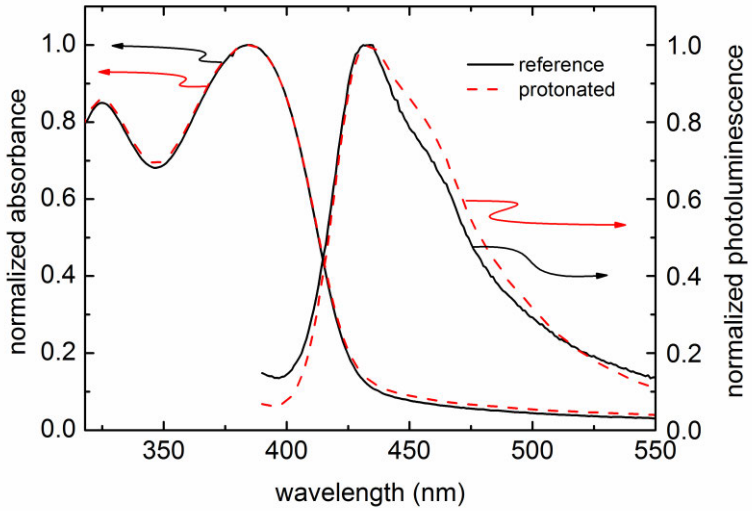

Figure 5.17: UV/Vis absorbance and photoluminescence emission spectra of PTA films prepared from $CHCl_3$ solutions without UV-light exposure (solid black line) and $CHCl_3$ exposed ~10 s to UV-light prior to spin-coating (dashed red line).

5.6 Ambient Stability Investigations

With regards to roll-to-roll production, ambient processing and stability are required, allowing for low-cost encapsulation. Organic semiconductors often degrade over time due to oxidation processes in presence of oxygen and water vapor. Therefore ambient stability of the PTA polymer in BG/BC OFETs was investigated and benchmarked against the widely used regioregular P3HT. The fabrication process was carried out in ambient atmosphere and the electrical characteristics were recorded under ambient light and a humidity level of 45-60 %. Figure 5.18 (a) and (b) show the output characteristics of PTA OFETs in comparison to P3HT devices. The source-drain channel current values are similar for both polymers but lower compared to PTA devices fabricated under argon atmosphere (see Figure 5.13). The linear regime at low V_{SD} is more pronounced and the contact resistance is lower than for devices fabricated under inert conditions. This can be attributed to (contact-) doping of the semiconductors due to water or oxygen.[196] The contact resistance of P3HT OFETs is even lower compared to PTA devices, ascribed to a lower hole injection barrier (0.3 eV, see page 60).

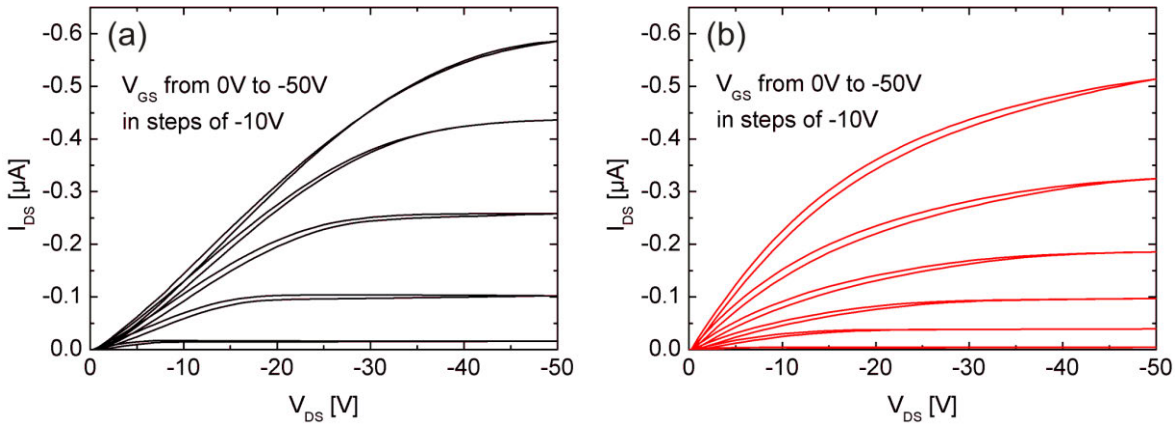

Figure 5.18: Output characteristics of PTA (a) and P3HT (b) FETs after fabrication and measurements in air and ambient light. (23-26°C, 45-60 % rh)

Table 5.4: Device parameters of BG/BC OFETs based on PTA in comparison to P3HT after storage in air (23-26°C, 45-60 % rh).

Sample	time	Mobility μ_{sat} [a] ($cm^2 V^{-1} s^{-1}$)	I (on/off) [b]	V_{so} (V)
PTA	as prepared	6.6×10^{-4}	1.1×10^{4}	-4
	1 week	8.3×10^{-4}	2.5×10^{4}	-3
	1 month	7.6×10^{-4}	1.8×10^{4}	-3
	2 months	6.3×10^{-4}	1.1×10^{4}	-2
	3 months	6.3×10^{-4}	2.6×10^{4}	-1
	4 months	6.3×10^{-4}	3.1×10^{4}	-1
	8 months	5.8×10^{-4}	1.8×10^{4}	0
	1 year	6.0×10^{-4}	2.6×10^{4}	0
P3HT	as prepared	2.5×10^{-4}	2.6×10^{3}	6
	1 week	2.7×10^{-4}	1.6×10^{3}	>10
	1 month	2.6×10^{-4}	3.2×10^{2}	>10
	2 months	2.1×10^{-4}	8.0×10^{1}	>10
	3 months	1.9×10^{-4}	6.6×10^{1}	>10
	4 months	1.6×10^{-4}	4.1×10^{1}	>10
	8 monts	8.0×10^{-5}	3.6×10^{1}	>10
	1 year	4.3×10^{-4}	4.9×10^{1}	~1

[a] μ_{sat} was calculated according to the gradual channel approximation,
[b] on-current I_{on} was taken at $V_{GS} = -50$ V, $V_{DS} = -50$V and off-current I_{off} at $V_{GS} = 0$ V, and $V_{GS} = -10$ V (for P3HT OFETs, being fully depleted for as prepared devices), $V_{DS} = -50$ V.

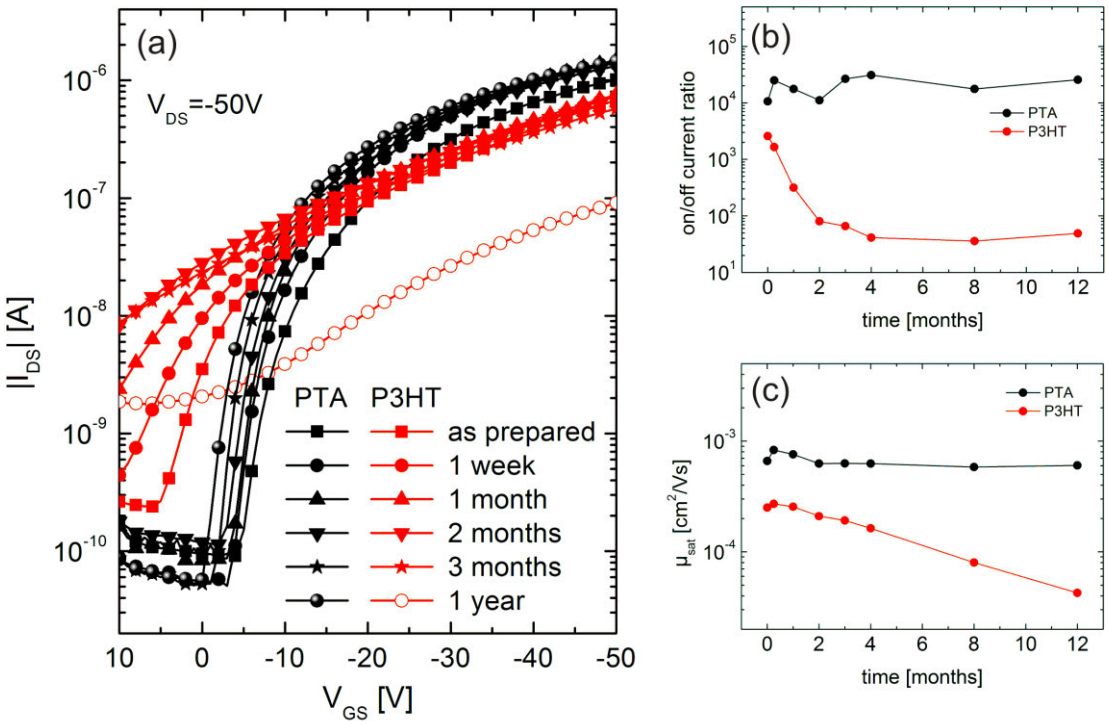

Figure 5.19: Semilogarithmic transfer characteristics (a) and extracted device parameter: on/off-current ratio (b) and saturation mobility (c) of PTA FETs (black) in comparison to P3HT (red) as a function of storing time measured in air and ambient light. (23-26°C, 45-60 % rh)

Several transfer characteristics and their extracted device parameters (mobility, on/off current ratio) as a function of storage time are displayed in Figure 5.19 (see also Table 5.4). The on/off current ratio of as prepared samples were determined to ~10^4 for PTA and ~10^2 for P3HT at V_{GS} = 0 V (and 10^3 for fully depleted P3HT FETs at V_{GS} = 10 V). The latter exhibited higher off-currents due to doping by oxygen and/or moisture.[38] This was also accompanied by a shift of the switch-on voltage to positive values. As a consequence of the deep lying HOMO level and the wide bandgap, even after storage of one year in ambient atmosphere (45-60 % rh, 23°C-26°C) PTA OFETs did not show any significant changes in device performance, providing excellent stability (Figure 5.19). Slight variations in field-effect mobilities and on/off ratios can be explained by varying levels of moisture and temperature. In contrast, P3HT FETs showed a large shift of the switch-on voltage to more positive values (>10 V) and a large decrease of the on/off current ratio (by a factor of ~40, see Figure 5.19 (b)) already after 3 months, due to doping.[38,75,197] Figure 5.19 (c) shows the gradually decreasing mobility of P3HT FET in comparison to the constant mobility values of PTA-based FETs over one year in air. Besides the deep lying HOMO level, being responsible for the excellent air stability, it is believed that the amorphous structure of PTA is also beneficial in comparison to the microcrystalline structure of P3HT. The latter exhibits grain boundaries which act as migration spots for water molecules and therefore increase the trap density.[75,198]

5.7 Conclusion

In conclusion, a novel air-stable polymer based on dimethylmethylene-bridged triarylamines was synthesized and investigated in BG/BC OFETs. This novel heterotriangulene polymer forms smooth amorphous films and reveal a clear p-type conductance. The optimization of electrode- and dielectric-polymer interfaces with various surface modification methods (HMDS, UV/ozone, O_2 plasma treatment) yielded mobilities of ~4 x 10^{-3} cm^2 $V^{-1}s^{-1}$ and on/off current ratios of ~10^5. It shows that PTA is a viable alternative for the best performing amorphous air-stable semiconducting polymers. Moreover, in the course of optimization the influence of different solvents on the device performance and optical properties (UV/Vis absorption and photoluminescence spectra) could be clearly attributed to hydrochloric acid which is formed in chloroform under UV-light and leads to protonation of the nitrogen on the PTA polymer. Due to its deeper lying HOMO level (E_{HOMO} = 5.1 eV) and wide bandgap (E_g = 2.9 eV) BG/BC PTA FETs fabricated, characterized and stored under ambient conditions showed excellent stability over months compared to P3HT. The latter showed a gradually decreasing performance in terms of on/off current ratio and mobility due to the well-known photo-oxidation of P3HT under ambient conditions, whereas the device parameter of PTA FETs remained high even after storing in air over one year. The combination of this robust performance with the ease of processing makes the new polymer a high potential candidate for large-scale low-cost production. There also appears to be considerable scope for further investigations regarding the significant sensitivity of the novel polymer in $CHCl_3$ solution to hydrochloric acid, due to protonation of the central nitrogen atom. This could enable the application of the novel PTA polymer as active material in pH-sensor elements.

6 Electrolyte-Gated Field-Effect Transistors for Sensing in Aqueous Media

Owing to the operational stability in direct contact with water combined with other desirable properties such as biocompatibility, mechanical softness, cost-effective processability on flexible substrates, electrolyte-gated organic field-effect transistor (EGOFET) based sensors constitute a highly promising novel sensor technology. Aside from the key features of sensors such as sensitivity, selectivity, reversibility and response time, the device stability is another important factor. Within this context, a combined study of poly(3-hexylthiophene)–based EGOFETs on various substrates is presented. In particular, the influences of different salt concentrations within the electrolyte and various gate electrode materials have been investigated. Furthermore, the limits of the stable operational window are evaluated and the effects when abandoning the latter are discussed. In addition, an explanation of the underlying mechanisms of degradations is given, being confirmed by the results of fluorescence microscopy and contact angle measurements. Moreover the possible origin of sensor drifts (decreasing currents) is addressed with long time investigations.[3]

The content of this chapter is based on work that has been published and was partly modified: K. Schmoltner, J. Kofler, A. Klug, E. List, *„Electrolyte-gated organic field-effect transistors for sensing in aqueous media“*, Organic Field-Effect Transistors XII; and Organic Semiconductors in Sensors and Bioelectronics VI, Zhenan Bao; Iain McCulloch; Ruth Shinar; Ioannis Kymissis, Editors, Proc. of SPIE 8831, 88311N (2013). Copyright 2013 Society of Photo Optical Instrumentation Engineers.

6.1 Introduction

Many sensing applications within biomedical diagnostics or environmental monitoring such as in-situ sensing of ions or biological substances require a stable operation in aqueous media. As mentioned in the fundamentals section 2.4, to obtain a water-stable OFET performance, low-voltage operation is crucial. Within this context electrolyte-gated OFETs are the transducers of choice, offering distinct advantages (see Figure 6.1). It is the direct contact between the organic

semiconductor and the electrolyte which enables low-voltage operation (below 1V) while monitoring high source-drain currents around a few µA. This is possible due to the formation of an electric double layer (EDL) at the electrolyte-organic semiconductor interface, exhibiting very high capacitance values (on the order of ~1-10 µF/cm^2).[127,132,133]

After the successful demonstration of the first water-gated OFET, several EGOFET based sensors for the detection of biomolecules such as DNA, dopamine, enzymes, proteins,[128-130] have been demonstrated and were excellently reviewed by Kergoat et al.[127] and Cramer et al.[120]. Moreover, we recently demonstrated the first electrolyte-gated OFET for selective and reversible ion detection, which is further discussed in chapter 7.

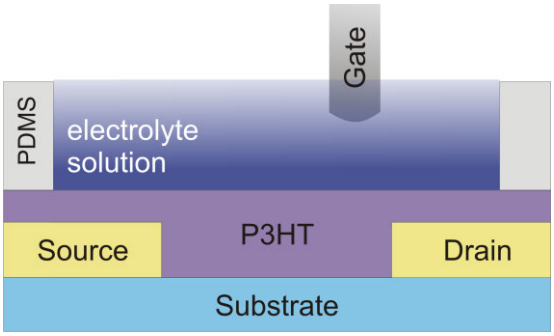

Figure 6.1: Scheme of an electrolyte-gated organic field-effect transistor.

However, in order to obtain a reliable sensor response, a stable device operation is crucial. In this context we present a combined study of the investigation of poly(3-hexylthiophene) (P3HT)–based EGOFETs on various substrates, gated using water and different concentrations of NaCl solutions. Moreover, the influences of different metal gate electrodes (Pt, Au) in comparison to an Ag/AgCl reference electrode are shown. The limits of stable operational windows were evaluated as well as the effects when abandoning the latter are discussed. Additionally contact angle measurements as well as fluorescence microscopy are conducted in order to understand the underlying mechanisms of degradation, and relevant electrochemical processes. Finally, after localizing the stable operational window long term stability measurements of EGOFET were performed to explain a potential sensor drift.

6.2 P3HT-based EGOFETs

EGOFETs were fabricated according to section 3.1 on different substrates such as glass, Si/SiO_2 or PET substrates. The structured source/drain electrodes exhibit channel length between L = 4 µm and 21 µm and channel width of W ~ 3 mm or W ~ 20 mm. Before the deposition of the semiconductor, HMDS was applied to SiO_2 and glass substrates via vapor phase deposition for an exposure time of 15 min. Adsorbed water on the substrate surface was removed by an annealing

step at 120°C in high vacuum (p ~ 4 x 10^{-5} mbar) for 1 h before a 4 g/L P3HT in toluene was deposited by spin coating. P3HT is known for its good film forming properties and very hydrophobic films. Both properties are necessary for water-gated transistors in order to prevent water molecules and ions to easily diffuse into the organic semiconductor film. The contact angles of water with the P3HT surfaces were determined to be ~105 ° independently of the underlying substrate. After adding the electrolyte (deionized (DI) water or various saline solutions (10^{-4} M to 10^{-2} M NaCl)) the EGOFETs were gated via an Ag/AgCl (3 M KCl) reference electrode, a 2 x 2 mm large and 50 nm thick gold (Au) pad or a platinum (Pt) electrode. Figure 6.2 shows typical samples with three P3HT-based EGOFETs with DI water as electrolyte before and during electrical conduction with an Ag/AgCl reference electrode.

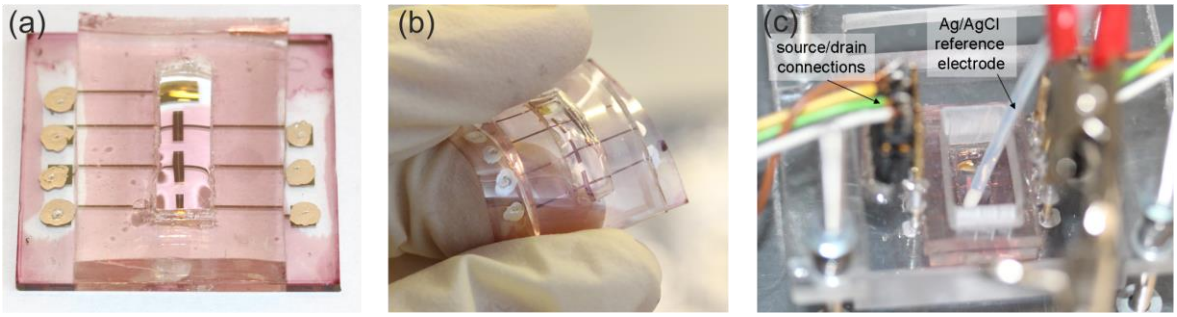

Figure 6.2: Typical sample with three P3HT-based EGOFETs with DI water as electrolyte on glass (a) and PET (b) before and after electrical contacted with Ag/AgCl reference electrode (c).

Figure 6.3 show the transfer and Figure 6.4 the output characteristics of typical P3HT-based EGOFETs with DI water as electrolyte, gated via an Ag/AgCl reference electrode. High on-currents of about 30 µA (V_{DS} = -0.4 V, V_{GS} = -0.5 V) were obtained due to the high W/L ratio, using an interdigital structure with L = 10 µm, and W = 20 mm (see inset in Figure 6.3). In Figure 6.3 (a) the transfer curves of three devices are compared, exhibiting only a slight device-to-device variation. The on/off-current ratios for the transfer curves at V_{DS}= -0.1 V are ~5 x 10^2 (on-current: V_{GS} = -0.5 V, off-current: V_{GS} = +0.2 V). In comparison, the on/off-current ratio in the saturation regime showed a lower value of about ~10^2, due to an increased leakage current. If the leakage current is on the order of the off-current, it significantly influences the on/off-ratio since $I_{DSoff} = I_{GS} + I_{DS}(V_{GS}<V_{so})$. The higher leakage current can be explained by a higher maximum applied potential difference (between drain-gate) of -0.7 V compared to -0.4 V in the linear regime. In general these high off-current, which originates from the leakage current, are considerable higher compared to OFETs based on conventional dielectrics instead of electrolytes. The threshold voltage in the saturation regime was determined to ~0 V and the mobility was estimated to be ~3 x 10^{-2} cm^2/Vs using a typical capacitance of 3 µF/cm^2 (for an Au/P3HT/water/Au system).[127] This is in good agreement with literature values.[127,132] Moreover, the origin of the small hysteresis can be attributed to charge polarization/ion movement in the electrolyte. These results, along with

the nice saturation behavior of the output characteristics in Figure 6.4 demonstrate a good overall device performance.

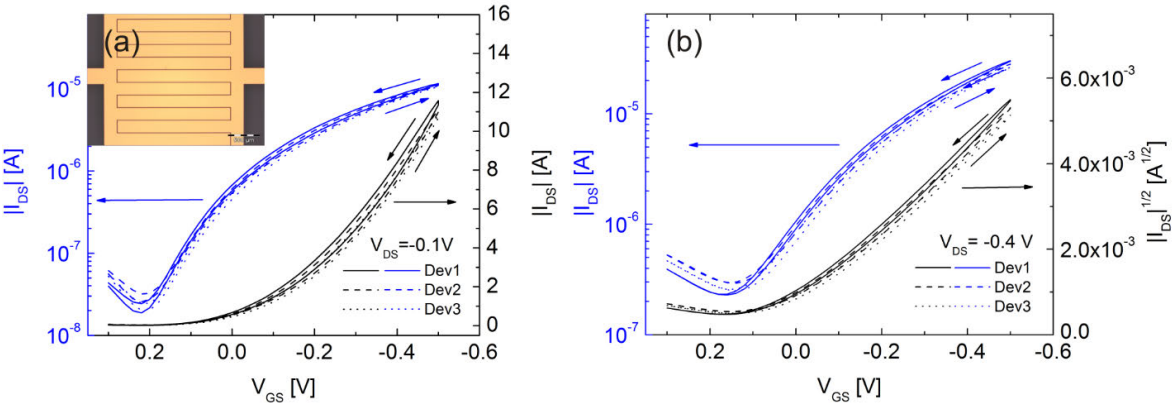

Figure 6.3:Transfer and semilogarithmic transfer curves of three P3HT-based EGOFETs gated via DI water with an Ag/AgCl reference electrode in the linear (a) and saturation (b) regime. Inset: micrograph of the interdigital gold source/drain structures before P3HT deposition (glass, L = 10 µm, W = 20 mm).

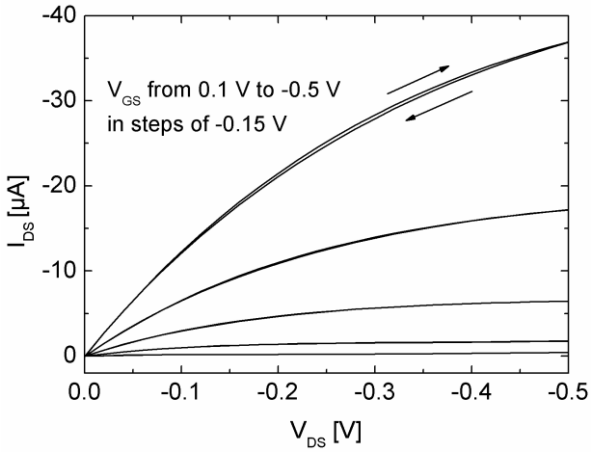

Figure 6.4: Output characteristics of a P3HT-based EGOFET (Dev1, above) gated via DI water with an Ag/AgCl reference electrode (W = 20 mm, L = 10 µm).

In Figure 6.5 (a) the transfer curves of devices with varying channel length (L = 5, 11, 21 µm) but same channel width (W = 3 mm) are compared, showing nice scaling behavior of the source-drain current. The on/off-current ratio and the threshold voltage in the saturation regime of the OFET with L = 21 µm, 11 µm and 5 µm channel were determined to I_{on}/I_{off} ~40, ~50, ~80, and V_{th} = -30 mV, -20 mV, +30 mV, respectively. Correspondingly, in linear regime the on/off-current ratios are higher (I_{on}/I_{off} ~100, ~120, ~250). The output characteristics of the shortest channel show nice saturation and no significant short-channel effects[75] (see Figure 6.5 (b)). It has been demonstrated that EGOFETs are most suitable for downscaling due to high transversal fields

generated by the very thin EDL, which inhibits short-channel effects.[199] Another advantage of electrolyte-gating is the lower contact resistance as reported by others.[200]

The maximum leakage current of about 200 nA is lower compared to EGOFETs with larger electrode area such as for interdigital structures (~ 480 nA). In detail, the electrode area is ~50 % smaller (2.6 mm^2) than the S/D electrodes of the interdigital structures (5.3 mm^2), being reflected in the corresponding leakage currents (see inset in Figure 6.5 (a)). With regards to EGOFET design this indicates, that the electrode areas in contact with the electrolyte should be kept small. Although the source/drain electrodes are not additionally encapsulated with e.g. a resin, the leakage current values are within an acceptable range. In general, the hydrophobic nature of P3HT impedes the ion penetration. Accordingly, the contact angle of DI water on P3HT layers was determined to ~105° (before electrical characterization), independent of the surface of the used substrate (glass, SiO_2 or PET).

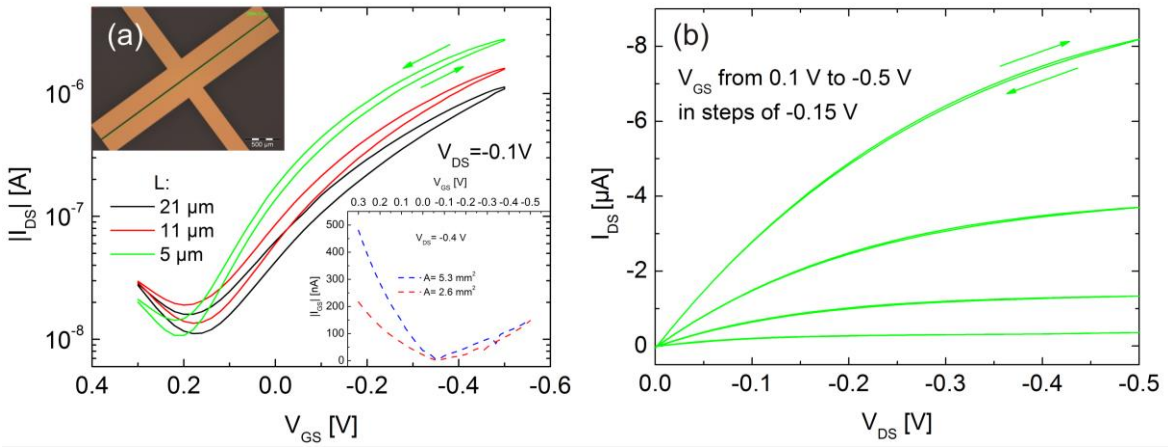

Figure 6.5: Semilogarithmic transfer curves of P3HT-based EGOFETs, gated via DI water with an Ag/AgCl reference electrode with different channel lengths but constant channel width: L = 21µm (black), L = 11 µm (red), L = 5 µm (green). Inset: micrograph of the gold source/drain structures before P3HT deposition and leakage current of EGOFET with different electrode areas. (b) Output characteristics of one of the EGOFETs compared (L = 5 µm, glass).

6.3 Influence of the Ion Concentration within the Electrolyte

In order to study the influence of the ion concentration (ionic strength) within the electrolyte on the device performance, NaCl solutions varying between 10^{-4} M and 10^{-2} M NaCl were used instead of DI H_2O. The corresponding semilogarithmic transfer curves and output characteristics are presented in Figure 6.6. In general, all measured devices show a threshold voltage shift to more negative values (V_{th} in saturation regime from -130 mV, -170 mV, -230 mV to -300 mV) upon increasing the NaCl concentration from DI H_2O to 10^{-4}, 10^{-3} and 10^{-2} M NaCl. On the other hand; the usually accompanied lower on-currents were not observed, since the slope of the transfer curves

increased. Consequently, the on-current slightly increased with increasing salt concentration. Moreover, the subthreshold slope decreased from 230 mV/dec to 190 mV/dec for the 10^{-2} M NaCl solution compared to the 2 orders of magnitude lower 10^{-4} M NaCl solution.

According to the models, describing the Debye-Helmholtz layer, the capacitance of the EDL increases with higher ionic strength of the solution, being an explanation for the slightly increased slope and nearly identical on-currents.[134] Since the substhreshold slope $S = \partial V_{GS}/\partial(logI_{DS})$ is closely related to the trap density at the semiconductor-electrolyte interface, the decreased value indicates a possible passivation of these traps. However, the V_{th}-shift might be explained by an enhanced screening of the surface charge (protons, hydroxyl ions) by more ions in the diffusion layer when the ionic strength is increased.[201] Similar results were obtained by Buth et al., who studied the influence of the pH and ionic strength on the performance of a α-sexithiophene based EGOFET.[132]

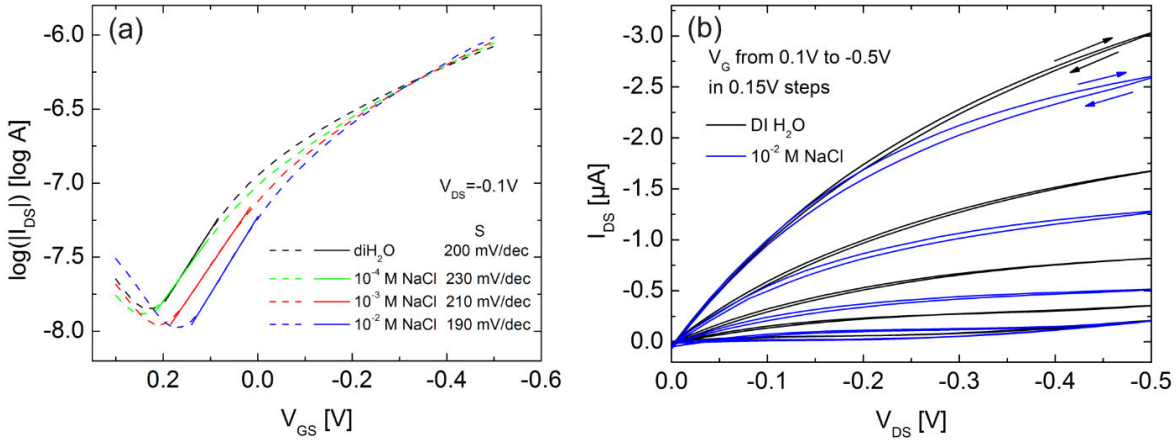

Figure 6.6: (a) Semilogarithmic transfer curve of P3HT-based EGOFETs gated via an Ag/AgCl reference electrode with different electrolyte solutions: DI H_2O (black), 10^{-4} M NaCl (green), 10^{-3} M NaCl (red) 10^{-2} M NaCl (blue);(b) Output characteristics of EGOFETs with DI H_2O (black) compared with 10^{-2} M NaCl solution as electrolyte (SiO_2, W = 3 mm, L = 4 µm).

Furthermore, a specific adsorption of ions at the semiconductor-electrolyte interfaces, introducing an additional capacitive contribution and thus altering the potential distribution, cannot be excluded. In general, it is important to note that the theoretical models of EDLs are simplified and experimentally verified only for specific and "highly defined" systems.[134] Already the considerations of EDLs for solid electrodes such as Pt, which are commonly used for many electrochemical investigations, are difficult, since it is difficult to get reproducible surface conditions (cleanliness, adsorbed impurities), which in turn changes the interface properties.

6.4 Influence of Various used Gate Electrodes

So far in this study only EGOFETs gated via an Ag/AgCl reference electrode have been presented. These reference electrodes function as a redox electrode with a fixed potential, i.e. the passage of current as well as different salt concentrations do not affect the electrode potential due to its nonpolarizable interface. Thus, any changes observed are due to changes at the semiconductor-electrolyte interface, which ideally constitutes a polarizable interface and are not due to changes at the electrode side. In a next step, P3HT-based EGOFETs were gated via Pt and Au electrodes. Basically, metal electrodes such as Pt can be used as quasi-reference electrodes, if the bulk solution and the potential of the electrodes do not change. A change in electrolyte concentration would result in a changed electrode potential.

Accordingly, the actual potentials of the quasi-reference electrode within a certain electrolyte have to be measured with respect to a reference electrode. For a Pt electrode, a potential of ~ 450 mV vs Ag/AgCl in 10^{-2} M NaCl was obtained. To contact the EGOFET via an Au electrode, an additional 2 x 2 mm Au pad was used and the potential was determined around ~250 mV vs Ag/AgCl in 10^{-2} M NaCl, exhibiting a strong drift.

To demonstrate the importance of an appropriate gate electrode, EGOFETs gated via Pt, Au and Ag/AgCl electrodes were investigated. Figure 6.7 shows the corresponding transfer characteristics, indicating a strong influence of the electrode used. Pt-electrode gated OFETs showed, a threshold voltage shift of about 400 mV to the positive direction (from -260 mV for Ag/AgCl to 140 mV for Pt in the linear regime) compared to Ag/AgCl gated, while the shape of the curve remains unchanged (see Figure 6.7 (b)). This is in good agreement with the measured potential of ~450 mV Pt vs Ag/AgCl, confirming the possible application of Pt as a quasi-reference electrode. On the contrary, this is not the case for the Au gate electrodes (pad), since the obtained threshold voltage shift does not match with the measured potential. Besides that the shape of the transfer curve completely changes, indicating that the interface/EDL at the electrode might also change (changing electrode potential). This altered behavior might be ascribed to the small electrode area of ~4 mm^2 in comparison to the P3HT coated S/D electrodes (~2.6 mm^2) which are of similar size and therefore strongly influences the voltage drop at the P3HT/electrolyte interface. Moreover, it might be also attributed to the non-reproducible Au surface due to the fabrication process as well as a possible reaction with the salt solution, especially chloride ions with Au.[202] This non-stable behavior has already been indicated by the potential drift of the Au electrode measured against the Ag/AgCl electrode.

This results show that, although the metal electrodes exhibit similar work functions around 5 eV (Au ~ 4.7-5.5 eV, Pt ~ 5.1-5.9),[80,203,204] it does not imply that similar threshold voltage shifts are

expected to occur. There are many other factors (as discussed above) which have a stronger influence on the V_{th}, such as the size of the electrode, contaminations and adsorbents on the surface, possible electrochemical reactions, etc. The investigation clearly demonstrates the importance of choosing an appropriate gate electrode and also indicates a good opportunity to tune V_{th}. Moreover, it highlights that sensing application inevitably require a reference electrode (nonpolarizable interface) so that the potential solely drops at the solution-semiconductor (polarizable) interface and potential changes consequently result in channel current variations.

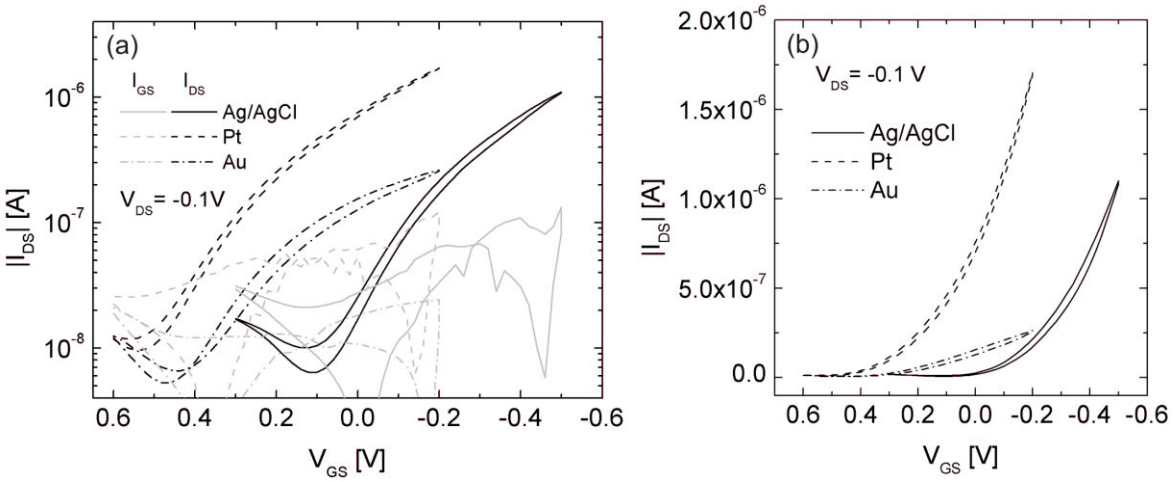

Figure 6.7: (a) Semilogarithmic and linear plotted (b) transfer curves of P3HT-based EGOFETs gated via different electrodes in 10^{-2} M NaCl in the linear regime: Ag/AgCl (solid line), Pt (dashed line), Au (dash-dotted line) (glass, W ~ 3 mm, L ~ 12 µm).

6.5 Stability Investigations of EGOFETs

With regards to sensor applications and a reliable sensor response, a stable device operation is crucial. Besides the environmental stability of EGOFETs, which is strongly dependent on the employed materials, the operational stability can be influenced by choosing a proper operational window with respect to the applied gate electrodes and electrolytes. In general, to allow for a good EGOFET performance all faradaic currents through the semiconductor-electrolyte interface (gate currents) should be avoided. Therefore, on the one hand an electrolyte with a large electrochemical window/high background limit[x,134] is needed to allow for a polarizable interface. On the other hand, a corresponding stable operational window for the applied potentials must be chosen. In our case, since we used aqueous electrolytes we are limited by the narrow stability range between oxygen and hydrogen evolution of water.

[x] The background limit is the potential at which significant cathodic and anodic current start to flow, when reduction (electrons flow from the electrode to the solution) and oxidation (electrons flow from the solution to the electrode) process start to appear, respectively.

Dynamic Operation

To investigate the limits of the stable operation window for our system and to demonstrate the device degradation when exceeding these operational potentials, P3HT-based EGOFETs gated via a Pt electrode in DI water were studied for different gate voltage sweeps. Figure 6.8 depicts the corresponding transfer curves, with maximum gate voltages of -500 mV and -700 mV. Maximum source-drain voltages of -500 mV were applied, resulting in a maximum potential difference ΔV of -1 V (at the beginning of the sweep) when V_{GS} is swept from +0.5 V to -0.5 V. These rather large voltages are applied for a few seconds since the gate voltage is swept with a rate of ~13 ms/mV. Anyhow, the transfer characteristics were reproducible within this voltage window (see black lines in Figure 6.8 (a)). However, when the gate voltage was swept from +0.7 V to -0.7 V, the subsequently recorded curve showed significant lower source-drain currents. Even though the voltage window was reduced again (+0.5 V, -0.5 V), the source-drain currents further decreased. The increased off-currents can be ascribed to higher leakage currents. These results indicate that once the potential exceeds a certain value or time, the current will continue to decrease also in case of a subsequent lower operational window. This decrease in current might be ascribed to bias-stress effects, but is more likely to be attributed to electrochemical reactions, leading to degradation of the semiconductor.

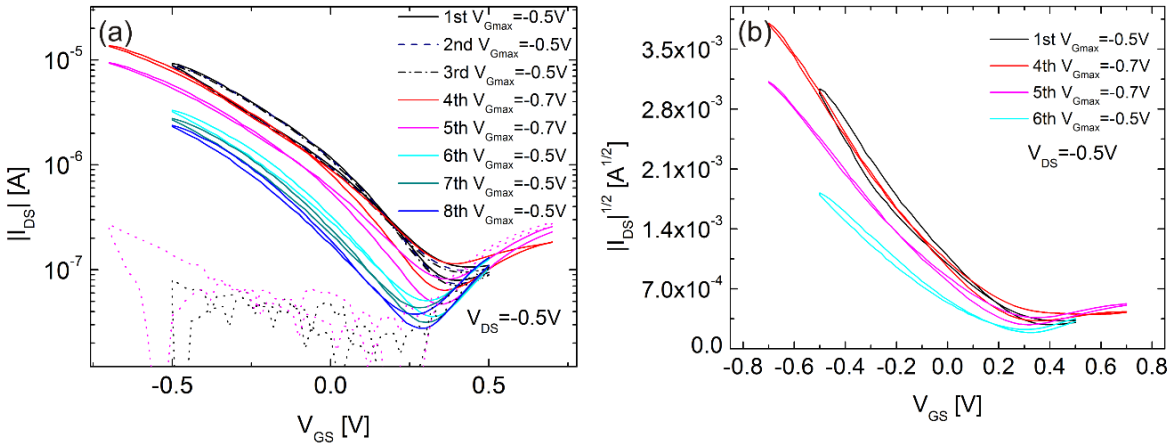

Figure 6.8. Semilogarithmic transfer curves (a) and square-root of the source-drain currents (b) vs. gate voltage of P3HT-based EGOFETs gated via Pt in DI H_2O at different maximum gate voltages (glass, W ~ 2.85 mm, L ~ 12 µm).

Static operation

To investigate the voltage-dependent current degradation versus time, the channel currents of exemplary P3HT-based EGOFETs with 10^{-2} M NaCl solution gated via Ag/AgCl were recorded at a constant working point. Figure 6.9 (a) shows the source-drain current vs. time at a stable working point (V_{DS} = -0.1 V, V_{GS} = -0.2 V). In the first 10-20 s an increasing current (black circles) is

observed, which can be ascribed to charging. Afterwards the current remains stable. If a gate voltage of -0.8 V instead of -0.2 V is applied (see Figure 6.9 (b), black stars), the channel current significantly decreases after ~ 60 s with time. After applying this high potential difference ΔV of -0.8 V (with respect to the source contact), the source-drain current significantly decreases with time also for a stable working point with low gate voltages (V_{GS} = -0.2 V) (see Figure 6.9 (a), red circles). This indicates that the measurements at elevated voltage changed the charge transfer properties significantly. In more detail, Figure 6.9 (c) shows the additional recorded gate and source currents during the measurement. It can be clearly seen that after a higher potential was applied, the leakage current significantly increased (red dashed line); a large part of the current flows from the source to the gate electrode, being responsible for the lower source-drain current. This was also confirmed by the recorded transfer curves after the static measurements, showing a decreased channel current as well as an increase in leakage current (Figure 6.9 (d)).

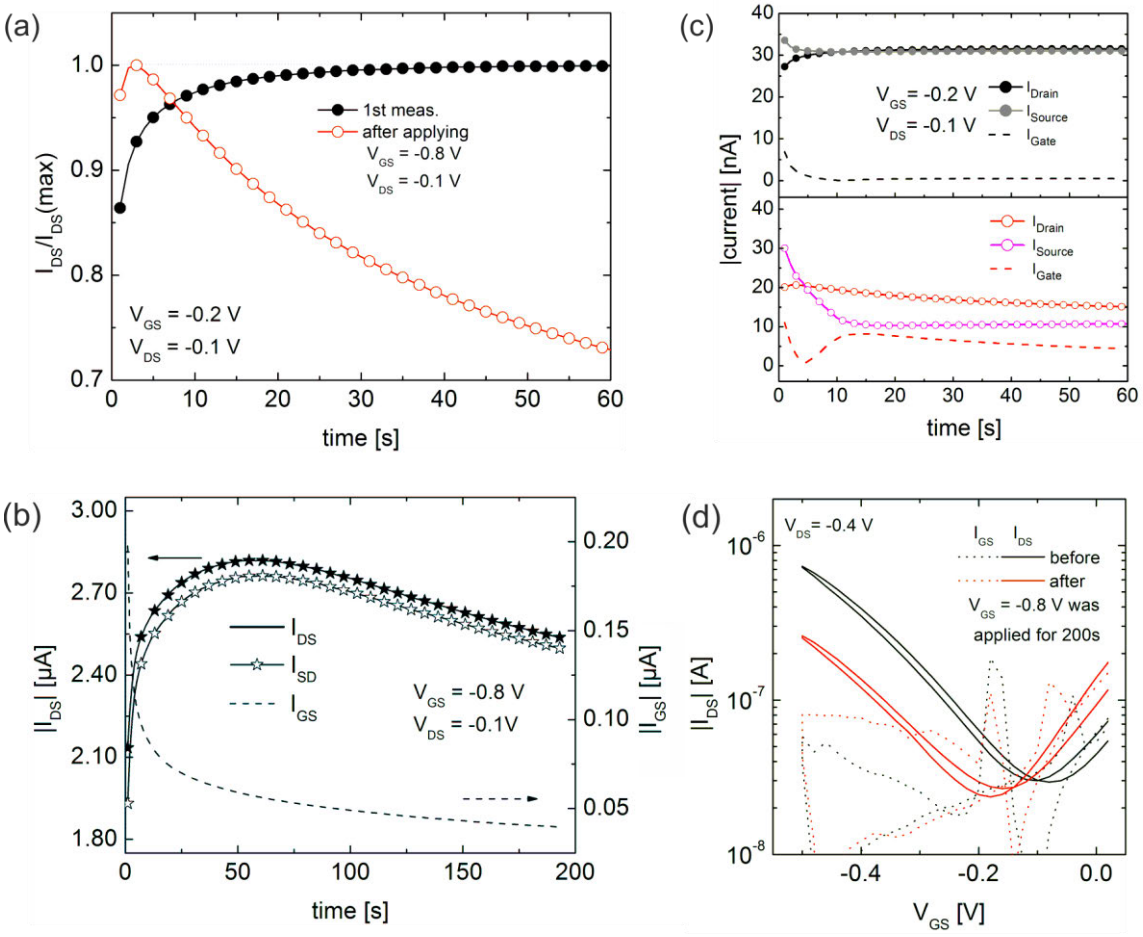

Figure 6.9. (a) Source-drain current vs. time at a stable operation point before (black) and after (red) applying a gate potential of -0.8 V for 200 s; (b) Source-drain current during applying -0.8 V at the gate electrode; (c) Source-drain currents (shown in (a)) with additionally measured source and gate currents; (d) Transfer characteristics before (black) and after (red) applying a gate potential of -0.8 V (glass, W ~ 3 mm, L ~ 4 µm).

An increasing gate current is a strong evidence for the occurrence of electrochemical reactions. The behavior of ion penetration and electrochemical doping has already been investigated to control the dimensionality of charge transport.[205] It was shown that the application of high voltages for extended operation times led to electrochemical doping of the whole film. Moreover it was demonstrated that materials properties like hydrophilictiy facilitates the ion penetration, leading to higher degree of electrochemical doping.

Effects on P3HT Films in Contact with Water after Exceeding a Stable Operational Window

After electrical characterization, a change of the wettability of the P3HT surface was observed for certain devices. This was usually the case if elevated potentials were applied, indicating the oxidation of P3HT. To investigate the corresponding contact angles of the P3HT surface, gold pads sufficiently large for contact angle measurements were evaporated on glass substrates. The thin P3HT films were deposited according to EGOFET fabrication (see section 3.1.3) and contacted via a DI H_2O droplet and a Pt electrode. After applying up to 1.5 V to the Pt/DI H_2O/P3HT/Au system the contact angle measurements of the P3HT surface with water revealed significantly decreased values (from 102 ° to 81 °), becoming more hydrophilic. In contrast, no significant contact angle variations (~5 °) were observed when the P3HT film was exposed to water for 30 min without applying a voltage. The effects of electrochemical doping on the P3HT surface wettability has already been demonstrated by others[206] and are in good agreement with our results. Moreover it was shown that these effects can be utilized for guiding water through microfluidic channels.[207]

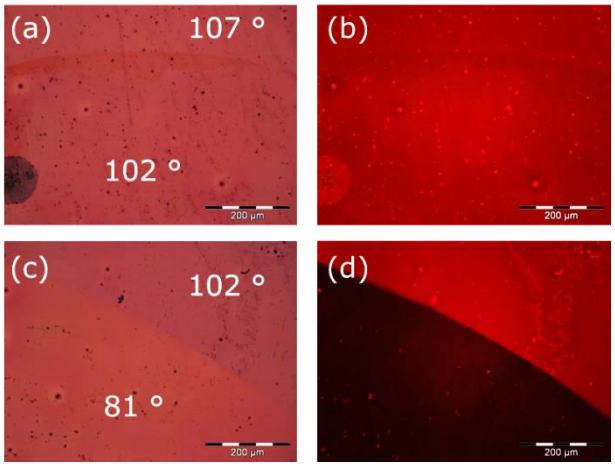

Figure 6.10: Micrograph (a,c) and fluorescence image (b,d) of a P3HT coated gold electrode after exposure to DI H_2O for 30 min (a,b) and after applying up to 1.5 V to the Au/P3HT/DI H_2O/Pt system (c,d). A significant color as well as fluorescence intensity change was observed after oxidizing the P3HT film.

Asides from the surface energy effects, the color of P3HT films also changed from violet to colorless (orange), accompanied by a decreased fluorescence upon electrochemical

doping/oxidative degradation (see Figure 6.10). These effects are well known from literature[38] and it was demonstrated that the decrease in fluorescence can be even exploited to investigate the time evolution of doping fronts.[208] Figure 6.11 shows the fluorescence image of EGOFETs after electrical characterization in 0.01 M NaCl and DI H_2O gated via Pt or Ag/AgCl electrode. In case of device 3 several transfer characteristics (-700 mV < V_{GS} < +300 mV) were recorded, whereas device 2 was only stressed few sweeps. The increased bias stress on device 3 results in a reduced fluorescence due to a higher degree of electrochemical doping compared to device 2. Their decrease is more pronounced at the source electrode, which can be attributed to a higher applied average potential difference between source-gate in comparison to drain-gate electrode: the drain potential is increased (from 0 V to -500 mV in 100 mV steps) after each gate sweep, while the source electrode is set to 0 V.

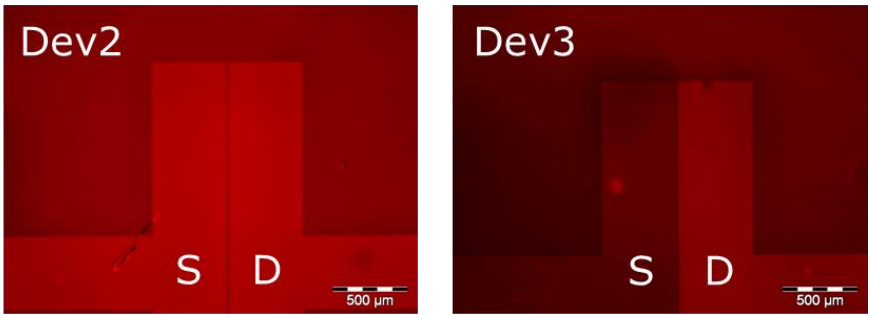

Figure 6.11: Fluorescence image of the source/drain electrodes of a P3HT EGOFET after contacting with 0.01 M NaCl in DI H_2O (Dev2) and recording transfer and output characteristic (Dev3) gated via Pt and Ag/AgCl.

We believe that the reason of the observed continuous current degradation can be ascribed to electrochemical reactions at the P3HT/electrolyte interface with hydroxide and chloride upon exceeding a certain potential. Moreover, the accompanied wettability increases as well as the fluorescence decline support the theory of oxidative degradation due to electrolysis of water. Kaihovirta et. al explained the observed degradation, which can even lead to vanishing current modulation at high potentials, to irreversible oxidative processes.[209] This over-oxidation might result in chain breaking and in the loss of conjugation as well as in the formation of sulfones, diketones, carboxylic acid, being an explanation for the loss in the electronic properties of the polythiophene.[210]

Long Term Stability

The obtained results demonstrate that EGOFETs using water or saline water solutions as an electrolyte must be operated well below 0.8 V. Accordingly, for long term stability monitoring, the channel current of an typical P3HT EGOFET gated via Ag/AgCl in DH_2O was recorded over two

hours at a stable working point within the linear regime (V_{DS} = -0.1 V, V_{GS} = -0.2 V), in order to avoid voltage dependent degradation (see Figure 6.12). During the first 30 minutes the channel current did not change significantly (0.4 nA/min). However, after that the decrease rate raised to ~1 nA/min, exhibiting a plateau in between (~45 – 65 s). The gate current remained stable around 1 nA.

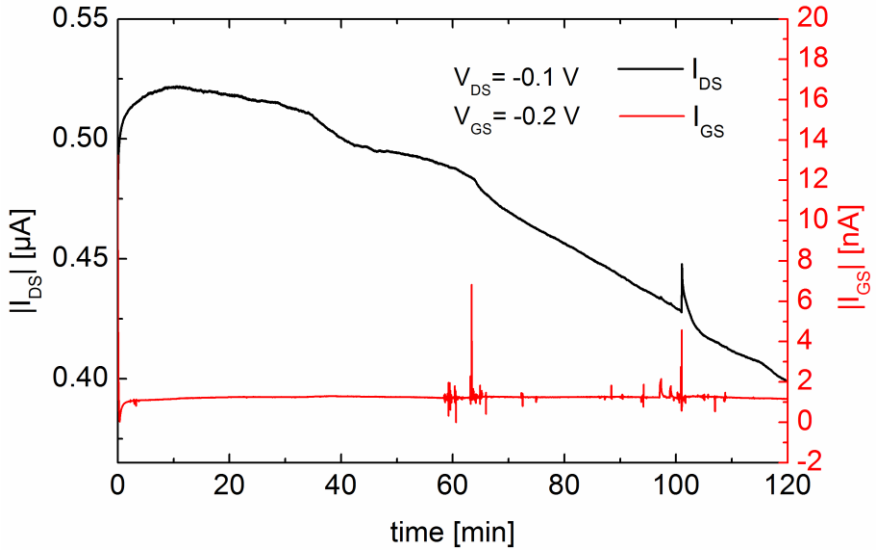

Figure 6.12: Source-drain current (black) and leakage current (red) vs. time of a P3HT EGOFET gated via Ag/AgCl in DIH_2O at a stable operation point recorded for 2h, (glass, W ~ 3 mm, L ~ 5 µm).

Moreover, before and after the prolonged measurement transfer curves were recorded (see Figure 6.13, black curves), featuring a similar current decrease after the long time measurements due to a threshold voltage shift to more negative values (dashed black curve). However, the comparison of these results with those of a reference device on the same sample exhibited similar tendencies (see Figure 6.13, blue curves). The reference device has been subjected to the electrolyte (DI H_2O) but has not been connected electrically (floating) during the long time measurements. This indicates that bias stress can be excluded as a reason for the decreased currents. It is more likely ascribed to the well-known P3HT degradation under ambient conditions (photo-oxidation)[38,175]. Furthermore, the diffusion of water molecules into semiconducting layer (P3HT) cannot be excluded[198] as another reason for the decreased current after long exposure to water electrolytes. Another indication of the migration of water into the P3HT film is the observed swelling/delamination when hydrophilic substrates (glass without HMDS treatment) were used. Figure 6.14 shows a dark field microscopy image of a typical P3HT film on glass after electrical characterization in water, exhibiting crack-like features.

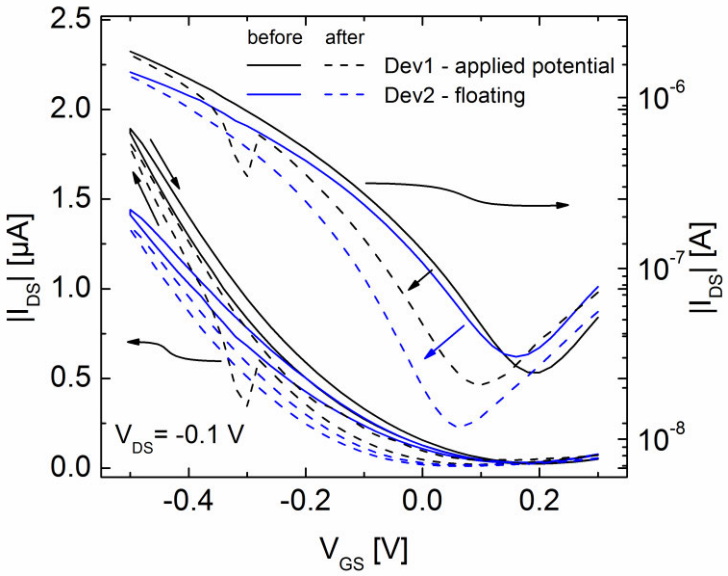

Figure 6.13: Semilogarithmic and linear transfer curves of P3HT-based EGOFETs gated via Ag/AgCl in DI H_2O in the linear regime before (solid line) and after the long time measurement (dashed line): Device 1 was measured during the long time test (black) and device 2 represents the reference device which was subjected to the DI H_2O but the electrodes were floating (blue) (glass, W ~ 3 mm, L ~ 5 µm).

Figure 6.14: Dark field microscope image of a P3HT film on glass (without HMDS coating) after exposure to water.

6.6 Conclusion

In summary, we have demonstrated P3HT-based EGOFETs gated in deionized water via an Ag/AgCl electrode, exhibiting a good overall performance with on-currents up to 30 µA. Due to the hydrophobic nature of P3HT the ion penetration is hindered so that negligible electrochemical reactions can occur within a water-stable window. We found that an increasing NaCl concentration (10^{-4} M – 10^{-2} M) results in significant threshold voltage shifts to more negative values, whereas the on-current showed a tendency to higher values, being ascribed to the higher capacitance of the EDL. The threshold voltage shifts might be explained by charge screening via an increased amount of ions within the diffusion layer. Moreover, we illustrated the importance of choosing appropriate gate electrodes by comparing Pt and Au electrodes with respect to a standard Ag/AgCl reference electrode. Pt-electrode-gated EGOFETs exhibited a significant shift of the threshold voltage, which was in good agreement with the measured potential difference in comparison to the Ag/AgCl electrode. On the contrary, completely altered transfer characteristics were obtained for EGOFETs gated with an Au electrode, which might be attributed to a non-stable electrode potential due to impurities on the surface as well as chemical reactions at the interfaces and the small electrode area. Moreover, this investigation indicated a good opportunity to tune the threshold voltages, being especially important for designing analogue and digital circuits. In general, the presented results are in good agreement with other reports of EGOFETs using other semiconductors (e.g. α-sexithiophene) or gate electrodes. Furthermore, we investigated the limits of a stable operating voltage window as well as the effects when abandoning the latter. A significant source-drain current decrease was observed when a high potential difference was applied. Accompanied with that, the leakage current significantly increased, which is a strong evidence for electrochemical reactions occurring. Moreover the wettability of the P3HT surfaces change to more hydrophilic films after applying high potentials. Asides from effects on the surface energy, the color of P3HT films changes from violet to colorless, accompanied by a decreased fluorescence which can be ascribed to electrochemical doping/oxidative degradation. Moreover the possible origin of sensor drifts (decreasing currents) has been addressed with long time investigations using a stable operational window. The comparable small current drifts of ~ 0.5 – 1 nA/min can be attributed to the well-known P3HT degradation under ambient conditions (photo-oxidation) and migration of water into the P3HT film rather than bias induced degradation.

To conclude, the presented results clearly demonstrate the influence of the salt concentration within the electrolyte and the influence of the applied electrode materials, being important factors for a proper design of EGOFET-based sensors including the evaluation of a stable operation window in order to obtain a reliable sensor response and avoid any electrochemical reactions to occur.

7 Ion-Selective Electrolyte-Gated Field Effect Transistor

Within the following chapter the first electrolyte-gated poly(3-hexylthiophene) thin film transistor for selective and reversible ion detection is presented. The inherent low voltage – high current operation of these electrolyte-gated transistors in combination with a state of the art ion selective membrane proofs to be a novel, versatile modular sensor concept. Based on field enhanced conduction, a sensitive linear response in the range of 10^{-6} to 10^{-1} M Na^+ with a slope of ~62 mV/dec was achieved. Furthermore this novel potentiometric sensor showed a reversible response and its selectivity was successfully tested against K^+ ions. This new concept is an important step towards a low-cost integrated ion sensor array for selective multiple ion detection, facilitated by a simple integration of different state of the art ion-selective membranes.

The content of this chapter is based on work that has been published and was partly modified: K. Schmoltner, J. Kofler, A. Klug, E. J. W. List-Kratochvil, „*Electrolyte-gated field effect transistor for selective and reversible ion detection*“ Adv. Mater. 25 (47), 6895-6899 (2013). Reproduced with permission from John Wiley and Sons.

7.1 Introduction

Ion sensors find their application in many different areas, ranging from food quality control where e.g. nitrate and nitrite concentration in meat and vegetables are of importance, or water monitoring for the detection of heavy metals (lead, cadmium, mercury and copper) to pharmaceutical and cosmetics industry where the concentration of e.g. fluoride and pH of tooth paste is of interest.[211] However, one of the most frequent routine applications of ion sensors is found within biomedical diagnostics e.g. the clinical analysis of blood. Within the human body electrolytes are in a delicate balance. For example electrolytes such as Na^+, K^+, Cl^-, HCO^-_3, Ca^{2+}, Mg^{2+} and H^+ ions are crucial for the regulation of the body's water balance or the activity of the nerves and muscle cells. An imbalance of these ion triggered by various diseases can even lead to life-threatening situations,

indicating the importance of high throughput clinical analyzer and point-of-care instruments.[212] To date, the potentiometric ion sensors in these systems are based on ion-selective electrodes (ISEs), which history goes back to the discovery of pH-sensitive glass in 1906 by Max Cremer.[213] Since the first commercial pH glass electrode was available (in 1930s), ISEs have been developed for a large number of inorganic and organic ions and became one of the most successful types of chemical sensors. This only became possible by the introduction of polymeric ion-selective membranes (ISMs) containing neutral or charged ionophores, which are available for the selective detection of many different ions. Moreover during the past decade the sensing abilities of ISMs have been improved to such an extent that it resulted in a "new wave of ion-selective electrodes".[214] This was achieved due to considerable improvements of the lower detection limit, new membranes, new sensing concepts and deeper theoretical understanding of the potentiometric response of ISMs. One of the current challenges includes the downscaling of ion sensor which requires suitable solid-state transducers in order to integrate sensor arrays to simultaneously detect multiple ions and allow for miniaturized ion-sensor systems for in-situ monitoring.

In this context electrolyte-gated OFETs seem to be the transducer of choice, exhibiting an excellent water-stable performance. In contrast to the conventional ion-sensitive FET architecture[96,114], where the analyte is in contact with a solid gate dielectric, EGOFETs benefit from a direct contact between the organic semiconductor and the analyte. The electric double layer of high capacitance ($\sim$1 - 10 μF cm^{-2})[127,128] formed at this interface enables low-voltage operation, which ensures a water-stable operation window, while the achieved source-drain currents (in the range of a few μA) are sufficiently high for further signal processing.

Compared to the ISE where the ion concentration is determined by measuring the electrical potentials with a voltmeter, FET-based sensors exhibit a considerable advantage, which is the impedance transformation at the spot of the measurement. The high impedance input signal (the gate potential) is potentiometrically measured by transforming it into an amplified source-drain current of low impedance. Therefore a rather simple electronic is needed for read-out. Moreover, owing to their intrinsic amplification FET based sensors typically reveal a high sensitivity. In conjunction with the outstanding features of organic electronic devices such as economic production, integration on flexible substrates and biocompatibility, low-cost disposable sensor assemblies are not a future vision anymore. So far, EGOFET-based sensors for the successful detection of biomolecules have been demonstrated using different sensing concepts. In order to obtain a sensitive as well as selective response different interfaces within the standard EGOFET architectures have been modified. One approach is the functionalization of the gate electrode (modifying gate-electrolyte interface) with self-assembled monolayers to selectively adsorb and

sense biomolecules e.g. dopamine down to pico-molar concentrations.[129] Another group presented the detection of penicillin by modifying the semiconductor/electrolyte interface with enzymes.[130]

However, based on this emerging EGOFET technology minimal investigations have been made on the selective sensing of ions. We recently demonstrated for the first time an EGOFET for selective and reversible ion detection.[4] A sensitive and selective response to sodium ions (Na^+) is obtained by introducing a state of the art ion-selective membrane, combining the aforementioned advantages of EGOFETs with the key sensing element of the well-established ISE technology. A detailed description of this novel concept and its sensor function is given in the next section. Before implementation, the ISMs were characterized within an ion-selective electrode configuration. The ion-selective EGOFETs based on poly(3-hexylthiophene) were electrically characterized with respect to their transistor performance as well as sensitivity to sodium ions. Furthermore, this potentiometric sensor was tested with respect to reversibility and selectivity against interfering potassium ions (K^+).

7.2 Novel Ion Sensing Concept

A schematic cross-section of the introduced ion-selective EGOFET is shown in Figure 7.1 (a), which basically consists of a bottom-contact P3HT EGOFET as transducer and an ionophore-doped polyvinylchloride (PVC) based ion-selective membrane (ISM) as the sensing element. The P3HT layer is in direct contact with an optimized inner filling solution (water containing 10^{-2} M NaCl), and separated via the ion-selective membrane from the analyte (water with different ion concentrations). The latter is in contact with an Ag/AgCl (3 M KCl) reference electrode. The mounted flow cell allows for a continuous exposure of the sensor device to different salt concentrations. This architecture is modular and facilitates the realization of ion-selective EGOFETs for the detection of various ions "simply" by introducing appropriate ISMs. The latter are well-established components which are usually applied in ion-selective electrodes.[215,216,217] Due to their vast dissemination they are available with a large variety of different ionophore-doped sensing membranes.[218] Their working principle is not based on a selective transport through the membrane as for example it is the case for filtration, osmosis or gas separation. In contrast, it relies on the ion movement over a few nanometers at the analyte-ISM and the ISM-inner filling solution interface forming a charge separation layer (see Figure 7.1 (c)). The arising phase boundary potentials at these interfaces result in an activity dependent membrane potential (E_{mem}) which is given by the Nernst equation:

$$E_{mem} = E^0 + \frac{RT}{z_i F} \ln\left(\frac{a_{analyte}}{a_{inner}}\right) \tag{7.1}$$

where E^0 is a constant, R the gas constant, z_i the valency of the analyte ion and F the Faraday's constant. In detail, this Nernstian membrane potential is determined by the ion activity difference between the analyte and the inner filling solution. In our case, the ion activity of the inner filling solution is kept constant (10^{-2} M NaCl) and the potential of the analyte is predefined through the Ag/AgCl gate electrode. Thus the potential of the inner filling solution is modulated solely by the ion activity in the analyte (see Figure 7.1 (b)). In fact, it is the potential of the inner filling solution (gate potential + membrane potential), hereby referred to as *effective gate potential*, which controls the source-drain current.

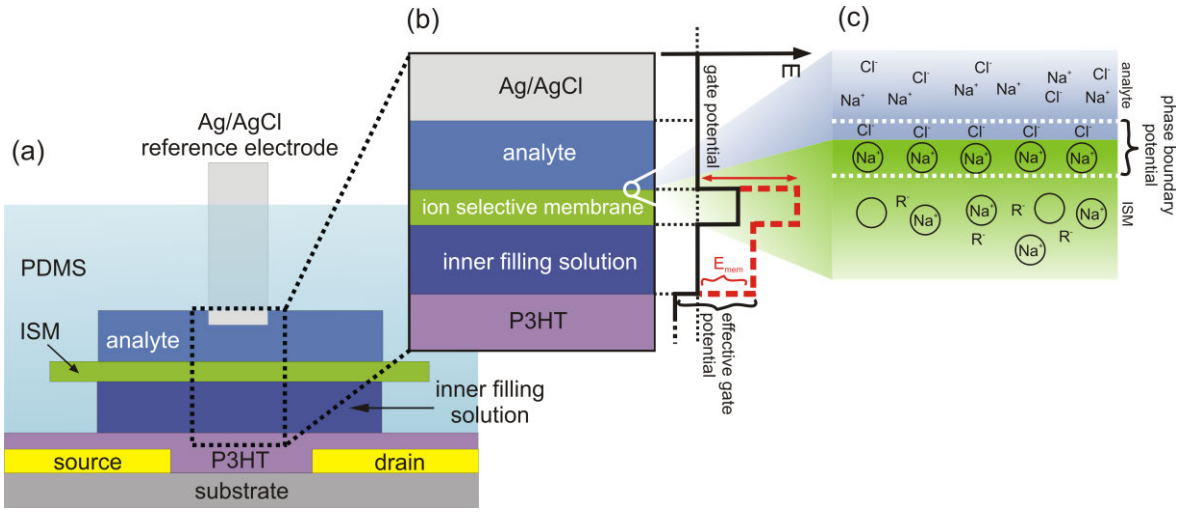

Figure 7.1: Cross section of an ion-selective EGOFET (a) and relevant interfaces to explain the sensor function (b): the bulk potentials in case of equal ion concentration in the analyte and the inner filling solution (black) and in case of lower concentration in the analyte (red dashed) are illustrated as well as the formation of the phase boundary potential at the analyte-ISM interface (c).

In contrast to other OFET sensor concepts, this approach is potentiometric and no direct modification of the organic semiconductor takes place which leads to a higher overall device stability. Since no binding happens at the interface (such as with enzymes etc.),[130] reversible detection is possible by simply flushing the device using a mounted flow cell. Thus no complex recovery process is needed. Moreover the transducer (EGOFET) is in direct contact with a constant optimized inner filling solution so that the performance (in terms of V_{th}, μ, g_m,…) of the EGOFET is not altered by a changed ion concentration as shown in chapter 6.3 p. 75. However, if the semiconducting layer is in contact with the analyte as shown by other approaches[219], the sensor signal relies on a mixed response of the ISM and the EGOFET due to a modified electrolyte/OSC interface. This can even lead to a deteriorated transistor performance, where the leakage current significantly increases when e.g. substances with a low electrochemical window or depolarizer[xi] are

[xi] Depolarizer is another word for an electroactive substance which is preferentially oxidized or reduced, and added to a solution to prevent an undesirable electrode reaction.

present within the analytes. We recently demonstrated that an ascorbic acid containing electrolyte leads to a P3HT-electrolyte interface which is not polarizable any more.[220] In contrast, for a proper transistor/sensor function the semiconductor-electrolyte interface should be ideally polarizable (high impedance, no faradaic current passing) in order to ensure that the potential solely drops only at this interface. On the other hand, the gate electrode should allow for faradaic current to pass without changing the potential of the electrode (non-polarizable) as well as being independent of the sample concentration. Hence, standard Ag/AgCl reference electrodes within a 3 M KCl inner filling solutions were used.

7.3 Fabrication of Ion-Selective EGOFETs

Ion-selective EGOFETs were fabricated according to section 3.1 on PET substrates. The structured source/drain electrodes exhibit channel length of ~ 7 µm, channel width of ~ 3 mm. Adsorbed water on the substrate surface was removed by an annealing step at 120°C in high vacuum ($p \sim 4 \times 10^{-5}$ mbar) for 1 h before a 4 g/L P3HT in toluene was deposited by spin coating. The films were dried at 60 °C in Argon (Ar) for ~10 min and subsequently at 120 °C under high vacuum ($p \sim 4 \times 10^{-5}$ mbar) for 1 h. All devices were assembled under inert atmosphere. In order to obtain a sensitive as well as selective response to sodium ions a state of the art, ionophore doped PVC based ISM as described by A. Cadogan[221] was introduced. In general these membranes consist of a polymeric matrix (PVC), ionic sites (hydrophobic ions) and an ionophore which is a specific ion selective component. The ionic sites are required to buffer the ion of interest (to maintain a constant ion activity) within the ISM so that the activity of the ions within the ISM does not depend on the activity in the analyte and therefore obtain a Nernstian ion-selective response.[xii,218,222] Accordingly, ISMs were prepared by dropcasting a high molecular weight polyvinyl chloride (31 wt.%, SelectophoreTM grade), 2-nitrophenyl octyl ether (2-NPOE) (68 wt.%), potassium tetrakis-((4-chlorophenyl)borate (KTpClPB) (0.7 wt.%) and sodium ionophore X (0.2 wt.%) in 5 mL tetrahydrofuran (THF), cocktail onto a glass slide. The dropcast membrane was dried overnight at ambient conditions and was peeled off the glass slide for further implementation on the P3HT-based EGOFET with a 10^{-2} M NaCl inner filling solution, confined by a PDMS reservoir (see Figure 7.2). All of the chemicals mentioned above were obtained from Fluka® Sigma-Aldrich and were used as received. Saline solutions were prepared in concentrations varying from 10^{-4} M to 10^{-1} M NaCl (99.5 %, p.a., ACS, ISO) and KCl (~99.0 %) in deionized water, respectively.

[xii] J. Kofler prepared the ISMs and for more background about ISMs in general as well as details about the preparation, the characterization and simulations please refer to his PhD thesis [222].

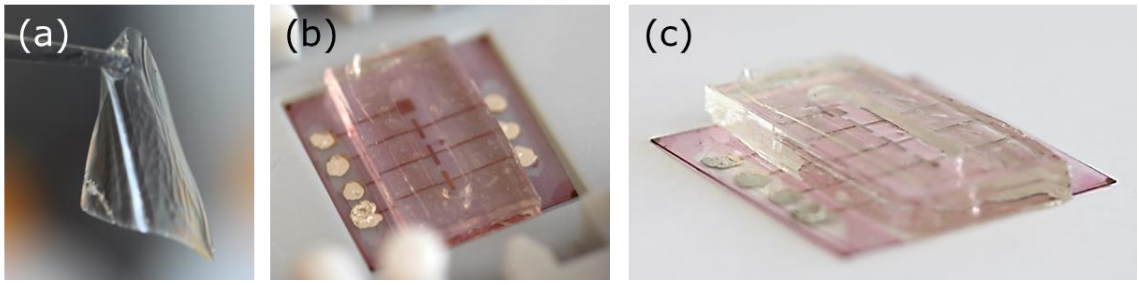

Figure 7.2: Ionophore-doped PVC based ISM (a) and implementation on a typical P3HT EGOFET with 10^{-2} M NaCl as electrolyte (b,c).

The reservoir and the flow cell for the ion-selective EGOFETs were made of PDMS as described in section 3.1.4.. Figure 7.3 (a) shows a finalized ion-selective EGOFET with an implemented Ag/AgCl reference electrode and a flow cell. In order to seal the flow cell and the reservoir of the inner filling solution, a pressure was applied by an appropriate fixture (see Figure 7.3 (c)). In comparison, a typical P3HT EGOFET without an ISM gated via an Ag/AgCl gate electrode, for reference measurements is shown as well (Figure 7.3 (b)). All electrical characterizations were done in air at ambient conditions (at same light conditions).

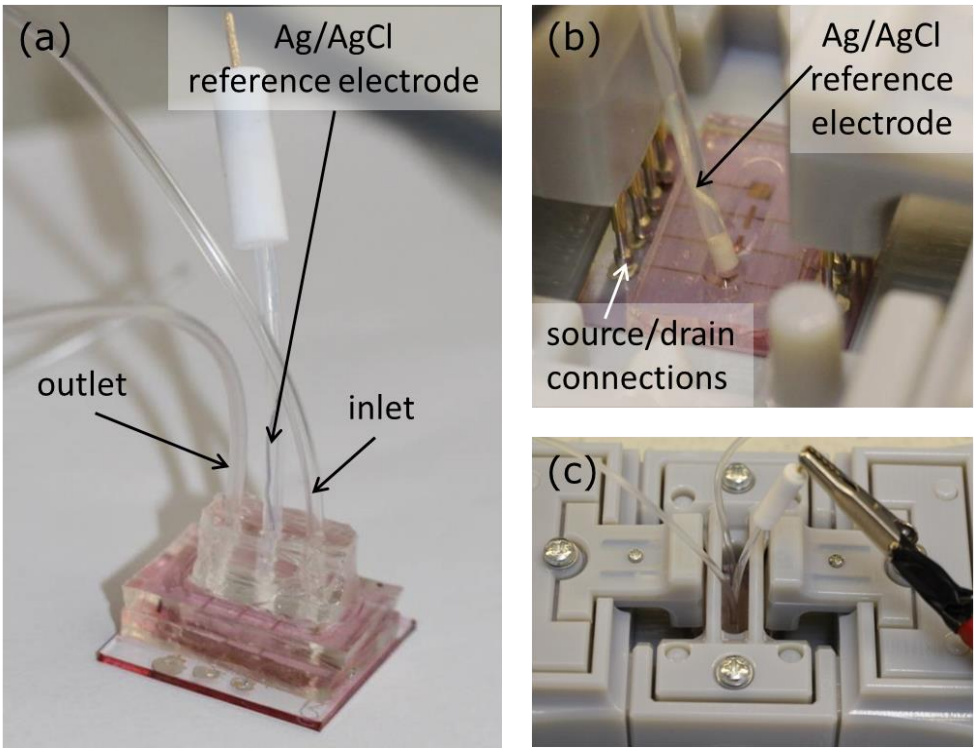

Figure 7.3: Typical ion-selective P3HT-based EGOFET with implemented Ag/AgCl gate electrode and flow cell (a) in comparison to a reference P3HT EGOFET without an ISM under test (b). A 3D printed measurements setup was used to electrically contact as well as to seal the flow cell with an appropriate fixture (c).

7.4 Characterization of the Na^+ selective ISM within an Ion-Selective Electrode

Before the Na^+ selective PVC based membranes were implemented into the EGOFET architecture, they were characterized with respect to sensitivity and selectivity in a typical ion-selective electrode configuration. Figure 7.4 shows the corresponding measurement setup: The total potential difference (electromotive force, EMF) between two Ag/AgCl reference electrodes which are separated by the ISM are measured under zero-current conditions. The measured EMF is the sum of local potential differences, arising at each electrochemical interface (see Figure 7.4): Ag/AgCl, AgCl/KCl, KCl/sample (liquid junction), sample/ISM, ISM/inner filling solution and inner filling solution/KCl interface. However, only the liquid junction potential and the membrane potential, which arises due to different activity dependent phase boundary potentials (PBPs) (Figure 7.4), are sample dependent. The other potentials are constant. The liquid junction potentials originate from the difference of ion mobility at the boundaries at the reference electrode but are negligible or constant when appropriate equitransferent bridge electrolyte of high concentrations (e.g. 3 M KCl) are used.[223,224] Accordingly, solely the membrane potential (E_{mem}) is considered. It is given by the activity dependent phase boundary potentials E_{PBP} arising at each side of the membrane (sample-ISM and ISM-inner filling solution) and depend on the ion activity in a Nernstian fashion (see eq. 7.2 – 7.4): E^0 is a constant, R the gas constant, z_i the valency of the analyte ion, F the Faraday's constant and a the corresponding activity of the target ion in the analyte and the inner filling solution, respectively.

$$EMF = E_{mem} = E_{PBP\_outer} - E_{PBP\_inner} \tag{7.2}$$

$$E_{mem} = E_a^0 + \frac{RT}{z_i F}\ln(a_{analyte}) - E_i^0 - \frac{RT}{z_i F}\ln(a_{inner}) \tag{7.3}$$

$$E_{mem} = E^0 + \frac{RT}{z_i F}\ln(\frac{a_{analyte}}{a_{inner}}) \tag{7.4}$$

In our case, the ion activity of the inner filling solution is kept constant (10^{-2} M NaCl) leading to e.q. 7.5, where the membrane potentials solely depends on the ion activity of the analyte and theoretically increases with 59.2 mV/dec:

$$E_{mem} = E^{0*} + \frac{0.05916}{z_i}\log(a_{analyte}) \tag{7.5}$$

A detailed explanation of the function of such ISMs is given by Bühlmann et al[218] and can be found within the PhD thesis of J. Kofler.[222]

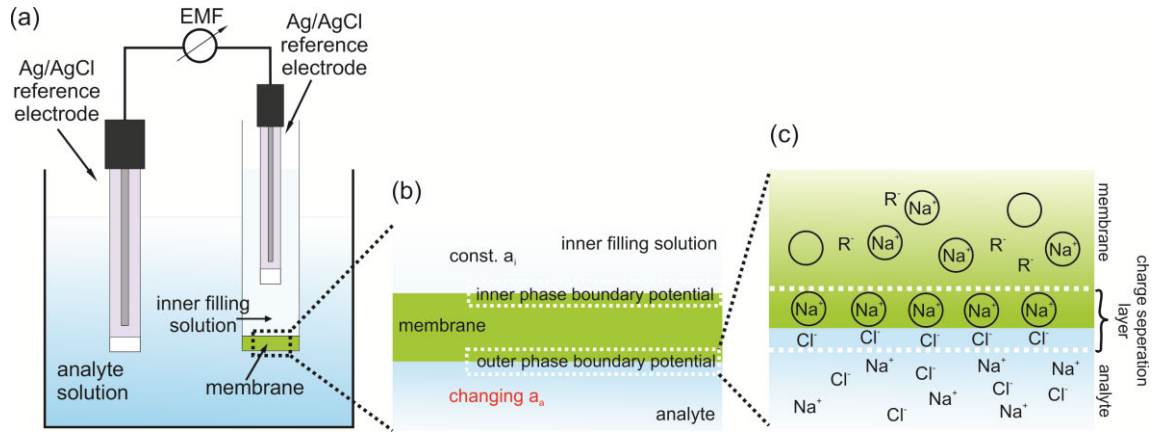

Figure 7.4: (a) Schematic ISE measurement setup exhibiting following interfaces: Ag / AgCl / KCl 3 M / sample / membrane / inner filling solution / KCl 3 M / AgCl / Ag. (b) Cross-section of the ISM interfaces and (c) section the ISM / analyte interface where the outer phase boundary potential results from a charge separation layer.

In order to investigate the sensitivity of the Na^+ ISE with a 10^{-2} M inner filling solution, the salt concentration was stepwise increased by adding saline solutions with a certain amount of NaCl (10^{-4} M – 10^{-1} M NaCl) to the analyte, while stirring and recording the potential difference (via a Keithley voltmeter) (see Figure 7.5 (a)). In addition, the response of the membrane to the interfering ion K^+ was measured by using KCl as an analyte (ee Figure 7.5 (b)). The results are presented in Figure 7.5 and Figure 7.6, showing a significant sensitive and selective response to Na^+.

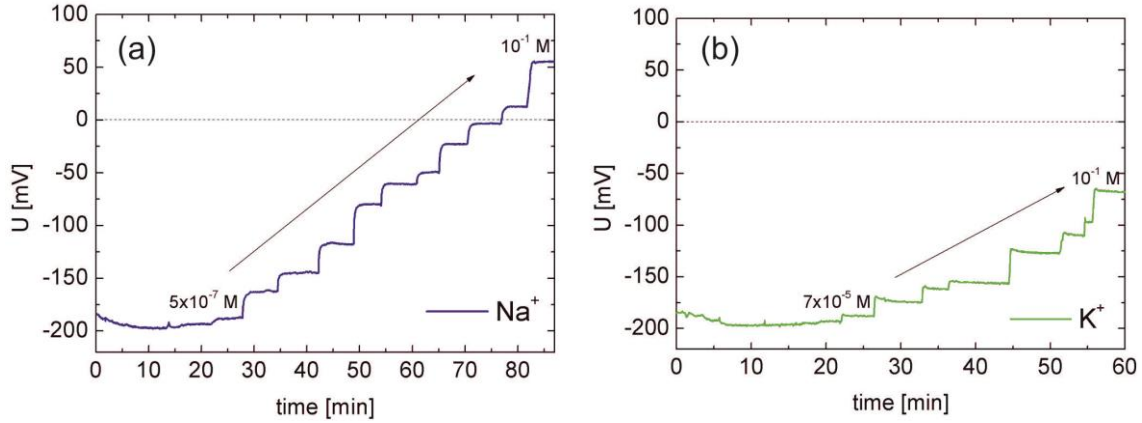

Figure 7.5: Potentiometric response of the PVC ISM while increasing the Na^+ (a) and the K^+ (b) concentration stepwise in case of an inner filling solution with 10^{-2} M NaCl.

Figure 7.6 depicts the measured potential difference versus the Na^+ and K^+ concentration, respectively. The lowest detection limit of the target ion was determined to be ~10^{-6} M Na^+. The results show a nice linear behavior in the range of 5 x 10^{-6} M to 10^{-1} M Na^+ with a slope of 52 mV/dec, compared to 58 mV/dec as reported in literature.[221] Moreover, a nice zero-crossing is observed at a concentration of 10^{-2} M NaCl, which corresponds to the inner filling solution. The

response curve for K^+ revealed a slope of 46 mV/dec, but a much smaller linear range between 5 x 10^{-3} M and 10^{-1} M K^+. This clearly demonstrates the Na^+ selectivity of the applied membrane.

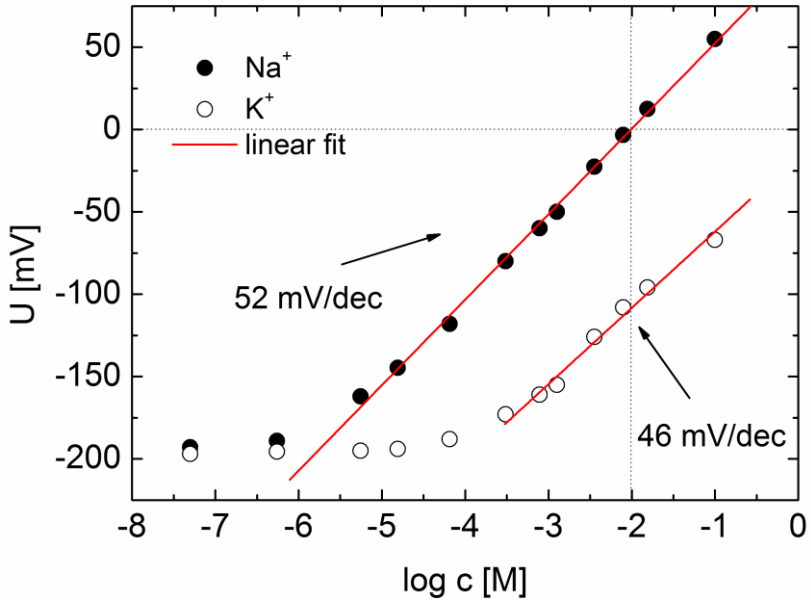

Figure 7.6: Potentiometric response versus the logarithmically plotted concentration of Na^+ (full symbols) and K^+ (open symbols) with a 10^{-2} M NaCl inner filling solution.

7.5 Characterization of Ion-Selective EGOFETs

After the evaluation of the ISM performance the ion-selective EGOFETs were characterized. Figure 7.7 shows the transfer (a) and output (b) characteristics of a typical Na^+ sensitive EGOFET with deionized (DI) water as analyte and a 10^{-2} M NaCl inner filling solution, exhibiting typical field-effect characteristics with a slight hysteresis. The transfer curve of this ion-sensitive EGOFET is shifted by ~ 200 mV to the negative direction when the target ion in the analyte is increased to 10^{-2} M Na^+. This threshold voltage (V_{th}) shift originates from a changed membrane potential. As already mentioned, this Nernstian membrane potential (see Figure 7.7 (c) and eq. 7.1) is determined by the ion activity difference between the analyte and the inner filling solution. As the ion activity of the inner filling solution is kept constant and the potential of the analyte is predefined through the Ag/AgCl gate electrode, the potential of the inner filling solution is modulated solely by the ion activity in the analyte (see Figure 7.7 (c)). This effective gate potential (gate potential + membrane potential) controls the source-drain current. Therefore, if the concentration of the target ion in the analyte is equal to the concentration in the inner filling solution (10^{-2} Na^+) the membrane potential is zero and the effective gate voltage matches the applied gate voltage (see Figure 7.7 (a) and (c), dotted line). Consequently no V_{th} shift is observed, and the characteristics are identical to an EGOFET without a Na^+ selective membrane where the Ag/AgCl gate electrode is directly immersed into the inner filling solution (see Figure 7.7 (a) and (c), dashed line). The reason for the

insignificantly increased off-current of the transfer curve with an ISM (dotted line) is a slightly larger leakage current. The mobility with and without an ISM in the saturation region was estimated to be ~2 x 10^{-2} cm^2/Vs using a typical capacitance of 3 $\mu F/cm^2$ (for an Au/P3HT/water/Au system),[127] which is in good agreement with other reported values.[82,127] These results clearly demonstrate that the implementation of an ISM does not influence the overall performance (on/off ratio ~10^2, maximum channel currents of ~10 µA) of the underlying EGOFET. However, when choosing the operational voltages it is important to consider the effective applied gate potential which should be well below 0.7 V to ensure a stable device operation and to avoid degradation due to doping and hydrolyses as we discussed in chapter 6.[3,127,132]

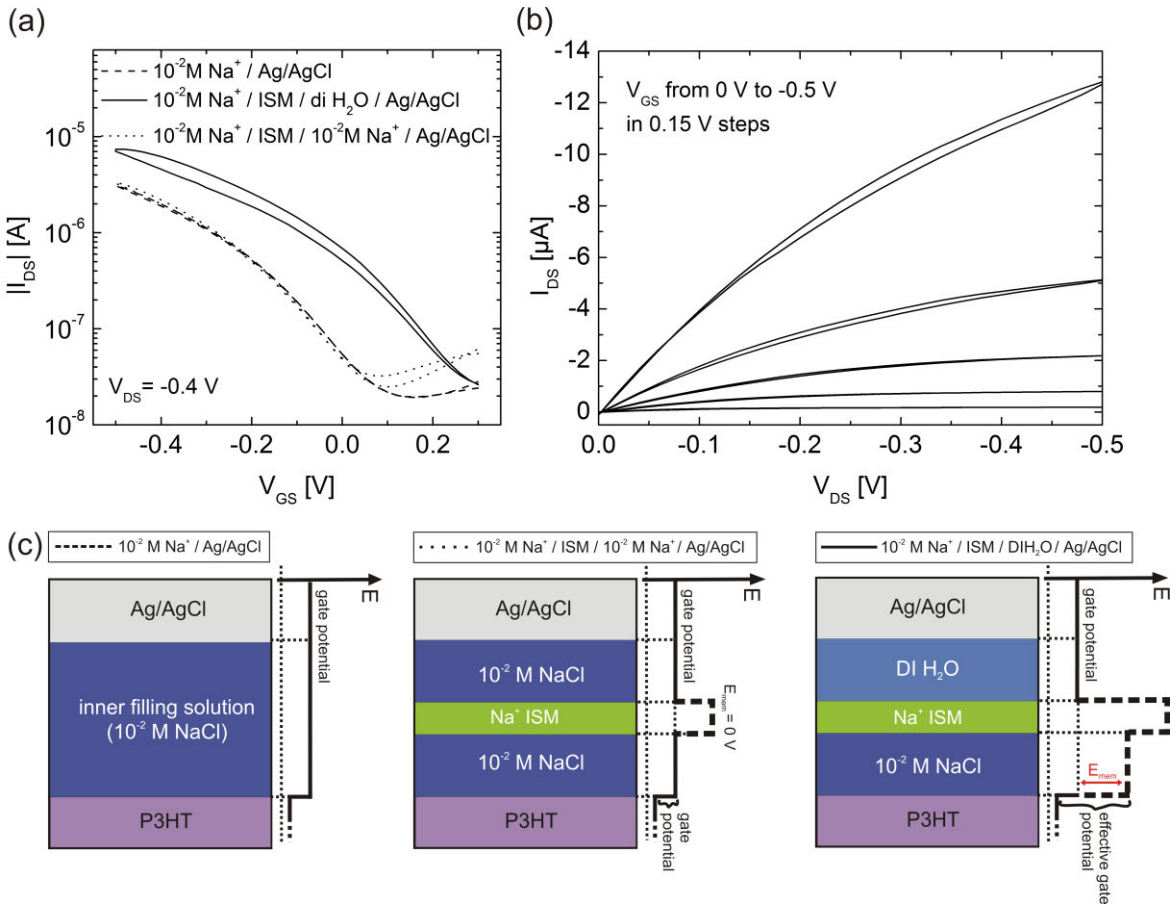

Figure 7.7: (a) Semilogarithmic transfer curve of a typical P3HT-based EGOFET without (dashed line) and with implemented ISM using DI H_2O (solid line) and 10^{-2} M Na^+ solution (dotted line) as an analyte. (b) Output characteristics of an ion-sensitive EGOFET using DI H_2O as an analyte. (c) Illustration of the modified gate potentials across the relevant interfaces of an ion-sensitive EGOFET without an ISM and a 10^{-2} M NaCl inner filling solution (left) compared with devices with an ISM and equal ion concentration in the analyte and the inner filling solution (E_{mem} = 0 V) (middle) and in case of lower concentration in the analyte (E_{mem} > 0 V) (right). Note that no potential difference between the Ag/AgCl electrode and electrolyte has been drawn, indicating that the liquid junction potential is negligible.

In order to demonstrate the sensitivity of the ion-selective EGOFET to Na^+, the source-drain current was recorded at a constant gate and source-drain potential while the Na^+ concentration in the water (analyte) was increased stepwise (see Figure 7.8, V_{DS} = -0.1 V, V_{GS} = -0.2 V). The Na^+ concentration was adjusted by adding a certain amount of different saline solutions (10^{-4} – 10^{-1} M NaCl) to a larger reservoir (200 ml DI H_2O beaker) which was connected via PVC tubing to the flow cell and further to retracing micro syringes (Fusion 400, Nexus 3000), producing a constant flow of 1 ml/min. As a sensitive response a source-drain current decrease of ~250-500 nA/dec (depending on the point of operation) was observed while varying the Na^+ concentration between 10^{-6} M and 10^{-1} M. The source-drain current decrease reflects the change in effective gate potential. The latter can be calculated by using the fitted transfer curve at V_{SD} = -0.1 V of the EGOFET without an ISM (see Figure 7.9). Alternatively, the transfer curve of the EGOFET with an ISM can be used (as mentioned before), if the Na^+ concentration in the inner filling solution and the analytes are equal. This measurement was performed before the sensitivity evaluation was carried out. Figure 7.9 (a) shows the transfer curve of an EGOFET without an ion-selective membrane in a 10^{-2} M NaCl electrolyte solution, gated via an Ag/AgCl reference electrode. Figure 7.9 (b) depicts the square root of the source-drain current versus the gate voltage including a corresponding polynomial fit. This equation, which describes the correlation of the gate voltage with the source-drain current, is required to estimate the effective applied gate voltage during the sensitivity measurements. Since drifts during the measurements cannot be totally excluded, the obtained values should be considered as estimations.

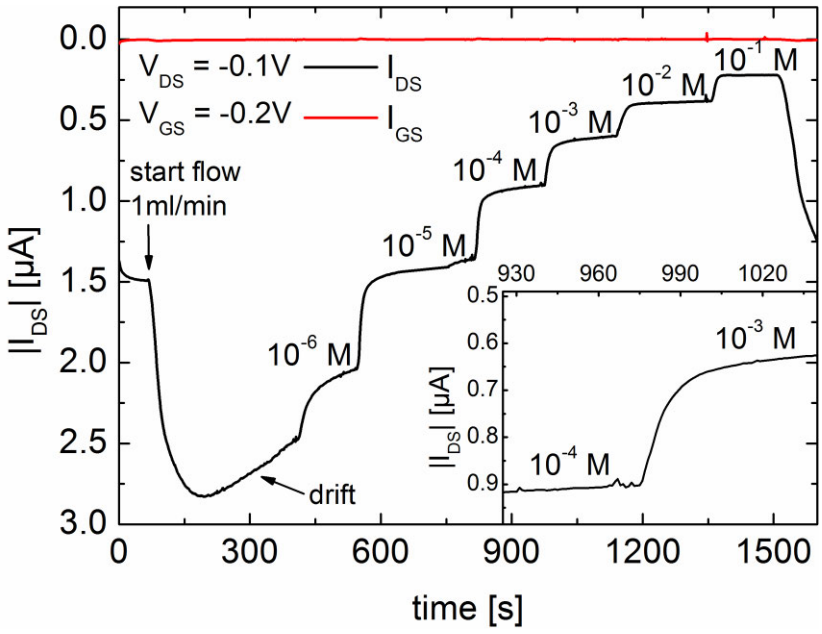

Figure 7.8: Source-drain current response to increasing Na^+ concentration of a typical ion-sensitive EGOFET with a PVC ion-selective membrane, exhibiting a response time of ~30 s (see inset).

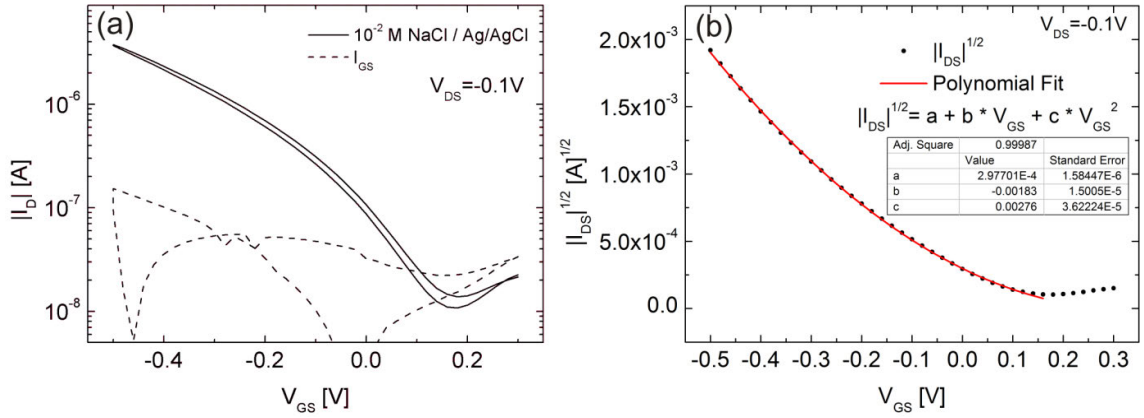

Figure 7.9: (a) Semilogarithmic transfer curve of a typical EGOFET without an ion-selective membrane in a 10^{-2} M NaCl electrolyte solution, gated via an Ag/AgCl reference electrode. (b) Square root of the source-drain current versus the gate voltage and corresponding polynomial fit.

Figure 7.10 shows the calculated effective gate voltage versus the Na^+ concentration following a linear relation with a slope of 62 mV/dec. This value is higher in comparison to the response obtained from the electrical characterization of the Na^+ ISM in an ion-selective electrode configuration of about 52 mV/dec. The increased response might be explained by the permanent flow of 1 mL/min for the ISEGOFET system. However, both values are in good agreement with the theoretically predicted value of 59.2 mV/dec, calculated from the Nernst equation at 25°C (see eq. 7.5). Variations of about ~7 mV/dec are in the expected error range, considering the fitting model for the EGOFET transfer curve as well as degradation effects due to the long continuous measurements. Nevertheless, the obtained values for the effective applied gate potential represent good estimations.

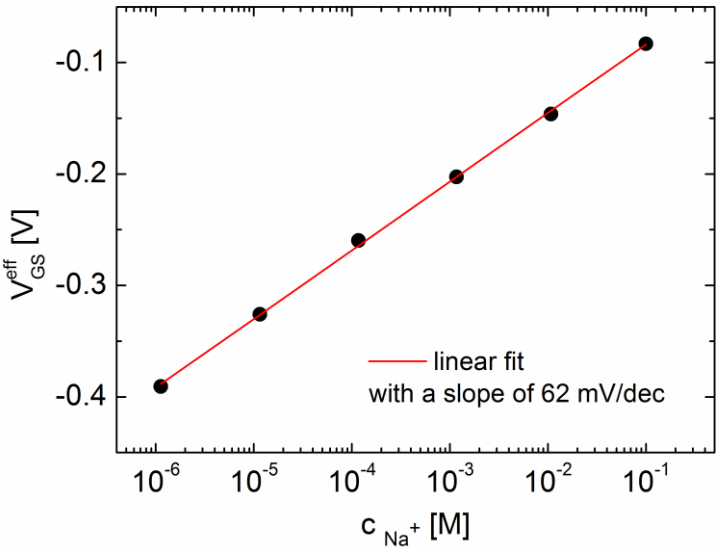

Figure 7.10: Calculated effective gate potential versus Na^+ concentration of an Na^+ ion-selective EGOFET with a 10^{-2} M NaCl inner filling solution.

The implementation of a flow cell was necessary to obtain a reversible sensor response and to lower the detection limit from 10^{-5} M Na^+ down to ~ 10^{-6} M Na^+.[225] This can be clearly seen by comparing the source-drain current before and after applying a flow of DI water through the cell (see Figure 7.8, first 300 s): if there is no flow, ions which diffuse out of the inner filling solution into the analyte lead to an artificially increased ion concentration in the vicinity of the ISM.[226] This results in a decreased effective gate potential (changed membrane potential) and further to a decreased source-drain current. If a flow is applied (after 300 s) this concentration is lowered, leading to a higher effective gate potential and consequently also to a higher source-drain current. These low Na^+ concentrations and the resulting high effective gate voltages (here < -400 mV) lead to significant drifts (decreasing channel currents, see Figure 7.8, 200 - 400 s). By increasing the concentration the effective applied gate voltage is decreased and the drift is reduced until it almost vanishes completely. Moreover, since no significant drift occurred when no voltages were applied, its origin is most probably ascribed to the high applied effective gate voltage which results in electrolysis of water at the electrolyte-semiconductor interface leading to device degradation. This drift can in principle be avoided by keeping the effective gate potential constant at a stable operating point, regardless of the ion concentration in the analyte. However, this requires a readjusting of the gate potential by an appropriate feedback mechanism.[227,228] The according adjustment of the gate potential corresponds directly to the membrane potential change and thus to the ion concentration in the analyte. An appropriate dynamic read-out protocol has been presented by Kofler et al.[220]

Moreover, note that the herein reported lowest detection limit (10^{-6} M Na^+) is not a property of the ion-sensitive EGOFET itself, but is rather determined by the ISM and the inner filling solution. In detail, ion fluxes through the membrane typically limit the lowest detection limit.[218] Suppression of these fluxes which lead detection limits in the nano-molar range might be achieved e.g. by using thicker membranes or a lower Na^+ concentration in the inner filling solution.[225,229] Furthermore, the response time of ~30 s is not a property of the ISM itself but it is rather how quickly the concentration within the flow cell approaches the concentration of the large reservoir (mixing time).[218] Consequently, the response time can be lowered by increasing the flow rate and decreasing the dead volume.

7.5.1 Reversibility and Selectivity

The reversible and selective response of the ion-sensitive EGOFET is shown in Figure 7.11. It demonstrates a rather fast response when the concentration was varied between 10^{-4} M Na^+ (base line) and 10^{-3} M Na^+. The selective response was tested with K^+ as interfering ion following 3 Na^+ concentration variation steps. The K^+ concentration was increased in a 10^{-4} M Na^+ background

solution to 10^{-2} M K^+ (two order of magnitude), showing a current variation of about 7 %. In comparison, by increasing from 10^{-4} M to 10^{-3} M Na^+ (one order of magnitude) a 5 times higher current change was detected, confirming the selectivity of the ion-sensitive EGOFET to Na^+ ions. This is in agreement with the obtained results of section 7.4, where the same PVC ISM was also characterized with respect to selectivity in an ion-selective electrode configuration between a range of 10^{-6} – 10^{-1} M K^+. The long-term current drift of ~0.3 % per minute at a reasonable gate voltage (see Figure 7.11), can be most likely ascribed to effects described in section 6.5 (page 78) such as the well-known P3HT degradation under ambient conditions or diffusion of water molecules into the P3HT film. The long-term stability of the newly presented ion sensor was not a main topic for this first proof of principle but will be one of the challenges for the future when pursuing highly promising sensor concepts based on EGOFETs. However, considering the utilization of the presented ion sensor for rapid self-testing applications the obtained small drifts during operation are in an acceptable range. Moreover, other materials exhibiting excellent air stability can be used instead of P3HT. We also fabricated EGOFETs based on the air-stable heterotriangluene but in contact with water the films delaminated and no functioning EGOFET could be measured. However, there are other very promising materials such as hydrogen-bonded semiconducting pigments.[40,230] For example an isoindigo-based polymer semiconductor was recently demonstrated in highly stable OFET sensors for selective detection in marine environment.[231]

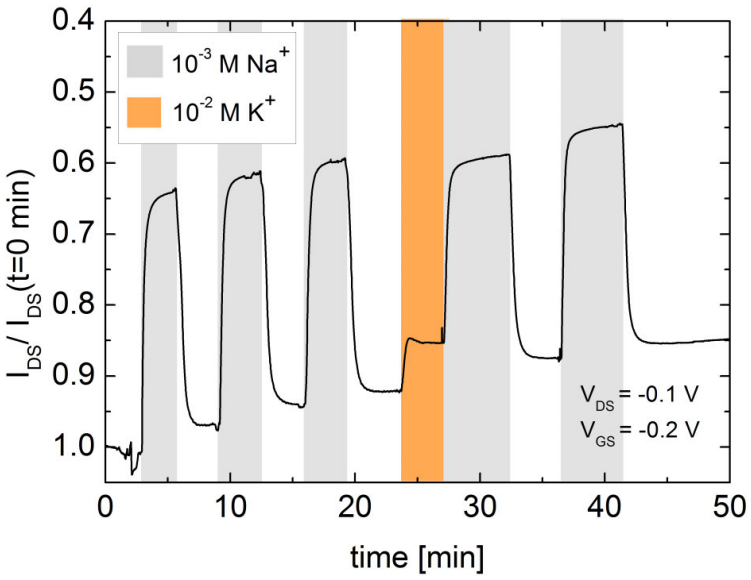

Figure 7.11: Response curve of a Na^+ selective EGOFET. The source-drain current was measured while the Na^+ concentrations were changed rapidly from 10^{-4} to 10^{-3} M and back. The selectivity was investigated by adding KCl to a 10^{-4} M Na^+ background solution to obtain 10^{-2} M K^+.

7.6 Conclusion

In conclusion, we have successfully demonstrated a novel sensor platform based on electrolyte-gated OFETs for selective and reversible ion detection. The novelty of this design compared to conventional ISFETs is the direct contact between the electrolyte and the semiconductor without the use of a solid dielectric, making low voltage operation in aqueous media feasible. Furthermore, this architecture benefits from a modular approach, allowing for the detection of various ions simply by choosing an appropriate ion-selective membrane. The presented potentiometric sensor based on a Na^+ sensitive PVC membrane showed a Nernstian behavior for a broad detection range between 10^{-6} M and 10^{-1} M Na^+. Moreover, a selective as well as reversible sensor response without a complex recovering process was achieved. Another highlight of this novel sensor concept is that the EGOFET is separated from the sample solutions so that the response is solely determined by the ISM response and the transducer performance is not altered. The investigation of the sensors further showed that for a stable sensor performance, the operation at a constant transistor working point is important. Based on this findings the successfully readjustment of the gate voltage with a dynamic read-out protocol was presented for a H^+ ion-selective EGOFET by Kofler et al.[220]. Next steps may include the replacement of the P3HT with a highly-stable semiconductor such as iso-indigo based materials as well as the implementation of hydrogels as inner filling solutions to obtain an all solid device. However, the presented results constitute an important step towards a low-cost integrated sensor array for multiple ion detection facilitated by a facile integration of different state of the art ISMs, being of high relevance for biomedical diagnostics, industrial process-, water-control and food-monitoring.

8 Summary and Conclusion

One main focus of the thesis was set on reliability issues of organic field-effect transistors (OFETs) in terms of air-stability of organic semiconductors, water-stable performance of OFETs as well as process-related instabilities leading to altered OFET performance. The second part of this thesis deals with electrolyte-gated organic field-effect transistors (EGOFETs) for sensing applications in aqueous media. In particular, the first ion-selective EGOFET for the detection of sodium ions is presented.

First, it was highlighted that equally important to the materials choice, also the manufacturing process has to be considered to obtain reliable well-performing OFETs. It is generally known that the processing conditions of the organic semiconductor as well as specific treatments of the substrate surface significantly influence the OFET performance. However, we demonstrated that already photolithographic processing to structure the source/drain electrodes of OFETs significantly influences the dielectric-semiconductor and/or electrode-semiconductor interfaces. This leads to altered electrical performance of bottom-gate bottom-contact OFETs based on P3HT. In particular, photoresist residuals within the channel results in substantial increase of the surface roughness, whereas the application of different remover chemicals can render the surface more hydrophilic, both resulting in a higher charge carrier trap density.

Apart from process related reliability issues, the environmental stability of OFETs is strongly dependent on the employed materials. Within this context a novel air-stable polymer based on dimethylmethylene-bridged triarylamines (PTA) was investigated in BG/BC OFETs. The newly synthesized amorphous organic semiconductor was characterized concerning morphological, optical, electrical and interface related properties. Optimization of electrode- and dielectric-polymer interfaces yielded mobilities of ~4 x 10^{-3} cm^2 $V^{-1}s^{-1}$ and on/off current ratios of ~10^5. This indicates that PTA is a viable alternative for the best performing amorphous air-stable semiconducting polymers. Moreover, a significant sensitivity to hydrochloric acid (within the solvent) was obtained in terms of electrical performance as well as optical properties, due to protonation of the central nitrogen atom. BG/BC PTA FETs fabricated, characterized and stored under ambient conditions showed excellent air stability over one year compared to P3HT. This can

can be attributed to PTA's deeper lying HOMO level (E_{HOMO} = 5.1 eV) and wide bandgap (E_g = 2.9 eV). The combination of this robust performance with the ease of processing makes the new polymer a high potential candidate for large-scale low-cost production.

The second main part of this thesis focused on electrolyte-gated OFETs as ideal candidates for transducer in sensing applications in aqueous media. We showed that P3HT-based EGOFETs gated in deionized water via an Ag/AgCl reference electrode exhibits a good overall performance with on-currents up to 30 µA. Due to the polarizable as well as hydrophobic nature of P3HT in water negligible faradaic current occur across the electrolyte-P3HT interface and the ion penetration is hindered within a water-stable window. The formation of an electric double layer at the P3HT side, with high capacitances allows a low voltage operation. Moreover, we found that an increasing NaCl concentration (10^{-4} M – 10^{-2} M) within water results in a modified transistor performance in terms of threshold voltage, on current and subthreshold slope. The importance of choosing appropriate gate electrodes is illustrated by comparing Pt and Au electrodes with respect to a standard Ag/AgCl reference electrode. Pt-electrode-gated EGOFETs exhibited only a shift of the threshold voltage, whereas the gold electrode led to a completely altered transistor characteristics, being not applicable as a quasi-reference electrode. The presented results clearly demonstrate the influence of the salt concentration within the electrolyte and the influence of the applied electrode materials, being important factors for a proper design of EGOFET based sensors. However, sensing applications always require a reference electrode (nonpolarizable interface) in order to ensure that the potential solely drops at the solution-semiconductor interface (polarizable) and that the gate electrode potential is independent of the sample concentration. This is important in order to ascribe any concentration changes occurring, to the sensing interface and thus to a modulated channel current. The evaluation of a stable operation window to obtain a reliable sensor response showed a significant source-drain current decrease when a high potential difference was applied. Accompanied with that, the leakage current significantly increased, the P3HT surface became more hydrophilic and the color changed as well as the fluorescence of these films decreased. Based on these effects it is believed that the reason of the observed degradation can be ascribed to electrochemical reactions/oxidative degradation upon exceeding a certain potential or a certain period of time at which a potential is applied. The comparable small current drifts observed for long time investigations using a stable operating window can be ascribed to the well-known P3HT degradation under ambient conditions (photo-oxidation) and migration of water into the P3HT film rather than bias induced degradation.

Based on these detailed investigation, we have successfully developed a novel sensor platform based on electrolyte-gated OFETs for selective and reversible ion detection. The novelty of this design compared to conventional ISFETs is the direct contact between the electrolyte and the

semiconductor without the use of a solid dielectric, making low voltage operation in aqueous media feasible. A sensitive and selective response to sodium ions (Na^+) is obtained by introducing a state of the art ion-selective membrane, combining the unique properties of EGOFETs with the key sensing element of the well-established ISE technology. This modular approach allows for the detection of various ions simply by choosing an appropriate ion-selective membrane. Based on a Na^+ sensitive PVC membrane this potentiometric sensor showed a Nernstian behavior for a broad detection range between 10^{-6} M and 10^{-1} M Na^+. Moreover, a selective as well as reversible sensor response without a complex recovering process was achieved. Another highlight is that the EGOFET is separated from the sample solutions so that the response is solely determined by the ISM response and the transducer performance is not altered. The investigation of the sensors further indicated that for a stable sensor performance, operation at a constant transistor working point is important. This has been successfully realized by following work including the readjustment of the gate voltage with a dynamic read-out protocol for a H^+ ion-selective EGOFET by J. Kofler and K. Schmoltner et al.[220] Next steps may include the replacement of the P3HT with a highly-stable semiconductor such as iso-indigo based materials as well as the implementation of hydrogels as inner filling solutions to obtain an all-solid device. In conclusion, the presented results constitute an important step towards a low-cost integrated sensor array for multiple ion detection, which is of high relevance for biomedical diagnostics, industrial process-, water-control and food-monitoring.

References

[1] K. Schmoltner, A. Klug, J. Kofler, E. J. W. List, *Proc. SPIE* **2012**, *8479*, 84790J.

[2] K. Schmoltner, F. Schlütter, M. Kivala, M. Baumgarten, S. Winkler, R. Trattnig, N. Koch, A. Klug, E. J. W. List, K. Müllen, *Polym. Chem.* **2013**, *4*, 5337.

[3] K. Schmoltner, J. Kofler, A. Klug, E. J. W. List-Kratochvil, *Proc. SPIE* **2013**, *8831*, 88311N.

[4] K. Schmoltner, J. Kofler, A. Klug, E. J. W. List-Kratochvil, *Adv. Mater.* **2013**, *25*, 6895.

[5] J. E. Lilienfeld, U.S. Patent 1 745 175, **1930**.

[6] J. Bardeen, W. H. Brattain, *Physical Review* **1948**, *74*, 230.

[7] http://www.aps.org/publications/apsnews/200011/history.cfm (01.06.2014)

[8] D. Kahng, M. M. Atalla, *IRE-AIEE Solid-State Devices Research Conference, Carnegie Institute of Technology*, Pittsburgh, PA, **1960**.

[9] http://www.nobelprize.org/nobel_prizes/physics/laureates/1956/ (01.06.2014)

[10] H. Klauk, *Organic Electronics,* John Wiley & Sons, Weinheim, Germany **2006**.

[11] H. Shirakawa, E. J. Louis, A. G. MacDiarmid, C. K. Chiang, A. J. Heeger, *J. Chem. Soc., Chem. Commun.* **1977**, 578.

[12] F. Bettelheim, W. H. Brown, M. K. Campbell, S. O. Farrell, *Introduction to General, Organic and Biochemistry*, 9th ed., Cengage Learning Services, Belmont, USA **2009**.

[13] D. R. Gamota, P. Brazis, K. Kalyansundaram, *Printed Organic and Molecular Electronics*, Kuwer Academic Publisher, Massachusetts **2004**.

[14] A. J. Heeger, *J. Phys. Chem. B* **2001**, *105*, 8475.

[15] K. Müllen, U. Scherf, *Organic Light Emitting Devices – Synthesis, Properties, and Applications*, Wiley-VCH Weinheim, Germany **2006.**

[16] G. Horowitz, *Adv. Mater*. **1998**, *10*, 365.

[17] H. Sirringhaus, *Adv. Mater.* **2005**, *17*, 2411.

[18] S. Günes, H. Neugebauer, N. S. Sariciftci, *Chem. Rev*. **2007**, *107* (4), 1324.

[19] M. Gaal, C. Gadermaier, H. Plank, E. Moderegger, A. Pogantsch, G. Leising, E. J. W. List, *Adv.Mater*. **2003**, *15*(14), 1165.

[20] D. A. Bernards, R. M. Owens, G. G. Malliaras, *Organic Semiconductors, in Sensor Applications,* Springer, New York **2008**.

[21] H. Yan, Z. Chen, Y. Zheng, C. Newman, J. R. Quinn, F. Dötz, M. Kastler, A. Facchetti, *Nature* **2009**, *457*, 679.

[22] H. Bronstein, Z. Chen, R. S. Ashraf, W. Zhang, J. Du, J. R. Durrant, P. S. Tuladhar, K. Song, S. E. Watkins, Y. Geerts, M. M. Wienk, R. a J. Janssen, T. Anthopoulos, H. Sirringhaus, M. Heeney, I. McCulloch, *J. Am. Chem. Soc.* **2011**, 133, 3272.

[23] P. F. Baude, D. A. Ender, M. A. Haase, T. W. Kelley, D. V. Muyres, S. D. Theiss, *App. Phys. Lett.* **2003**, *82*, 3964.

[24] H. E. A. Huitema, G. H. Gelinck, J. B. P. H. van der Putten, K. E. Kuijk, C. M. Hart, E. Cantatore, D. M. de Leeuw, *Adv. Mater.* **2002**, *14*, 1201.

[25] J. T. Mabeck, G. G. Malliaras, *Anal. Bioanal. Chem.* **2006**, *384*, 343.

[26] N. A. Kotov, J. O. Winter, I. P. Clements, E. Jan, B. P. Timko, S. Campidelli, S. Pathak, A. Mazzatenta, C. M. Lieber, M. Prato, R. V. Bellamkonda, G. a. Silva, N. W. S. Kam, F. Patolsky L. Ballerini, *Adv. Mater.* **2009**, *21*, 3970.

[27] T. Someya, A. Dodabalapur, A. Gelperin, H. E. Katz, Z. Bao, *Langmuir* **2002,** *18*, 5299.

[28] M. Irimia-Vladu, P. A. Troshin, M. Reisinger, L. Shmygleva, Y. Kanbur, G. Schwabegger, M. Bodea, R. Schwödiauer, A. Mumyatov, J. W. Fergus, V. F. Razumov, H. Sitter, N. S. Sariciftci, S. Bauer, *Adv. Funct. Mater.* **2010**, *20*, 4069.

[29] M. Berggren, A. Richter-Dahlfors, *Adv. Mater.* **2007**, *19*, 3201.

[30] T. N. Sorrell, *Organic Chemistry*, 2nd ed., University Science Books, Sausalito, California **2006**.

[31] Z. Bao, J. Locklin, *Organic Field-Effect Transistors*, CRC Press, Boca Raton **2007**.

[32] I. Kymissis, *Organic Field Effect Transistor: Theory, Fabrication and Characterization*, Springer, New York, USA **2009**.

[33] O. D. Jurchescu, M. Popinciuc, B. J. V. Wees, T. T. M. Palstra, *Adv. Mater.* **2007**, *19*, 688.

[34] Y. Yuan, G. Giri, A. L. Ayzner, A. P. Zoombelt, S. C. B. Mannsfeld, J. Chen, D. Nordlund, M. F. Toney, J. Huang, Z. Bao, *Nat. Commun*. **2014**, *5*, 3005

[35] T. W. Kelley, D. V. Muyres, P. F. Baude, T. P. Smith, T. D. Jones, *Mater. Res. Soc. Symp. Proc.* **2003**, *771*, 169.

[36] H. Sirringhaus, *Science* **1998**, *280*, 1741.

[37] H. Sirringhaus, P. J. Brown, R. H. Friend, M. M. Nielsen, K. Bechgaard, B. M. W. Langeveld-Voss, A. J. . H. Spiering, R. A. J. Janssen, E. W. Meijer, P. Herwing, D. M. de Leeuw, *Nature* **1999**, *401*, 685.

[38] M. S. A. Abdou, F. P. Orfino, Y. Son, S. Holdcroft, *Macromolecules* **1997**, *7863*, 4518.

[39] I. McCulloch, M. Heeney, C. Bailey, K. Genevicius, I. Macdonald, M. Shkunov, D. Sparrowe, S. Tierney, R. Wagner, W. Zhang, M. L. Chabinyc, R. J. Kline, M. D. McGehee, M. F. Toney, *Nat. Mater.* **2006**, *5*, 328.

[40] E. D. Głowacki, M. Irimia-Vladu, M. Kaltenbrunner, J. Gsiorowski, M. S. White, U. Monkowius, G. Romanazzi, G. P. Suranna, P. Mastrorilli, T. Sekitani, S. Bauer, T. Someya, L. Torsi, N. S. Sariciftci, *Adv. Mater.* **2013**, *25*, 1563.

[41] U. Zschieschang, F. Ante, T. Yamamoto, K. Takimiya, H. Kuwabara, M. Ikeda, T. Sekitani, T. Someya, K. Kern, H. Klauk, *Adv. Mater.* **2010**, *22*, 982.

[42] C. Wang, H. Dong, W. Hu, Y. Liu, D. Zhu, Chem. Rev. **2012**, *112*, 2208.

[43] D. M. de Leeuw, M. M. J. Simenon, a. R. Brown, R. E. F. Einerhand, *Synth. Met.* **1997**, *87*, 53.

[44] Q. Tang, H. Li, Y. Liu, W. Hu, *J. Am. Chem. Soc.* **2006**, *128*, 14634.

[45] C. R. Newman, C. D. Frisbie, A. Demetrio, S. Filho, J. Bre, *Chem. Mater.* **2004**, *16*, 4436.

[46] C. Kittel, *Introduction to Solid State Physics*, John Wiley and Sons, New York, **1986**.

[47] V. Coropceanu, J. Cornil, D. da Silva Filho, Y. Olivier, R. Silbey, J.-L. Brédas, *Chem. Rev.* **2007**, *107*, 926.

[48] P. G. Le Comber, W. E. Spear, *Phys. Rev. Lett*. **1970**, *25*, 509.

[49] G. Horowitz, R. Hajlaou, P. Delannoy, *J. Phys. III* **1995**, *5*, 355.

[50] E. J. Meijer, *Charge transport in disordered organic field-effect transistors,* PhD Thesis, University of Technology Delft, **2003**.

[51] G. Horowitz, H. E. Hajlaoui, R. Hajlaoui, *J. Appl. Phys.* **2000**, *87*, 4456.

[52] N. Tessler, Y. Preezant, N. Rappaport, Y. Roichman, *Adv. Mater.* **2009**, *21*, 2741.

[53] H. Bässler, *Phys. Status Solidi B* **1993**, *175*, 15.

[54] A. Miller, E. Abrahams, *Phys. Rev.* **1960**, *120*, 745.

[55] M. C. J. M. Vissenberg, M. Matters, *Phys. Rev. B* **1998**, *57*, 12964.

[56] M. D. McGehee, E. K. Miller, D. Moses, A. J. Heeger, *Advances in Synthetic Metals: Twenty Years of Progress in Science and Technology*, (Eds.: P. Bernier, S. Lefrant, G. Bidan), Elsevier Science S. A., Lausanne, **1999**.

[57] A. N. Aleshin, S. R. Williams, A. J. Heeger, *Synth Me*t **1998**, *94*, 173.

[58] http://www.sigmaaldrich.com/catalog/product/aldrich/655201 (02.06.2014)

[59] D. F. Barbe, C. R. Westgate, *J. Phys. Chem. Solids* **1970**, *31*, 2679.

[60] A. Tsumura, H. Koezuka, T. Ando, *Appl. Phys. Lett.* **1986**, *49*, 1210.

[61] K.-Y. Jen, G. G. Miller, R. L. Elsenbaumer, *J. Chem. Soc. Chem. Commun.* **1986**, *5*, 1346.

[62] A. Assadi, C. Svensson, M. Willander, O. Ingan s, *Appl. Phys. Lett.* **1988**, *53*, 195.

[63] M. Shur, *Physics of Semiconductor Devices*, Prentice-Hall, Englewood Cliffs, NJ **1990**.

[64] T. Sekitani, T. Someya, *Mater. Today* **2011**, *14*, 398.

[65] G. H. Gelinck, P. Heremans, K. Nomoto, T. D. Anthopoulos, *Adv. Mater.* **2010**, *22*, 3778.

[66] V. Vaidya, S. Member, S. Soggs, J. Kim, A. Haldi, J. N. Haddock, B. Kippelen, D. M. Wilson, *IEEE Trans. CIRCUITS Syst.* **2008**, *55*, 1177.

[67] L. Zhou, A. Wanga, S.-C. Wu, J. Sun, S. Park, T. N. Jackson, *Appl. Phys. Lett.* **2006**, *88*, 083502.

[68] E. Cantatore, T. C. T. Geuns, G. H. Gelinck, E. V. Veenendaal, A. F. A. Gruijthuijsen, L. Schrijnemakers, S. Drews, D. M. D. Leeuw, *IEEE J. Solid-State Circuits* **2007**, *42*, 84.

[69] S. M. Sze, *Physics of Semiconductor Devices*, 3rd ed., John Wiley and Sons, **2007**.

[70] D. Boudinet, G. Le Blevennec, C. Serbutoviez, J.-M. Verilhac, H. Yan, G. Horowitz, *J. Appl. Phys.* **2009**, *105*, 084510.

[71] G. Horowitz, R. Hajlaoui, H. Bouchriha, R. Bourguiga, M. Hajlaoui, *Adv. Mater.* **1998**, *10*, 923.

[72] G. Horowitz, P. Lang, M. Mottaghi, H. Aubin, *Adv. Funct. Mater.* **2004**, *14*, 1069.

[73] Y.-Y. Noh, N. Zhao, M. Caironi, H. Sirringhaus, *Nature Nanotech.* **2007**, *2*, 784

[74] M. L. Chabinyc, J.-P. Lu, R. A. Street, Y. Wu, P. Liu, B. S. Ong, *J. Appl. Phys.* **2004**, *96*, 2063.

[75] A. Klug, A. Meingast, G. Wurzinger, A. Blümel, K. Schmoltner, U. Scherf, E. J. W. List, *Proc. of SPIE* **2011**, *8118*, 811809.

[76] R. A. Street, A. Salleo, *Appl. Phys. Lett.* **2002**, *81*, 2887.

[77] Y. Roichman, N. Tessler, *Appl. Phys. Lett.* **2002**, *80*, 151.

[78] T. J. Richards, H. Sirringhaus, *J. Appl. Phys.* **2007**, *102*, 094510.

[79] D. Natali, M. Caironi, *Adv. Mater.* **2012**, *24*, 1357.

[80] S. Rentenberger, A. Vollmer, E. Zojer, R. Schennach, N. Koch, *J. Appl. Phys.* **2006**, *100*, 053701.

[81] P. Lin, F. Yan, *Adv. Mater.* **2012**, *24*, 34.

[82] L. Kergoat, B. Piro, M. Berggren, G. Horowitz, M.-C. Pham, *Anal. Bioanal. Chem.* **2012**, *402*, 1813.

[83] J. Janata, M. Josowicz, *Nat. Mater.* **2003**, *2*, 19.

[84] A. Klug, K. Schmoltner, E. J. W. List, *Proc. of SPIE* **2010**, *7779*, 77790G1.

[85] G. Scarpa, A.-L. Idzko, S. Götz, S. Thalhammer, *Macromol. Biosci.* **2010**, *10*, 378.

[86] H. Katz, *Electroanalysis* **2004**, *16*, 1837.

[87] D. J. Macaya, M. Nikolou, S. Takamatsu, J. T. Mabeck, R. M. Owens, G. G. Malliaras, *Sensors Actuators B Chem.* **2007**, *123*, 374.

[88] A. Klug, M. Denk, T. Bauer, M. Sandholzer, U. Scherf, C. Slugovc, E. J. W. List, *Org. Electron.* **2013**, *14*, 500.

[89] A. Das, R. Dost, T. Richardson, M. Grell, J. J. Morrison, M. L. Turner, *Adv. Mater.* **2007**, *19*, 4018.

[90] W. Hu, Y. Liu, Y. Xu, S. Liu, S. Zhou, D. Zhu, B. Xu, C. Bai, C. Wang, *Thin Solid Films* **2000**, *360*, 256.

[91] L. Torsi, A. Dodabalapur, L. Sabbatini, P. G. Zambonin, *Sensors Actuators B Chem.* **2000**, *67*, 312.

[92] B. Crone, A. Dodabalapur, A. Gelperin, L. Torsi, H. E. Katz, A. J. Lovinger, Z. Bao, *Appl. Phys. Lett.* **2001**, *78*, 2229.

[93] T. Someya, H. E. Katz, A. Gelperin, A. J. Lovinger, A. Dodabalapur, *Appl. Phys. Lett.* **2002**, *81*, 3079.

[94] L. Torsi, A. Tafuri, N. Cioffi, M. C. Gallazzi, A. Sassella, L. Sabbatini, P. G. Zambonin, *Sensors Actuators B* **2003**, *93*, 257.

[95] Z.-T. Zhu, J. T. Mason, R. Dieckmann, G. G. Malliaras, *Appl. Phys. Lett.* **2002**, *81*, 4643.

[96] C. Bartic, B. Palan, A. Campitelli, G. Borghs, *Sensors Actuators B* **2002**, *83*, 115.

[97] C. Bartic, G. Borghs, *Anal. Bioanal. Chem.* **2005**, *384*, 354.

[98] C. Bartic, A. Campitelli, S. Borghs, *Appl. Phys. Lett.* **2003**, *82*, 475.

[99] T. Someya, A. Dodabalapur, J. Huang, K. C. See, H. E. Katz, *Adv. Mater.* **2010**, *22*, 3799.

[100] T. Someya, T. Sekitani, S. Iba, Y. Kato, H. Kawaguchi, T. Sakurai, *Proc. Natl. Acad. Sci. USA* **2004**, *101*, 9966.

[101] T. Someya, Y. Kato, T. Sekitani, S. Iba, Y. Noguchi, Y. Murase, H. Kawaguchi, T. Sakurai, *Proc. Natl. Acad. Sci. USA* **2005**, *102*, 12321.

[102] T. Sekitani, T. Someya, *Adv. Mater.* **2010**, *22*, 2228.

[103] H. Klauk, U. Zschieschang, J. Pflaum, M. Halik, *Nature* **2007**, *445*, 745.

[104] M. J. Panzer, C. D. Frisbie, *J. Am. Chem. Soc.* **2007**, *129*, 6599.

[105] L. Herlogsson, *Electrolyte-Gated Organic Thin-Film Transistors*, PhD thesis, Linköpings Universitet, Sweden, **2011.**

[106] C. Liao, F. Yan, *Polym. Rev.* **2013**, *53*, 352.

[107] D. Elkington, N. Cooling, W. Belcher, P. Dastoor, X. Zhou, *Electronics* **2014**, *3*, 234.

[108] M. E. Roberts, S. C. B. Mannsfeld, N. Queraltó, C. Reese, J. Locklin, W. Knoll, Z. Bao, *Proc. Natl. Acad. Sci. U. S. A.* **2008**, *105*, 12134.

[109] G. Scarpa, A.-L. Idzko, A. Yadav, S. Thalhammer, *Sensors* **2010**, *10*, 2262.

[110] M. E. Roberts, A. N. Sokolov, Z. Bao, *J. Mater. Chem.* **2009**, *19*, 3351. b816386c

[111] L. Torsi, G. M. Farinola, F. Marinelli, M. C. Tanese, O. H. Omar, L. Valli, F. Babudri, F. Palmisano, P. G. Zambonin, F. Naso, *Nat. Mater.* **2008**, *7*, 412.

[112] M. L. Hammock, A. N. Sokolov, R. M. Stoltenberg, B. D. Naab, Z. Bao, *ACS Nano* **2012**, *6*, 3100.

[113] P. Bergveld, *Sensors Actuators B* **2003**, *88*, 1.

[114] P. Bergveld, *IEEE Trans. Biomed. Eng.* **1972**, *BME-19*, 342.

[115] S. Ritjareonwattu, Y. Yun, C. Pearson, M. C. Petty, *IEEE Sens. J.* **2012**, *12*, 1181.

[116] T. Ji, P. Rai, S. Jung, V. K. Varadan, *Appl. Phys. Lett.* **2008**, *92*, 233304.

[117] M.-J. Spijkman, J. J. Brondijk, T. C. T. Geuns, E. C. P. Smits, T. Cramer, F. Zerbetto, P. Stoliar, F. Biscarini, P. W. M. Blom, D. M. de Leeuw, *Adv. Funct. Mater.* **2010**, *20*, 898.

[118] A. Caboni, E. Orgiu, E. Scavetta, M. Barbaro, A. Bonfiglio, *Appl. Phys. Lett.* **2009**, *95*, 123304.

[119] S. Lai, M. Demelas, G. Casula, P. Cosseddu, M. Barbaro, A. Bonfiglio, *Adv. Mater.* **2013**, *25*, 103.

[120] T. Cramer, A. Campana, F. Leonardi, S. Casalini, A. Kyndiah, M. Murgia, F. Biscarini, *J. Mater. Chem. B* **2013**, *1*, 3728.

[121] S. H. Kim, K. Hong, W. Xie, K. H. Lee, S. Zhang, T. P. Lodge, C. D. Frisbie, *Adv. Mater.* **2012**, *25*, 1822.

[122] L. Herlogsson, X. Crispin, N. D. Robinson, M. Sandberg, O.-J. Hagel, G. Gustafsson, M. Berggren, *Adv. Mater.* **2007**, *19*, 97.

[123] S. Ono, K. Miwa, S. Seki, J. Takeya, *Appl. Phys. Lett.* **2009**, *94*, 063301.

[124] J. H. Cho, J. Lee, Y. Xia, B. Kim, Y. He, M. J. Renn, T. P. Lodge, C. D. Frisbie, *Nat. Mater.* **2008**, *7*, 900.

[125] J. Lee, L. G. Kaake, J. H. Cho, X.-Y. Zhu, T. P. Lodge, C. D. Frisbie, *J. Phys. Chem. C* **2009**, *113*, 8972.

[126] M. Hamedi, L. Herlogsson, X. Crispin, R. Marcilla, M. Berggren, O. Inganäs, *Adv. Mater.* **2009**, *21*, 573.

[127] L. Kergoat, L. Herlogsson, D. Braga, B. Piro, M.-C. Pham, X. Crispin, M. Berggren, G. Horowitz, *Adv. Mater.* **2010**, *22*, 2565.

[128] L. Kergoat, B. Piro, M. Berggren, M.-C. Pham, A. Yassar, G. Horowitz, *Org. Electron.* **2012**, *13*, 1.

[129] S. Casalini, F. Leonardi, T. Cramer, F. Biscarini, *Org. Electron.* **2012**, *14*, 156.

[130] F. Buth, A. Donner, M. Sachsenhauser, M. Stutzmann, J. A Garrido, *Adv. Mater.* **2012**, *24*, 4511.

[131] M. Magliulo, A. Mallardi, M. Y. Mulla, S. Cotrone, B. R. Pistillo, P. Favia, I. Vikholm-Lundin, G. Palazzo, L. Torsi, *Adv. Mater.* **2013**, *25*, 2090.

[132] F. Buth, D. Kumar, M. Stutzmann, J. A. Garrido, *Appl. Phys. Lett.* **2011**, *98*, 153302.

[133] A. Laiho, L. Herlogsson, R. Forchheimer, X. Crispin, M. Berggren, *Proc. Natl. Acad. Sci. U. S. A.* **2011**, *108*, 15069.

[134] A. J. Bard, L. R. Faulkner, *Electrochemical Methods: Fundamentals and Applications*, 2nd ed., John Wiley & Sons Inc., **2001**.

[135] H. S. White, G. P. Kittlesen, M. S. Wrighton, *J. Am. Chem. Soc.* **1984**, *106*, 5375.

[136] E. W. Paul, A. J. Ricco, M. S. Wrighton, *J. Phys. Chem.* **1985**, *89*, 1441.

[137] Y. Wen, Y. Liu, Y. Guo, G. Yu, W. Hu, *Chem. Rev.* **2011**, *111*, 3358.

[138] S. Gamerith, A. Klug, H. Scheiber, U. Scherf, F. Moderegger, E. J. W. List, *Adv. Funct. Mater.* **2007**, *17*, 3111.

[139] A. Blümel, A. Klug, S. Eder, U. Scherf, E. Moderegger, E. J. W. List, *Org. Electron.* **2007**, *8*, 389.

[140] B. D. Gates, Q. Xu, M. Stewart, D. Ryan, C. G. Willson, G. M. Whitesides, *Chem. Rev.* **2005**, *105*, 1171.

[141] Mircorchemicals GmbH, Ulm, Germany; www.microchemicals.de

[142] TECHNIC FRANCE, http://technic.fr/v2/technic_france_advanced_photoresist_strippers (16.08.2012)

[143] J. A. Voorthuyzen, K. Keksin, P. Bergveld, *Surf. Sci.* **1987**, *187*, 201.

[144] H.-C. Tiao, Y.-J. Lee, Y.-S. Liu, S.-H. Lee, C.-H. Li, M.-Y. Kuo, *Org. Electron.* **2012**, *13*, 1004.

[145] H.-J. Butt, K. Graz, M. Kappl, *Physics and Chemistry of Interfaces*, Wiley-VCH Verlag GmbH & Co. KGaA, Weinheim, **2003**; chapter 7, p.118.

[146] B. Stadlober, U. Haas, H. Gold, A. Haase, G. Jakopic, G. Leising, N. Koch, S. Rentenberger, E. Zojer, *Adv. Funct. Mater.* **2007**, *17*, 2687.

[147] J. Kofler, DA, master thesis, *Fabrication and investigation of micro – and nano – fluidic devices: Fundamental aspects and sensor applications*, Master Thesis, Graz University of Technology, **2011**.

[148] M. Zhang, H. N. Tsao, W. Pisula, C. Yang, A. K. Mishra, K. Müllen, *J. Am. Chem. Soc.* **2007**, *129*, 3472.

[149] S. Allard, M. Forster, B. Souharce, H. Thiem, U. Scherf, *Angew. Chemie* **2008**, *47*, 4070.

[150] T. Sekitani, Y. Noguchi, U. Zschieschang, H. Klauk, T. Someya, *Proc. Natl. Acad. Sci. U. S. A.* **2008**, *105*, 4976.

[151] L. A. Majewski, J. W. Kingsley, C. Balocco, A. M. Song, *Appl. Phys. Lett.* **2006**, *88*, 222108.

[152] MicroChemicals GmbH; Lithography Trouble Shooting 2012; http://www.microchemicals.eu/brochure.html

[153] C. Goldmann, C. Krellner, K. P. Pernstich, S. Haas, D. J. Gundlach, B. Batlogg, *J. Appl. Phys.* **2006**, *99*, 034507.

[154] A. Schoonveld, *Transistors based on ordered organic semiconductors*, PhD Thesis, University of Groningen, Netherlands **1999**.

[155] L.-L. Chua, R. H. Friend, P. K. H. Ho, *Appl. Phys. Lett.* **2005**, *87*, 253512.

[156] S. G. J. Mathijssen, M. Kemerink, A. Sharma, M. Cölle, P. A. Bobbert, R. A. J. Janssen, D. M. de Leeuw, *Adv. Mater.* **2008**, *20*, 975.

[157] M.-H. Yoon, C. Kim, A. Facchetti, T. J. Marks, *J. Am. Chem. Soc.* **2006**, *128*, 12851.

[158] D. Knipp, . A. Street, A. l kel, J. Ho, *J. Appl. Phys.* **2003**, *93*, 347.

[159] H. Klauk, M. Halik, U. Zschieschang, F. Eder, G. Schmid, C. Dehm, *Appl. Phys. Lett.* **2003**, *82*, 4175.

[160] Y. Qiu, Y. Hu, G. Dong, L. Wang, J. Xie, Y. Ma, *Appl. Phys. Lett.* **2003**, *83*, 1644.

[161] J. Veres, S. D. Ogier, S. W. Leeming, D. C. Cupertino, S. Mohialdin Khaffaf, *Adv. Funct. Mater.* **2003**, *13*, 199.

[162] S. Lim, S. Kim, J. Lee, M. Kim, D. Kim, T. Zyung, *Synth. Met.* **2005**, *148*, 75.

[163] I. Yagi, K. Tsukagoshia, Y. Aoyagi, *Appl. Phys. Lett.* **2005**, *86*, 103502.

[164] N. Koch, *ChemPhysChem* **2007**, *8*, 1438.

[165] A. Facchetti, *Chem. Mater.* **2011**, *23*, 733.

[166] H. N. Tsao, D. M. Cho, I. Park, M. R. Hansen, A. Mavrinskiy, D. Y. Yoon, R. Graf, W. Pisula, H. W. Spiess, K. Müllen, *J. Am. Chem. Soc.* **2011**, *133*, 2605.

[167] Z. Chen, M. J. Lee, R. S. Ashraf, Y. Gu, S. Albert-Seifried, M. M. Nielsen, B. Schroeder, T. D. Anthopoulos, M. Heeney, *Adv. Mater.* **2012**, *24*, 647.

[168] S. Wang, M. Kappl, I. Liebewirth, M. Müller, K. Kirchhoff, W. Pisula, K. Müllen, *Adv. Mater.* **2011**, *24*, 417.

[169] S. Dong, H. Zhang, L. Yang, M. Bai, Y. Yao, H. Chen, L. Gan, T. Yang, H. Jiang, S. Hou, L. Wan, X. Guo, *Adv. Mater.* **2012**, *24*, 5576.

[170] K.-J. Baeg, D. Khim, D.-Y. Kim, J. B. Koo, I.-K. You, W. S. Choi, Y.-Y. Noh, *Thin Solid Films* **2010**, *518*, 4024.

[171] G. Wang, T. Hirasa, D. Moses, A. J. Heeger, *Synth. Met.* **2004**, *146*, 127.

[172] J. Veres, S. Ogier, S. Leeming, B. Brown, D. Cupertino, H. House, P. O. Box, *Mater. Res.* **2002**, *708*, 1.

[173] W. Zhang, J. Smith, R. Hamilton, M. Heeney, J. Kirkpatrick, K. Song, S. E. Watkins, T. Anthopoulos, I. McCulloch, *J. Am. Chem. Soc.* **2009**, *131*, 10814.

[174] E. Meijer, *Synth. Met.* **2004**, *142*, 53.

[175] H.-H. Liao, C.-M. Yang, C.-C. Liu, S.-F. Horng, H.-F. Meng, J.-T. Shy, *J. Appl. Phys.* **2008**, *103*, 104506.

[176] I. McCulloch, C. Bailey, M. Giles, M. Heeney, I. Love, M. Shkunov, D. Sparrowe, S. Tierney, *Chem. Mater.* **2005**, *17*, 1381. 1.

[177] R. Abbel, M. Wolffs, R. A. A. Bovee, J. L. J. van Dongen, X. Lou, O. Henze, W. J. Feast, E. W. Meijer, A. P. H. J. Schenning, *Adv. Mater.* **2009**, *21*, 597.

[178] Z. Jiang, T. Ye, C. Yang, D. Yang, M. Zhu, C. Zhong, J. Qin, D. Ma, *Chem. Mater.* **2011**, *23*, 771.

[179] Z. Fang, V. Chellappan, R. D. Webster, L. Ke, T. Zhang, B. Liu, Y.-H. Lai, *J. Mater. Chem.* **2012**, *22*, 15397.

[180] Z. Fang, T. L. Teo, L. P. Cai, Y. H. Lai, A. Samoc, M. Samoc, *Org. Lett.* **2009**, *11*, 1.

[181] Z. Fang, X. H. Zhang, Y. H. Lai, B. Liu, *Chem. Commun.* **2009**, 920.

[182] T. Yamamoto, *Bull. Chem. Soc. Jpn*. **1999**, *72*, 621.

[183] T. Yamamoto, *Prog. Polym. Sci.* **1992**, *17*, 1153.

[184] J. F. Rusling, S. L. Suib, *Adv. Mater.* **1994**, *6*, 922.

[185] S. Hautecloque, *Journal of Photochemistry* **1980**, *14*, 157.

[186] P. E. Hoggard, A. J. Bridgeman, H. Kunkely, A. Vogler, *Inorganica Chim. Acta* **2004**, *357*, 639.

[187] S. Kappaun, S. Horner, A.-M. Kelterer, K. Waich, F. Grasse, M. Graf, L. Romaner, F. Niedermair, K. Müllen, A. C. Grimsdale, R. Saf, E. J. W. List, E. Zojer, C. Slugovc, *Macromol. Chem. Phys.* **2008**, *209*, 2122.

[188] I. Dumsch, C. J. Kudla, U. Scherf, *Macromol. Rapid Commun.* **2009**, *30*, 840.

[189] M. Vetrichelvan, S. Valiyaveettil, *Chem. Eur. J.* **2005**, *11*, 5889.

[190] S. Kappaun, S. Horner, A.-M. Kelterer, K. Waich, F. Grasse, M. Graf, L. Romaner, F. Niedermair, K. Müllen, A. C. Grimsdale, R. Saf, E. J. W. List, E. Zojer, C. Slugovc, *Macromol. Chem. Phys.* **2008**, *209*, 2122.

[191] G. Garrido, E. Koort, C. Rafols, E. Bosch, T. Rodima, I. Leito, M. Roses, *J. Org. Chem.* **2006**, *71*, 9062;

[192] A. Wan, J. Hwang, F. Amy, A. Kahn, *Org. Electron.* **2005**, *6*, 47.

[193] W.-K. Kim, J.-L. Lee, *Appl. Phys. Lett.* **2006**, *88*, 262102.

[194] S. Grecu, M. Roggenbuck, A. Opitz, W. Brütting, *Org. Electron.* **2006**, *7*, 276.

[195] J. Veres, S. Ogier, G. Lloyd, D. de Leeuw, *Chem. Mater.* **2004**, *16*, 4543.

[196] B. H. Hamadani, H. Ding, Y. Gao, D. Natelson, *Phys. Rev. B* **2005**, *72*, 235302.

[197] S. Hoshino, M. Yoshida, S. Uemura, T. Kodzasa, N. Takada, T. Kamata, K. Yase, *J. Appl. Phys.* **2004**, *95*, 5088.

[198] E. Said, O. Larsson, M. Berggren, X. Crispin, *Adv. Funct. Mater.* **2008**, *18*, 3529.

[199] L. Herlogsson, Y.-Y. Noh, N. Zhao, X. Crispin, H. Sirringhaus, M. Berggren, *Adv. Mater.* **2008**, *20*, 4708.

[200] D. Braga, M. Ha, W. Xie, C. D. Frisbie, *Appl. Phys. Lett.* **2010**, *97*, 193311.

[201] A. Härtl, J. A. Garrido, S. Nowy, R. Zimmermann, C. Werner, D. Horinek, R. Netz, M. Stutzmann, *J. Am. Chem. Soc.* **2007**, *129*, 1287.

[202] Y. Ling, *J. Electrochem. Soc.* **1997**, *144*, 2689.

[203] J. Hölzl, F. K. Schulte, *Solid Surface Physics; Work Function of Metals*, (Eds. G. Höhler) Springer-Verlag, Berlin, **1979**.

[204] D. R. Lide, Ed., *CRC Handbook of Chemistry and Physics*, 87th ed., 12-114, CRC Press **2006**.

[205] O. Larsson, A. Laiho, W. Schmickler, M. Berggren, X. Crispin, *Adv. Mater.* **2011**, *23*, 4764.

[206] L. Robinson, J. Isaksson, N. D. Robinson, M. Berggren, *Surf. Sci.* **2006**, *600*, L148.

[207] L. Robinson, A. Hentzell, N. D. Robinson, J. Isaksson, M. Berggren, *Lab Chip* **2006**, *6*, 1277.

[208] V. Bychkov, P. Matyba, V. Akkerman, M. Modestov, G. Brodin, C. K. Law, M. Marklund, L. Edman, *Phys. Rev. Lett.* **2011**, *107*, 016103.

[209] N. Kaihovirta, H. Aarnio, C.-J. Wikman, C.-E. Wilén, R. Österbacka, *Adv. Funct. Mater.* **2010**, *20*, 2605.

[210] U. Barsch, F. Beck, Electrochim. Acta **1996**, *41*, 1761.

[211] www.nico2000.net, (06.05.2014)

[212] A. Lewenstam, *Electroanalysis* **2014**, *26*, 1171.

[213] M. Dole, *J. Chem. Educ.* **1980**, *57*, 134.

[214] J. Bobacka, A. Ivaska, A. Lewenstam, *Chem. Rev.* **2008**, *108*, 329.

[215] E. Bakker, E. Pretsch, *Anal. Chem.* **2002**, 420.

[216] N. Abramova, A. Bratov, *Sensors* **2009**, *9,* 7097.

[217] S. V. Lamaka, M.G. Taryba, M. L. Zheludkevich, M. G. S. Ferreira, *Electroanalysis* **2009**, *21*, 2447.

[218] P. Bühlmann, L. D. Chen, in *Supramol. Chem. From Mol. to Nanomater.* (Eds.: P. A. Gale, J. W. Steed), John Wiley & Sons, Ltd., **2012**, pp. 2539–2577.

[219] K. Melzer, A. M. Münzer, E. Jaworska, K. Maksymiuk, A. Michalska, G. Scarpa, *Org. Electron.* **2014**, *15*, 595.

[220] J. Kofler, K. Schmoltner, A. Klug, E. J. W. List-Kratochvil, *Appl. Phys. Lett.* **2014**, *104*, 193305.

[221] A. Cadogan, Z. Gao, A. Lewenstam, A. Ivaska, D. Diamond, *Anal. Chem.* **199**2, *64*, 2496.

[222] J. Kofler, PhD thesis in preparation, University of Technology Graz.

[223] E. Bakker, P. Bühlmann, E. Pretsch, *Chem. Rev.* **1997**, *97*, 3083.

[224] W. E. Morf, *Anal. Chem*. **1977**, *49*, 810.

[225] A. Ceresa, T. Sokalski, E. Pretsch, *J. Electroanal. Chem.* **2001**, *501*, 70.

[226] S. Mathison, E. Bakker, *Anal. Chem.* **1998**, *70*, 303.

[227] P. Bergveld, *Sens. Actuators* **1981**, *1*, 17.

[228] P. Bergveld, *IEEE Trans. Biomed. Eng.* **1968**, BME 15,102.

[229] E. Bakker, E. Pretsch, *Trends in Anal. Chem.* **2001**, *20*, 11.

[230] M. Irimia- ladu, E. D. Głowacki, P. A Troshin, G. Schwabegger, L. Leonat, D. K. Susarova, O. Krystal, M. Ullah, Y. Kanbur, M. A. Bodea, V. F. Razumov, H. Sitter, S. Bauer, N. S. Sariciftci, *Adv. Mater.* **2011**, *24*, 375.

[231] O. Knopfmacher, M. L. Hammock, A. L. Appleton, G. Schwartz, J. Mei, T. Lei, J. Pei, Z. Bao, *Nat. Commun.* **2014**, *5*, 2954.

Appendix

Within the appendix the original publications which are the basis of this thesis are included:

[1**] Photolithographic processing and its influence on the performance of organic field-effect transistors**
K. Schmoltner, A. Klug, J. Kofler and E. J.W. List
Proceedings of SPIE 8479, Organic Semiconductors in Sensors & Bioelectronics V, 84790J, (**2012**)

[2**] A heterotriangulene polymer for air-stable organic field-effect transistors**
K. Schmoltner, F. Schlütter, M. Kivala, M. Baumgarten, S. Winkler, R. Trattnig, N. Koch, A. Klug, E. J. W. List and K. Müllen
Polymer Chemistry 4, 5337-5344 (**2013**)

[3**] Electrolyte-gated field effect transistors for sensing applications in aqueous media**
K. Schmoltner, J. Kofler, A. Klug and E. J. W. List-Kratochvil
Proceedings of SPIE 8831, Organic Field-Effect Transistors XII; Organic Semiconductors in Sensors & Bioelectronics VI, 88311N (**2013**)

[4**] Electrolyte-gated field effect transistor for selective and reversible ion detection**
K. Schmoltner*, J. Kofler*, A. Klug and E. J. W. List-Kratochvil,
Advanced Materials 25 (47), 6895–6899 (**2013**)

*both authors contributed equally.

Photolithographic processing and its influence on the performance of organic field-effect transistors

K. Schmoltner,[a] A. Klug,[a] J. Kofler,[a] E. J. W. List*[a,b]
[a]NanoTecCenter Weiz Forschungsgesellschaft mbH, Franz-Pichler-Strasse 32, 8160 Weiz, Austria;
[b]Institute of Solid State Physics, Graz University of Technology, Petersgasse 16, 8010 Graz, Austria

ABSTRACT

We report on the influence of photolithographic processing of source/drain electrodes on the device performance of regioregular poly(3-hexylthiophene)-based bottom-gate bottom-contact organic field-effect transistors (OFETs). The presented results demonstrate that it is not only the processing conditions of the organic semiconductor influencing relevant device parameters, but it is also the preceding process steps including the structuring of electrodes via lift-off which significantly determine the OFET performance. In particular, the effects of photoresist residuals within the active channel region and the influence of the application of various lift-off chemicals were thoroughly investigated by contact angle measurements, atomic force microscopy and electrical characterization of OFET-based devices. By modifying the dielectric/semiconductor and/or electrode/semiconductor interfaces, the applied chemicals are shown to affect the device performance in terms of switch-on voltage, subthreshold swing and on/off-current ratio. The present study emphasizes the necessity for the optimization of the manufacturing process in order to obtain reproducible high-performing OFETs and OFET-based sensors.

Keywords: Organic field-effect transistor, OFET, OFET fabrication, organic semiconductors, plastic electronics
*emil.list@ntc-weiz.at; phone 0043 316 876 8000; fax 0043 316 876 8040; ntc-weiz.at

1. INTRODUCTION

Organic field-effect transistors (OFETs)[1,2] have been in focus of intense research for more than 20 years. They have developed rapidly, driven by the outstanding properties of organic compounds which enable the realization of cheap, lightweight, large-area, flexible electronic circuits.[3,4] Successful realizations of flexible displays[5,6,7], radio-frequency identification tags[8,9] as well as OFET-based sensors[10,11,12] were presented. Recent advances in this field were not only possible due to extensive research and development of high-mobility[13] and solution-processable organic semiconductors[14] but also because of the technological progress concerning the manufacturing process. Accordingly, besides the optimization of organic semiconductors, whose charge-carrier mobility values (of 0.1 - 1 $cm^2\ V^{-1}s^{-1}$)[15,16] already exceed the benchmark values of amorphous silicon, big focus is also set on improving the OFET performance from the device physics and manufacturing point of view (e.g. downscaling for low-voltage applications and higher operational frequencies[17]). For the deposition/structuring of the components of organic field-effect transistors several processing techniques have been employed. Aside from inkjet printing,[18] other printing techniques (screen-, offset-, gravure-printing), soft lithography[19] and imprint lithography, photolithography is one of the well-developed and widely used processes.[20] It provides a straightforward method to process large-area substrates, enabling parallel patterning as well as down-scaling with feature sizes as low as ~40 nm[21]. Since it is a well-established method in today's integrated circuit fabrication based on inorganic semiconductors, its application in organic electronics benefits from the available knowledge. However, there are significant drawbacks including high process and equipment costs and limitations when pattering the organic semiconductor (e.g. delamination, degradation effects). In this study photolithographic patterning via lift-off was applied for structuring the source/drain electrodes of OFETs including the following process steps: preparation of the substrate surface, coating of a photoresist, softbake, alignment and exposure through a photomask, post-exposure bake, development, metallization, removal (see Figure 1).

Organic Semiconductors in Sensors and Bioelectronics V, edited by Ruth Shinar, Ioannis Kymissis,
Proc. of SPIE Vol. 8479, 84790J · © 2012 SPIE · CCC code: 0277-786/12/$18 · doi: 10.1117/12.930445

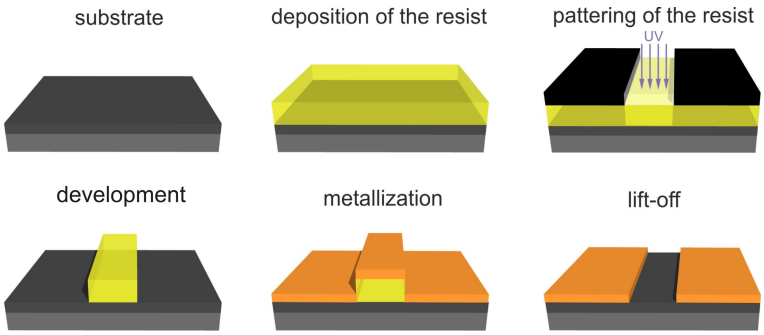
substrate
deposition of the resist
pattering of the resist
UV
development
metallization
lift-off

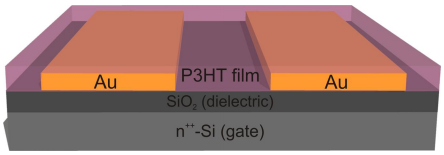
Au
P3HT film
Au
SiO2 (dielectric)
n++-Si (gate)

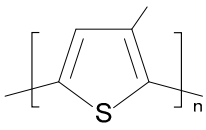
S
n

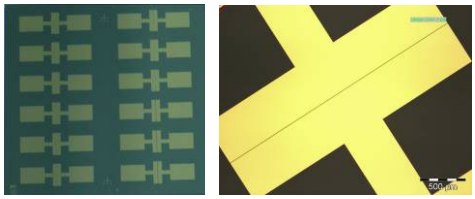

Figure 3. Typical sample with 12 structured gold source/drain electrodes (left) and corresponding micrograph (right).

The semiconducting polymer regioregular poly(3-hexylthiophene) (P3HT, Plexcore® OS) was dissolved in toluene or chloroform with a concentration of 2 g/l. Before the deposition of the semiconductor, adsorbed water on the SiO_2 surface was removed by an annealing step at 120°C in high vacuum ($p \sim 4x10^{-5}$ mbar) for 1 h. After spin-coating the semiconductor the films were first dried at 60°C in argon for approximately 10 min and subsequently at 120°C in high vacuum ($p \sim 4x10^{-5}$ mbar) for 1h. All devices were assembled and characterized under inert atmosphere in argon-filled glove boxes. The electrical characteristics were measured using an Agilent B1500A Parameter Analyzer and gradual channel approximation was used to calculate the mobility μ in the saturation regime.[25]

3. RESULTS AND DISCUSSION

3.1 Influence of photoresist residuals on the OFET performance

After photolithographic structuring of the source/drain electrodes the samples were investigated with scanning electron microscopy (SEM, Raith e-line) and tapping-mode atomic force microscopy (AFM, Veeco Instruments). Figure 4 (a) and (b) show SEM and AFM images of the channel between the gold source/drain electrodes after lift-off with *n*-methyl-2-pyrrolidon (NMP). The SEM image reveals areas with dark spots on the SiO_2 surface, which are also observable in the AFM image in terms of height variations up to ~8 nm. Since SiO_2 usually has a very smooth surface and the SEM image shows significant material contrast, these features most likely can be ascribed to photoresist residuals. Their origin might be a high degree of crosslinking of the negative resist, being increased for higher temperatures. The temperature input in combination with the corresponding radiation during thermal evaporation of the metal might lead to crosslinking and therefore reducing removability.[26] In order to remove these resist residuals, alternative removers (TechniStrip™ NI555 and P1316) were used, which rather dissolve the crosslinked resist than peeling it off the substrate. SEM and AFM images confirmed the successful removal of the photoresist with these strippers (Figure 4 (d,e,f)). The corresponding line section of the AFM image shows a very smooth SiO_2 surface within the channel without any residual chemicals.

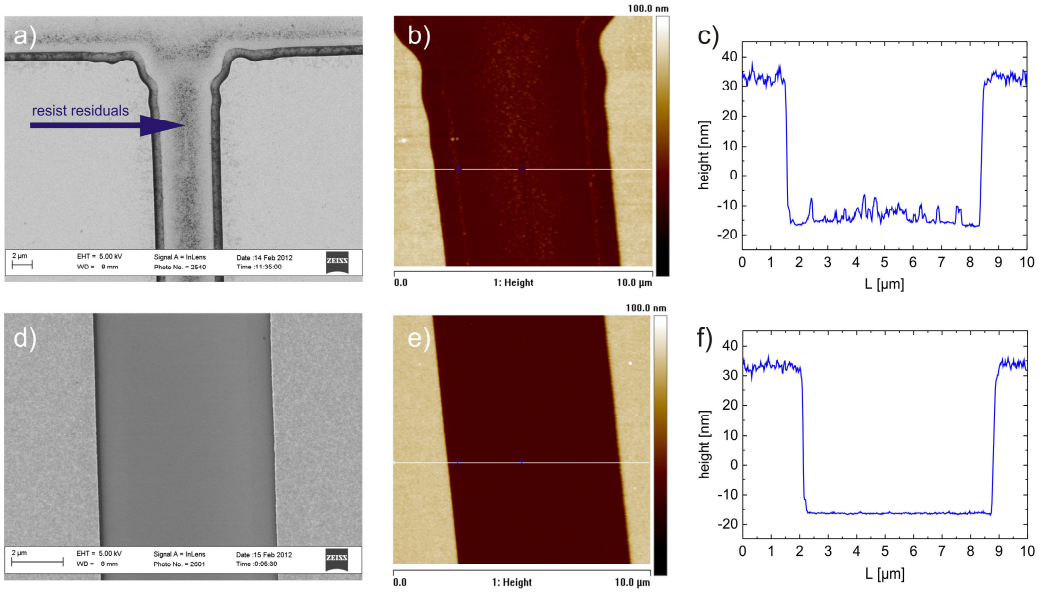

Figure 4. SEM (a,d) and AFM (b,e) images and line sections (c,f) of the structured channel on SiO_2 after lift-off with NMP showing photoresist residuals (top) and without residuals after using the remover TechniStrip™ P1316 (bottom).

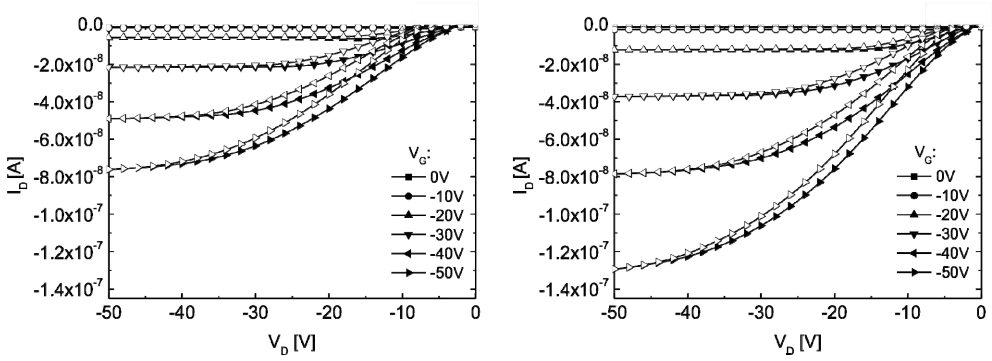
0.0
-2.0x10-8
-4.0x10-8
-6.0x10-8
-8.0x10-8
-1.0x10-7
-1.2x10-7
-1.4x10-7
ID [A]
-50
-40
-30
-20
-10
0
VD [V]
VG:
0V
-10V
-20V
-30V
-40V
-50V

Besides the morphological investigations, the contact angles of deionized water (DI-H_2O) and diiodomethane on the SiO_2 surface were determined in order to investigate the influence of the applied lift-off chemicals on the surface polarity. Table 2 summarizes the results, also including relevant device parameters of corresponding P3HT-based BG/BC OFETs. The application of P1316 significantly changed the SiO_2 surface energy from hydrophobic (contact angle of DI-H_2O ~70°), when NMP and NI555 was used, to hydrophilic (contact angle of DI-H_2O ~11°). Not only the surface energy of SiO_2 was affected, but also the gold surface showed modified contact angles of DI-H_2O and diiodomethane, being an issue for morphology changes at the electrode/semiconductor interface and therefore being relevant for injection properties. Moreover, an additional cleaning step with acetone, isopropanol and rinsing with deionized water slightly changed the contact angles as well, in particular hydrophobizing the surface when applied after removing with P1316.

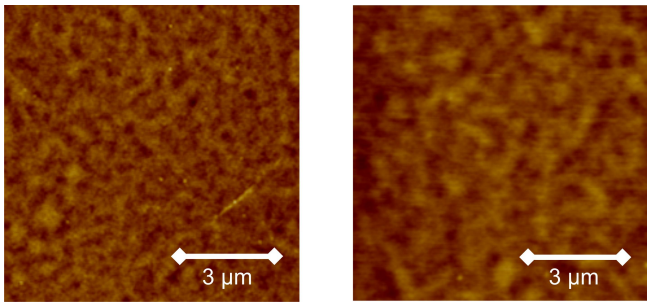

Figure 6. AFM height images of P3HT on SiO_2 when different removers were used for the lift-off process: (left) NMP-NI555 and (right) NMP-P1316; color code from black to white corresponds to a z-data range of 5nm.

Table 2: Contact angles on SiO_2 and gold (thermally evaporated) after using different lift-off chemicals and relevant OFET parameters of corresponding P3HT-based BG/BC devices ($L \approx 25$ mm, $W \approx 2.85$ mm): saturation field-effect mobility μ_{sat} (at V_D = -50V, V_G = -35V calculated according to gradual channel approximation), on/off-current ratio I(on/off) (I_{on}: V_G = -50V, I_{off}: V_G = 0V at V_D = -50V), switch-on voltage V_{so}, subthreshold slope S and percentage of I_D at $V_D = V_G$ = -50V in output characteristics with respect to value in transfer characteristics I_{on}*(O-T)*.

Substrate	**Treatment**	**Contact angle (°)**		**Mobility μ_{sat} ($cm^2\ V^{-1}\ s^{-1}$)**	***I* (on/off)**	**V_{so} (V)**	***I_{on} (O-T)* (%)**
		H_2O	**Diiodmethan**				
SiO_2	NMP – NI555	70.6	59.9	1.8×10^{-4}	5.6×10^{3}	-4	82
Gold	NMP – NI555	59.5	22.6				
SiO_2	NMP-NI555 – acetone–ISO	71.5	60.2	1.9×10^{-4}	6.8×10^{3}	-4	82
Gold	NMP-NI555 – aceton–ISO	63	24.5				
SiO_2	NMP – P1316	11.7	47.3	2.1×10^{-4}	1.5×10^{4}	-12	73
Gold	NMP – P1316	32.1	4.4				
SiO_2	NMP-P1316 – acetone-ISO	32.1	53.3	1.6×10^{-4}	1.6×10^{4}	-9	72
Gold	NMP-P1316 – acetone-ISO	40.2	14.7				

Figure 7 depicts the output characteristics, the semilogarithmic transfer curves as well as the square-root of the channel current vs. gate voltage of typical P3HT-based BG/BC OFETs when different lift-off chemicals were applied. As indicated above and shown by other groups,[36,37] chemicals modifying the surface properties of the dielectric significantly influence the performance of organic field-effect transistors. Accordingly, OFETs treated with remover P1316 showed a more negative switch-on voltage and a larger hysteresis, indicating a higher trap density due to a larger number of OH-groups on the more hydrophilic surface.[29,38] This is in agreement with the results of the contact angle measurements. Moreover, by comparing the maximum currents in Figure 7, the OFETs treated with P1316 (more hydrophilic surface) yielded ~16% lower drain current (at V_G = -50 V, V_D = -50 V) as well as a lower I_{on} *(O-T)* ratio (see Table 2), which again is a sign for a larger trap density. Although OFETs with NI555-treated SiO_2 exhibited lower channel currents in the reverse sweep as well, the effect ascribed to charge-carrier trapping is not as pronounced as for OFETs with the hydrophilic SiO_2 surface. In accordance with the results of the contact angle measurements, an additional cleaning step of the sample with isopropanol and acetone after the lift-off process did not significantly change the performance of

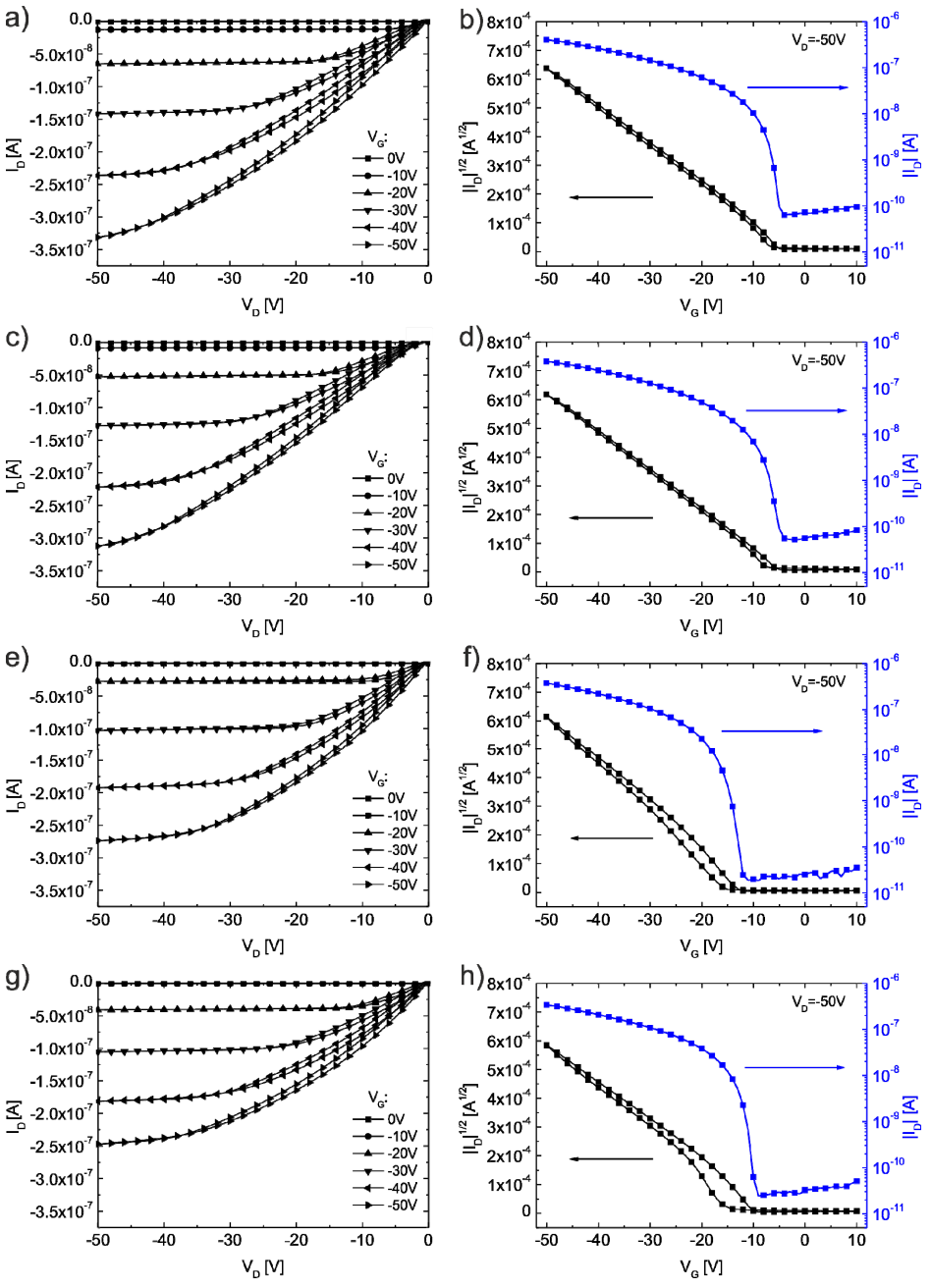
a)
b)
c)
d)
e)
f)
g)
h)
I_D [A]
V_D [V]
V_G:
0V
-10V
-20V
-30V
-40V
-50V
V_D=-50V
$|I_D|^{1/2}$ [$A^{1/2}$]
$|I_D|$ [A]
V_G [V]

4. SUMMARY AND CONCLUSIONS

In summary, we demonstrated that photolithographic processing to structure the source/drain electrodes of organic field-effect transistors can significantly influence the dielectric/semiconductor and/or electrode/semiconductor interfaces, leading to a modification of the electrical performance of bottom-gate bottom-contact OFETs based on P3HT. In particular, photoresist residuals within the channel of OFETs lead to decreased field-effect mobilities, lower on/off-current ratios and higher subthreshold slopes, originating from a substantial increase of the surface roughness and the associated charge carrier trap density. The application of additional remover chemicals successfully dissolved the observed photoresist residuals affecting the OFET performance. If, however, a remover chemical was used which renders the substrate surface more hydrophilic, the corresponding devices showed significantly larger negative threshold voltages indicating higher trap densities at the semiconductor/dielectric interface originating from a larger number of OH-groups on the surface. To conclude, the presented results clearly demonstrate that process chemicals have a distinct influence on the device performance of organic field-effect transistors, making it inevitably necessary to focus not only on the constituting OFET materials but also on the manufacturing process for obtaining reproducible well-performing OFETs and OFET-based sensors.

ACKNOWLEDGEMENTS

The authors gratefully acknowledge M. Postl and P. Hierzer from NTC Weiz GmbH as well as C. Koch and T. Rinke from MicroChemicals GmbH for support and discussions. For financial support the Styrian Government (projects BioOFET 2 and MIEC-DEVs) is acknowledged.

REFERENCES

[1] Horowitz, G., "Organic Field-Effect Transistors," Adv. Mater. 10(5), 365-377 (1998).
[2] Bao, Z. and Locklin, J., [Organic Field-Effect Transistors], CRC Press, Boca Raton (2007).
[3] Sekitani, T., and Someya, T., "Human-friendly organic integrated circuits," Mater. Today 14(9), 398–407 (2011).
[4] Gelinck, G., Heremans, P., Nomoto, K., and Anthopoulos, T.D., "Organic transistors in optical displays and microelectronic applications," Adv. Mater. 22(34), 3778–3798 (2010).
[5] Huitema, H.E. a., Gelinck, G.H., van der Putten, J.B.P.H., Kuijk, K.E., Hart, C.M., Cantatore, E., and de Leeuw, D.M., "Active-matrix displays driven by solution-processed polymeric transistors," Adv. Mater. 14(17), 1201–1204 (2002).
[6] Vaidya, V., Member, S., Soggs, S., Kim, J., Haldi, A., Haddock, J.N., Kippelen, B., and Wilson, D.M., "Comparison of pentacene and amorphous silicon AMOLED display driver circuits," 55(5), IEEE Trans. Circuits Syst. I, Reg. Papers 1177–1184 (2008).
[7] Zhou, L., Wanga, A., Wu, S.-C., Sun, J., Park, S., and Jackson, T.N., "All-organic active matrix flexible display," Appl. Phys. Lett. 88(8), 083502 (2006).
[8] Baude, P. F., Ender, D. A., Haase, M. A., Kelley, T. W., Muyres, D. V. and Theiss, S. D., "Pentacene-based radio-frequency identification circuitry," Appl. Phys. Lett. 85(22), 3964-3966 (2003).
[9] Cantatore, E., Geuns, T.C.T., Gelinck, G.H., Veenendaal, E.V., Gruijthuijsen, A.F.A., Schrijnemakers, L., Drews, S., and Leeuw, D.M.D., "A 13.56-MHz RFID system based on organic transponders," IEEE J. Solid-State Circuits 42(1), 84–92 (2007).
[10] Someya, T., Dodabalapur, A., Huang, J., See, K.C., and Katz, H.E., "Chemical and physical sensing by organic field-effect transistors and related devices," Adv. Mater. 22(34), 3799–3811 (2010).
[11] Mabeck, J.T., and Malliaras, G.G., "Chemical and biological sensors based on organic thin-film transistors," Anal. Bioanal. Chem. 384(2), 343–353 (2006).
[12] Berggren, M., and Richter-Dahlfors, a., "Organic Bioelectronics," Adv. Mater. 19(20), 3201–3213 (2007).
[13] Zhang, M., Tsao, H.N., Pisula, W., Yang, C., Mishra, A.K., and Müllen, K., "Field-effect transistors based on a benzothiadiazole-cyclopentadithiophene copolymer," J. Am. Chem. Soc. 129(12), 3472–3473 (2007).
[14] Allard, S., Forster, M., Souharce, B., Thiem, H., and Scherf, U., "Organic semiconductors for solution-processable field-effect transistors (OFETs)," Organ. Electron. 4070 – 4098 (2008).
[15] Yan, H., Chen, Z., Zheng, Y., Newman, C., Quinn, J.R., Dötz, F., Kastler, M., and Facchetti, A., "A high-mobility electron-transporting polymer for printed transistors," Nature 457(7230), 679–686 (2009).
[16] Bronstein, H., Chen, Z., Ashraf, R.S., Zhang, W., Du, J., Durrant, J.R., Tuladhar, P.S., Song, K., Watkins, S.E., et al., "Thieno[3,2-b]thiophene-diketopyrrolopyrrole-containing polymers for high-performance organic field-effect transistors and organic photovoltaic devices," J. Am. Chem. Soc. 133(10), 3272–3275 (2011).
[17] Sekitani, T., Noguchi, Y., Zschieschang, U., Klauk, H., and Someya, T., "Organic transistors manufactured using inkjet technology with subfemtoliter accuracy," Proc. Natl. Acad. Sci. U.S.A. 105(13), 4976–4980 (2008).
[18] Gamerith, S., Klug, A., Scheiber, H., Scherf, U., Moderegger, E. and List, E. J. W., "Direct Ink-Jet Printing of Ag-Cu Nanoparticle and Ag-Precursor Based Electrodes for OFET Applications," Adv. Funct. Mater. 17, 3111-3118 (2007).
[19] Blümel, A., Klug, A., Eder, S., Scherf, U., Moderegger, E. and List, E. J. W., "Micromolding in capillaries and microtransfer printing of silver nanoparticles as soft-lithographic approach for the fabrication of source/drain electrodes in organic field-effect transistors," Org. Electron. 8, 389-395 (2007).
[20] Wen, Y., Liu, Y., Guo, Y., Yu, G., and Hu, W., "Experimental techniques for the fabrication and characterization of organic thin films for field-effect transistors," Chem. Rev. 111(5), 3358–3406 (2011).
[21] Gates, B.D., Xu, Q., Stewart, M., Ryan, D., Willson, C.G., and Whitesides, G.M., "New approaches to nanofabrication: molding, printing, and other techniques," Chem. Rev. 105(4), 1171–1196 (2005).

[22] Majewski, L. A., Kingsley, J. W., Balocco, C. and Song, A. M., "Influence of processing conditions on the stability of poly(3-hexylthiophene)-based field-effect transistors," Appl. Phys. Lett. 88, 222108 (2006).
[23] Mircorchemicals GmbH, Ulm, Germany; www.microchemicals.de
[24] TECHNIC FRANCE; http://technic.fr/v2/technic_france_advanced_photoresist_strippers
[25] Horowitz, G., Lang, P., Mottaghi, M., and Aubin, H., "Extracting parameters from the current-voltage characteristics of organic field-effect transistors," Adv. Funct. Mater. 14(11), 1069–1074 (2004).
[26] MicroChemicals GmbH; Lithography Trouble Shooting 2012; http://www.microchemicals.eu/brochure.html
[27] Goldmann, C., Krellner, C., Pernstich, K.P., Haas, S., Gundlach, D.J., and Batlogg, B., "Determination of the interface trap density of rubrene single-crystal field-effect transistors and comparison to the bulk trap density," J. Appl. Phys. 99(3), 034507 (2006).
[28] Schoonveld, A., PhD Thesis, "Transistors based on ordered organic semiconductors," University of Groningen, Netherlands (1999).
[29] Chua, L.-L., Zaumseil, J., Chang, J.-F., Ou, E. C.-W., Ho, P. K.-H., Sirringhaus, H. and Friend, R. H., "General observation of n-type field-effect behaviour in organic semiconductors," Nature 434, 194-199 (2005).
[30] Mathijssen, S.G.J., Kemerink, M., Sharma, a., Cölle, M., Bobbert, P. a., Janssen, R. a. J., and de Leeuw, D.M., "Charge trapping at the dielectric of organic transistors -Visualized in real time and space," Adv. Mater. 20(5), 975–979 (2008).
[31] Yoon, M.-H., Kim C., Facchetti, A., Marks,.T. J., "Gate dielectric chemical structure - Organic field-effect transistor performance correlations for electron, hole and ambipolar organic semiconductors," J. Am. Chem. Soc. 128, 12851–12869 (2006).
[32] Knipp, D., Street, R. a., Vo lkel, a., and Ho, J., "Pentacene thin film transistors on inorganic dielectrics: Morphology, structural properties, and electronic transport," J. Appl. Phys. 93(1), 347 (2003).
[33] Klauk, H., Halik, M., Zschieschang, U., Eder, F., Schmid, G., and Dehm, C., "Pentacene organic transistors and ring oscillators on glass and on flexible polymeric substrates," Appl. Phys. Lett.s 82(23), 4175 (2003).
[34] Natali, D., and Caironi, M., "Charge injection in solution-processed organic field-effect transistors: physics, models and characterization methods," Adv. Mater. 24(11), 1357–1387 (2012).
[35] Qiu, Y., Hu, Y., Dong, G., Wang, L., Xie, J., and Ma, Y., "H_2O effect on the stability of organic thin-film field-effect transistors," Appl. Phys. Lett. 83(8), 1644 (2003).
[36] Veres, J., Ogier, S.D., Leeming, S.W., Cupertino, D.C., and Mohialdin Khaffaf, S., "Low-k insulators as the choice of dielectrics in organic field-effect transistors," Adv. Funct. Mater. 13(3), 199–204 (2003).
[37] Lim, S., Kim, S., Lee, J., Kim, M., Kim, D., and Zyung, T., "Surface-treatment effects on organic thin-film transistors," Synth. Met. 148(1), 75–79 (2005).
[38] Yagi, I., Tsukagoshia, K. and Aoyagi, Y., "Modification of the electric conduction at the pentacene/SiO_2 interface by surface termination of SiO_2," Appl. Phys. Lett. 86, 103502 (2005).
[39] Koch, N., "Organic electronic devices and their functional interfaces," Chemphyschem 8(10), 1438–1455 (2007).

Polymer Chemistry

RSC Publishing

PAPER

View Article Online
View Journal | View Issue

A heterotriangulene polymer for air-stable organic field-effect transistors†

Cite this: *Polym. Chem.*, 2013, **4**, 5337

Kerstin Schmoltner,[a] Florian Schlütter,[b] Milan Kivala,[b] Martin Baumgarten,[b] Stefanie Winkler,[cd] Roman Trattnig,[a] Norbert Koch,[cd] Andreas Klug,[a] Emil J. W. List*[ae] and Klaus Müllen*[b]

Received 19th January 2013
Accepted 5th March 2013

DOI: 10.1039/c3py00089c

www.rsc.org/polymers

We report on a novel air-stable p-type heterotriangulene polymer (**PTA**) for large-area organic field-effect transistor (OFET) applications. The newly synthesized amorphous organic semiconductor was characterized concerning morphological, optical, electrical and interface related properties and revealed a saturation mobility of $\sim 4.2 \times 10^{-3}$ cm^2 V^{-1} s^{-1} and an on/off current ratio of $\sim 10^5$ in bottom-gate/bottom-contact (BG/BC) OFETs. The influence of several interface modifications was investigated in order to optimize the device performance. **PTA** FETs exhibited excellent air stability over several months and a superior performance compared to the widely used poly(3-hexylthiophene)-based OFETs. Moreover, we show that hydrochloric acid in chloroform leads to protonation of the nitrogen atoms on the **PTA** polymer, resulting in a significant change of the electrical characteristics of OFETs.

Introduction

During the past two decades the fast progress in research on novel small molecule and π-conjugated polymer based organic semiconductors[1–3] has led to successful realizations of simple electronic circuits for low-cost radio-frequency identification tags,[4,5] flexible large-area displays,[6,7] as well as for sensing devices.[8,9] In particular, to enable cost-effective, simple large-scale roll-to-roll production, solution-processable organic semiconductors with good electric properties in OFETs, *i.e.* high charge carrier mobilities, high on/off current ratios and low threshold voltages, are imperative. π-Conjugated oligomers and polymers have proved to be good candidates with excellent performance, reaching the benchmark of amorphous silicon with charge carrier mobilities of 0.1–6.2 cm^2 V^{-1} s^{-1}.[10–14] Regioregular poly(3-hexylthiophene) (P3HT), for example, is by far one of the most widely investigated p-type polymers exhibiting charge carrier mobility values up to 0.1–0.4 cm^2 V^{-1} s^{-1}.[15,16]

However, P3HT forms microcrystalline films and its mobility is strongly influenced by morphological changes depending on processing conditions.[17–19] In comparison, amorphous polymers such as poly(triarylamines) (PTAAs) cannot compete with the mobilities of crystalline ones ($\sim 10^{-3}$ to 10^{-2} cm^2 V^{-1} s^{-1}), although their ease of processing with high reproducibility as well as robust electrical performance are beneficial.[20–22] Since most large-scale roll-to-roll printing techniques are applied under ambient conditions, air-stability of organic semiconductors is required. In this context, P3HT shows poor performance, due to a relatively low ionization potential leading to degradation effects in the presence of light.[23–26] In general, a significant improvement in air stability can be obtained by increasing the ionization potential above 5 eV.[27,28]

Here we report on a heterotriangulene polymer (**PTA**) as an alternative organic semiconductor for air stable organic field-effect transistors synthesized in a straightforward procedure (see Fig. 1 (a)). Due to the bridging dimethylmethylene groups good solubility of **PTA** in organic solvents is ensured without the attachment of additional solubilizing groups (*e.g.* long alkyl chains), leading to thermally stable amorphous films with enhanced device stability.[29] Furthermore, the electron delocalization between the central nitrogen and the benzene moieties is enhanced by the planarization, which results in an improved conjugation along the polymer chains. The crucial air stability is, however, provided by the low lying HOMO level ($E_{HOMO} = 5.1$ eV)

[a]*NanoTecCenter Weiz Forschungsgesellschaft m.b.H., Franz-Pichler-Straße 32, A-8160 Weiz, Austria. E-mail: emil.list@ntc-weiz.at; Fax: +43 316 876 8040; Tel: +43 316 876 8000*

[b]*Max-Planck-Institut für Polymerforschung, Ackermannweg 10, 55021, Mainz, Germany. E-mail: muellen@mpip-mainz.mpg.de*

[c]*Helmholtz Zentrum Berlin für Materialien und Energie GmbH Elektronenspeicherring BESSY II, Albert-Einstein-Str. 15, 12489 Berlin, Germany*

[d]*Institut für Physik, Humboldt-Universität zu Berlin, Brook-Taylor-Strasse 6, D-12489 Berlin, Germany*

[e]*Institute of Solid State Physics, Graz University of Technology, Petersgasse 16, A-8010 Graz*

† Electronic supplementary information (ESI) available: Photoluminescence spectra of toluene *vs.* $CHCl_3$ solutions and the influence of UV-light, UV/Vis absorption and photoluminescence spectra of PTA films, surface morphology of a P3HT film, UPS results of P3HT and work function of different treated Au, output characteristics of PTA FETs with different interface treatments, Evolution of device parameters of PTA and P3HT FETs under ambient conditions. See DOI: 10.1039/c3py00089c

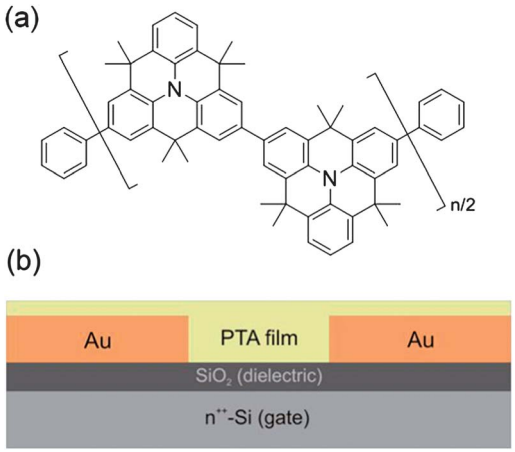

Fig. 1 (a) Chemical structure of the **PTA** polymer. (b) Schematic representation of bottom-gate/bottom-contact (BG/BC) OFETs (not to scale).

and wide bandgap (E_g = 2.9 eV) of **PTA**. The potential of heteroatriangulenes as p-type semiconductors was recently shown by dendrimeric derivatives of **PTA**, exhibiting an enhanced hole transporting ability in organic light emitting diodes (OLEDs) together with an improved thermal and morphological stability.[30,31,32]

Aside from the intrinsic properties of the organic semiconductor, the device architecture, its interfaces and thus the applied surface treatments determine the OFET stability under ambient conditions.[33] We focus on bottom-gate/bottom-contact (BG/BC) OFETs based on **PTA** (see Fig. 1(b)) and investigate the influence of several surface treatments on the device performance. We show that the utilization of chloroform as a solvent leads to a protonation of the nitrogen atom on the **PTA** polymer, which has a significant influence on the electrical characteristics of OFETs. Finally, the ambient stability of **PTA** OFETs over months is benchmarked against P3HT OFETs.

Experimental section

Synthesis of the monomer

2,6-Dibromo-4,4,8,8,12,12-hexamethyl-8,12-dihydro-4*H*-benzo[1,9]quinolizino[3,4,5,6,7-*defg*]acridine (DTPABr$_2$). *N*-Bromosuccinimide (0.487 g, 2.74 mmol) was added to a solution of 4,4,8,8,12,12-hexamethyl-8,12-dihydro-4*H*-benzo[1,9]quinolizino[3,4,5,6,7-*defg*]acridine (**DTPA**) (0.5 g, 1.37 mmol) in $CHCl_3$ (40 mL) at 0 °C over a period of 20 min. While warming up to room temperature, the resulting solution was stirred in the dark overnight. The reaction was quenched with a saturated aqueous solution of $Na_2S_2O_3$. The resulting mixture was extracted with CH_2Cl_2 (3×) and the combined organic fractions were dried with $MgSO_4$. After filtration and evaporation of the solvent, the residue was subjected to column chromatography (silica, *n*-hexane–CH_2Cl_2 4 : 1). Final recrystallization from ethanol yielded **DTPABr$_2$** as a white powder (0.55 g, 77%). ^{1}H NMR ($CDCl_3$, 250 MHz, δ): 1.51 (s, 6H), 1.53 (s, 12H), 7.08 (t, $J_1 = J_2 = 6.3$ Hz, 1H), 7.29 (d, $J = 7.5$ Hz, 4H), 7.37 (dd, $J_1 = J_2 = 2.5$ Hz, 4H). ^{13}C NMR ($CDCl_3$, 63 MHz, δ): 132.2, 131.6, 131.5, 131.2, 131.0, 129.4, 126.5, 126.1, 123.5, 115.8, 35.6, 33.0, 32.5, 29.7. FD-MS (8 kV): m/z = 521.9 (100%, M^+). ESI-HR MS calcd for $C_{27}H_{25}Br_2N$ ([M + H]$^+$) 522.0432, found 522.0441. Anal. calcd for $C_{27}H_{25}Br_2N$: C 61.97%, H 4.82%, N 2.68%; found: C 61.89%, H 4.94%, N 2.67%.

Polymerization

PTA. Bis(1,5-cycloocatdiene)nickel(0) (460 mg, 1.67 mmol), 1,5-cyclooctadiene (181 mg, 0.21 mL, 1.67 mmol) and 2,2′-bipyridine (261 mg, 1.67 mmol) were added to a flame-dried 100 mL Schlenk flask, dissolved in 7 mL of anhydrous toluene and *N*,*N*-dimethylformamide (2 : 1) and stirred for 30 min at 65 °C in the absence of light. A solution of 2,6-dibromo-4,4,8,8,12,12-hexamethyl-8,12-dihydro-4*H*-benzo[1,9]quinolizino[3,4,5,6,7-*defg*]acridine (**DTPABr$_2$**) (350 mg, 0.67 mmol) in 23 mL of anhydrous toluene at 65 °C was added quickly *via* a double-tipped needle and the resulting mixture was stirred for two days at 85 °C in the absence of light. After addition of 1 mL of bromobenzene the mixture was stirred for additional two hours. Subsequently the reaction mixture was poured into 160 mL of MeOH–HCl (30 : 1) and stirred for one hour and the precipitate was filtered. After repeated precipitation in MeOH–HCl, the polymer was subjected to Soxhlet extraction using acetone and hexane. The final precipitation led to a white solid (160 mg, 66%). ^{1}H NMR (CD_2Cl_2, 250 MHz, δ): 1.67 (br, 6H), 1.76 (br, 12H), 7.09 (br, 1H), 7.40 (br, 2H), 7.62 (br, 4H). SEC (THF, PS-standard): M_w = 17 800 g mol^{-1}, PDI = 1.7, DP ∼ 49.

Materials and characterization

The applied compounds were purchased from Sigma-Aldrich, Fluka, Fisher Scientific, VWR and Acros. Field desorption mass spectra were obtained on a VG Instruments ZAB 2-SE-FPD spectrometer, with data collected between m/z 110 and 3300. Size-exclusion chromatography (SEC) analysis was performed with SDV (PSS) columns (106, 104, and 500 Å porosity) connected to RI and UV (254 nm) detectors against polystyrene standards with THF as an eluting solvent. High resolution mass spectrometry was performed on an ESI-Q-TOF system (maXis, Bruker Daltonics, Germany). The instrument was operated in wide pass quadrupole mode, for MS experiments, with the TOF data being collected between m/z 100 and 5000. NMR measurements were recorded on a Bruker AVANCE 250 system. The proton and carbon spectra were measured in CD_2Cl_2 at 298.3 K and the spectra were referenced for the residual $CHDCl_2$ at $\delta(^1H)$ = 5.32 ppm. Cyclic voltammetry was measured on a Princeton Applied Research Parstat 2273 instrument with anhydrous dichloromethane under an argon atmosphere. Tetrabutylammonium hexafluorophosphate (n-Bu_4NPF_6) was used as a conductive salt at a concentration of 0.1 mol L^{-1}. Ferrocene was added as an internal standard (1 mM). The peaks were calibrated according to the oxidation peak of ferrocene for HOMO level calculation. The voltage was ramped by 100 mV s^{-1}. Half-step potentials were used for the evaluation. No reduction peaks were observed. Thermogravimetric analysis data were acquired on a Mettler TGA/SDTA 851e at a heating rate of 10 K min^{-1} under a nitrogen atmosphere.

Optical absorption spectra were measured using a Perkin Elmer Lambda 900 UV/VIS spectrometer. A spectrofluorophotometer Shimadzu RF-5301PC was used to record photoluminescence and all spectra were corrected according to the detector characteristics.

For ultraviolet photoelectron spectroscopy (UPS) studies **PTA** and P3HT were spin-coated from toluene solution on Si/SiO_2/Au substrates, with the gold being thermally evaporated and subsequently exposed to lift-off chemicals in order to obtain the same conditions as with the OFETs. The UPS measurements were performed using a multitechnique ultra high vacuum (UHV-) apparatus (base pressure: 1×10^{-10} mbar) and a helium-gas-discharge lamp (21.218 eV) with a very low photon flux (*ca.* 100 times attenuated compared to standard commercial sources) in order to reduce any irradiation damage. All spectra were recorded at room temperature and normal emission using a hemispherical Specs Phoibos 100 energy analyzer with 120 meV energy resolution for UPS. To determine the work function, secondary electron cutoffs were recorded with the sample biased to −10 V to clear the analyzer work function.

Fabrication of organic field-effect transistors

OFET devices were fabricated in bottom-gate/bottom-contact (BG/BC) architecture on silicon substrates (1 inch × 1 inch). The heavily doped silicon (n^{++}-Si) was used as a common bottom gate and the 200 nm thermally grown SiO_2 as a gate dielectric ($C_i = 17.3$ nF cm^{-2}). 50 nm gold source/drain (*S*/*D*) electrodes with a 2 nm chrome adhesion layer were structured using conventional lift-off processing. The channel width and the channel length were 2.85 mm and 25 μm, respectively. **PTA** and regioregular poly(3-hexylthiophene) (Plexcore® OS, purchased from Sigma-Aldrich) were dissolved in toluene with a concentration of 2 g L^{-1} and 3 g L^{-1}. In order to optimize the wetting behavior of the semiconductor and the device performance, the surface of some samples was modified before depositing the semiconductor. Hexamethyldisilazane (97% purity degree, SSE Optihot VB20 hotplate) was applied *via* vapor phase deposition for various exposure times. Certain samples were treated by UV/ozone or O_2-plasma to hydrophilize the surface and form a thin AuO_x layer on the gold electrodes.[34] A UV-Lamp 6035 Hg (Ar) was used for 10 min UV-light exposure of the SiO_2 surface and the gold electrodes. The O_2-plasma treatment was done using a Femto plasma etch plant (diener electronic) with exposure times of 5 min and a power of 100 W. All devices were assembled under an inert atmosphere, except those used for ambient stability investigations. In order to remove adsorbed water on the SiO_2, the substrates were also annealed at 120 °C in high vacuum for 1 h before the application of the semiconductors (only for inert assembling). After spin-coating the semiconductor, the films were first dried at 60 °C in argon (Ar) for ∼10 min and subsequently at 120 °C under high vacuum ($p \sim 4 \times 10^{-5}$ mbar) for 1 h.

Thin film and device characterization

To investigate the surface morphology of the thin **PTA** films, atomic force microscopy (AFM) (Veeco Dimension V AFM equipped with a Nanoscope V controller) was used in tapping mode. The electrical characteristics were measured in an argon-filled glove box and in air under ambient conditions using an Agilent B1500 Parameter Analyzer. Gradual channel approximation was used to calculate the field-effect mobility μ in the saturation regime. The subthreshold slope *S* was obtained from the inverse slope of the linear fit of $\log|I_{DS}|$ *vs.* V_{GS} in the subthreshold regime.

Results and discussion

Material synthesis and characterization

The straightforward synthetic route towards polymer **PTA** is shown in Scheme 1. The dimethylmethylene-bridged triarylamine **DTPA** was prepared according to the literature in three steps.[35,36] Monomer **DTPABr$_2$** was obtained after twofold bromination using *N*-bromosuccinimide (NBS) in stoichiometric amounts. Following the standard Yamamoto conditions and endcapping using bromobenzene, **PTA** was obtained in 51% overall yield.[37,38] After removal of the low molar mass fraction by repeated Soxhlet extraction and precipitation, the weight-average molecular weight of **PTA** was determined by size-exclusion chromatography (SEC) using a poly(styrene) standard in THF and was found to be 17 800 g mol^{-1} (PDI = 1.7), which corresponds to a molecular structure of approximately 49 **DTPA** repeating units. **PTA** showed good solubility in organic solvents, *e.g.*, THF, toluene, dichloromethane and

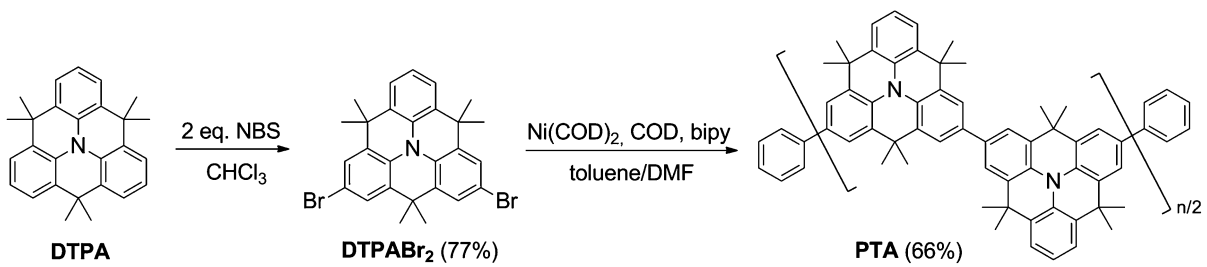

DTPA **DTPABr$_2$** (77%) **PTA** (66%)

Scheme 1 Schematic representation of the synthesis of **PTA**. COD = 1,5-cyclooctadiene, bipy = 2,2′-bipyridine, NBS = *N*-bromosuccinimide, and DMF = *N*,*N*-dimethylformamide.

1,2-dichlorobenzene enabling its characterization by ^{1}H NMR spectroscopy. The ^{1}H NMR spectrum revealed broad signals between 7.6 and 7.0 ppm corresponding to the aromatic protons of the heterotriangulene subunits and a broad signal at 1.7 ppm caused by its methyl-groups at the bridges, with correct signal intensities. Thermogravimetric analysis (TGA) showed good thermal stability up to 400 °C (Fig. 2(a)) (decomposition temperature at 5% weight loss is 456 °C). Cyclic voltammetry of **PTA** was measured at room temperature (see Fig. 2(b)) and the HOMO level of the polymer in solution was estimated using the onset oxidation potential relative to the ferrocene standard according to eqn (1).[39] This resulted in a HOMO energy level of 5.01 eV (see below and Table 1).

$$E^{\mathrm{HOMO}} = [(E^{\mathrm{ox}}_{\mathrm{onset}} - E^{\mathrm{reference}}_{\mathrm{onset}}) + 4.8]\ \mathrm{eV} \quad (1)$$

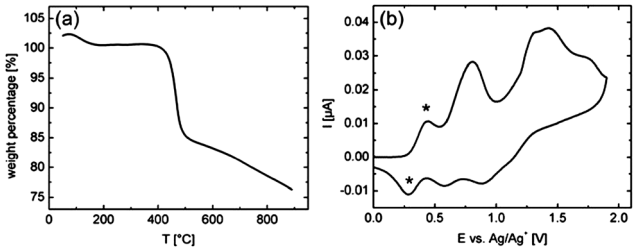

Fig. 2 (a) TGA of **PTA** at a heating rate of 10 K min^{-1} under a nitrogen atmosphere. (b) Cyclic voltammogram of **PTA** reported *vs.* ferrocene (anodic scans are shown, 10^{-3} M in 0.1 M Bu_4PF_6–CH_2Cl_2 at a scan rate of 50 mV s^{-1}). The asterisks denote the Fc^+/Fc oxidation/reduction process.

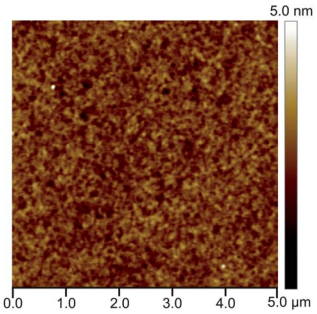

Fig. 3 AFM topographic image of a typical **PTA** film on SiO_2 (scan size 5 µm × 5 µm).

Table 1 UV/Vis maximum absorption wavelength and maximum emission wavelength (λ_{max}), bandgap energy (E_g), ionization potential (E_{HOMO}) and energy of the LUMO level (E_{LUMO}) of the **PTA** polymer

Solution	Absorption (λ_{max}, nm)	Emission (λ_{max}, nm)	E_g^{opt}[a] (eV)	E_{HOMO} (eV)	E_{LUMO}[d] (eV)
Toluene	323, 382	425	2.9	5.1[b]	2.2
$CHCl_3$	324, 382	4724, 547		5.0[c]	

[a] Estimated from the onset of absorption in the solid state (see ESI). [b] Obtained from ultraviolet photoelectron spectroscopy. [c] *HOMO* levels were calculated from the measured first oxidation potential *versus* Fc/Fc^+ according to eqn (1). [d] Calculated using optical bandgap energy.

Thin film morphology

Fig. 3 shows the topographic image of a typical **PTA** film on SiO_2 after annealing at 120 °C for 1 h in high vacuum ($p \sim 4 \times 10^{-5}$ mbar). The film exhibits a very smooth surface with a root-mean-squared roughness of ~0.4 nm. The amorphous, disordered morphology was confirmed by X-ray diffraction analysis (Siemens D501, Cu-tube in Bragg–Brentano configuration). No scattering patterns were observed (not shown).

Energy levels and optical properties

To investigate the photophysical properties of the **PTA** polymer, UV/Vis absorption spectra and photoluminescence spectra were recorded in diluted solutions of toluene and $CHCl_3$ (5×10^{-3} g L^{-1}) (Fig. 4 and Table 1). The UV/Vis absorption maximum of **PTA** in toluene and $CHCl_3$ is at 383 nm and a second maximum is found at ~323 nm. The photoluminescence spectra of **PTA** in toluene and $CHCl_3$ differ significantly. The fluorescence spectrum of the toluene solution exhibits a maximum at 425 nm. In contrast, for the $CHCl_3$ solution the initial blue emission (at 425 nm) is significantly decreased and a second emission peak appears at 547 nm. Accordingly, a coloration of the $CHCl_3$ solution (from colorless to brown) was observed within a few seconds when the solutions were prepared under ambient light or exposed to UV-light, while equivalent toluene solutions remained colorless (see ESI†). This suggests that the coloration is caused by a halochromic effect, resulting from the well-known dissociation of $CHCl_3$ under UV-light at which hydrochloric acid (HCl) is formed leading to protonation of the central nitrogen (N-protonation).[40–43] UV/Vis absorption measurements in the solid state revealed an optical bandgap of 2.9 eV (see ESI†).

The energy levels of the **PTA** polymer and their alignment with respect to the Au Fermi-level were determined by ultraviolet photoelectron spectroscopy (UPS). **PTA**'s low binding energy onset is 0.7 eV below the Fermi-level (E_F) (Fig. 5(a)). Together with the work function (Φ = 4.4 eV, Fig. 5(a)) determined from the secondary electron cutoff, the ionization energy (IE) is 5.1 eV (Table 1). This is in good agreement with the result from cyclic voltammetry (E_{HOMO} = 5.0 eV). The lowest unoccupied molecular orbital level was estimated by taking into

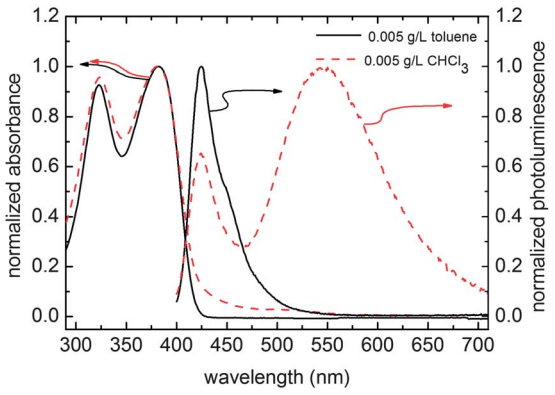

Fig. 4 UV/Vis absorbance and photoluminescence emission spectra of **PTA** in toluene (solid black line) and in chloroform (dashed red line).

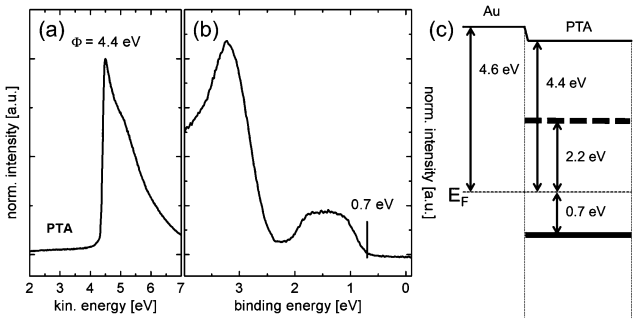

Fig. 5 (a) Secondary electron cut-off and (b) valence region UPS spectra of **PTA** on Au/SiO_2 substrates. (c) Schematic energy levels of **PTA** with respect to gold.

account the optical energy gap of 2.9 eV (Table 1), resulting in the energy level scheme in Fig. 5(b). The deep HOMO level and the wide bandgap are responsible for the good stability of the **PTA** polymer under ambient conditions. In contrast, P3HT has its ionization energy at 4.5 eV (see ESI†).

Additionally we also focused on the polymer/gold interface in order to correlate injection properties with the electrical characteristics. The hole injection barrier between gold and **PTA** is 0.7 eV and the interface dipole $\Delta\Phi$ is −0.2 eV. The determined work function of gold with 4.6 eV is rather low, but can be explained by hydrocarbon contaminations on the gold due to handling in air and exposure to chemicals used in the lift-off process, reducing the surface dipole as shown by Rentenberger and coworkers.[34] In accordance we demonstrate that depending on the conditions prior to the measurements, different Au work function values varying between 4.4 eV and 4.7 eV were measured (see ESI†).

Characterization of organic field-effect transistors

Investigations of **PTA** based BG/BC OFETs revealed a clear p-type transport of the novel material with a rather strong influence of the applied surface treatments. Fig. 6(a) shows the transfer characteristics of **PTA** OFETs with different surface treatments (Table 2). The highest saturation mobility of 4.2×10^{-3} cm^2 V^{-1} s^{-1} and on/off current ratio of $\sim 10^5$ were obtained for OFETs with HMDS treatment. These results are similar to the literature values of other fully amorphous semiconductors such as PTAAs.[20] Fig. 6(b) depicts the output characteristics of a typical device, showing a negligible hysteresis. However, the absence of a clear linear characteristic at low drain voltages indicates a significant contact resistance, which can be ascribed to a high hole injection barrier, resulting from the energy mismatch of the **PTA** HOMO level and the low gold work function due to storing in air. This emphasizes that fabrication processes are strongly correlated with charge injection/contact resistance of the electrodes.[44,45] To improve the injection of charge carriers, the gold contacts were UV/ozone and O_2 plasma treated inducing a thin AuO_x layer which increases the work function.[34,46,47] The treatment improved the linear region of the output characteristics (shown in the ESI†), but at the same time one order of magnitude lower source-drain currents and mobility values ($\sim 2 \times 10^{-4}$ cm^2 V^{-1} s^{-1}) were obtained (see

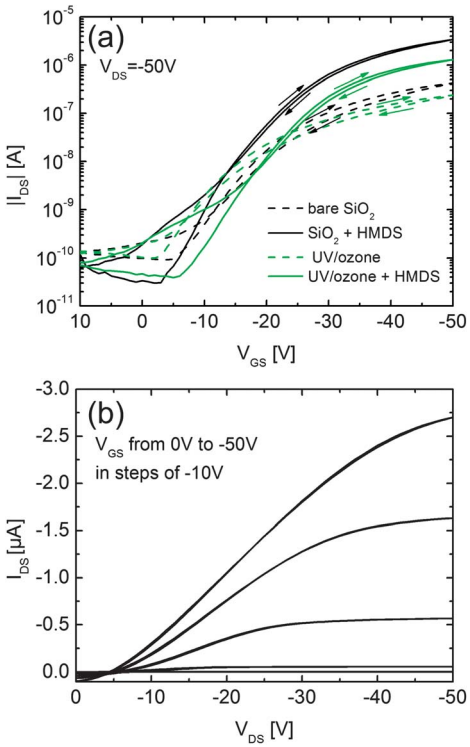

Fig. 6 (a) Transfer characteristics of **PTA** OFETs with different surface treatments: bare SiO_2 (dashed black line), 15 min HMDS treatment (solid black line), UV/ozone treatment with (dashed green line) and without (solid green line) HMDS. (b) Output characteristics of a typical **PTA** OFET with HMDS treatment.

Fig. 6(a) and Table 2). This can be ascribed to a higher density of hydroxyl (OH–) groups induced by UV/ozone or O_2 plasma treatment, which act as traps on the SiO_2 dielectric.[48,49] Additionally, O_2 plasma treated devices showed a positive switch-on voltage (V_{so}), and low on/off current ratios (high off-currents, high subthreshold slope S) (see Table 2), which is most likely due to doping of the semiconductor.[50] By deactivating the OH-groups and decreasing the polar component on SiO_2 with HMDS treatment, the mobility could be increased again ($\sim 2.1 \times 10^{-3}$ cm^2 V^{-1} s^{-1}, Fig. 6(a)).[51,52] The modified performance of the **PTA** FETs due to different interface treatments can be attributed to a change of the hole injection barrier, the surface polarity, consequently an increased/decreased charge carrier trap density and doping, rather than changes in morphology.[21]

BG/BC OFETs were also fabricated to investigate the influence of $CHCl_3$ as a solvent and the corresponding protonation reaction on the electrical properties of the **PTA** polymer. Fig. 7 displays the output characteristics of a **PTA** OFET (protonated) when the $CHCl_3$ solution was exposed to UV-light ($\sim$10 s, wavelength of 254 nm and 366 nm) prior to spin-coating. Solution of reference OFETs (non-protonated), also shown, were not exposed to UV-light and ambient light was kept at a minimum. For these devices, similar to the results for toluene, the output characteristics show a significant contact resistance. This is not the case with protonated (UV-light exposed) $CHCl_3$ solution, indicated also by good saturation behavior. Accordingly, the transfer curve shows a higher off-current and a shift of

Table 2 Device parameters of BG/BC OFETs based on **PTA** with different surface treatments

Surface modification	HMDS treatment[a]	Mobility μ_{sat}[b] ($cm^2\ V^{-1}\ s^{-1}$)	I[c] (on/off)	V_{so} (V)	S (V per dec)
O_2 plasma	—	1.8×10^{-4}	8.8×10^{1}	>10	15.7
UV/ozone	—	1.5×10^{-4}	2.3×10^{3}	−3	5.5
Bare SiO_2	—	4.1×10^{-4}	4.4×10^{3}	−5	5.9
O_2 plasma	HMDS 15 min	4.9×10^{-4}	8.3×10^{2}	7	8.3
UV/ozone	HMDS 5s	2.1×10^{-3}	2.8×10^{4}	−6	5.3
Bare SiO_2	HMDS 15 min	4.2×10^{-3}	1.0×10^{5}	−3	4.3

[a] Different exposure times were used due to wetting problems. [b] μ_{sat} was calculated according to the gradual channel approximation. [c] On-current extracted at $V_{GS} = -50$, $V_{DS} = -50$ V and off-current at $V_{GS} = 0$ V, $V_{DS} = -50$ V.

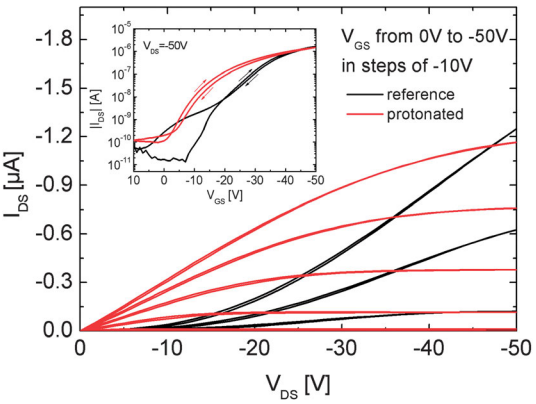

Fig. 7 Output and transfer (inset) characteristics of **PTA** OFETs with (black lines) and without (red lines) UV-light exposure of the $CHCl_3$ solution prior to spin-coating in an argon atmosphere.

the switch-on voltage to more positive values. Both effects are most probably assigned to (contact-) doping of the **PTA** polymer.

The ambient stability of the **PTA** polymer in BG/BC OFETs was investigated and benchmarked against the widely used regioregular P3HT. The fabrication process was carried out in ambient atmosphere and the electrical characteristics were recorded under ambient light and a humidity level of approximately 45–60%. Fig. 8(a) and (b) show the output characteristics of **PTA** OFETs in comparison to P3HT devices. The source-drain channel current values are similar for both polymers but lower compared to **PTA** devices fabricated under an argon atmosphere (see Fig. 6). The linear regime at low V_{SD} is more pronounced and the contact resistance is lower than for devices fabricated under inert conditions. This can be attributed to (contact-) doping of the semiconductors due to water or oxygen.[53] The contact resistance of P3HT OFETs is even lower compared to **PTA** devices, ascribed to a lower hole injection barrier (0.3 eV, see ESI†).

Several transfer characteristics as a function of storage time are displayed in Fig. 8(c) (extracted device parameters are listed in the ESI†). The on/off current ratios of as-prepared samples were determined to be $\sim 10^4$ for **PTA** and $\sim 10^2$ for P3HT at $V_{GS} =$ 0 V (and 10^3 for fully depleted P3HT FETs at $V_{GS} = 10$ V). The latter exhibited higher off-currents due to doping by oxygen and/or moisture.[23] This was also accompanied by a shift of the switch-on voltage to positive values. As a consequence of the deep lying HOMO level and the wide bandgap, even after

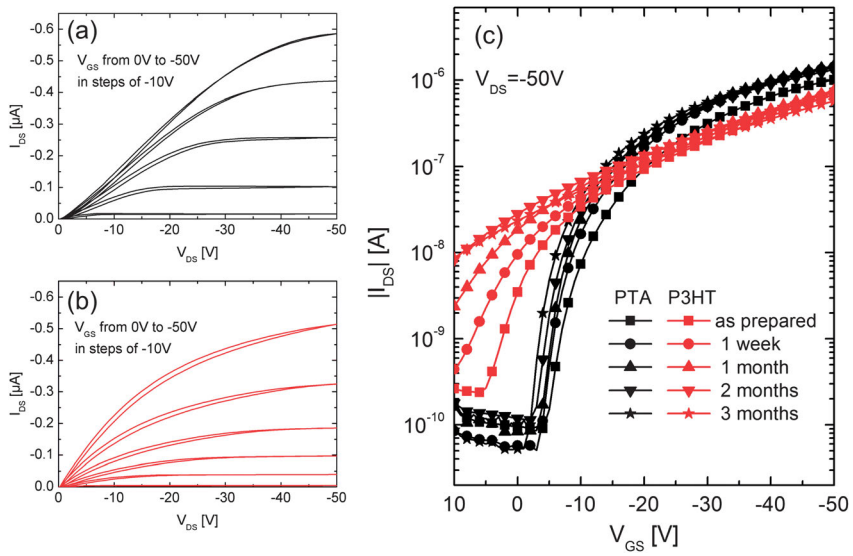

Fig. 8 Output characteristics of **PTA** (a) and P3HT (b) FETs after fabrication and measurements in air and ambient light. (c) Semi-logarithmic transfer characteristics of **PTA** (black) and P3HT (red) as a function of time measured in air and ambient light. (23–26 °C, 45–60% rh).

storage of 3 months in ambient atmosphere (~45 to 60% rh, 23–26 °C) **PTA** OFETs did not show any significant changes in device performance, providing excellent stability. In contrast, P3HT FETs showed a shift of the switch-on voltage to more positive values (>10 V) and a large decrease of the on/off current ratio (by a factor of ~40).[23,26,54] Moreover, the amorphous structure of **PTA** is believed to be beneficial in comparison to the microcrystalline structure of P3HT with its grain boundaries, acting as migration spots for water molecules which increase the trap density.[26]

Conclusions

In conclusion, a novel air-stable polymer based on dimethylmethylene-bridged triarylamines was synthesized and investigated in BG/BC OFETs. The optimization of electrode/- and dielectric/polymer interfaces yielded mobilities of $\sim 4 \times 10^{-3}$ $cm^2 V^{-1} s^{-1}$ and on/off current ratios of $\sim 10^5$, showing that **PTA** is a viable alternative for the best performing amorphous air-stable semiconducting polymers. Due to its deeper lying HOMO level ($E_{HOMO} = 5.1$ eV) and wider bandgap ($E_g = 2.9$ eV) BG/BC **PTA** FETs fabricated, characterized and stored under ambient conditions showed excellent stability over months compared to P3HT. The combination of this robust performance with the ease of processing makes the new polymer a high potential candidate for large-scale low-cost production. There also appears to be considerable scope for further investigations regarding the significant sensitivity of the novel polymer in $CHCl_3$ solution to hydrochloric acid, due to protonation of the central nitrogen atom. This could enable the application of the novel **PTA** polymer as an active material in pH-sensor elements.

Acknowledgements

The authors gratefully acknowledge Alfred Neuhold and Prof. Roland Resel for XRD investigations. Stefan Sax and Sebastian Nau from NTC Weiz GmbH are acknowledged for support and discussions. The authors thank Prof. Jürgen P. Rabe for granting access to UPS measurements. For financial support the Styrian Government (projects BioOFET 2, GZ:A3-11.B-36/2010-5) and the Transregio SFB TR 49 (Frankfurt, Mainz, Kaiserslautern) are acknowledged.

Notes and references

1 C. Wang, H. Dong, W. Hu, Y. Liu and D. Zhu, *Chem. Rev.*, 2012, **112**, 2208.
2 A. Facchetti, *Chem. Mater.*, 2011, **23**, 733.
3 H. Sirringhaus, *Adv. Mater.*, 2005, **17**, 2411.
4 E. Cantatore, T. C. T. Geuns, G. H. Gelinck, E. V. Veenendaal, A. F. A. Gruijthuijsen, L. Schrijnemakers, S. Drews and D. M. D. Leeuw, *IEEE J. Solid-State Circuits*, 2007, **42**, 84.
5 P. F. Baude, D. A. Ender, M. A. Haase, T. W. Kelley, D. V. Muyres and S. D. Theiss, *Appl. Phys. Lett.*, 2003, **82**, 3964.
6 H. E. a. Huitema, G. H. Gelinck, J. B. P. H. van der Putten, K. E. Kuijk, C. M. Hart, E. Cantatore and D. M. de Leeuw, *Adv. Mater.*, 2002, **14**, 1201.
7 G. Gelinck, P. Heremans, K. Nomoto and T. D. Anthopoulos, *Adv. Mater.*, 2010, **22**, 3778.
8 J. T. Mabeck and G. G. Malliaras, *Anal. Bioanal. Chem.*, 2006, **384**, 343.
9 M. Berggren and A. Richter-Dahlfors, *Adv. Mater.*, 2007, **19**, 3201.
10 H. N. Tsao, D. M. Cho, I. Park, M. R. Hansen, A. Mavrinskiy, D. Y. Yoon, R. Graf, W. Pisula, H. W. Spiess and K. Müllen, *J. Am. Chem. Soc.*, 2011, **133**, 2605.
11 Z. Chen, M. J. Lee, R. S. Ashraf, Y. Gu, S. Albert-Seifried, M. M. Nielsen, B. Schroeder, T. D. Anthopoulos and M. Heeney, *Adv. Mater.*, 2012, **24**, 647.
12 H. Bronstein, Z. Chen, R. S. Ashraf, W. Zhang, J. Du, J. R. Durrant, P. S. Tuladhar, K. Song, S. E. Watkins, Y. Geerts, M. M. Wienk, R. A. J. Janssen, T. Anthopoulos, H. Sirringhaus, M. Heeney and I. McCulloch, *J. Am. Chem. Soc.*, 2011, **133**, 3272.
13 S. Wang, M. Kappl, I. Liebewirth, M. Müller, K. Kirchhoff, W. Pisula and K. Müllen, *Adv. Mater.*, 2012, **24**, 417.
14 S. Dong, H. Zhang, L. Yang, M. Bai, Y. Yao, H. Chen, L. Gan, T. Yang, H. Jiang, S. Hou, L. Wan and X. Guo, *Adv. Mater.*, 2012, **24**, 5576.
15 H. Sirringhaus, *Science*, 1998, **280**, 1741.
16 K.-J. Baeg, D. Khim, D.-Y. Kim, J. B. Koo, I.-K. You, W. S. Choi and Y.-Y. Noh, *Thin Solid Films*, 2010, **518**, 4024.
17 H. Sirringhaus, P. J. Brown, R. H. Friend, M. M. Nielsen, K. Bechgaard, B. M. W. Langeveld-Voss, A. J. H. Spiering, R. A. J. Janssen, E. W. Meijer, P. Herwing and D. M. de Leeuw, *Nature*, 1999, **401**, 685.
18 G. Wang, J. Swensen, D. Moses and A. J. Heeger, *J. Appl. Phys.*, 2003, **93**, 6137.
19 G. Wang, T. Hirasa, D. Moses and A. J. Heeger, *Synth. Met.*, 2004, **146**, 127.
20 S. Veres, S. Ogier, B. Leeming, D. Brown, H. Cupertino, H. ouse and P. O. Box, *Mater. Res.*, 2002, **708**, 1.
21 J. Veres, S. D. Ogier, S. W. Leeming, D. C. Cupertino and S. Mohialdin Khaffaf, *Adv. Funct. Mater.*, 2003, **13**, 199.
22 W. Zhang, J. Smith, R. Hamilton, M. Heeney, J. Kirkpatrick, K. Song, S. E. Watkins, T. Anthopoulos and I. McCulloch, *J. Am. Chem. Soc.*, 2009, **131**, 10814.
23 M. S. A. Abdou, F. P. Orfino, Y. Son and S. Holdcroft, *Macromolecules*, 1997, **7863**, 4518.
24 E. Meijer, *Synth. Met.*, 2004, **142**, 53.
25 H.-H. Liao, C.-M. Yang, C.-C. Liu, S.-F. Horng, H.-F. Meng and J.-T. Shy, *J. Appl. Phys.*, 2008, **103**, 104506.
26 A. Klug, A. Meingast, G. Wurzinger, A. Blümel, K. Schmoltner, U. Scherf and E. J. W. List, *Proc. SPIE*, 2011, **8118**, 811809.
27 I. McCulloch, M. Heeney, C. Bailey, K. Genevicius, I. Macdonald, M. Shkunov, D. Sparrowe, S. Tierney, R. Wagner, W. Zhang, M. L. Chabinyc, R. J. Kline, M. D. McGehee and M. F. Toney, *Nat. Mater.*, 2006, **5**, 328.
28 I. McCulloch, C. Bailey, M. Giles, M. Heeney, I. Love, M. Shkunov, D. Sparrowe and S. Tierney, *Chem. Mater.*, 2005, **17**, 1381.

29 R. Abbel, M. Wolffs, R. A. A. Bovee, J. L. J. van Dongen, X. Lou, O. Henze, W. J. Feast, E. W. Meijer and A. P. H. J. Schenning, *Adv. Mater.*, 2009, **21**, 597.
30 Z. Jiang, T. Ye, C. Yang, D. Yang, M. Zhu, C. Zhong, J. Qin and D. Ma, *Chem. Mater.*, 2011, **23**, 771.
31 Z. Fang, V. Chellappan, R. D. Webster, L. Ke, T. Zhang, B. Liu and Y.-H. Lai, *J. Mater. Chem.*, 2012, **22**, 15397.
32 F. Schlütter, F. Rossel, M. Kivala, V. Enkelmann, J.-F. Gisselbrecht, P. Ruffieux, R. Fasel and K. Müllen, *J. Am. Chem. Soc.*, 2013, **135**, 4550.
33 L. A. Majewski, J. W. Kingsley, C. Balocco and A. M. Song, *Appl. Phys. Lett.*, 2006, **88**, 222108.
34 S. Rentenberger, A. Vollmer, E. Zojer, R. Schennach and N. Koch, *J. Appl. Phys.*, 2006, **100**, 053701.
35 Z. Fang, T. L. Teo, L. P. Cai, Y. H. Lai, A. Samoc and M. Samoc, *Org. Lett.*, 2009, **11**, 1.
36 Z. Fang, X. H. Zhang, Y. H. Lai and B. Liu, *Chem. Commun.*, 2009, 920.
37 T. Yamamoto, *Bull. Chem. Soc. Jpn.*, 1999, **72**, 621.
38 T. Yamamoto, *Prog. Polym. Sci.*, 1992, **17**, 1153.
39 J. F. Rusling and S. L. Suib, *Adv. Mater.*, 1994, **6**, 922.
40 S. Hautecloque, *J. Photochem.*, 1980, **14**, 157.
41 P. E. Hoggard, A. J. Bridgeman, H. Kunkely and A. Vogler, *Inorg. Chim. Acta*, 2004, **357**, 639.
42 S. Kappaun, S. Horner, A.-M. Kelterer, K. Waich, F. Grasse, M. Graf, L. Romaner, F. Niedermair, K. Müllen, A. C. Grimsdale, R. Saf, E. J. W. List, E. Zojer and C. Slugovc, *Macromol. Chem. Phys.*, 2008, **209**, 2122.
43 I. Dumsch, C. J. Kudla and U. Scherf, *Macromol. Rapid Commun.*, 2009, **30**, 840.
44 A. Wan, J. Hwang, F. Amy and A. Kahn, *Org. Electron.*, 2005, **6**, 47.
45 D. Natali and M. Caironi, *Adv. Mater.*, 2012, **24**, 1357.
46 W.-K. Kim and J.-L. Lee, *Appl. Phys. Lett.*, 2006, **88**, 262102.
47 B. Stadlober, U. Haas, H. Gold, A. Haase, G. Jakopic, G. Leising, N. Koch, S. Rentenberger and E. Zojer, *Adv. Funct. Mater.*, 2007, **17**, 2687.
48 S. G. J. Mathijssen, M. Kemerink, A. Sharma, M. Cölle, P. a. Bobbert, R. a. J. Janssen and D. M. de Leeuw, *Adv. Mater.*, 2008, **20**, 975.
49 L. Chua, J. Zaumseil, J. Chang and E. C. Ou, *Nature*, 2005, **434**, 194.
50 S. Grecu, M. Roggenbuck, A. Opitz and W. Brütting, *Org. Electron.*, 2006, **7**, 276.
51 J. Veres, S. Ogier, G. Lloyd and D. de Leeuw, *Chem. Mater.*, 2004, **16**, 4543.
52 S. Lim, S. Kim, J. Lee, M. Kim, D. Kim and T. Zyung, *Synth. Met.*, 2005, **148**, 75.
53 B. H. Hamadani, H. Ding, Y. Gao and D. Natelson, *Phys. Rev. B: Condens. Matter Mater. Phys.*, 2005, **72**, 235302.
54 S. Hoshino, M. Yoshida, S. Uemura, T. Kodzasa, N. Takada, T. Kamata and K. Yase, *J. Appl. Phys.*, 2004, **95**, 5088.

Electronic Supplementary Information for

A Heterotriangulene Polymer for Air-stable Organic Field-Effect Transistors

Kerstin Schmoltner,[a] Florian Schlütter,[b] Milan Kivala,[b] Martin Baumgarten,[b] Stefanie Winkler,[c,d] Roman Trattnig,[a] Norbert Koch,[c,d] Andreas Klug,[a] Emil J. W. List,[a,e] Klaus Müllen[b]

[a] *NanoTecCenter Weiz Forschungsgesellschaft m.b.H., Franz-Pichler-Straße 32, A-8160 Weiz, Austria*
[b] *Max-Planck-Institut für Polymerforschung, Ackermannweg 10, 55021, Mainz, Germany*
[c] *Helmholtz Zentrum Berlin für Materialien und Energie GmbH Elektronenspeicherring BESSY II, Albert-Einstein-Str. 15, 12489 Berlin, Germany*
[d] *Institut für Physik, Humboldt-Universität zu Berlin, Brook-Taylor-Strasse 6, D-12489 Berlin, Germany*
[e] *Institute of Solid State Physics, Graz University of Technology, Petersgasse 16, A-8010 Graz, Austria*

Table of contents

1. Synthesis 2
2. Photoluminescence spectra of toluene vs. $CHCl_3$ solutions and the influence of UV-light exposure 2
3. Absorption and photoluminescence spectra of PTA films 3
4. Surface morphology of a P3HT film 3
5. Energy levels of P3HT and work function of differently treated Au 3
6. Output characteristics of PTA based OFETs with different interface treatments 4
7. Evolution of device parameters of PTA and P3HT OFETs under ambient conditions 6

1. Synthesis

4,4,8,8,12,12-hexamethyl-8,12-dihydro-4H-benzo[1,9]quinolizino[3,4,5,6,7-defg]acridine (DTPA) was synthesized according to literature from methyl 2-iodobenzoate and methyl 2-aminobenzoate. [1, 2]

2. Photoluminescence spectra of toluene vs. $CHCl_3$ solutions and the influence of UV-light exposure

Fig. S1 shows the photoluminescence spectra of 1g/L **PTA** in toluene and chloroform solution under different pre-conditions. The solid black line displays the fluorescence spectra of solutions which were prepared under ambient condition, under yellow light and kept in dark until the measurements (blue dashed line) and exposed to UV-light (~10 s, with wavelengths of 254 nm, 366 nm) (red dashed/dotted line). In contrast to the toluene solutions, the chloroform solutions spectra exhibit a significant influence of the ambient/UV-light exposure. A second peak appears around ~565 nm. The corresponding inset depicts a color change of the $CHCl_3$ solution from colorless to brown solution when exposed to ambient light. The observed effects can be ascribed to the dissociation of $CHCl_3$ under ambient light or UV-light at which hydrochloric acid (HCl) [5,6] is formed and protonation of the central nitrogen happens. Even if the $CHCl_3$ solution was prepared under yellow light and kept in dark, a non-negligible emission from 500 nm to 650 nm appears but is not as pronounced as for solutions prepared under ambient light or exposed to UV-light. This can be explained by short ambient light exposure during mounting the sample in the spectrofluorophotometer as well as the light influence during the measurements. Moreover, it cannot be excluded that the used $CHCl_3$ has already contained a small amount of HCl. The ~10 nm blue-shift of the emission maxima (at 434 nm) in comparison to the spectra of 0.005g/L solution shown in **Fig. 4** in the main text can be ascribed to the high concentration (1g/L) resulting in self absorption of these solutions.

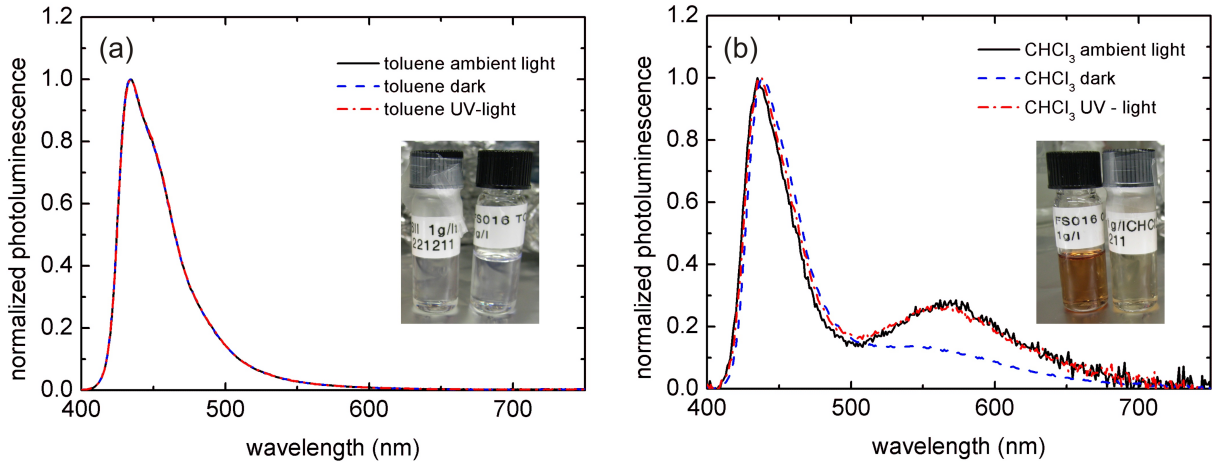

Fig. S1 Photoluminescence emission spectra of 1g/L PTA solution in toluene (a) and chloroform (b) after preparation under ambient conditions (black solid line), in dark (blue dashed line) and after exposure to UV-light (red dashed/dotted line). Inset: corresponding solutions when prepared under ambient light (left) and in dark (right).

3. Absorption and photoluminescence spectra of PTA films

Fig. S2 displays the UV/Vis absorption spectra and photoluminescence spectra of **PTA** films spin-coated from 2g/L toluene and chloroform solutions. The UV/Vis absorption maxima of **PTA** films were at 383 nm and 325 nm. The fluorescence spectrum of films prepared from toluene and $CHCl_3$ solution exhibits a maximum at 434 nm and 436 nm, respectively. Compared to the results obtained for **PTA** solutions, the spectra of films showed no significant influence of the used solvent, which can be explained by the fact that the solutions for film deposition were prepared and spin-coated under inert atmosphere in absence of UV-light (no discoloration, no protonation effects were observed). Subsequently the films were dried under high vacuum ($p \sim 4 \times 10^{-5}$ mbar) at 120°C to remove residual solvents.

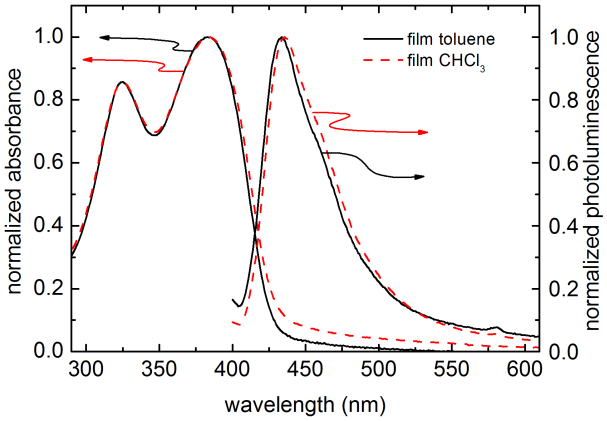

Fig. S2 UV/Vis absorbance and photoluminescence emission spectra of **PTA** films prepared from toluene (solid black line) and chloroform (dashed red line) solutions.

4. Surface morphology of a P3HT film

Fig. S3 shows the topographic image of a typical **P3HT** film on SiO_2 after annealing at 120°C for 1h in high vacuum ($p \sim 4 \cdot 10^{-5}$ mbar). The film exhibits a very smooth surface with a root-mean-squared roughness of ~0.4 nm.

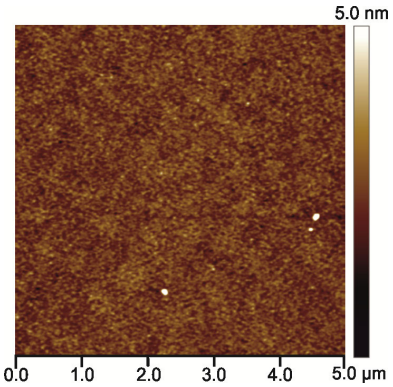

Fig. S3 AFM topographic image of a typical P3HT film on SiO_2 (scan size 5 µm x 5 µm).

5. Energy levels of P3HT and work function of differently treated Au

Fig. S4 shows the results of ultraviolet photoelectron spectroscopy (UPS) of the P3HT polymer to determine the absolute location of the energy levels of P3HT and the relative alignment at the interface to gold. The secondary electron cut-off was found at 4.2 eV with respect to the Fermi level (E_F) and, in conjunction with the binding

energy of the emission onset of 0.3 eV below the Fermi level, the corresponding ionization energy could be determined to 4.5 eV (see **Fig. S4 (a)**). The lowest unoccupied molecular orbital can be estimated (E_{LUMO} = 2.6 eV) by using the optical gap energy of 1.9 eV, which was determined from UV/Vis absorption measurements in solid state (film of 2g/l toluene, not shown). The corresponding energy level scheme is shown in **Fig. S4 (b)**.

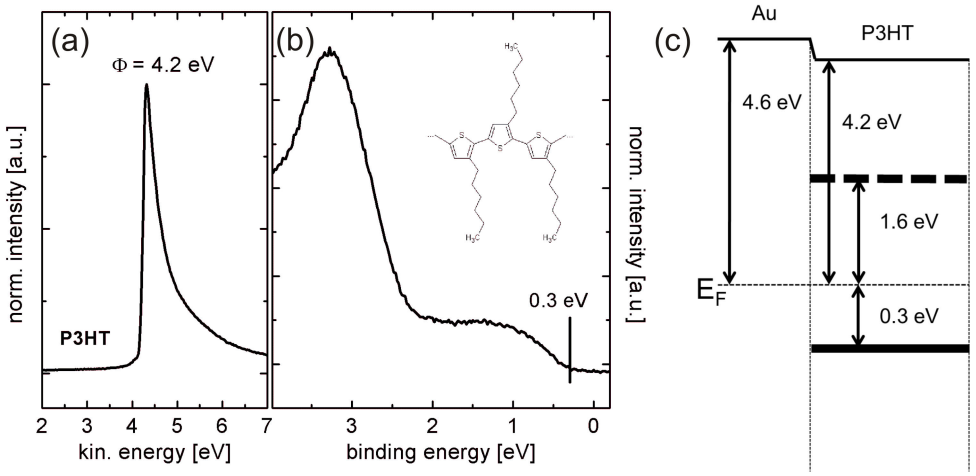

Fig. S4 (a) Secondary electron cut-off and (b) valence region UPS spectra of P3HT on Au/SiO_2 substrates. (c) Schematic energy levels of P3HT with respect to gold.

As mentioned in the main text, the work function of the gold with 4.6 eV is rather low. This can be explained by hydrocarbon contaminations on gold, which lower the surface dipole and therefore the work function. [3] Correspondingly, to determine the influence of different treatments and storing conditions on the work function of gold, various gold substrates were investigated. To resemble the conditions in the device after evaporation of gold, the sample was exposed to the lift-off chemicals used during the source/drain structuring process. The work function of these gold films subsequently stored in argon was determined to 4.58 eV (**Au**, **Table S1**). When the samples were stored in air (for ~2-3 days), the work function was lowered by about 0.15 eV ($\mathbf{Au_{air}}$, **Table S1**). Films exposed to the lift-off chemicals, which were additionally treated with 15 min HMDS, revealed a work function of 4.53 eV ($\mathbf{Au^{HMDS}}$). The highest work function of 4.65 eV (still low due to storing in air) was obtained for gold films without any additional treatment ($\mathbf{Au_{air}^{pristine}}$, **Table S1**). The obtained values are in good agreement with results from literature. [3, 4]

Table S1: Work functions of differently treated gold films; **Au**: exposed to lift-off chemicals and stored in Ar, $\mathbf{Au_{air}}$: exposed to lift-off chemicals and stored in air, $\mathbf{Au^{HMDS}}$: exposed to lift-off chemicals and HMDS, then stored in Ar; $\mathbf{Au_{air}^{pristine}}$: without treatment but stored in air.

Sample	**Au**	$\mathbf{Au_{air}}$	$\mathbf{Au^{HMDS}}$	$\mathbf{Au_{air}^{pristine}}$
Φ (eV)	4.58	4.43	4.53	4.65

6. Output characteristics of PTA based OFETs with different interface treatments

Fig. S5 depicts output characteristics of **PTA** based OFETs with UV/ozone **(b)** and O_2 plasma **(c)** treatment of the dielectric surface and the electrodes compared to a reference device without surface modification **(a)** (all samples were prepared without HMDS treatment). **Fig. S5 (b)** reveals that the UV/ozone treatment of the source/drain electrodes improves the charge carrier injection slightly seen by an improved linear characteristics at low drain voltages. Moreover, the channel current is lower which can be explained by a higher density of OH-groups on SiO_2 (caused by the UV/ozone exposure), leading to charge carrier trapping. The output

characteristics of OFETs with O_2 plasma exposure of the electrode-/dielectric surface show good saturation without injection problems (see **Fig. S5 (c)**), being mostly ascribed to (contact-) doping.

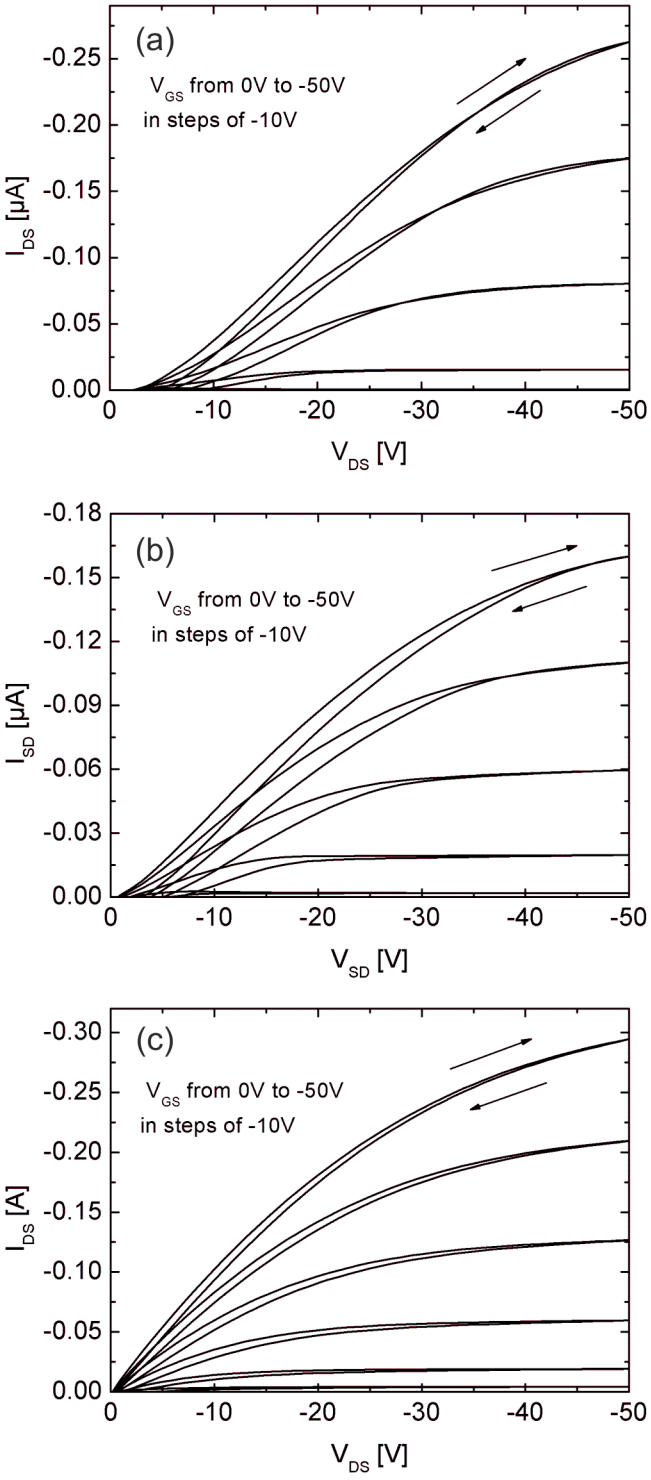

Fig. S5 Output characteristics of **PTA** OFETs with different interface treatments: (a) bare SiO_2, (b) UV/ozone and (c) O_2 plasma treatment, (L = 25 µm, W = 2.85 mm, without HMDS exposure).

7. Evolution of device parameters of PTA and P3HT OFETs under ambient conditions

Table S2 depicts the extracted device parameters of **PTA** and P3HT FETs over time when fabrication and characterization was done in air under ambient conditions. OFETs based on the novel polymer **PTA** did not show any significant change in performance even after storage over 3 months. Slight variations in field-effect mobilities and on/off ratios can be explained by varying levels of moisture and temperature. No degradation was observed, in contrast to P3HT devices, which exhibited gradually decreasing on/off ratios and increasing switch-on voltages due to doping effects.

Table S2: Device parameters of BG/BC OFETs based on **PTA** in comparison to P3HT after storage in air (23-26°C, 45-60 % rh).

Sample	time	Mobility μ_{sat} [a] ($cm^2 V^{-1} s^{-1}$)	I (on/off) [b]	V_{so} (V)
PTA	as prepared	6.6×10^{-4}	1.1×10^{4}	-4
	1 week	8.3×10^{-4}	2.5×10^{4}	-3
	1 month	7.6×10^{-4}	1.8×10^{4}	-3
	2 months	6.3×10^{-4}	1.1×10^{4}	-2
	3 months	6.3×10^{-4}	2.6×10^{4}	-1
P3HT	as prepared	2.5×10^{-4}	2.6×10^{3}	6
	1 week	2.7×10^{-4}	1.6×10^{3}	>10
	1 month	2.6×10^{-4}	3.2×10^{2}	>10
	2 months	2.1×10^{-4}	8.0×10^{1}	>10
	3 months	1.9×10^{-4}	6.6×10^{1}	>10

[a] μ_{sat} was calculated according to the gradual channel approximation
[b] on-current I_{on} was taken at V_{GS}=-50V, V_{DS}=-50V and off-current I_{off} at V_{GS}=0V, and V_{GS}=-10V (for P3HT OFETs, being fully depleted for as prepared devices), V_{DS}=-50V

[1] Z. Fang, T. L. Teo, L. P. Cai, Y. H. Lai, A. Samoc, M. Samoc, *Org. Lett.*, 2009, **11**, 1.
[2] Z. Fang, X. H. Zhang, Y. H. Lai, B. Liu, *Chem. Commun.*, 2009, 920.
[3] S. Rentenberger, A. Vollmer, E. Zojer, R. Schennach, and N. Koch, *J. Appl. Phys.*, 2006, **100**, 053701.
[4] A. Wan, J. Hwang, F. Amy, and A. Kahn, *Org. Electron.*, 2005, **6**, 47.
[5] S. Hautecloque, *Journal of Photochemistry*, 1980, **14**, 157.
[6] P. E. Hoggard, A. J. Bridgeman, H. Kunkely, A. Vogler, *Inorg. Chim. Acta*, 2004, **357**, 639.

Electrolyte-gated organic field-effect transistors for sensing in aqueous media

K. Schmoltner,[a] J. Kofler,[a] A. Klug,[a] E. J. W. List-Kratochvil*[a,b]
[a]NanoTecCenter Weiz Forschungsgesellschaft mbH, Franz-Pichler-Strasse 32, 8160 Weiz, Austria;
[b]Institute of Solid State Physics, Graz University of Technology, Petersgasse 16, 8010 Graz, Austria

ABSTRACT

For the emerging fields of biomedical diagnostics and environmental monitoring, where sensor platforms for in-situ sensing of ions and biological substances in appropriate aqueous media are required, electrolyte-gated organic field-effect transistors (EGOFETs) seem to be the transducers of choice. Due to the formation of an electric double layer at the electrolyte/organic semiconductor interface, they exhibit a very high capacitance allowing for low-voltage and water-stable operation. In combination with the outstanding properties of organic devices like biocompatibility, low-temperature processability on flexible substrates, as well as the possibility to tune the physical and chemical properties enhancing the selectivity and sensitivity, EGOFET-based sensors are a highly promising novel sensor technology. In order to obtain a reliable sensor response, a stable device operation is crucial. Within this context, we present a combined study of poly(3-hexylthiophene)–based EGOFETs on various substrates. In particular, the influences of different concentrations of NaCl in the electrolyte and various gate electrode materials, to tune the threshold voltage have been investigated. Furthermore, the limits of the stable operational window are evaluated and the effects when abandoning the latter are discussed.

Keywords: Electrolyte-gated organic field-effect transistor, EGOFET, OFET-based sensors, biosensors, organic semiconductors
*emil.list-kratochvil@ntc-weiz.at; phone 0043 316 876 8000; fax 0043 316 876 8040; ntc-weiz.at

1. INTRODUCTION

Aside from the main application of organic field-effect transistors (OFETs) in display and integrated circuit technology[1,2], OFETs have been proven to be excellent candidates as transducers for many sensing applications.[3,4,5,6,7] Owing to the outstanding features of organic devices, which are processable at low temperatures, economic production,[8] miniaturization and integration on flexible substrates are feasible, leading to smart (disposable) sensor assemblies for health-, food- and environmental monitoring.[9,10] Another property of organic compounds is the good biocompatibility,[11] which is of high importance when it comes to biomedical applications and the envisioned human interfacing, e.g. artifical skin, in-situ measurements of vital parameters, or monitoring the health conditions via E-textiles. Here, benefiting from the "soft" nature as well as the similarity of building blocks, organic materials outperform the inorganic counterparts significantly. Moreover, the chemical and physical properties of organic compounds can be tuned in order to obtain a distinct sensitivity and selectivity with respect to target analytes.

Another advantage of OFETs compared to other sensor concepts (e.g. based on resistors), is the inherent signal amplification, which results in higher sensitivity.[12] OFET-based sensors are transducers and amplifiers at the same time and there are well established methods to miniaturize and integrate them into complex circuits including further signal processing. They benefit also from fast response times and low power consumption. In view of these exceptional features, integrated low-cost (disposable) sensor tags for multi-analyte detection are not a future vision anymore. Accordingly, several examples of OFET-based chemical sensors have been demonstrated, ranging from detection of small molecules such as NH_3,[13] NO_2,[14,15] O_2,[16] vapors (e.g. 1-hexanol, ethanol)[17,18,19] and humidity[20] to ions[21] and complex biomolecules[22,23,24].

Organic Field-Effect Transistors XII; and Organic Semiconductors in Sensors and Bioelectronics VI, edited by Zhenan Bao, Iain McCulloch, Ruth Shinar, Ioannis Kymissis Proc. of SPIE Vol. 8831, 88311N
 · doi: 10.1117/12.2024135

Especially, for the emerging fields of biomedical diagnostics and environmental monitoring, sensing of ions (e.g. Na^+, K^+, Ca^{2+}, pH,…) and biological substances (e.g. DNA, enzymes, hormones, …) in appropriate aqueous media is of particular interest. In order to obtain a stable operation in aqueous analytes, low-voltage operation is required. Here electrolyte-gated OFETs are the transducers of choice, offering distinct advantages. They benefit from a direct contact between the organic semiconductor and the analytes (electrolyte). It is this interface between the analytes (electrolyte) and the semiconductor, which enables low-voltage operation (below 1V) at high source-drain currents around a few µA. This is due to the formation of an electric double layer (EDL) at the electrolyte/organic semiconductor interface with a very high capacitance (on the order of ~1-10 µF/cm^2)[25,26,27]. Figure 1 illustrates a p-type EGOFET in case of a negative applied gate potential, leading to the formation of an EDL at the gate/electrolyte and the semiconductor/electrolyte interface via migration of cations and anions to the respective interfaces. In detail, the EDL at the gate side consists of electrons within the metal and cations in the electrolyte, while at the semiconductor side holes and anions form the EDL. Within the electrolyte the ion layer is composed of 2 layers, the Helmholtz layer and the diffusion layer. The first consists basically of a solvent molecule layer in direct contact with the metal or semiconductor and a solvated ion layer. The diffusion layer, on the other hand, describes the layer of free ions, which migrate under electrostatic interaction and thermal motion. The excess of these ions decreases with increasing distance from the gate/- or semiconductor/electrolyte interface.[28] Therefore the potential drops only at the interfaces at the double layer, which typically exhibits a very small thickness, leading to very high capacitance values. Consequently, low voltage operation within a water-stable window is possible while the obtained source-drain currents remain sufficiently high for further signal processing.

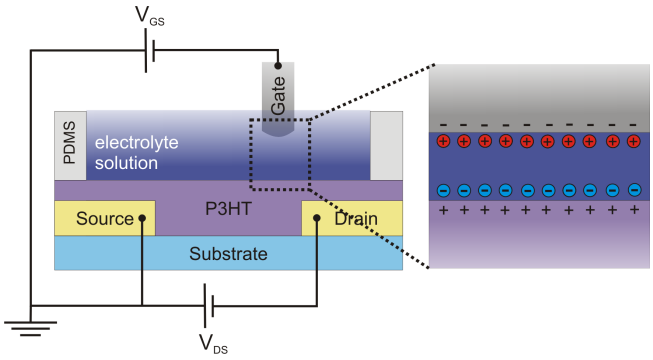

Figure 1. Scheme of an electrolyte-gated p-type organic field-effect transistor.

Owing to this exceptional property, electrolyte-gated OFETs were first recognized and subject of intense research in the field of low-voltage/ low-power applications, where they are good alternatives for OFETs based on solid dielectrics such as conventional oxide gate insulators, high-k dielectrics or ultrathin organic layers.[29]

An important milestone for sensing of biomolecules was then set by Kergoat et al., who reported on the stable operation of water-gated OFETs, making in-situ sensing of ions and biological substances in an appropriate aqueous medium possible.[25] Recent advances in this field include the successful detection of biomolecules such as DNA, dopamine, enzymes, proteins[30,31 32,33] as well as studies of the influence of pH and ionic strength on the performance of electrolyte-gated FETs[26]. Advances in OTFT-based biosensors operating in aqueous media as well as achievements in the field of EGOFETs are excellently reviewed by Kergoat et al.[25] and Cramer et al.[34]

While electrochemical doping of the semiconductor is highly unwanted for EGOFETs, the working principle of organic electrochemical transistors (OECTs)[35] relies exactly on this process. In comparison to EGOFETs, where the conducting channel is formed via charge accumulation due to the application of a sufficiently high gate field, OECTs are turned on or off via electrochemical doping or dedoping mechanisms, altering the conductivity of the electrically conducting polymer. Basically the architecture of OECTs is the same as for EGOFETs (see Figure 2). However, a charge-transfer process across the electrolyte/polymer interface is required.[3] First OECT-based chemical sensors were reported by Wrighton et al. in 1985, where transistors based on polyaniline operated in an aqueous electrolyte solution, showing a response to small changes in pH as well as to redox reagents.[36] However, the drawback of OECTs is the slow switching speed and therefore slow response times.

In analogy to the inorganic semiconductor technology, organic ion-sensitive FETs (ISOFETs) are one of the most widley investigated FETs operating in aqueous media.[37,21] Here the electrolyte is in direct contact with the gate dielectric and a reference electrode is used as the gate electrode (see Figure 2). The electric field across the insulating gate dielectric is influenced by the ions at the electrolyte/dielectric interface, thus modulating the channel current. With this concept successful detection of pH changes has been realized using silicon nitride as proton-sensitive layer[21] as well as the sensing of biomolecules (e.g. glucose) has been demonstrated by immobilization of an enzymatic layer (glucose oxidase) on a tantalum oxide dielectric.[24] This showed that in general the selectivity towards a certain analyte can be induced by modifying the gate dielectric with a proper functionalization. Moreover, attempts for the detection of specific ions have been reported by Rai et al.[38], but to our knowledge no reversible and selective ion sensor based on the conventional ISFET concept has been presented so far.
However based on the emerging EGOFET technology, we recently demonstrated for the first time an electrolyte-gated OFET for selective and reversible ion detection.[39] A sensitive and selective response to sodium ions was obtained by introducing a state-of-the-art ion-selective membrane. Based on field-enhanced conduction, a sensitive linear Nernstian response (~62 mV/dec) for a broad detection range of 10^{-6} to 10^{-1} M NaCl was achieved. These results constitute an important step towards a low-cost integrated sensor array for multiple ion detection facilitated by a simple integration of different state-of-the-art ion-selective membranes.
This as well as the above mentioned achievements demonstrates that the utilization of EGOFET-based sensors ushered in a new era of biological and ion sensing.

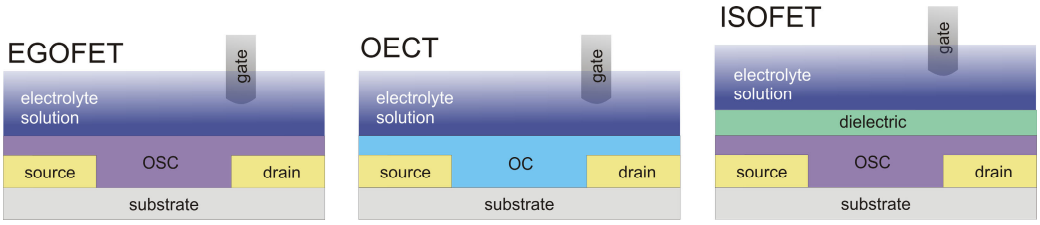

Figure 2. Scheme of an electrolyte-gated organic field-effect transistor (EGOFET), an organic electrochemical transistor (OECT) and an ion-sensitive organic field-effect transistor (ISOFET).

Aside from the key features of sensors such as sensitivity, selectivity, reversibility and response time, the device stability is another important factor in order to obtain a reliable sensor response.[40] In this context we present a combined study of the investigation of poly(3-hexylthiophene) (P3HT)–based EGOFETs on various substrates, gated using water and different concentrations of NaCl solutions. Moreover, the influences of different metal gate electrodes (Pt, Au) in comparison to an Ag/AgCl reference electrode are shown. In particular, the limits of stable operational windows were evaluated as well as the effects when abandoning the latter are discussed.

2. SAMPLE FABRICATION

EGOFET devices were fabricated on 1 inch x 1 inch glass, Si/SiO_2 or PET substrates (Melinex®, DuPont Teijin Films). Conventional lift-off processing was used to structure the 50 nm gold source/drain (S/D) electrodes with 2 nm chromium adhesion layer (channel length L = 4 µm - 21 µm, channel width W ~ 3 mm or W ~ 20 mm).[41] Before the deposition of the semiconductor, hexamethyldisilazane (97% purity degree, SSE Optihot VB20 hotplate) was applied to the SiO_2 and glass substrates via vapor phase deposition for an exposure time of 15 min, and adsorbed water on the substrate surface was removed by an annealing step at 120°C in high vacuum ($p \sim 4x10^{-5}$ mbar) for 1 h. Regioregular poly(3-hexylthiophene) (Plexcore® OS purchased from Sigma-Aldrich) was then deposited via spin-coating from a 4 g/l toluene solution and dried at 60°C in Argon (Ar) for ~10 min and subsequently at 120°C under high vacuum ($p \sim 4 \cdot 10^{-5}$ mbar) for 1 h. All devices were assembled under inert atmosphere. Deionized (DI) water and saline solutions, which were prepared in concentrations varying from 10^{-4} M to 10^{-2} M NaCl (99.5%, p.a., ACS, ISO) in DI water, were used as electrolytes. A reservoir, which was made of polydimethylsiloxane (PDMS, Sylgard 184) via a soft molding process including a curing step of ~1 h at 100 °C was used to confine the electrolyte. The EGOFETs were gated via an Ag/AgCl (3M KCl) reference electrode, a 2 x 2 mm large and 50 nm thick gold (Au) pad or a platinum (Pt) electrode. Typical samples with three P3HT-based EGOFETs with DI water as electrolyte before and after electrical conduction with an

Ag/AgCl reference electrode are shown in Figure 3. The electrical characterization was done in air at ambient conditions using an Agilent B1500 Parameter Analyzer. Gradual channel approximation was used to calculate the field-effect mobility μ, and the threshold voltage was determined by linear fitting of the square-root of the channel current vs. the gate voltage in the saturation regime.

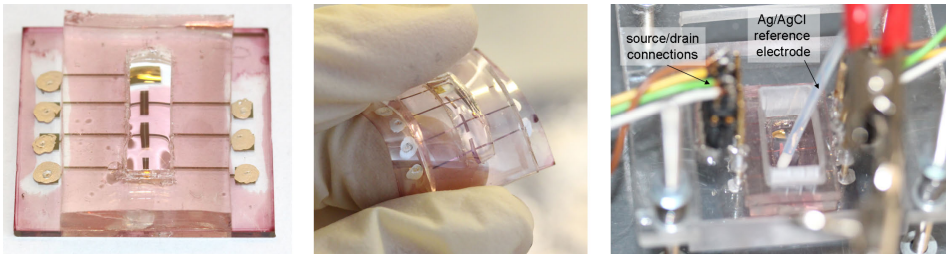

Figure 3. Typical sample with three P3HT-based EGOFETs with DI water as electrolyte on glass and PET before and after electrical conduction with Ag/AgCl reference electrode.

3. RESULTS AND DISCUSSION

Figure 4 and 5 show the transfer and output characteristics of typical P3HT-based EGOFETs with DI water as electrolyte, gated via an Ag/AgCl reference electrode. High on-currents of about 30 μA (V_{DS} = -0.4 V, V_{GS} = -0.5 V) were obtained due to the high W/L ratio, using an interdigital structure with L = 10 μm, and W = 20 mm (see inset in Figure 4). In Figure 4 (a) the transfer curves of three devices are compared, exhibiting only a slight device-to-device variation. The on/off-current ratios for the transfer curves at V_{DS}= -0.1 V are ~5 x 10^2 (on-current: V_{GS} = -0.5 V, off-current: V_{GS}= +0.2 V). In comparison, the on/off-current ratio in the saturation regime showed a lower value of about ~10^2 due to an increased leakage current, being responsible for the higher off-current. The higher leakage can be explained by a higher maximum applied potential difference of -0.7 V compared to -0.4 V in the linear regime. The threshold voltage in the saturation regime was determined to ~0 V and mobility was estimated to be ~3 x 10^{-2} cm^2/Vs using a typical capacitance of 3 $\mu F/cm^2$ (for an Au/P3HT/water/Au system)[25], being in good agreement with literature values. Moreover, the origin of the observed small hysteresis can be attributed to charge polarization/ion movement in the electrolyte. These results, along with the nice saturation behavior of the output characteristics in Figure 5 demonstrate a good overall device performance.

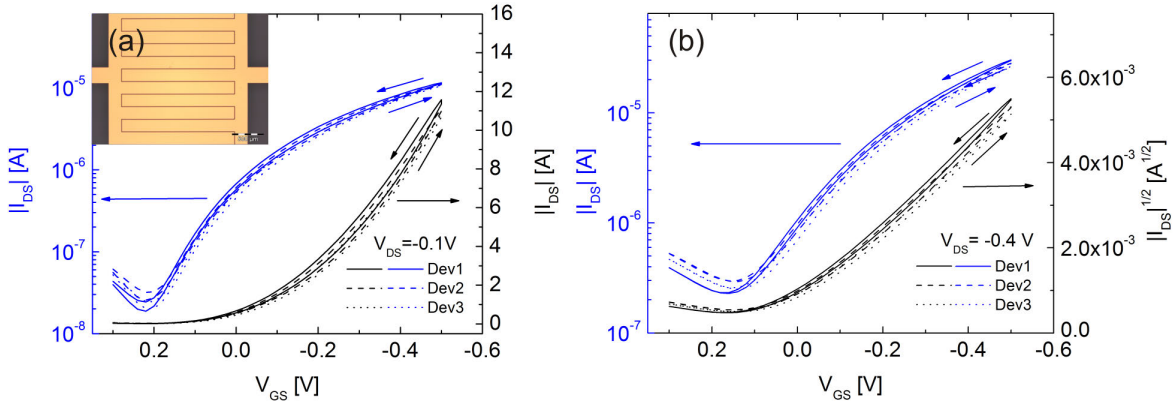

Figure 4.Transfer and semilogarithmic transfer curves of three P3HT-based EGOFETs gated via DI water with an Ag/AgCl reference electrode in the linear (a) and saturation (b) regime. Inset: micrograph of the interdigital gold source/drain structures before P3HT deposition (L = 10 μm, W = 20 mm).

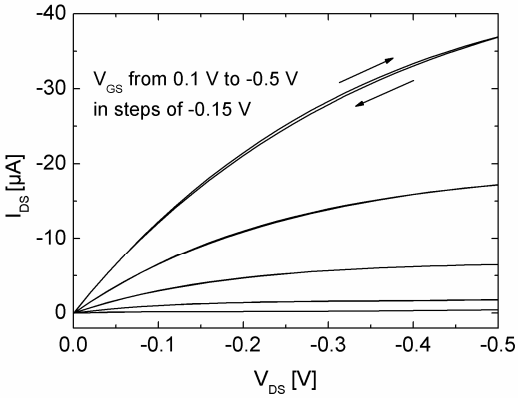

Figure 5. Output characteristics of one of the three P3HT-based EGOFETs gated via DI water with an Ag/AgCl reference electrode (W = 20 mm, L = 10 µm).

In Figure 6 (a) the transfer curves of devices with varying channel length (L = 5, 11, 21 µm) but same channel width (W = 3 mm) are compared, showing nice scaling behavior of the source-drain current. The on/off-current ratio and the threshold voltage in the saturation regime of the OFET with L = 21 µm, 11 µm and 5µm channel were determined to I_{on}/I_{off} ~40, ~50, ~80, and V_{th} = -30 mV, -20 mV, +30 mV, respectively. The output characteristics of the shortest channel shows nice saturation, no significant short-channel effects[42] were observed (see Figure 6 (b)). It has been demonstrated that EGOFETs are most suitable for downscaling due to high transversal fields generated by the very thin EDL, inhibiting short-channel effects.[43] Another advantage of electrolyte-gating is the lower contact resistance as reported by others.[44] Furthermore, the maximum leakage current of about 200 nA is lower compared to EGOFETs with larger electrode area such as for interdigital structures (~ 480 nA). In detail, the electrode area is ~50 % smaller (2.6 mm^2) than the S/D electrodes of the interdigital structures (5.3 mm^2), being reflected in the corresponding leakage currents (see inset in Figure 6 (a)). Although the source/drain electrodes are not additionally encapsulated with e.g. a resin, the leakage current values are within an acceptable range. In general, the hydrophobic nature of P3HT impedes the ion penetration. Accordingly, the contact angle of DI water on P3HT layers was determined to ~105°, independent of the surface of the used substrate (glass, SiO_2 or PET).

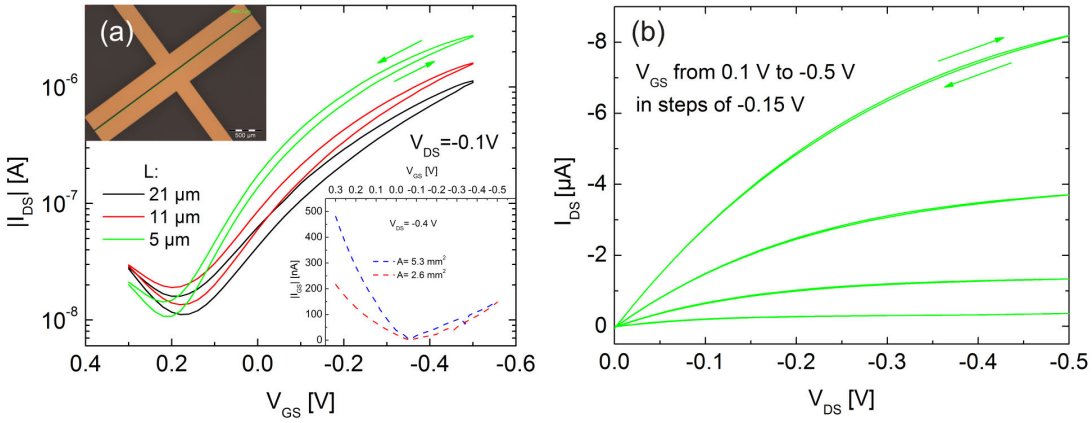

Figure 6. Semilogarithmic transfer curves of P3HT-based EGOFETs, gated via DI water with an Ag/AgCl reference electrode with different channel lengths but constant channel width: L = 21µm (black), L = 11 µm (red), L = 5 µm (green). Inset: micrograph of the gold source/drain structures before P3HT deposition and leakage current of EGOFET with different electrode areas. (b) Output characteristics of one of the EGOFETs compared (L = 5 µm).

In order to study the influence of the ion concentration within the electrolyte on the device performance, NaCl solutions varying between 10^{-4} M and 10^{-2} M NaCl were used instead of DI H_2O. The corresponding semilogarithmic transfer curves and output characteristics are presented in Figure 7. In general, for all measured devices a threshold voltage shift to more negative values (V_{th} in saturation regime from -130 mV ,-170 mV, -230 mV to -300 mV) was observed upon increasing the NaCl concentration from DI H_2O to 10^{-4}, 10^{-3} and 10^{-2} M NaCl. On the other hand; the usually accompanied lower on-currents were not observed, since the slope of the transfer curves increased. Therefore the on-current slightly increased with increasing salt concentration. Moreover, the subthreshold slope decreased from 230 mV/dec to 190 mV/dec for the 10^{-2} M NaCl solution compared to the 2 orders of magnitude lower 10^{-4} M NaCl solution. According to the models describing the Debye-Helmholtz layer, the capacitance of the EDL increases with higher ionic strength of the solution, being an explanation for the slightly increased slope and nearly remaining on-currents.[28] However, the V_{th}-shift might be explained by an enhanced screening of the surface charge (protons, hydroxyl ions) by more ions in the diffusion layer when the ionic strength is increased.[45] Similar results were obtained by Buth et al., who studied the influence of the pH and ionic strength on the performance of a α-sexithiophene based EGOFET.[26]

Furthermore, a specific absorption of ions at the semiconductor/electrolyte interfaces, introducing an additional capacitive contribution and thus altering the potential distribution, cannot be excluded. In general, it is important to note that the theoretical models of EDLs are simplified and experimentally verified for specific and "highly defined" systems.[28] Already the considerations of EDLs for solid electrodes such as Pt, which are commonly used for many electrochemical investigations, are difficult, since it is difficult to get reproducible surface conditions (cleanliness, adsorbed impurities), which in turn changes the interface properties.

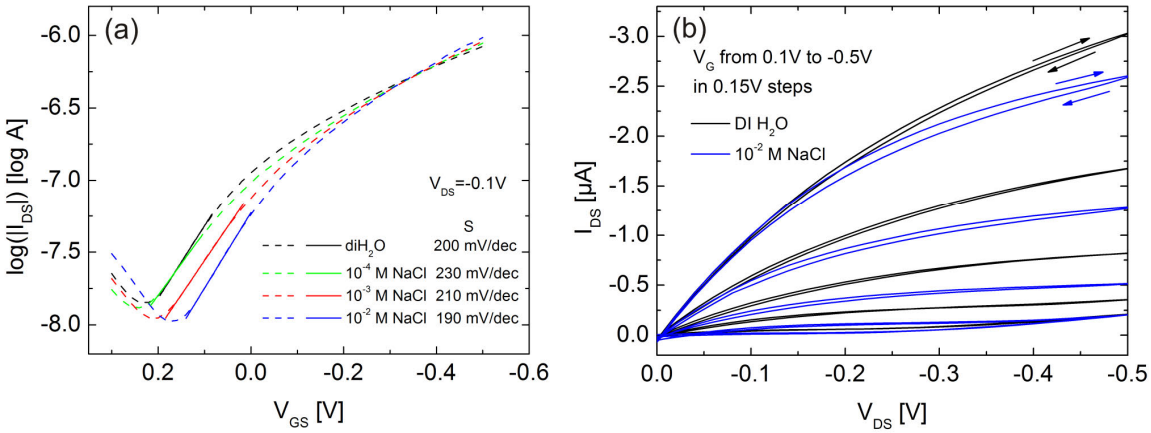

Figure 7. (a) Semilogarithmic transfer curve of P3HT-based EGOFETs gated via an Ag/AgCl reference electrode with different electrolyte solutions: DI H_2O (black), 10^{-4} M NaCl (green), 10^{-3} M NaCl (red) 10^{-2} M NaCl (blue); (b) Output characteristics of EGOFETs with DIH_2O (black) compared with 10^{-2} M NaCl solution as electrolyte (SiO_2, W = 3 mm, L = 4 µm).

So far in this study only EGOFETs gated via an Ag/AgCl reference electrode have been presented. These reference electrodes function as a redox electrode with a fixed potential. Thus, any changes observed are due to changes at the semiconductor/electrolyte interface and not due to changes at the electrode side. In a next step, P3HT-based EGOFETs were gated via Pt and Au electrodes. Basically, metal electrodes such as Pt and Au can be used as quasi-reference electrodes, if the bulk solution and the potential of the electrodes do not change, but actual potentials are required to be measured with respect to a reference electrode.

For a Pt electrode, a potential of ~ 450 mV vs Ag/AgCl in 10^{-2} M NaCl was obtained. To contact the EGOFET via an Au electrode, an additional 2 x 2 mm Au pad was used and the potential was determined around ~250 mV vs Ag/AgCl in 10^{-2} M NaCl, exhibiting a strong drift.

To demonstrate the importance of an appropriate gate electrode, EGOFETs gated via these metal electrodes were investigated. Figure 8 shows the corresponding transfer characteristics, indicating a strong influence of the used electrode. When gated via Pt electrode, a threshold voltage shift of about 400 mV to the positive direction (from -260 mV for Ag/AgCl to 140 mV for Pt in the linear regime) compared to Ag/AgCl gating is obtained, while the shape of the curve remains (see Figure 8 (b)). This is in good agreement with the measured potential of ~450 mV Pt vs Ag/AgCl, confirming the possible application of Pt as quasi-reference electrode. On the contrary, this is not the case for gating with the Au pad, since the obtained threshold voltage shift does not match with the measured potential. Besides that the shape of the transfer curve completely changes, indicating that the interface/EDL at the electrode might also change (changing electrode potential). Moreover, this altered behavior might be also ascribed to the small electrode area of ~ 4 mm^2, the non-reproducible Au surface due to the fabrication process as well as a possible reaction with the salt solution, especially chloride ions with Au.[46] This non-stable behavior has already been indicated by the potential drift of the Au electrode measured against the Ag/AgCl electrode.

This results prove that, although the used metal electrodes exhibit similar work functions around 5 eV (Au ~ 4.7-5.5 eV, Pt ~ 5.1-5.9),[47,48,49] this does not imply that similar threshold voltage shifts are expected to occur. There are many other factors (as discussed above) which have a stronger influence on the V_{th}, such as the size of the electrode, contaminations and adsorbents on the surface, possible electrochemical reactions, etc. However, the investigation clearly demonstrates the importance of choosing an appropriate gate electrode as well as indicates a good opportunity to tune V_{th}.

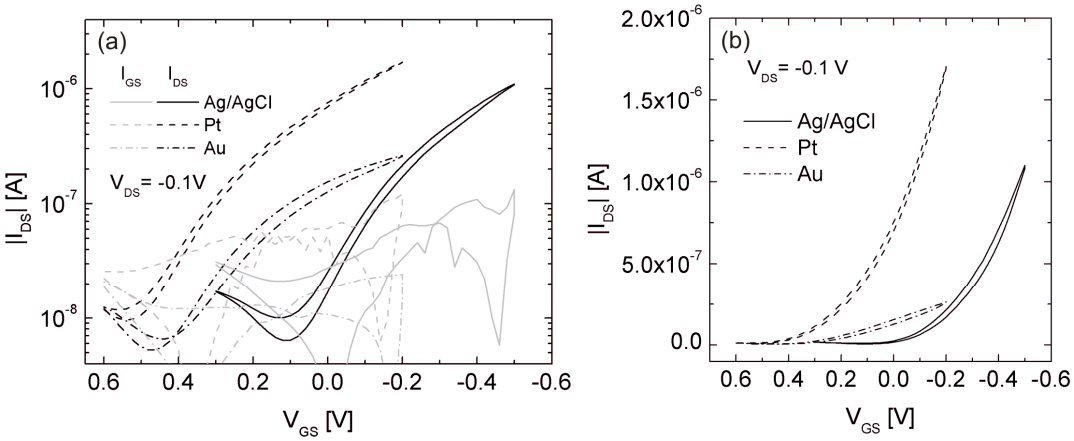

Figure 8. (a) Semilogarithmic and linear plotted (b) transfer curves of P3HT-based EGOFETs gated via different electrodes in 10^{-2} M NaCl in the linear regime: Ag/AgCl (solid line), Pt (dashed line), Au (dash-dotted line) (Glass, W ~ 3 mm, L ~ 12 µm).

Moreover, with regards to the operational stability, it is important to choose a proper operational window with respect to the applied electrodes. Therefore, to investigate the limits of the stable operation window and to demonstrate the device degradation when exceeding operatinal potentials, P3HT-based EGOFETs gated via a Pt electrode in DI water were studied when different maximum gate voltages were applied. Figure 9 depicts the corresponding transfer curves, with maximum gate voltages of -500 mV and -700 mV. Maximum source-drain voltages of -500 mV were applied, resulting in a maximum potential difference ΔV of -1 V when V_{GS} is swept from +0.5 V to -0.5 V. These rather large voltages are applied for a few seconds only since the gate voltage is swept with a rate of ~13 ms/mV. Anyhow, the transfer characteristics were reproducible within this voltage window (see black lines in Figure 9 (a)). However, when the gate voltage was swept from +0.7 V to -0.7 V, the subsequently recorded curve showed significant lower source-drain currents. Even though the voltage window was reduced again (+0.5 V, -0.5 V), the source-drain currents further decreased. The increased off-currents can be ascribed to higher leakage currents. These results indicate that once the potential exceeds a certain value or time, the current will continue to decrease also in case of a subsequent lower operational window. This decrease in current might be ascribed to bias-stress effects, but is more likely to be attributed to electrochemical reactions, leading to degradation of the semiconductor. An increasing gate current is a strong evidence

for the occurrence of electrochemical reactions. The behavior of ion penetration and electrochemical doping has already been investigated with respect to control the dimensionality of charge transport.[50] It was shown that the application of high voltages for extended operation times led to electrochemical doping of the whole film.

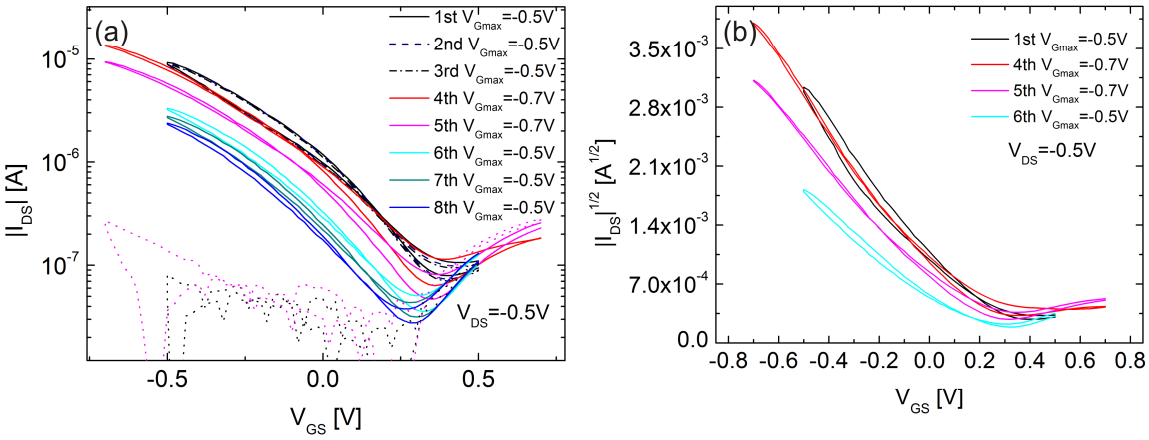

Figure 9. Semilogarithmic transfer curves (a) and square-root of the source-drain currents vs. gate voltage of P3HT-based EGOFETs gated via Pt in DI H_2O when different maximum gate voltages were applied (glass, W ~ 2.85 mm, L ~ 12 µm).

To investigate the influence of time on the voltage-dependent current degradation, the channel currents of exemplary P3HT-based EGOFETs with 10^{-2} NaCl solution gated via Ag/AgCl were recorded. Note that here an Ag/AgCl reference gate electrode was used to ensure the actual applied potential also within the electrolyte. Figure 10 (a) shows the source-drain current vs. time at a constant working point (V_{DS} = -0.1 V, V_{GS} = -0.2 V). In the first 10-20 s an increasing current is observed (black), which can be ascribed to charging. Then the current remains stable, but when a gate voltage of -0.8 V is applied, after ~ 60 s the channel current significantly decreases with time (see Figure 10 (b), black line). After applying this potential difference ΔV of -0.8 V (with respect to the source contact), the source-drain current was again recorded for lower V_{GS} = -0.2 V and a significantly decreasing current with time was observed (see Figure 10 (a), red line), indicating that the measurements at elevated voltage changed the charge transfer properties of the semiconductor. In more detail, Figure 10 (c) shows the additional recorded gate and source currents during the measurement. It can be clearly seen that after a higher potential was applied, the leakage current significantly increased (red dashed line); a large part of the current flows from the source to the gate electrode, being responsible for the lower source-drain current. This was also confirmed by the recorded transfer curves after the time-dependent measurements, showing a decreased channel current as well as an increase in leakage current (Figure 10 (d)). We believe that the reason of the observed degradation can be ascribed to electrochemical reactions at the P3HT/electrolyte interface with hydroxide and chloride upon exceeding a certain potential or a certain period of time at which a potential is applied. However, the exact underlying mechanism is currently under investigation.

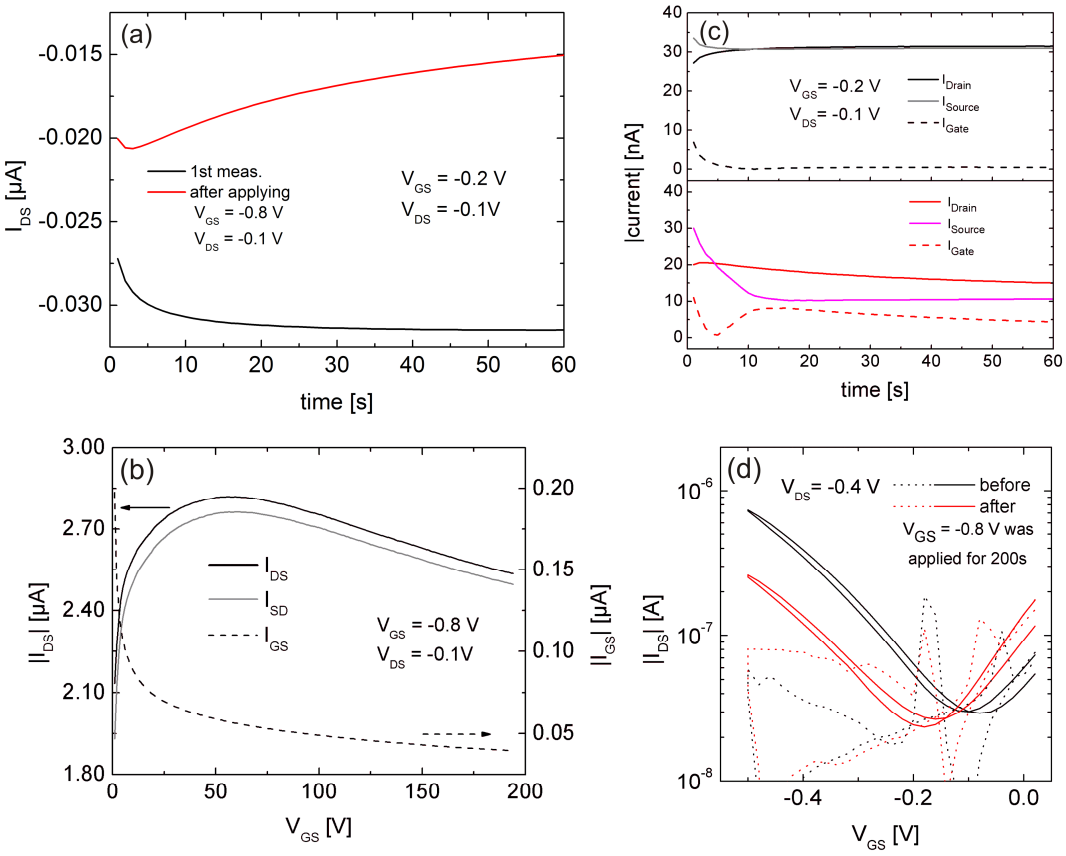

Figure 10. (a) Source-drain current vs. time at a stable operation point before (black) and after (red) applying a gate potential of -0.8 V for 200 s; (b) Source-drain current during applying -0.8 V at the gate electrode; (c) Source-drain currents (shown in (a)) with additionally measured source and gate currents; (d) Transfer characteristics before (black) and after (red) applying a gate potential of -0.8 V (glass, W ~ 3 mm, L ~ 4 µm).

4. SUMMARY AND CONCLUSION

In summary, we have demonstrated P3HT-based EGOFETs gated in deionized water via an Ag/AgCl electrode, exhibiting a good overall performance with on-currents up to 30 µA. Due to the hydrophobic nature of P3HT the ion penetration is hindered so that negligible electrochemical reactions can occur within a water-stable window. We found that an increasing NaCl concentration (10^{-4} M – 10^{-2} M) within water results in significant threshold voltage shifts to more negative values, whereas the on-current showed a tendency to higher values, being ascribed to the higher capacitance of the EDL. The threshold voltage shifts might be explained by charge screening via an increased amount of ions within the diffusion layer. Moreover, we illustrated the importance of choosing appropriate gate electrodes by comparing Pt and Au electrodes with respect to a standard Ag/AgCl reference electrode. Pt-electrode-gated EGOFETs exhibited a significant shift of the threshold voltage, which was in good agreement with the measured potential difference in comparison to the Ag/AgCl electrode. On the contrary, a completely altered transfer characteristics was obtained for EGOFETs gated with an Au electrode, which might be attributed to a non-stable electrode potential due to impurities on the surface as well as chemical reactions at the interfaces. In general, the presented results are in good agreement with other reports of EGOFETs using other semiconductors (e.g. α-sexithiophene) or gate electrodes. Furthermore, we investigated the operational stability within certain gate-potential windows and the effects when abandoning the latter. We observed a significant source-drain current decrease when a high potential difference was

applied. Accompanied with the lower source-drain currents an increasing leakage current was observed, which is a strong evidence for electrochemical reactions. To conclude, the presented results clearly demonstrate the influence of the salt concentration within the electrolyte and the influence of the applied electrode materials, being important factors for a proper design of EGOFET-based sensors including the evaluation of a stable operation window in order to obtain a reliable sensor response.

ACKNOWLEDGEMENTS

The authors gratefully acknowledge the Styrian Government (projects BioOFET 2 (GZ: A3-11.B-36/2010-5) and MIEC-DEVs (GZ: A3-11.M-32/2011-5)) for financial support.

REFERENCES

[1] Sekitani, T., and Someya, T., "Human-friendly organic integrated circuits," Mater. Today 14(9), 398–407 (2011).
[2] Gelinck, G., Heremans, P., Nomoto, K., and Anthopoulos, T. D., "Organic transistors in optical displays and microelectronic applications," Adv. Mater. 22(34), 3778–3798 (2010).
[3] Mabeck, J. T. and Malliaras, G. G., "Chemical and biological sensors based on organic thin-film transistors," Anal. Bioanal. Chem. 384, 343-353 (2006).
[4] Lin, P. and Yan, F., "Organic thin-film transistors for chemical and biological sensing," Adv. Mater. 24(1), 34–51 (2012).
[5] Kergoat, L., Piro, B., Berggren, M., Horowitz, G., and Pham, M.-C., "Advances in organic transistor-based biosensors: from organic electrochemical transistors to electrolyte-gated organic field-effect transistors," Anal. Bioanal. Chem. 402(5), 1813–1826 (2012).
[6] Berggren, M. and Richter-Dahlfors, A., "Organic Bioelectronics," Adv. Mater. 19, 3201-3213 (2007).
[7] Janata, J. and Josowicz, M., "Conducting polymers in electronic chemical sensors," Nat. Mater. 2(1), 19–24 (2003).
[8] Gamerith, S., Klug, A., Scheiber, H., Scherf, U., Moderegger, E. and List, E. J. W., "Direct Ink-Jet Printing of Ag-Cu Nanoparticle and Ag-Precursor Based Electrodes for OFET Applications," Adv. Funct. Mater. 17, 3111-3118 (2007).
[9] Bernards, D., Owens, R. M. and Malliaras, G. G., [Organic Semiconductors in Sensor Applications], Springer, Berlin, Heidelberg (2008).
[10] Klug, A., Schmoltner, K. and List, E. J. W., "Organic field-effect transistors applicable for gas and ion detection," Proc. of SPIE 7779, 77790G1-15 (2010).
[11] Scarpa, G., Idzko, A.-L., Götz, S., and Thalhammer, S., "Biocompatibility studies of functionalized regioregular poly(3-hexylthiophene) layers for sensing applications," Macromol. Biosci. 10 (4), 378–383 (2010).
[12] Katz, H. E., "Chemically Sensitive Field-Effect Transistors and Chemiresistors: New Materials and Device Structures," Electroanal. 16(22), 1837-1842 (2004).
[13] Klug, A., Denk, M., Bauer, T., Sandholzer, M., Scherf, U., Slugovc, C., and List, E. J. W., "Organic field-effect transistor based sensors with sensitive gate dielectrics used for low-concentration ammonia detection," Organ. Electron. 14(2), 500–504 (2013).
[14] Das, A., Dost, R., Richardson, T., Grell, M., Morrison, J. J., and Turner, M. L., "A Nitrogen Dioxide Sensor Based on an Organic Transistor Constructed from Amorphous Semiconducting Polymers," Adv. Mater. 19(22), 4018–4023 (2007).
[15] Hu, W., Liu, Y., Xu, Y., Liu, S., Zhou, S., Zhu, D., Xu, B., Bai, C., and Wang, C., "The gas sensitivity of a metal-insulator-semiconductor field-effect transistor based on Langmuir Blodgett films of a new asymmetrically substituted phthalocyanine," Thin Solid Films 360, 256–260 (2000).
[16] Torsi, L., Dodabalapur, A., Sabbatini, L., and Zambonin, P., "Multi-parameter gas sensors based on organic thin-film-transistors," Sens. Actuators, B 67(3), 312–316 (2000).

[17] Crone, B. Dodabalapur, A. Gelperin, A., Torsi, L., Katz, H. E., Lovinger, A. J. and Bao, Z., "Electronic sensing of vapors with organic transistors," Appl. Phys. Lett. 78(15), 2229-2231 (2001).
[18] Someya, T., Katz, H. E., Gelperin, A., Lovinger, A. J. and Dodabalapur, A., "Vapor sensing with α,ω-dihexylquarterthiophene field-effect transistors: The role of grain boundaries," Appl. Phys. Lett. 81(16), 3079-3081 (2002).
[19] Torsi, L., Tafuri, A., Cioffi, N., Gallazzi, M. C., Sassella, A., Sabbatini, L., and Zambonin, P. G., "Regioregular polythiophene field-effect transistors employed as chemical sensors," Sens. Actuators, B 93, 257–262 (2003).
[20] Zhu, Z.-T., Mason, J. T., Dieckmann, R., and Malliaras, G. G., "Humidity sensors based on pentacene thin-film transistors," Appl. Phys. Lett. 81(24), 4643-4645 (2002).
[21] Bartic, C., Palan, B., Campitelli, A., and Borghs, G., "Monitoring pH with organic-based field-effect transistors," Sens. Actuators, B 83, 115–122 (2002).
[22] Bartic, C. and Borghs, G., "Organic thin-film transistors as transducers for (bio)analytical applications," Anal. Bioanal. Chem. 384, 354-365 (2006).
[23] Someya, T., Dodabalapur, A., Gelperin, A., Katz, H. E., and Bao, Z., "Integration and Response of Organic Electronics with Aqueous Microfluidics," Langmuir 18(13), 5299–5302 (2002).
[24] Bartic, C., Campitelli, A., and Borghs, S., "Field-effect detection of chemical species with hybrid organic/inorganic transistors," Appl. Phys. Lett. 82(3), 475-477 (2003).
[25] Kergoat, L., Herlogsson, L., Braga, D., Piro, B., Pham, M.-C., Crispin, X., Berggren, M., and Horowitz, G., "A water-gate organic field-effect transistor," Adv. Mater. 22(23), 2565–2569 (2010).
[26] Buth, F., Kumar, D., Stutzmann, M., and Garrido, J. A., "Electrolyte-gated organic field-effect transistors for sensing applications," Appl. Phys. Lett. 98(15), 153302 (2011).
[27] Laiho, A., Herlogsson, L., Forchheimer, R., Crispin, X., and Berggren, M., "Controlling the dimensionality of charge transport in organic thin-film transistors," Proc. Natl. Acad. Sci. U.S.A. 108(37), 15069–15073 (2011).
[28] Bard, A. J. and Faulkner, L. R., [Electrochemical Methods: Fundamentals and Applications], second ed., John Wiley & Sons Inc., 12-18, 544-575 (2001).
[29] Kim, S. H., Hong, K., Xie, W., Lee, K. H., Zhang, S., Lodge, T. P., and Frisbie, C. D., "Electrolyte-Gated Transistors for Organic and Printed Electronics," Adv. Mater. 25(13), 1822–1846 (2012).
[30] Kergoat, L., Piro, B., Berggren, M., Pham, M.-C., Yassar, A., and Horowitz, G., "DNA detection with a water-gated organic field-effect transistor," Organ. Electron. 13(1), 1–6, (2012).
[31] Casalini, S., Leonardi, F., Cramer, T., and Biscarini, F., "Organic field-effect transistor for label-free dopamine sensing," Organ. Electron. 14, 156-163, (2012).
[32] Buth, F., Donner, A., Sachsenhauser, M., Stutzmann, M., and Garrido, J. A., "Biofunctional electrolyte-gated organic field-effect transistors," Adv. Mater. 24(33), 4511–4517 (2012).
[33] Magliulo, M., Mallardi, A., Mulla, M. Y., Cotrone, S., Pistillo, B. R., Favia, P., Vikholm-Lundin, I., Palazzo, G., and Torsi, L., "Electrolyte-gated organic field-effect transistor sensors based on supported biotinylated phospholipid bilayer," Adv. Mater. 25(14), 2090–2094 (2013).
[34] Cramer, T., Campana, A., Leonardi, F., Casalini, S., Kyndiah, A., Murgia, M., and Biscarini, F., "Water-gated organic field effect transistors – opportunities for biochemical sensing and extracellular signal transduction," J. Mater. Chem. B 1(31), 3728-3741 (2013).
[35] White, H. S., Kittlesen, G. P., and Wrighton, M. S., "Chemical Derivatization of an Array of Three Gold Microelectrodes with Polypyrrole: Fabrication of a Molecule-Based Transistor," J. Am. Chem. Soc. 106, 5375–5377 (1984).
[36] Paul, E. W., Ricco, A. J., and Wrighton, M. S., "Resistance of Polyanillne Films as a Function of Electrochemical Potential and the Fabrication of Poiyanlline-Based Microelectronic Devices," J. Phys. Chem. 89(8), 1441–1447 (1985).
[37] Bergveld, P., "Thirty years of ISFETOLOGY What happened in the past 30 years and what may happen in the next 30 years," Sens. Actuators, B 88, 1–20 (2003).
[38] Ji, T., Rai, P., Jung, S., and Varadan, V. K., "In vitro evaluation of flexible pH and potassium ion-sensitive organic field effect transistor sensors," Appl. Phys. Lett. 92(23), 233304 (2008).
[39] Schmoltner, K., Kofler, J., Klug, A. and List-Kratochvil, E. J. W. „Electrolyte-gated organic field-effect transistor for selective reversible ion detection," Adv. Mater. in press.

[40] Schmoltner, K., Schlütter, F., Kivala, M., Baumgarten, M., Winkler, S., Trattnig, R., Koch, N., Klug, A., List, E. J. W. and Müllen, K., "A heterotriangulene polymer for air-stable organic field-effect transistors," Polym. Chem. (2013) [doi:10.1039/c3py00089c].
[41] Schmoltner, K., Klug, A., Kofler, J., and List, E. J. W. "Photolithographic processing and its influence on the performance of organic field-effect transistors," Proc. SPIE 8479, 84790J (2012).
[42] Klug, A., Meingast, A., Wurzinger, G., Blümel, A., Schmoltner, K., Scherf, U. and List, E. J. W. "Organic field-effect transistors: a combined study on short-channel effects and the influence of substrate pre-treatment on ambient stability," Proc. SPIE 8118, 811809 (2011).
[43] Herlogsson, L., Noh, Y.-Y., Zhao, N., Crispin, X., Sirringhaus, H., and Berggren, M., "Downscaling of Organic Field-Effect Transistors with a Polyelectrolyte Gate Insulator," Adv. Mater. 20(24), 4708–4713 (2008).
[44] Braga, D., Ha, M. J., Xie, W. , Frisbie, C. D., "Ultralow contact resistance in electrolyte-gated thin film transistors," Appl. Phys. Lett 97, 193311 (2010).
[45] Härtl, A., Garrido, J. A, Nowy, S., Zimmermann, R., Werner, C., Horinek, D., Netz, R., and Stutzmann, M., "The ion sensitivity of surface conductive single crystalline diamond," J. Am. Chem. Soc. 129(5), 1287–1292 (2007).
[46] Ling, Y., "The Electrochemical Oxidation of Gold in 0.6 M NaCl and 0.3 M Na2SO4 Solutions," J. Electrochem. Soc. 144(8), 2689 (1997).
[47] Rentenberger, S., Vollmer, A., Zojer, E., Schennach, R., and Koch, N., "UV⁄ozone treated Au for air-stable, low hole injection barrier electrodes in organic electronics," J. Appl. Phys. 100(5), 053701 (2006).
[48] Hölzl, J., and Schulte, F. K., [Solid Surface Physics; Work Function of Metals], Höhler, G., Ed., Springer-Verlag, Berlin, (1979).
[49] Lide, D. R., Ed. [CRC Handbook of Chemistry and Physics], 87th ed., 12-114, CRC Press (2006).
[50] Larsson, O., Laiho, A., Schmickler, W., Berggren, M., and Crispin, X., "Controlling the dimensionality of charge transport in an organic electrochemical transistor by capacitive coupling," Adv. Mater. 23(41), 4764–4769 (2011).

ADVANCED MATERIALS
www.advmat.de

Electrolyte-Gated Organic Field-Effect Transistor for Selective Reversible Ion Detection

*Kerstin Schmoltner, Johannes Kofler, Andreas Klug, and Emil J. W. List-Kratochvil**

Organic field-effect transistors (OFETs) have already been proven to be suitable candidates as transducers for various sensor applications.[1–4] Owing to their intrinsic amplification, OFET based sensors typically reveal a high sensitivity. In conjunction with the outstanding features of organic electronic devices such as economic production, integration on flexible substrates and biocompatibility, low-cost disposable sensor assemblies are not a future vision anymore. Especially, the emerging fields of medical diagnostics and environmental monitoring require sensor platforms for in-situ sensing of ions and biological substances in appropriate aqueous media. Within these fields, sensor arrays for multiple ion detection (e.g., Na^+, K^+, Ca^{2+}, pH) for biomedical diagnostics, food-monitoring as well as for industrial process- and water-control are of particular interest.[5] Regarding these sensing applications, electrolyte-gated organic field-effect transistors (EGOFETs) are the transducers of choice. In contrast to conventional ion-sensitive OFETs[5–9] or FETs (ISFETs),[10–12] where the analyte is in contact with a solid gate dielectric, EGOFETs benefit from a direct contact between the organic semiconductor and the analyte. The electric double layer of high capacitance (1–10 μF cm^{-2}) formed at this interface enables low-voltage operation, which ensures a water-stable operation window, while the achieved source-drain currents (in the range of a few μA)[13–15] are sufficiently high for further signal processing.[6]

The high potential of electrolyte-gated OFETs was first indicated by Kergoat et al. who reported on the stable operation of water-gated OFETs.[13] Recent advances in this field include the successful detection of biomolecules such as DNA, dopamine, enzymes and proteins.[16–19] Additionally, the influence of pH and ionic strength of the electrolyte on the performance of EGOFETs were studied.[3,14] However, to our knowledge no organic ion-selective EGOFET has been shown.

With this contribution we demonstrate a novel, modular and versatile EGOFET-sensor platform for reversible and selective ion detection. Based on an electrolyte-gated poly(3-hexylthiophene) thin film transistor and a state-of-the-art sodium ion (Na^+) selective membrane,[20] a sensitive linear response in the range of 10^{-6} to 10^{-1} M Na^+ with a slope of ≈62 mV dec^{-1} was achieved. Furthermore, this potentiometric sensor showed a reversible response and its selectivity was successfully tested against interfering potassium ions (K^+). This new concept proves to be an important step towards a low-cost integrated ion-sensor array for selective multiple ion detection.

A schematic cross-section of the introduced ion-sensitive EGOFET is shown in **Figure 1**a, consisting of a bottom-contact poly(3-hexylthiophene) (P3HT) FET in direct contact with an optimized inner filling solution (water containing 10^{-2} M NaCl), acting as an electrolyte gate and separated via a polyvinylchloride (PVC) based ion-selective membrane (ISM) from the analyte. The latter is in contact with an Ag/AgCl (3 M KCl) reference electrode. The mounted flow cell enables a continuous exposure of the sensor device to different salt concentrations. This architecture is modular and facilitates the realization of ion-selective EGOFETs for the detection of various ions "simply" by introducing appropriate ISMs. The latter are well-established components which are usually applied in ion-selective electrodes.[21–23] Due to their vast dissemination they are available with a large variety of different ionophore-doped sensing membranes.[24] Their working principle is not based on a selective transport through the membrane as, for example, in case of filtration, osmosis or gas separation. In contrast, it relies on the ion movement over a few nanometers within the charge separation layer at the sample/membrane interface, leading to an activity-dependent membrane potential. A detailed explanation of the function of such ISMs is, for example, given by Bühlmann et al.[24] Important sensor parameters such as lowest detection limit and selectivity can be tuned by modifying the membrane.[25]

In contrast to other OFET sensor concepts, this approach is potentiometric and no direct modification of the organic semiconductor takes place, which leads to a higher overall device stability. Moreover, since no binding happens at the interface (such as with enzymes etc.),[18] reversible detection is possible by simply flushing the device using a mounted flow cell. Thus no complex recovery process is needed.

Figure 1 also shows the transfer (b) and output (c) characteristics of a typical Na^+ sensitive EGOFET with deionized (DI) water as analyte and a 10^{-2} M NaCl inner filling solution, exhibiting typical field-effect characteristics with a slight hysteresis. The transfer curve of this ion-sensitive EGOFET is shifted by ≈200 mV to the negative direction when the target ion in the analyte is increased to 10^{-2} M Na^+. This threshold voltage (V_{th}) shift originates from a non-zero membrane potential. In detail, this Nernstian membrane potential (see Figure 1a and Equation (1) is determined by the ion activity difference between the analyte and the inner filling solution. As the ion activity of the inner

K. Schmoltner,[+] J. Kofler,[+] Dr. A. Klug,
Prof. Dr. E. J. W. List-Kratochvil
NanoTecCenter Weiz Forschungsgesellschaft mbH
Franz-Pichler Straße 32, A-8160 Weiz, Austria
E-mail: E.List@tugraz.at
Prof. Dr. E. J. W. List-Kratochvil
Institute of Solid State Physics
Graz University of Technology
Petersgasse 32, A-8010, Graz, Austria

[+]K. Schmoltner and J. Kofler contributed equally to this work.

DOI: 10.1002/adma.201303281

ADVANCED MATERIALS
www.advmat.de

www.MaterialsViews.com

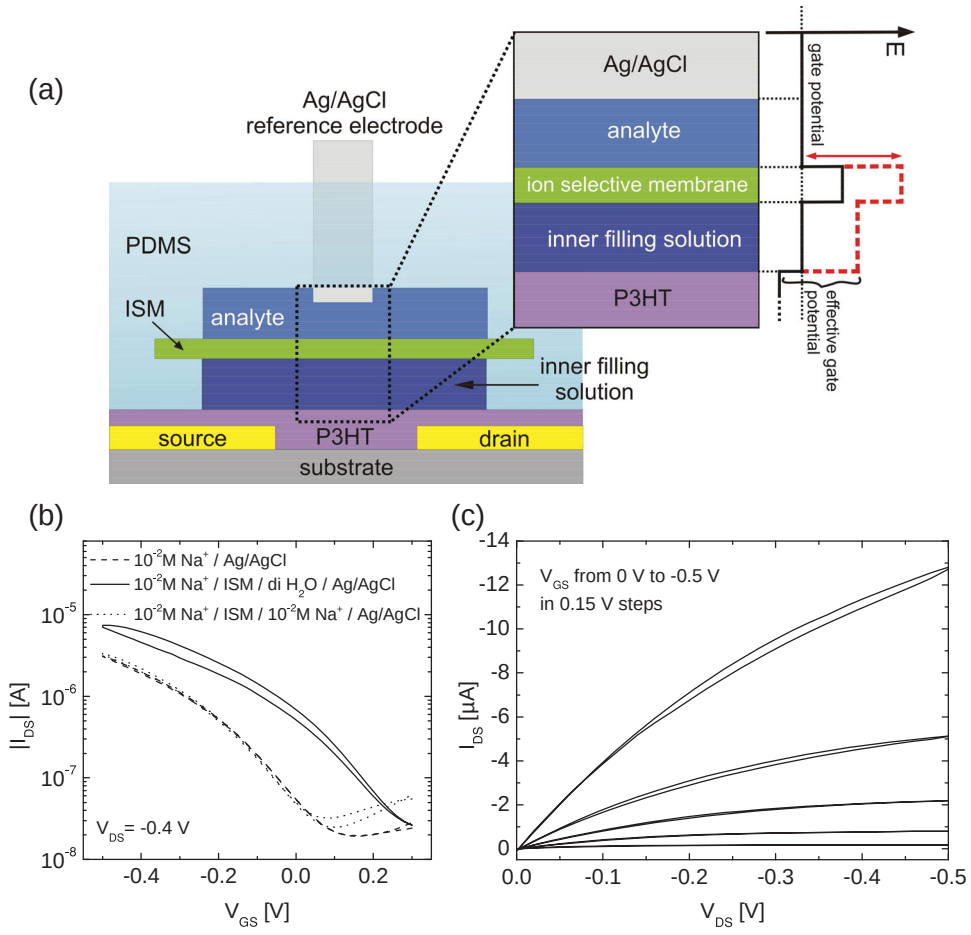

Figure 1. a) Cross section of an ion-sensitive EGOFET: the bulk potentials in case of equal ion concentration in the analyte and the inner filling solution (black) as well as in case of lower concentration in the analyte (red dashed) are illustrated. b) Semilogarithmic transfer curve of a typical P3HT-based EGOFET without (dashed line) and with implemented ISM using DI H_2O (solid line) and 10^{-2} M Na^+ solution (dotted line) as an analyte. c) Output characteristics of an ion-sensitive EGOFET using DI H_2O as an analyte.

filling solution is kept constant and the potential of the analyte is predefined through the Ag/AgCl gate electrode, the potential of the inner filling solution is modulated solely by the ion activity in the analyte (see Figure 1a). In fact, it is the potential of the inner filling solution (gate potential + membrane potential), hereby referred to as effective gate potential, which controls the source-drain current. Therefore, if the concentration of the target ion in the analyte is equal to the concentration in the inner filling solution (10^{-2} Na^+), the membrane potential is zero and the effective gate voltage matches the applied gate voltage. Consequently no V_{th} shift is observed, and the characteristics are identical to an EGOFET without a Na^+ selective membrane where the Ag/AgCl gate electrode is directly immersed into the inner filling solution (see Figure 1 b, dashed line). The reason for the insignificantly increased off-current of the transfer curve with an ISM (dotted line) is a slightly larger leakage current. The mobility with and without an ISM in the saturation region was estimated to be $\approx 2 \times 10^{-2}$ cm^2 V^{-1} s^{-1} using a typical capacitance of 3 µF cm^{-2} (for an Au/P3HT/water/Au system)[13], which is in good agreement with other reported values.[1,13] These results clearly demonstrate that the implementation of an ISM does not influence the overall performance (on/off ratio $\approx 10^2$, maximum channel currents of ≈10 µA) of the underlying EGOFET. However, when choosing the operational voltages, it is important to consider the effective applied gate potential which should be well below 0.7 V to ensure a stable device operation and to avoid degradation due to doping and hydrolyses. [13,14]

In order to demonstrate the sensitivity of the ion-selective EGOFET to Na^+, the source-drain current was recorded at a constant gate and source-drain potential while the Na^+ concentration in the water (analyte) was increased stepwise (see **Figure 2**a, $V_{DS} = -0.1$ V, $V_{GS} = -0.2$ V). The Na^+ concentration was adjusted by adding a certain amount of different saline solutions (10^{-4} – 10^{-1} M NaCl) to a larger reservoir (200 ml DI H_2O beaker) which was connected via PVC tubing to the flow cell and further to retracing micro syringes, producing a constant flow of 1 ml/min. As a sensitive response a source-drain current decrease of ≈250–500 nA dec^{-1} (depending on the point of operation) was observed while varying the Na^+ concentration between 10^{-6} M and 10^{-1} M. The source-drain current decrease reflects the change in effective gate potential. The latter can be calculated by using the fitted transfer curve at $V_{SD} = -0.1$ V (see Supporting Information) of the EGOFET without an ISM.

Adv. Mater. **2013**,
DOI: 10.1002/adma.201303281

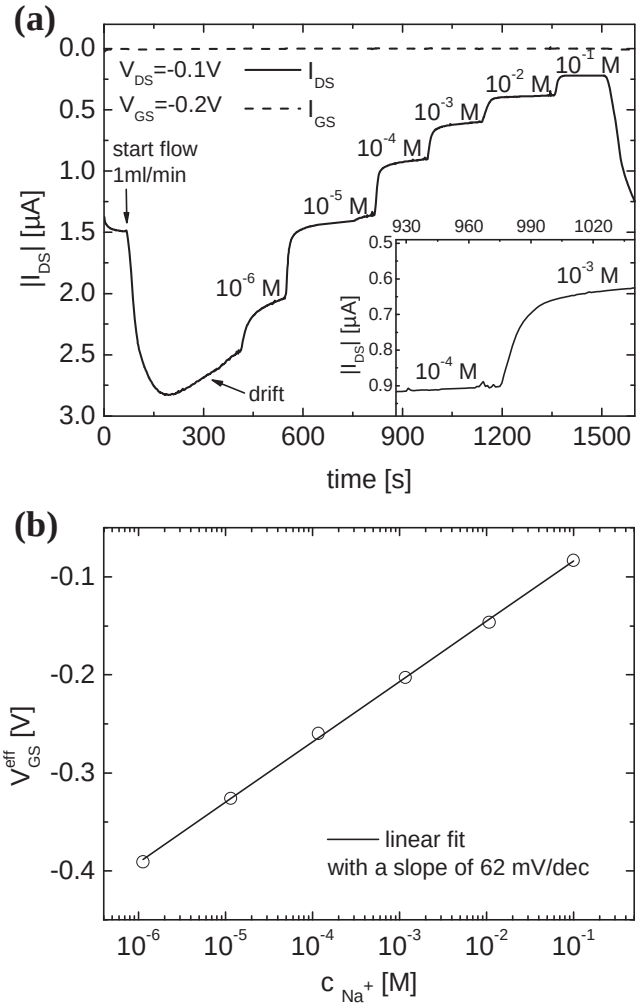

Figure 2. a) Source-drain current response to increasing Na^+ concentration of a typical ion-sensitive EGOFET with a PVC ion-selective membrane, exhibiting a response time of ≈30 s (see inset). b) Calculated effective gate potential versus Na^+ concentration (see Supporting Information).

Alternatively, the transfer curve of the EGOFET with an ISM can be used (as mentioned before), if the Na^+ concentration in the inner filling solution and the analytes are equal. Figure 2b shows the calculated effective gate voltage versus the Na^+ concentration following a linear relation with a slope of 62 mV dec^{-1}. Accordingly, the ion-selective PVC membranes were also tested in an ion-selective electrode configuration and the electrical characterization revealed a sensitive response of about 52 mV dec^{-1} (see Supporting Information). Both values are in good agreement with the theoretically predicted value of 59.2 mV dec^{-1}, calculated from the Nernst equation at 25 °C, which describes the membrane potential across the membrane as follows[23]

$$E = E^0 + \frac{RT}{z_i F} \ln\left(\frac{a_{analyte}}{a_{inner}}\right) \quad (1)$$

where E^0 is a constant, R the gas constant, z_i the valency of the analyte ion, F the Faraday's constant and a the corresponding activity of the target ion in the analyte and the inner filling solution, respectively. Variations of about ≈7 mV dec^{-1} are in the expected error range, considering the fitting model for the EGOFET transfer curve as well as degradation effects due to the long continuous measurements. Nevertheless, the obtained values for the effective applied gate potential represent good estimations.

The implementation of a flow cell was necessary to obtain a reversible sensor response and to lower the detection limit from 10^{-5} M Na^+ down to ≈10^{-6} M Na^+.[26] This can be clearly seen by comparing the source-drain current before and after applying a flow of DI water through the cell (see Figure 2, first 300 s): if there is no flow, ions which diffuse out of the inner filling solution into the analyte lead to an artifically increased ion concentration in the vicinity of the ISM.[27] This results in a decreased effective gate potential and further to a decreased source-drain current. If a flow is applied (after 300 s), this concentration is lowered, leading to a higher effective gate potential and consequently also to a higher source-drain current. These low Na^+ concentrations and the resulting high effective gate voltages (here < −400 mV) lead to significant drifts (decreasing channel currents, see Figure 2a, 200–400 s). By increasing the concentration the effective applied gate voltage is decreased and the drift is reduced until it almost vanishes completely. Moreover, since no significant drift occurred when no voltages were applied, its origin is most probably ascribed to the electrolysis of water at the electrolyte/semiconductor interface leading to device degradation. This drift can in principle be avoided by keeping the effective gate potential constant at a stable operating point, regardless of the ion concentration in the analyte. However, this requires a readjusting of the gate potential by an appropriate feedback mechanism.[28,29] The according adjustment of the gate potential corresponds directly to the membrane potential change and thus to the ion concentration in the analyte. An appropriate read-out circuit is currently under investigation.

Moreover, note that the herein reported lowest detection limit (10^{-6} M Na^+) is not a property of the ion-sensitive EGOFET itself, but is rather determined by the ISM and the inner filling solution. In detail, ion fluxes through the membrane typically limit the lowest detection limit. Suppression of these fluxes which leads to detection limits in the nano-molar range can be achieved e.g., by using thicker membranes or a lower Na^+ concentration in the inner filling solution.[25,26,30]

Furthermore, the response time of ≈30 s is not a property of the ISM itself but rather related to how quickly the concentration within the flow cell reaches the concentration of the large reservoir (mixing time).[24] Consequently, the response time can be lowered by increasing the flow rate and decreasing the dead volume.

The reversible and selective response of the ion-sensitive EGOFET is shown in **Figure 3**. It demonstrates a rather fast response when the concentration was varied between 10^{-4} M Na^+ (base line) and 10^{-3} M Na^+. The selective response was tested with K^+ as interfering ion following 3 Na^+ concentration variation steps. The K^+ concentration was increased in a 10^{-4} M Na^+ background solution to 10^{-2} M K^+ (two orders of magnitude), showing a current variation of about 7%. In comparison, by increasing from 10^{-4} M to 10^{-3} M Na^+ (one order of magnitude), a 5 times higher current change was

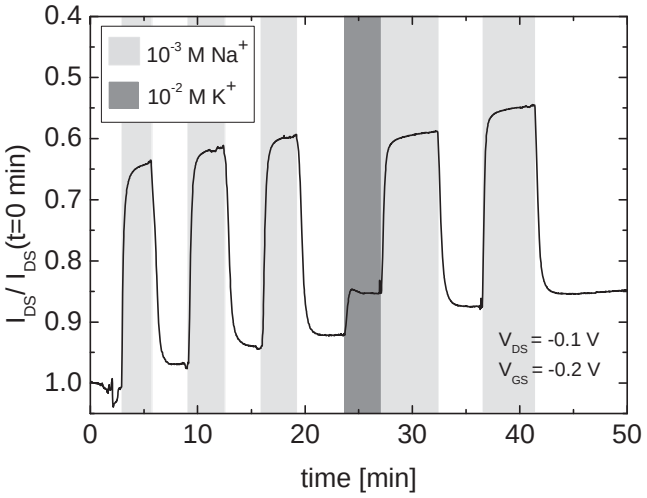

Figure 3. Response curve of a Na^+ selective EGOFET. The source-drain current was measured while the Na^+ concentrations were changed rapidly from 10^{-4} to 10^{-3} M and back. The selectivity was investigated by adding K^+ to a 10^{-4} M Na^+ background solution to obtain 10^{-2} M K^+.

detected, confirming the selectivity of the ion-sensitive EGOFET to Na^+ ions. When the same PVC ISM was also characterized with respect to selectivity in an ion-selective electrode configuration between a range of 10^{-6} – 10^{-1} M K^+, the significant selective response to Na^+ could be confirmed (see Supporting Information). The long-term current drift of ≈0.3% per minute at a reasonable gate voltage (see Figure 3), can be most likely ascribed to bias-stress effects. The long-term stability[31] of the newly presented ion sensor is not a main topic in this letter but will be one of the challenges for the future when pursuing highly promising sensor concepts based on EGOFETs. However, considering the utilization of the presented ion sensor for rapid self-testing applications, the obtained small drifts during operation are in an acceptable range.

In conclusion, we have successfully demonstrated a novel sensor platform based on electrolyte-gated OFETs for selective and reversible ion detection. The novelty of this design compared to conventional ISFETs is the direct contact between the electrolyte and the semiconductor without the use of a solid dielectric, making low-voltage operation in aqueous media feasible. Furthermore, this architecture benefits from a modular approach, allowing for the detection of various ions simply by choosing an appropriate ion-selective membrane. The presented potentiometric sensor based on a Na^+ sensitive PVC membrane showed a Nernstian behavior for a broad detection range between 10^{-6} M and 10^{-1} M Na^+. Moreover, a selective as well as reversible sensor response without a complex recovering process was achieved. These results constitute an important step towards a low-cost integrated sensor array for multiple ion detection facilitated by a facile integration of different state-of-the-art ISMs, being of high relevance for biomedical diagnostics, food-monitoring, industrial process- and water-control.

Experimental Section

The reservoir and the flow cell for the ion-sensitive EGOFETs were made of polydimethylsiloxane (PDMS, Sylgard 184) via a soft molding process, including a curing step of ≈1 h at 100 °C. In order to seal off the flow cell and the reservoir of the inner filling solution, a pressure was applied by an appropriate fixture. The EGOFETs were fabricated on PET substrates (Melinex, DuPont Teijin Films) and the 50 nm gold source/drain (S/D) electrodes with 2 nm chromium adhesion layer were structured using conventional lift-off processing (channel length ≈7 µm, channel width ≈3 mm). Regioregular poly(3-hexylthiophene) (Plexcore OS purchased from Sigma-Aldrich) was deposited via spin-coating from a 4 g L^{-1} toluene solution and dried at 60 °C in Argon (Ar) for ≈10 min and subsequently at 120 °C under high vacuum ($p \approx 4 \times 10^{-5}$ mbar) for 1 h. All devices were assembled under inert atmosphere. In order to obtain a sensitive as well as selective response to sodium ions, a state-of-the-art ionophore-doped PVC based ISM as described by A. Cadogan[20] was introduced. The ISM membranes were prepared by drop-casting a high molecular weight polyvinyl chloride (31 wt%, Selectophore grade), 2-nitrophenyl octyl ether (2-NPOE) (68 wt%), potassium tetrakis-((4-chlorophenyl)borate (KTpClPB) (0.7 wt%) and sodium ionophore X (0.2 wt%) in 5 mL tetrahydrofuran (THF) cocktail onto a glass slide. The drop-cast membrane was allowed to dry overnight at ambient conditions and was peeled off the glass slide for further implementation. All of the chemicals mentioned above were obtained from Fluka Sigma-Aldrich and were used as received. Saline solutions were prepared in concentrations varying from 10^{-4} M to 10^{-1} M NaCl (99.5%, p.a., ACS, ISO) and KCl (>99.0%) in deionized water, respesctively. The electrical characterization of all devices was done in ambient air conditions (at same light conditions) using an Agilent B1500 Parameter Analyzer. Gradual channel approximation was used to calculate the field-effect mobility in the saturation regime.

Supporting Information

Supporting Information is available from the Wiley Online Library or from the author.

Acknowledgements

For financial support the Styrian Government (projects BioOFET 2 and MIEC-DEVs) is acknowledged.

Received: July 16, 2013
Revised: August 15, 2013
Published online:

[1] L. Kergoat, B. Piro, M. Berggren, G. Horowitz, M.-C. Pham, *Anal. Bioanal. Chem.* **2012**, *402*, 1813.
[2] P. Lin, F. Yan, *Adv. Mater.* **2012**, *24*, 34.
[3] J. T. Mabeck, G. G. Malliaras, *Anal. Bioanal. Chem.* **2006**, *384*, 343.
[4] A. Klug, M. Denk, T. Bauer, M. Sandholzer, U. Scherf, C. Slugovc, E. J. W. List, *Org. Electron.* **2013**, *14*, 500.
[5] A. Bratov, N. Abramova, A. Ipatov, *Anal. Chim. Acta* **2010**, *678*, 149.
[6] C. Bartic, B. Palan, A. Campitelli, G. Borghs, *Sens. Actuators, B* **2002**, *83*, 115.
[7] C. Gao, X. Zhu, J. Choi, C. H. Ahn, in *IEEE Transducers '03, The 12th International Conference on Solid State Sensors Actuators and Microsystems*, Boston **2003**, 1172.
[8] C. Bartic, A. Campitelli, S. Borghs, *Appl. Phys. Lett.* **2003**, *82*, 475.
[9] T. Ji, P. Rai, S. Jung, V. K. Varadan, *Appl. Phys. Lett.* **2008**, *92*, 233304.
[10] P. Bergveld, *Sens. Actuators, B* **2003**, *88*, 1.
[11] P. Bergveld, *IEEE Trans. Biomed. Eng.* **1970**, *BME 17*, 70.
[12] S. V. Dzyadevych, A. P. Soldatkin, A. V. El'skaya, C. Martelet, N. Jaffrezic-Renault, *Anal. Chim. Acta* **2006**, *568*, 248.

DOI: 10.1002/adma.201303281

[13] L. Kergoat, L. Herlogsson, D. Braga, B. Piro, M.-C. Pham, X. Crispin, M. Berggren, G. Horowitz, *Adv. Mater.* **2010**, *22*, 2565.
[14] F. Buth, D. Kumar, M. Stutzmann, J. A. Garrido, *Appl. Phys. Lett.* **2011**, *98*, 153302.
[15] A. Laiho, L. Herlogsson, R. Forchheimer, X. Crispin, M. Berggren, *Proc. Natl. Acad. Sci. U.S.A.* **2011**, *108*, 15069.
[16] L. Kergoat, B. Piro, M. Berggren, M.-C. Pham, A. Yassar, G. Horowitz, *Org. Electron.* **2012**, *13*, 1.
[17] S. Casalini, F. Leonardi, T. Cramer, F. Biscarini, *Org. Electron. 2012*, *14*, 156.
[18] F. Buth, A. Donner, M. Sachsenhauser, M. Stutzmann, J. A. Garrido, *Adv. Mater.* **2012**, *24*, 4511.
[19] M. Magliulo, A. Mallardi, M. Y. Mulla, S. Cotrone, B. R. Pistillo, P. Favia, I. Vikholm-Lundin, G. Palazzo, L. Torsi, *Adv. Mater.* **2013**, *25*, 2090.
[20] A. Cadogan, Z. Gao, A. Lewenstam, A. Ivaska, D. Diamond, *Anal. Chem.* **1992**, *64*, 2496.
[21] E. Bakker, E. Pretsch, *Anal. Chem.* **2002**, 420.
[22] N. Abramova, A. Bratov, *Sensors* **2009**, *9*, 7097.
[23] S. V. Lamaka, M. G. Taryba, M. L. Zheludkevich, M. G. S. Ferreira, *Electroanal.* **2009**, *21*, 2447.
[24] P. Bühlmann, L. D. Chen, in *Supramolecular Chemistry: From Molecules to Nanomaterials* (Eds: P. A. Gale, J. W. Steed), John Wiley & Sons, Ltd., **2012**, pp. 2539–2577.
[25] E. Bakker, E. Pretsch, *Trends in Anal. Chem.* **2001**, *20*, 11.
[26] A. Ceresa, T. Sokalski, E. Pretsch, *J. Electroanal. Chem.* **2001**, *501*, 70.
[27] S. Mathison, E. Bakker, *Anal. Chem.* **1998**, *70*, 303.
[28] P. Bergveld, *Sens. Actuators* **1981**, *1*, 17.
[29] P. Bergveld, *IEEE Trans. Biomed. Eng.* **1968**, *BME 15*,102.
[30] K. Schmoltner, F. Schlütter, M. Kivala, M. Baumgarten, S. Winkler, R. Trattnig, N. Koch, A. Klug, E. J. W. List, K. Müllen, *Polym. Chem.* **2013**, 10.1039/c3py00089c.
[31] Z. Szigeti, T. Vigassy, E. Bakker, E. Pretsch, *Electroanal.* **2006**, *18*, 1254.

ADVANCED MATERIALS

Supporting Information

for *Adv. Mater.*, DOI: 10.1002/adma. 201303281

Electrolyte-Gated Organic Field-Effect Transistor for Selective Reversible Ion Detection

*Kerstin Schmoltner, Johannes Kofler, Andreas Klug, and Emil J. W. List-Kratochvil**

Supporting Information

for *Adv. Mater.*, DOI: 10.1002/adma.201303281

Electrolyte-gated organic field-effect transistor for selective reversible ion detection

*Kerstin Schmoltner, Johannes Kofler, Andreas Klug, Emil J. W. List-Kratochvil**

K. Schmoltner, J. Kofler, Dr. A. Klug, Prof. Dr. E. J. W. List-Kratochvil
NanoTecCenter Weiz Forschungsgesellschaft mbH
Franz-Pichler Straße 32, A-8160 Weiz, Austria
E-mail: E.List@tugraz.at
Prof. Dr. E. J. W. List-Kratochvil
Institute of Solid State Physics,
Graz University of Technology
Petersgasse 32, A-8010 Graz, Austria

Before the ion-selective PVC based membranes (ISMs) were implemented into the EGOFET architecture, they were characterized with respect to sensitivity and selectivity in a typical ion-selective electrode configuration. A 10^{-2} M NaCl inner filling solution and two Ag/AgCl reference electrodes were used, resulting in the following setup: Ag/AgCl electrode / 10^{-2} M NaCl / ISM / analyte / Ag/AgCl electrode. To investigate the sensitivity to Na^+, the salt concentration was stepwise increased by adding saline solutions with a certain amount of NaCl (10^{-4} M – 10^{-1} M NaCl) to the analyte, while stirring and recording the potential difference (via a Keithley voltmeter) (see **Figure S1**(a)). In addition, the response of the membrane to the interfering ion K^+ was measured by using KCl as an analyte. The results are presented in **Figure** S1 and **S2**, showing a significant sensitive and selective response to Na^+.

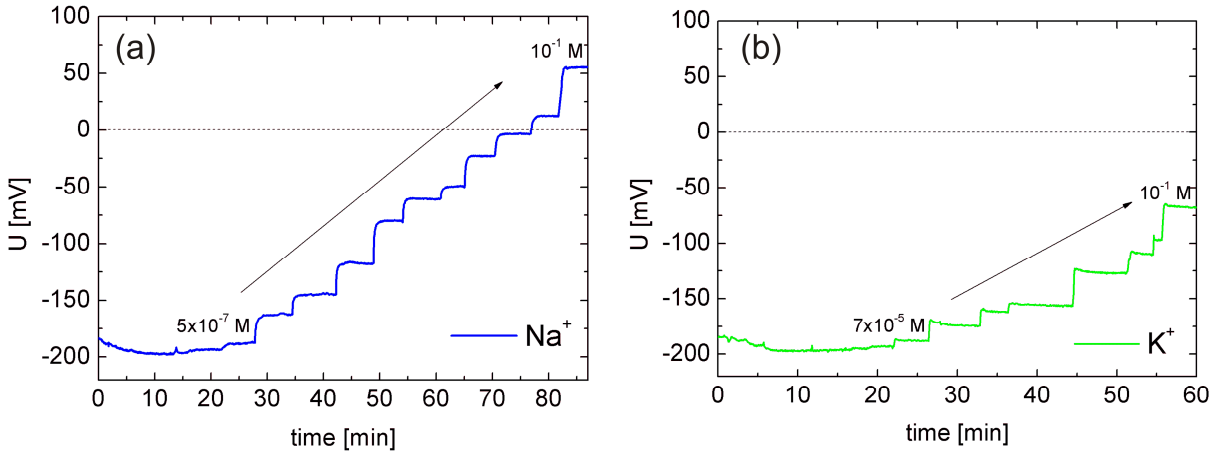

Figure S1. Potentiometric response of the PVC ISM while increasing the Na^+ (a) and the K^+ (b) concentration stepwise.

The lowest detection limit of the target ion was determined to be ~10^{-6} M Na^+ (see Figure S2). The results show a nice linear behavior in the range of 5 x 10^{-6} M to 10^{-1} M Na^+ with a slope of 52 mV/dec, compared to 58 mV/dec as reported in literature.[1] The response curve for K^+ revealed a slope of 46 mV/dec, but a much smaller linear range between 5 x 10^{-3} and 10^{-1} M K^+. This clearly demonstrates the Na^+ selectivity of the applied membrane.

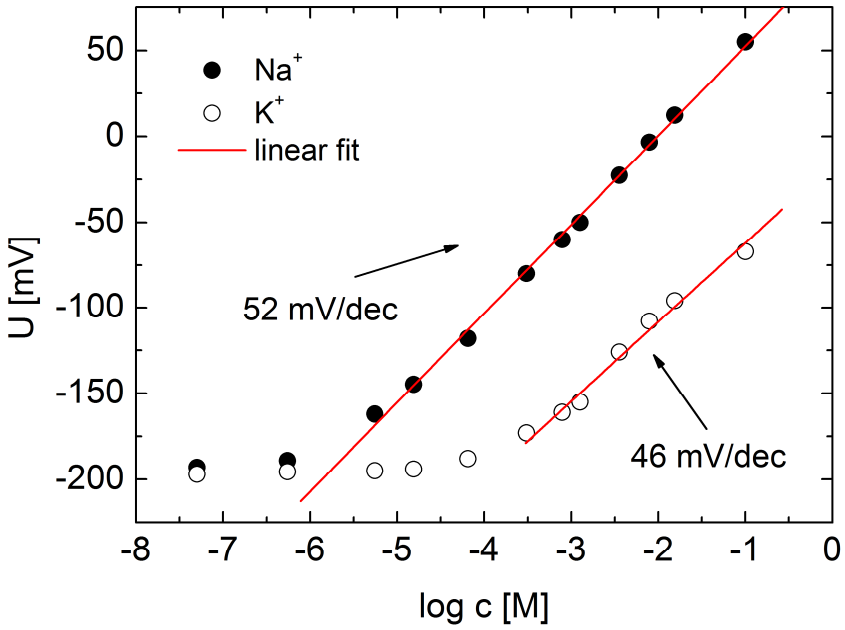

Figure S2. Potentiometric response versus the logarithmically plotted concentration of Na^+ (full symbols) and K^+ (open symbols).

Transfer curve and fit parameter of an electrolyte-gated ion-sensitive field-effect transistor

Figure S3 (a) shows the transfer curve of an EGOFET without an ion-selective membrane in a 10^{-2} M NaCl electrolyte solution, gated via an Ag/AgCl reference electrode. This measurement was performed before the sensitivity evaluation was carried out at a constant operating point (V_{DS} = -0.1 V, V_{GS} = -0.2 V) (see Figure 2 in the main text). Figure S3 (b) depicts the square root of the source-drain current versus the gate voltage including a corresponding polynomial fit. This equation (see Figure S3 (b)), which describes the correlation of the gate voltage with the source-drain current, is required to estimate the effective applied gate voltage during the sensitivity measurements (see Figure 2 (b) in the main text). Since drifts during the measurements cannot be totally excluded, the obtained values should be considered as estimations.

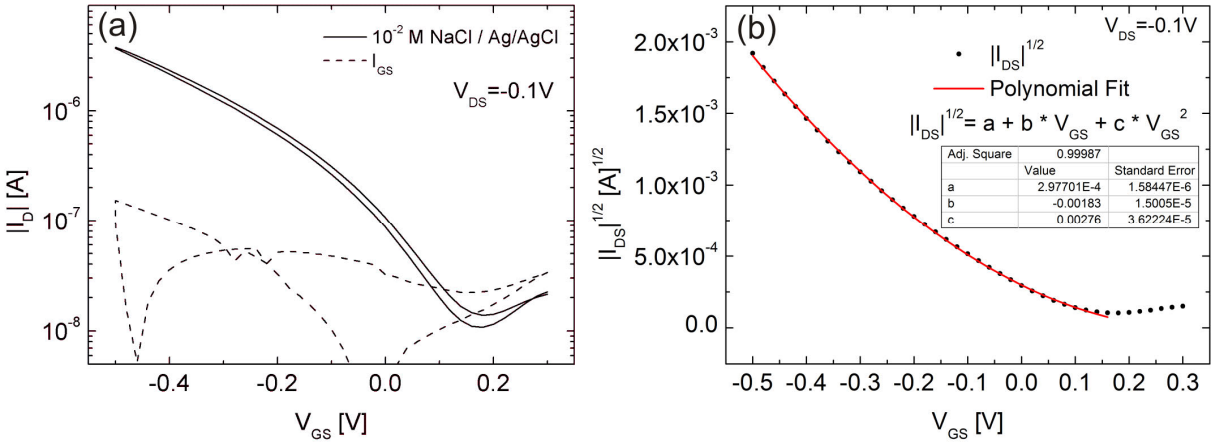

Figure S3. Semilogarithmic transfer curve of a typical EGOFET without an ion-selective membrane (a). Square root of the source-drain current versus the gate voltage and corresponding polynomial fit (b).

References

[1] A. Cadogan, Z. Gao, A. Lewenstam, A. Ivaska, and D. Diamond, *Anal. Chem.* **199**2, *64*, 2496.